UNSW SYDNEY

Studies in the absorption of vapours by liquids : the absorption of zinc vapour in molten lead

Author:
Warner, Noel Alfred

Publication Date:
1958

DOI:
https://doi.org/10.26190/unsworks/11789

License:
https://creativecommons.org/licenses/by-nc-nd/3.0/au/
Link to license to see what you are allowed to do with this resource.

Downloaded from http://hdl.handle.net/1959.4/67095 in https://unsworks.unsw.edu.au on 2024-04-20

UNSW
>015046940

T541.3453
40

THE UNIVERSITY OF NEW SOUTH WALES
LIBRARY

Permission has been granted by the Head of the School in which this thesis was submitted for it to be consulted after 2 weeks... and copied after ...2 weeks...

This permission is contained in the Administration file "Availability of H.D. Theses" and applies only to those theses lodged with the University before the use of Disposition Declaration forms.

N.S.W. UNIVERSITY OF TECHNOLOGY

SCHOOL OF CHEMICAL ENGINEERING

STUDIES IN THE ABSORPTION OF VAPOURS BY LIQUIDS

THE ABSORPTION OF ZINC VAPOUR IN MOLTEN LEAD

DOCTOR OF PHILOSOPHY THESIS

N.S

N. A. W A R N E R

January, 1958

UNIVERSITY OF N.S.W.
27972 26. FEB. 75
LIBRARY

ABSTRACT

The countercurrent absorption of zinc vapour in molten lead has been analysed using the additive diffusional resistance concepts.

The contacting of zinc vapour with molten lead is shown to be a true absorption, not a condensation, and the conventional gas absorption theories are shown to apply to the absorption of a metallic vapour in a liquid metal at an elevated temperature.

Fundamental studies of disc column performance are reported and the importance of the relative interfacial velocity in the gas phase mass transfer process has been illustrated and a new mass transfer factor, the "relative j_D" factor has been introduced.

A simple correlation, relating the gas film mass transfer coefficient, the diffusion coefficient and the gas phase pressure drop, has been established by vaporisation studies in a disc column. The relationship provides excellent support to the $^2/_3$ exponent on the diffusivity. In previous investigations of irrigated systems, the true effect of diffusivity is shown to have been masked by relative velocity effects.

By using room temperature analogues of the zinc absorption in molten lead packed column, the flow characteristics of the irrigating liquid lead and the mass transfer properties of the packing under non-wetting conditions are evaluated, thereby allowing correlation of the zinc absorption data with ammonia absorption experiments on the same packing.

For correlating the zinc and ammonia absorption data, a new variable quantity, "the effective holdup ratio", has been introduced. The results of the zinc absorption studies suggest that the total liquid holdup is effective in the absorption process, because of the increased mobility of

the semistagnant liquid, when a liquid metal irrigates a packed bed, compared to the very slow movement of the static holdup usually observed in aqueous or organic liquid irrigated systems.

.....

CONTENTS

CHAPTER 6

CHAPTER 7

CHAPTER 8

SECTION B

INVESTIGATION OF THE ABSORPTION OF ZINC VAPOUR IN MOLTEN LEAD

CHAPTER 9

CHAPTER 10

CHAPTER 11

CHAPTER 12

.....

CHAPTER 1

INTRODUCTION

UNIVERSITY OF NEW SOUTH WALES KENSINGTON

During the past few years considerable attention has been given to the development of a process in which zinc can be produced in a blast furnace. In August 1957, the first full account of the production of zinc in a blast furnace was reported by Morgan (76). Prior to this date numerous patents appeared on various aspects of the process. The relevant patents and the underlying theoretical aspects were summarised by Morgan (76) and the development of the process by the Imperial Smelting Corporation at Avonmouth, England, outlined.

A study of the problems, associated with the development of the zinc blast furnace, showed that the process could only be thermally efficient if the gas generated in the furnace contained a considerable quantity of carbon dioxide. Using the conventional types of condensers, it had been previously possible to condense zinc only from gases substantially free from carbon dioxide. The primary problem, on which the development of the process depended, was therefore the condensation of zinc from a gas containing a relatively low concentration of zinc vapour and a considerable amount of carbon dioxide. Conventional cooling methods, when applied to such gaseous mixtures, result in the oxidation of the zinc by the carbon dioxide and the subsequent formation of "blue powder", which has only very limited commercial application and cannot be coalesced by heating above the zinc melting point, because of the oxide coating on the particles.

The solution to the problem of oxidation of the zinc by carbon dioxide, when the gaseous mixture was cooled, was to shock chill the gases by passing them through narrow water cooled tubes. In such a system the

condensation took place in the bulk of the gas phase, with any particles of dust or fume acting a nuclei for the formation of small droplets. These droplets cooled below their melting point before coalescing and zinc dust was formed, which was carried forward and collected in filter bags. The zinc dust thus formed was found to contain 98% metallic zinc, proving that shock chilling had prevented undue oxidation during the condensation. However, due to even the slight oxidation, the zinc dust could not be readily coalesced even if brought into contact with a bath of molten zinc.

Two different methods have been proposed for recovering the zinc in liquid form from the gaseous mixture. The method favoured by the New Jersey Zinc Co., U.S.A., was to contact the gases with a shower of molten zinc. A description of this process has been published (1). The method developed by the Imperial Smelting Corporation outlined by Morgan (76) was to contact the gases with molten lead. As liquid lead, even when containing 2-3% zinc, can be pumped and handled with ease, any of the methods used for absorbing gases in liquids were available to provide the desired contacting. Particularly promising results were obtained by passing the furnace gases into a chamber showered with molten lead by the action of a rotor dipping into a pool of lead. The lead was cooled as it left this unit causing separation of liquid zinc. Continuous removal of both heat and zinc from the furnace gases was obtained by pumping the lead through a circuit consisting of the "condenser", an external cooler and a zinc separation vessel, from which the zinc produced is continuously withdrawn and the lead returned to the "condenser".

A typical operation of the blast furnaces now in production at Avonmouth yields gas leaving the charge containing 5-6% Zn and 8-10% CO_2.

Such a gas mixture has an equilibrium re-oxidation temperature of 960 - 1000°C. The primary object of the molten lead contacting stage is to remove the zinc from the gas phase very rapidly to prevent the re-oxidation reaction:-

$$CO_2 + Zn = CO + ZnO$$

For a gas containing 5% Zn, the following figures are given by Morgan (76) for the countercurrent scrubbing with cool liquid lead saturated with zinc.

TABLE 1.1

TYPICAL COUNTERCURRENT "CONDENSER" OPERATING DATA

Based on Figures by Morgan (76)

A. Gas Phase

5% Zn at 1000°C
Cooled to 450°C

B. Lead Phase

Circulation rate	= 420 ton/ton Zn produced
Inlet temp.	= 440°C
Inlet composition	= 2.02% Zn (sat'd.)
Outlet temp.	= 570°C
Outlet composition	= 2.26% Zn
Saturation at Outlet temp.	= 4.90%

C. Zinc Recovery

% of Total recovered as molten zinc	= 89%

The high lead circulation rate, shown in Table 1.1, and therefore the small rise in zinc concentration, is needed to fulfil the heat removal requirements. The 11% of zinc, which is not recovered as liquid zinc, is recovered in the dross periodically removed from the "condenser" and from the scrubbing system through which the "condenser" exhaust gases pass.

Morgan (76) and the patent literature refer to the gas - liquid lead contacting stages as condensers. Such a nomenclature suggests a lack of understanding of the fundamental mechanism involved, as does the statement made by Morgan (76) when describing these units:-

> "Rapid cooling tends to promote fog formation but the seriousness of this aspect is reduced by (a) the high superheat of the gases, which have a dew point of about 650°C and leave the furnace at 900 - 1000°C; and (b) the presence of a rain of unsaturated lead in which droplets of zinc are formed, but are themselves scrubbed by the intense rain of lead."

The statement quoted implies that discrete drops of zinc are formed in the contacting stage, because the gas temperature in the vicinity of the lead rain falls below the dew point and it is these droplets of zinc which are collected by the scrubbing action of the lead showers.

This is considered not to be the case at all. The transfer of zinc from the gas phase into the liquid lead is clearly a diffusion controlled mass transfer operation. The zinc must diffuse from the bulk of the furnace gases through the laminar gas film on the gas - liquid lead interface and must then diffuse into the bulk of the lead phase. Hence at no stage would the zinc be present in particulate form.

Zinc droplets would be formed in the bulk of the gas phase, only if the bulk gas temperature fell below the dew point of its zinc vapour content. As the dew point of the inlet gases is approximately 650°C, the gas inlet temperature 1000°C approximately and the outlet lead temperature approximately 570°C, it is very difficult to conceive the bulk gas temperature as falling below the dew point, when the temperature drops associated with the transfer of heat from the hot gases to the cooler lead

are taken into account and when it is realised that the zinc content of the gases will decrease approximately exponentially as the gas traverses the "condenser", with the corresponding decrease in the dew point temperature of the gas mixture.

It is therefore suggested that a more appropriate nomenclature for the gas - liquid lead contacting stages would be to call these units "absorbers", as it would appear that the fundamental mechanism involved is basically what is known as gas absorption.

The industrially important operations of gas absorption, liquid - liquid extraction, leaching and distillation are all cases where mass is transferred from one phase to another and are therefore collectively termed mass transfer operations. The transfer of mass from one phase to another or from one point to another in the same phase is by diffusion.

The transfer of mass in a stagnant fluid, in the absence of convection currents, is by the process of molecular diffusion. Molecular diffusion is also the mechanism of material transfer in fluids, which are in laminar flow with all particles of the fluid moving along parallel paths. Molecular diffusion occurs also in the turbulent flow of fluids, but in this case there is an additional mechanism called eddy diffusion.

Turbulent flow is characterised by the formation of eddy currents or swirls, which cause a cross mixing of thefluid elements, which in laminar flow are moving parallel to each other. The mixing of the fluid elements in turbulent flow greatly facilitates the transfer of mass between points of unequal concentration. Therefore, in turbulent fluids, the molecular diffusion accounts for only a small portion of the diffusional transport, whereas eddy diffusion is the principle mechanism.

However, even in turbulent flow, the eddies and convection currents die out as a phase boundary is approached. Thus at the phase interface there exists a laminar film, through which the tranfer of mass can be by molecular diffusion only. Although eddy diffusion in turbulent flow is very rapid, compared to the inherently slow process of molecular diffusion, the overall rate of transfer of mass from one phase to another is largely dependent upon the rate of molecular diffusion of the component being transferred through the laminar film adjacent to the phase boundary.

The aim of this research project was therefore to study the mechanism of the absorption of zinc vapour in molten lead and to see if the conventional gas absorption theories, developed for non-metallic systems at or near room temperature, could be applied to the absorption of a metallic vapour in a liquid metal at an elevated temperature.

Metallic vapour - liquid metals systems have not previously been analysed from this point of view and thus there have been no similar investigations reported in the literature. For this reason, a conventional literature survey is not presented in this thesis, but instead, the experimental investigations are prefaced by a short section covering the theoretical aspects required as a general basis for the project.

Since this research program was initiated in 1953, several workers have reported mass transfer studies in liquid metal systems. Although no data has yet been published for the absorption of a metallic vapour in a liquid metal, the mass transfer studies reported by Bonilla (7) in 1955, Dunn, Bonilla, Ferstenberg and Gross (20) in 1956 and Maxwell and Storrow (69) in 1957, require special mention as they constitute advances in the related

fields of diffusional transport in liquid metal systems.

Bonilla (7) summarised the studies of numerous investigators working in the molten metal and fused salt mass transfer field, including the more detailed experiments later published by Dunn, Bonilla, Ferstenberg and Gross (20). Two experiments, designed to study the rate of mass transfer between two liquid phases at an elevated temperature, were reported by Bonilla (7). The rate of mass transfer in the two liquid phase lead - zinc systems was investigated, but no successful results were obtained because of experimental difficulties. An investigation was also made of the diffusional resistance within drops of fused LiCl - KCl eutectic rising through a bath of molten cadmium. The mass transfer coefficients for transport of cadmium into drops of the molten eutectic were comparable to those predicted from Higbie's Penetration Theory (39). The conclusion reached was that the performance of fused salt - liquid metal spray columns could at least be roughly estimated for design purposes from the existing theories, provided the droplet size was known.

Dunn, Bonilla, Ferstenberg and Gross (20) studied the rates of mass transfer for solid metal shapes dissolving in mercury at room temperature. The systems studied were natural convection at horizontal cylinders, forced convection flow in tubes and forced convection flow through packed beds. The results of these room temperature studies followed substantially the correlations developed for non-metals at room temperature and therefore it was suggested that mass transfer operations in liquid metals could be predicted from the accepted correlations, at least for preliminary design purposes.

Maxwell and Storrow (69) reported data for the room temperature vaporisation of mercury from amalgamated surfaces into gas streams. The

mass transfer data obtained in these studies were correlated using the accepted methods, showing that the transfer of a metallic vapour into a gas stream at room temperature is basically the same as other vaporisation processes.

As the experiments undertaken during the course of the program covered a large number of diverse fields, which by themselves would appear to have little bearing on the main theme, at various stages throughout the thesis, theoretical aspects and literature reviews are included in the relevant chapters so as to preserve the continuity of the discussions, rather than presenting these diverse aspects at the beginning of the thesis, where their real significance would not be appreciated.

The experimental work can be broadly classified into two sections. Section A contains the fundamental studies of disc column performance, whilst in Section B the investigation proper of the absorption of zinc vapour in molten lead is presented.

Although the disc column was finally found unsatisfactory for investigating the absorption of zinc vapour in molten lead, the fundamental studies reported would have been required, had the disc column proved suitable for the application. As these studies were virtually completed, before the disc column was finally rejected and as the conclusions reached in these experiments were considered to be of general application and were used in the final assessment of the zinc absorption studies, these fundamental studies of Section A are considered to be an integral part of the experimental program.

THEORETICAL ASPECTS

CHAPTER 2

LIQUID LEAD - ZINC ALLOYS

ZINC DIFFUSIVITY AND ACTIVITY

2.1 Diffusion in Liquid Lead - Zinc Alloys

Compared with the numerous data available on solid state diffusion, the studies of diffusion in liquid metals are very limited and are mainly restricted to the mercury amalgams over small ranges of temperature and composition. The general difficulty of measuring diffusion coefficients in both liquids and gases at high temperatures has been that of eliminating convection currents. A review of experimental work in this field covering work up to 1951 was given by Jost (51). More recent papers include those by Hoffman (44) on self-diffusion in mercury, Morgan and Kitchener (75) on diffusion of carbon and cobalt in liquid iron, Grace and Derge (35) and Rothman and Hall (91) on the diffusion of bismuth in bismuth - lead alloys and Niwa et al. (80), who studied diffusion in the following liquid systems: Sn - Pb, Bi - Pb, Sb - Pb, Cd - Pb, Sn - Bi and Sb - Sn.

There have, however, been no data reported for diffusion in liquid lead - zinc alloys.* In the absence of such data, an estimate had to be made of the diffusion coefficient in this system, as it was realised that such information would be required for the study of zinc vapour absorption in molten lead. The existing theories, enabling a prediction to be made of the diffusion coefficient in the liquid state, were therefore reviewed.

* Although Bonilla and co-workers had previously reported a single value of the diffusion coefficient of zinc in liquid lead (N.Y.O. 3088, 3090 U.S. A.E.C.), a personal communication to Bonilla (February 1957) indicated that there was no reliable diffusion data available on the Pb - Zn system, and suggested the use of a form of the Stokes-Einstein equation for arriving at an estimate.

Einstein (21) and Eyring (32) have both proposed theoretical equations, from which the diffusion coefficient can be obtained. Both these theories consider the diffusivity and viscosity as being closely related rate processes and predict activation energies of diffusion and viscosity as being essentially equal. The Stokes-Einstein and the Eyring equations relating the viscosity and the diffusion coefficient have identical temperature coefficients, but the diffusivities differ by a factor of about 3π in magnitude.

The Stokes-Einstein (21) equation, derived on the basis of hydrodynamic theory, in which it is assumed that the diffusing species is very large compared to the particle size of the medium gives

$$D = \frac{kT}{6\pi r \eta} \qquad \ldots\ldots 2.1$$

where k is the Boltzmann constant, r is the radius of the diffusing particle and η is the viscosity of the medium, which is considered as being continuous.

The Eyring equation (32) takes the discontinuity in "jump-distances" in the medium into account by three parameters in the place of r but for monatomic liquids can be reduced to a form similar to the Stokes-Einstein equation:

$$D = \frac{kT}{2 r \eta} \qquad \ldots\ldots 2.2$$

The variation of D with temperature is therefore determined by the variation of the viscosity and hence the usual form of expressing experimental diffusion data is by the Arrhenius type of equation

$$D = D_o \exp. \frac{-\Delta H}{RT} \qquad \ldots\ldots 2.3$$

where ΔH = activation energy and the constant D_o are found experimentally.

Neither of these theories provides a reliable method of calculating

diffusion coefficients from accessible data.

It has been suggested (32) that the Stokes-Einstein equation, modified by a small numerical factor, should be applicable to a solute molecule of size comparable with that of the solvent molecules. Support of this view was given by Morgan and Kitchener (75), who compiled a table of the available data for diffusion in amalgams, and showed that, for elements near mercury (i.e. the solvent) in the periodic table, the data conformed very approximately with a modified Stokes-Einstein equation

$$D = \frac{kT}{3\pi\eta r} \qquad \ldots\ldots 2.4$$

However, for other elements in the same table, which were further removed from mercury in the periodic table, the original Stokes-Einstein gave values closer to the reported experimental values. The values used for r by Morgan and Kitchener (75) in the calculations were the "metallic radii" for 12-co-ordination as given by Wells (126).

Rothman and Hall (91) used their measured coefficients of the self-diffusion of lead to calculate the radius of the diffusing particle. At 350°C the radii obtained using equations 2.1 and 2.2 were:

Eyring equation:- $r = 6.73$ to 7.12 Å

Stokes-Einstein equation:- $r = 0.715$ to 0.757 Å

The range given for each equation was because of differences in the reported viscosity data for lead. Thus the agreement between the calculated radii and the usually accepted radii of lead (whether "metallic radius" or "ionic radius") was better when the Stokes-Einstein equation was used. Similar observations were made by Hoffman (44) who studied self-diffusion in mercury. Rothman and Hall (91) did not extend the analysis of the radius to an assessment of what the diffusing entity was, as they considered their data to be of insufficient accuracy.

Several workers including Jost (51) and Niwa et al. (80) have suggested that the unit of flow in metals is the metal ion. The basis behind this proposal is that in most non-electrolyte liquids, it has been found that the following empirical relationship between the activation energy of viscosity $\Delta H_{vis.}$ and the energy of vaporisation L_o

$$L_o / \Delta H_{vis.} \doteqdot 3 \text{ to } 4 \qquad \ldots\ldots 2.5$$

However, the ratio $L_o / \Delta H_{vis.}$ in most metals is between 8 and 25. Hence, it has been assumed that the unit of flow in metals is much smaller than the unit of vaporisation. Since the latter is the neutral atom, the former would appear to be the metal ion. If the ratio $L_o / \Delta H_{vis.}$ is therefore ammended by the ratio of the ionic and atomic volumes, values of 3 to 4 for metals are also obtained

i.e. $$\frac{L_o}{\Delta H_{vis.}} \cdot \left(\frac{r_{ion}}{r_{atom}}\right)^3 \text{ for metals} \doteqdot 3 \text{ to } 4 \qquad \ldots\ldots 2.6$$

Niwa et al. (80) suggested that their diffusion data for the following liquid systems Sn - Pb, Bi - Pb, Sb - Pb, Cd - Pb, Sn - Bi and Sb - Sn, could be "intuitively explained in terms of metal ions stripped of the conduction electrons", but no attempt was made by these authors to quantitatively analyse their diffusion data in such terms.

As the studies reported by Niwa et al. (80) are the only comprehensive source of diffusion in dilute liquid lead alloys, their results are of particular interest to this investigation, as they allow an assessment to be made of the applicability of the theoretical equations to such systems.

A review of the various equations proposed showed that calculations based on the Stokes-Einstein equation, equation 2.1, in which the radius of the diffusing particle is taken as the ionic radius ("crystal" radius of Pauling) as given by Wells (126), gave calculated values of the

diffusion coefficient, which were of similar order to those obtained experimentally by Niwa et al. (80).

The calculated values using the above procedure are compared to the experimental data for diffusion in dilute liquid lead alloys in Table 2.1.

TABLE 2.1

DIFFUSION IN DILUTE LIQUID LEAD ALLOYS

Diffusate	Temperature °C	$D_{obs.} \times 10^5$ cm.^{2}/sec. *	$D_{calc.} \times 10^5$ cm.^{2}/ sec. †	$D_{obs.}/D_{calc.}$
Sn	450	2.6	3.6	0.72
	510	3.9	4.5	0.87
	550	4.3	5.1	0.84
	600	5.5	5.8	0.95
Bi	450	5.0	3.5	1.43
	500	6.2	4.1	1.51
	550	7.3	4.9	1.49
	600	8.3	5.5	1.51
Sb	450	3.1	4.1	0.76
	500	4.1	4.8	0.86
	550	5.5	5.8	0.95
	600	6.4	6.6	0.97
Cd	450	3.9	2.6	1.50
	500	5.0	3.1	1.61
	550	6.0	3.7	1.62
	600	6.8	4.2	1.62

* Experimental data reported by Niwa et al. (80)

† Calculated using Stokes-Einstein equation, radius of diffusing particle taken as the ionic radius tabulated by Wells (126) and viscosity data given in Liquid Metals Handbook (65).

The agreement between the calculated and experimental values shown in Table 2.1 is considered to be fair only. The biggest departures are exhibited for Bi - Pb and Cd - Pb alloys, in which cases the experimental values are approximately 1.5 times the calculated values. As Grace and Derge (35) and Rothman and Hall (91) also obtained data which was substantially in agreement with the data of Niwa et al. (80) for diffusion of bismuth in dilute lead alloys, the large departure from the calculated value cannot fairly be attributed to experimental errors, but must indicate a deficiency in the theoretical equation. Also it is doubtful if any structural interpretation should be made of the choice of the ionic radius as the relevant radius in the diffusion process.

However, the procedure, used in the calculations, has given values of diffusion coefficients, which are closer than those calculated using the Eyring equation, the Stokes-Einstein equation using the "metallic radii" or the modified Stokes-Einstein equation proposed by Morgan and Kitchener (75).

The same method of calculation was applied to the experimental data of Schwartz (94) for diffusion in dilute mercury alloys at 25°C. The results of these calculations are shown in Table 2.2.

TABLE 2.2

DIFFUSION IN DILUTE MERCURY AMALGAMS

TEMPERATURE = 25°C

Diffusate	$D_{obs.} \times 10^5$ $cm.^2/sec.$ *	$D_{calc.} \times 10^5$ $cm.^2/sec.$ †	$D_{obs.}/D_{calc.}$
Li	0.93	2.35	0.40
Na	0.86	1.49	0.58
K	0.71	1.06	0.67
Cs	0.64	0.83	0.77
Au	0.73	1.03	0.71
Zn	2.4	1.91	1.26
Cd	2.0	1.45	1.38
Tl	1.18	1.48	0.80
Sn	2.1	1.98	1.06
Pb	2.1	1.68	1.25
Bi	1.5	1.91	0.79

* Experimental data reported by Schwartz (94)

† Calculated using Stokes-Einstein equation, radius of diffusing particle taken as the ionic radius tabulated by Wells (126) and viscosity data given in Liquid Metals Handbook (65).

The agreement between the experimental and calculated values shown in Table 2.2 is quite good except for the alkali metal data and the figure observed for the diffusion of gold. It is interesting to note that, for the highly electropositive alkali metals, a calculation using the metallic radii as given by Wells (127) rather than the ionic radii, gives values closer to the observed experimental data. A comparison of the two methods of calculation for the alkali metals diffusing in dilute mercury amalgams is shown in Table 2.3.

TABLE 2.3

DIFFUSION OF ALKALI METALS IN DILUTE MERCURY AMALGAMS

Comparison of the Use of the Ionic Radii and Metallic Radii in the Stokes-Einstein Equation

Experimental Data Reported by Schwartz (94)

Diffusate	$\frac{D_{obs.}}{D_{calc.}}$ Using Ionic Radii	$\frac{D_{obs.}}{D_{calc.}}$ Using Metallic Radii
Li	0.40	1.04
Na	0.58	1.16
K	0.67	1.18
Cs	0.77	1.28

Although a structural interpretation could possibly be made, based on the calculations shown in Tables 2.2 and 2.3, such a procedure is considered unwise at this stage. However, for estimating the diffusion coefficient of zinc in dilute lead alloys, it is considered that sufficient justification has been presented for basing the calculation on the Stokes-Einstein equation with the radius of the diffusing particle being taken as the ionic radius as given by Wells (126). The values of the diffusion coefficient of zinc in dilute lead alloys, calculated using the suggested procedure, are shown in Table 2.4. If these data were to be used at higher zinc concentrations, they would have to be corrected by the equations proposed by Eyring (32):-

$$D = D_i \ (1 + d \ (\ln \gamma)/d(\ln x)) \qquad \ldots\ldots 2.7$$

where D_i = the diffusion coefficient at infinite dilution
γ = activity coefficient of the diffusing species
x = mole fraction of the diffusing species.

TABLE 2.4

CALCULATED DIFFUSION COEFFICIENTS

FOR ZINC IN DILUTE LEAD ALLOYS

Temperature °C	$D_{calc.} \times 10^5$ cm.^{2}/sec.
450	3.5
500	4.1
550	4.9
600	5.5
650	6.3
700	7.0
750	7.8

2.2 Activity of Zinc in Liquid Lead - Zinc Alloys

The activity of zinc in lead - zinc alloys has been determined experimentally by vapour pressure and e.m.f. measurements.

Jellinek and Wannow (48) determined the zinc activity by a dynamic vapour pressure measurement with carrier gas technique.

Recently Kleppa (56) used the e.m.f. technique to measure the zinc activity. Kleppa's experimental results showed remarkable agreement with the earlier vapour pressure measurements of Jellinek and Wannow.

Both these experimental investigations give activity data, which agrees very closely with values calculated from a semi-theoretical equation derived by Lumsden (62). Lumsden proposed an equation to represent the change in free energy when one gram-atom of a liquid lead-zinc alloy is formed from its liquid components, based on a thermodynamic study of all the available information of the lead - zinc system.

From Lumsden's free energy of mixing expression, the partial molar free energy change of either component can be obtained, thus allowing the activities to be evaluated. Williams and Davey (131) undertook the arduous task of evaluating the zinc activities by this method for a wide range of temperatures and alloy compositions. It is from these workers' calculated data that the zinc activities, were obtained.

Selected values of the zinc activity from the extensive tables compiled by Williams and Davey (131), using the Lumsden (62) free energy of mixing expression, are given in Table 2.5.

To calculate the vapour pressure of zinc over lead - zinc alloys, the zinc activity and the vapour pressure of pure zinc ($a_{Zn} = 1$) must be known for the given temperature and alloy composition. Kelley (52) has deduced an expression for the free energy change on the vaporisation of liquid to gaseous zinc, thus allowing the vapour pressure of pure zinc to be evaluated at any temperature. Kelley remarked that the vapour pressure equation derived from his free energy change on vaporisation equation fitted "the reliable experimental data virtually exactly".

Davey (19) has calculated the vapour pressure of liquid zinc from the melting point to the normal boiling point, based on Kelley's free energy equation. The values calculated by Davey are shown in Table 2.6.

TABLE 2.5

SELECTED CALCULATED ZINC ACTIVITY DATA IN LIQUID Pb - Zn ALLOYS

Calculations by Williams and Davey (131) Based on Lumsden's Equation (62)

Temp. °C	x_{Zn}	γ_{Zn}	a_{Zn}	Temp. °C	x_{Zn}	γ_{Zn}	a_{Zn}
350	0.005	37.15	0.186	600	0.005	9.98	0.050
350	0.010	36.21	0.362	600	0.010	9.81	0.098
350	0.020	34.27	0.685	600	0.020	9.48	0.190
350	0.030	32.41	0.972	600	0.040	8.85	0.354
				600	0.060	8.28	0.497
400	0.005	26.42	0.132	600	0.080	7.75	0.620
400	0.010	25.75	0.258	600	0.100	7.25	0.725
400	0.020	24.54	0.491	600	0.120	6.80	0.815
400	0.040	22.16	0.886	600	0.140	6.37	0.892
				600	0.160	5.98	0.957
450	0.005	19.72	0.099				
450	0.010	19.28	0.193	650	0.005	8.35	0.042
450	0.020	18.44	0.369	650	0.010	8.22	0.082
450	0.040	16.86	0.674	650	0.020	7.97	0.159
450	0.060	15.47	0.928	650	0.040	7.47	0.299
				650	0.060	7.03	0.422
500	0.005	15.24	0.076	650	0.080	6.61	0.529
500	0.010	14.93	0.149	650	0.100	6.22	0.622
500	0.020	14.35	0.287	650	0.120	5.86	0.703
500	0.040	13.21	0.528	650	0.140	5.52	0.773
500	0.060	12.19	0.731	650	0.160	5.20	0.833
500	0.080	11.27	0.902	650	0.180	4.92	0.886
				650	0.200	4.65	0.930
550	0.005	12.19	0.061	650	0.220	4.39	0.966
550	0.010	11.94	0.119	650	0.240	4.15	0.996
550	0.020	11.51	0.230				
550	0.040	10.69	0.427				
550	0.060	9.94	0.596				
550	0.080	9.25	0.740				
550	0.100	8.60	0.860				
550	0.120	8.02	0.962				

TABLE 2.6

VAPOUR PRESSURE OF PURE ZINC

Calculations by Davey (19) Based on Kelley's equation (62)

Temp. °C	P_{Zn} (atm.)	P_{Zn} (mm. Hg.)
419.5	0.000203	0.154
420	0.000205	0.156
430	0.000279	0.212
440	0.000371	0.282
450	0.000491	0.373
460	0.000647	0.492
470	0.000845	0.642
480	0.001094	0.831
490	0.001403	1.066
500	0.001786	1.358
510	0.002286	1.737
520	0.002884	2.192
530	0.003614	2.747
540	0.004508	3.426
550	0.005598	4.254
560	0.006855	5.208
570	0.008418	6.395
580	0.01030	7.830
590	0.01253	9.523
600	0.01517	11.53
610	0.01820	13.83
620	0.02183	16.59
630	0.02618	19.90
640	0.03097	23.54
650	0.03673	27.94
660	0.04335	32.95
670	0.05105	38.80
680	0.5957	45.27
690	0.06918	52.58
700	0.08072	61.35
710	0.09354	71.09
720	0.1079	82.00
730	0.1245	94.58
740	0.1429	108.6
750	0.1637	124.4
800	0.3081	234.2
850	0.5500	418.0
900	0.9297	706.6
907	0.9980	758.5

2.3 Nomenclature (c.g.s. units throughout)

a_{Zn} = activity of zinc in zinc - lead alloy referred to standard state $a_{Zn} = 1$ for pure liquid zinc at the same temperature

D = diffusion coefficient

$D_{calc.}$ = diffusion coefficient calculated

$D_{obs.}$ = diffusion coefficient experimentally observed

D_o = constant in Arrheius type equation

ΔH = activation energy for diffusion

$\Delta H_{vis.}$ = activiation energy for viscosity

k = Boltzmann constant

L_o = energy of evaporation

p_{Zn} = zinc partial pressure

R = universal gas constant

r = radius of the diffusing entity

r_{atom} = atomic radius

r_{ion} = ionic radius

T = absolute temperature

x_{Zn} = mole fraction zinc in zinc - lead alloy

η = coefficient of viscosity

γ_{Zn} = activity coefficient of zinc in zinc - lead alloy

CHAPTER 3

MOLECULAR DIFFUSION IN GASES

ZINC VAPOUR DIFFUSION IN NITROGEN

Theoretical advances in the diffusion in gases have largely been due to physicists because of the intimate relation between diffusion and the kinetic theory of gases. Two basically different theories relating diffusion with the molecular properties of the component gases have been advanced. The chief difference in the two theories is the prediction of the variation of the diffusion coefficient with gas composition. The Stefan-Maxwell (115)(68) theory predicts no variation, whereas the Meyer-Jeans (73)(47) expression predicts a maximum variation of $33\,1/3\%$ with composition.

Experimental studies indicate the diffusion coefficient in binary gaseous systems as being only very slightly, if at all, affected with the composition of the binary mixture. Because of this the Stefan-Maxwell expression is usually considered to give the more accurate representation of the gaseous diffusion process.

Modifications of these original expressions derived from kinetic theory were made by Arnold (2) and Gilliland (31) to yield empirical expressions from which the diffusion coefficient can be estimated. Hirchfelder, Bird and Spotz (41)(40)(42) have more recently proposed a new approach allowing diffusion coefficients to be predicted from accessible data.

There has been very little experimental data reported for the diffusion of metallic vapours in gases. Several investigators have measured the diffusion of metallic vapours in flames at high temperatures but the accuracy of these measurements is extremely doubtful.

Van der Held and Miesowicz (38) and Spier (113) measured the diffusion

coefficients of sodium vapour in nitrogen and mercury and cadmium vapour in nitrogen, respectively. These investigators measured the diffusion coefficient at room temperature and a pressure of 1 mm. Hg. and 2 mm. Hg., respectively. The metallic vapour was excited by a condensed discharge and allowed to diffuse against a stream of nitrogen in a tube. The intensity of radiation along the tube, measured photographically, allowed the diffusion coefficients to be evaluated.

Mullaly and Jacques (79) measured the diffusion coefficient of mercury vapour in nitrogen at room temperature. The vapour gradient along a uniform tube was obtained by allowing mercury vapour and iodine vapour to simultaneously diffuse into the tube from opposite ends. As fast as the vapours diffused towards one another, they combined and a deposit of mercury iodides was formed, where the vapours met in the tube, allowing the boundary conditions over a measured diffusion length to be evaluated, and the diffusion coefficient to be calculated.

Gilliland (31) determined the diffusion coefficient of mercury in air at atmospheric pressure and at a temperature of 341°C by observing the rate of vaporisation from a capillary tube maintained at a uniform temperature to eliminate convection currents. Gilliland's experimental data is of particular interest to this investigation, as it represents the closest approach to the conditions, under which the diffusion coefficient of zinc vapour was required to be estimated for analysing the zinc vapour absorption in molten lead data.

As there has been no data reported for the diffusion of zinc vapour in nitrogen, the three methods available for predicting diffusion coefficients are reviewed and an attempt is made to determine the most suitable form for estimating the diffusion coefficient of zinc vapour in nitrogen.

3.1 Estimation of Gas Phase Diffusion Coefficients

3.1.1 Arnold Method

The Arnold method (2) for the prediction of diffusion coefficients is based essentially on the expression proposed by Stefan-Maxwell (115)(68), modified by Sutherland (119) to allow for the effect of intermolecular forces in increasing the resistance to diffusion.

$$D_{12} = \frac{B\sqrt{\frac{1}{M1} + \frac{1}{M2}}\; T^{3/2}}{S^2 P\left(1 + \frac{C}{T}\right)} \qquad \ldots\ldots 3.1$$

The factor $\frac{1}{1 + \frac{C}{T}}$ is due to Sutherland (119) who developed his theory of diffusion on the same basis as his theory of viscosity (120). Sutherland gave the following expression for evaluating C for the mixture, from the corresponding Sutherland constants of the components of the mixture

$$C = F\sqrt{C_1 C_2}$$

The factor F depending on the ratio of the molecular volumes as given below:-

V_2/V_1	1	2	3	4	5	6	7	8	9	10
F	1.00	0.98	0.953	0.920	0.894	0.875	-	0.838	-	0.805

Arnold evaluated the term S representing the distance between centres of two molecules of different species at contact by the equation:-

$$S = (V_1^{\frac{1}{3}} + V_2^{\frac{1}{3}}) \qquad \ldots\ldots 3.2$$

The molecular volumes V_1 and V_2 were calculated by application of Kopps' law of additive volumes, which states that the value V is an additive function of the atomic volumes. The cube root of V is a measure of the molecular diameter. The values of atomic volumes for the elements were compiled by Le Bas (58).

The value of the constant B can be predicted from kinetic theory.

Arnold evaluated this constant according to the several theoretical approaches. Comparison with existing experimental data indicated that the value of B according to Jeans (47) was the best representation of the available data.

Therefore Arnold proposed as his final equation for the prediction of diffusion coefficients:-

$$D_{12} = \frac{0.00837\, T^{3/2} \sqrt{\frac{1}{M_1} + \frac{1}{M_2}}}{P\left(V_1^{\frac{1}{3}} + V_2^{\frac{1}{3}}\right)^2} \left(\frac{1}{1 + \frac{C}{T}}\right) \qquad \ldots\ldots 3.3$$

3.1.2. Gilliland Method

Gilliland (31) developed an empirical formula based on the Stefan-Maxwell original classical kinetic theory equation:-

$$D_{12} = \frac{B\, T^{3/2} \sqrt{\frac{1}{M_1} + \frac{1}{M_2}}}{S^2\, P} \qquad \ldots\ldots 3.4$$

This equation is the same as that used as a basis by Arnold except that it does not contain the Sutherland modification $(1 + \frac{C}{T})$. The procedure followed by Gilliland for evaluating the distance S between the centres of two unlike molecules at collision was the same as proposed by Arnold.

The constant B was determined by correlating the available experimental diffusivity data with the result:-

$$D_{12} = \frac{0.0043\, T^{3/2} \sqrt{\frac{1}{M_1} + \frac{1}{M_2}}}{P\left(V_1^{\frac{1}{3}} + V_2^{\frac{1}{3}}\right)^2} \qquad \ldots\ldots 3.5$$

Gilliland also correlated the experimental data by the form of equation used by Arnold (i.e. containing the Sutherland modification) but concluded that the correlation of the data by this method was not as good as his empirical expression.

3.1.3 Hirschfelder, Bird and Spotz Method

The more rigorous kinetic theory of gases, as developed by Chapman and Cowling (10), can be employed to give improved expressions for predicting the transport properties of gases. The viscosity, equation of state, coefficient of diffusion and other physical properties of gases are intimately connected with the law of force between the individual molecules.

Hirschfelder, Bird and Spotz (41)(40)(42) have evaluated the transport properties of gases making use of a realistic model of molecular interaction. The form used for the potential energy of interaction between molecules is the form which has proven very satisfactory for explaining the equation of state of simple non-polar gases. Non-polar gases have an energy of attraction, which varies with the inverse sixth power of the distance between centres of adjacent molecules, and a repulsive energy, which varies with the inverse twelfth power. For non-polar gases, the inverse sixth-power of attraction can be justified rigorously. The inverse twelfth power for the energy of repulsion has no real theoretical foundation. However, Lennard-Jones (59) has shown for non-polar gases that it suffices to explain the available second virial coefficient data, and is a good approximation of the short-range repulsive forces.

The Lennard-Jones potential energy function for non-polar molecules can be written as a function of the distance between the molecules

$$\varphi(r) = 4\varepsilon\left[\left(\frac{\sigma}{r}\right)^{12} - \left(\frac{\sigma}{r}\right)^{6}\right] \qquad \ldots\ldots 3.6$$

where σ and ε are adjustable parameters known as the force constants, which are characteristic of the chemical species of the colliding molecules. The potential energy of interaction between molecules is independent of

temperature and only the parameters σ and ϵ are required to describe the potential for the approach of two non-polar gas molecules.

The parameter ϵ is the maximum energy of attraction and σ is the value of r for which the potential energy of interaction is zero. The significance of these parameters can be seen from Fig. 3.1.

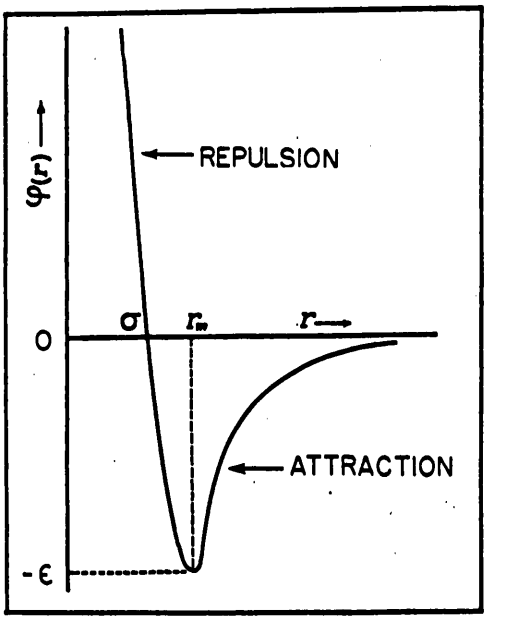

Fig. 3.1 - Lennard-Jones potential energy of molecular interaction as a function of distance r between the two molecules
When $r > r_m$ molecules are attracted
When $r < r_m$ molecules repel one another

The potential energy of interaction of polar and non-polar molecules and polar-polar molecules is different from the Lennard-Jones expression and therefore the following discussions are only true for non-polar molecules. As the investigations carried out in this research project are with non-polar molecules, only this case is considered. However, the

appropriate treatment for the other types of interaction is given by Hirschfelder, Curtiss and Bird (5).

The parameters σ and ε are best calculated from experimental viscosity or second virial coefficient data. Although the statistical mechanical theory underlying these calculations is extremely involved and the computations themselves rather complex, tabulated functions are available (76)(7)(69), which enable the calculations to be made quite readily.

The use of the force constants obtained from viscosity data is preferred for transport property calculations, whereas parameters calculated from second virial coefficients should be used for calculations of equations of state and thermodynamic data.

The relation between the coefficient of viscosity η and the force constants is given for pure non-polar gases as

$$\eta \times 10^7 = \frac{266.93 \ (MT)^{\frac{1}{2}}}{\sigma^2 \ \Omega^{(2,2)*}} \qquad \ldots\ldots 3.7$$

In the absence of viscosity data Hirschfelder, Curtiss and Bird (5) recommended the following empirical equations for estimating the force constants. These equations supercede those previously published in an earlier work (40)(42).

$$\varepsilon/k = 0.77 \ T_c \qquad \ldots\ldots 3.8$$

$$\varepsilon/k = 1.15 \ T_b \qquad \ldots\ldots 3.9$$

$$\varepsilon/k = 1.92 \ T_m \qquad \ldots\ldots 3.10$$

$$b_o = 0.75 \ V_c = 18.4 \ T_c/p_c \qquad \ldots\ldots 3.11$$

$$b_o = 2.0 \ V_b^{(liq)} \qquad \ldots\ldots 3.12$$

$$b_o = 2.3 \ V_m^{(sol)} \qquad \ldots\ldots 3.13$$

Where $$b_o = 1.2615 \ \sigma^3 \qquad \ldots\ldots 3.14$$

If a single value of viscosity is available, then either ε/k or σ may be estimated empirically and the other constant determined by substitution in the viscosity equation.

Hirschfelder, Bird and Spotz (40)(42) showed that there are some substances, which the force constants could not be obtained from the experimental viscosity data. For these substances there was no possible choice of ε/k and σ, which would lead to the observed temperature dependence. This was because their simple model of intermolecular potential (designed for spherical non-polar molecules) does not strictly apply in these cases. These anomalous gases fell into the following classes:-

(a) Polar Molecules

H_2O, NH_3, HB_r, HCN, HI, $HgCl_2$

The energy of interaction of polar molecules is quite different from that of non-polar molecules. As the experiments carried out in this thesis did not require estimation of transport properties of polar molecules, the treatment of polar molecules for estimating transport properties will not be given. Hirschfelder, Curtiss and Bird (5) have outlined the appropriate procedure.

(b) Metal Vapours and Valence-unsaturated Molecules:

Hg, Cd, Zn

The collisions of valence-unsaturated molecules sometimes follow one potential energy curve and sometimes another. At large separations their energy of attraction is perfectly normal, but at shorter distances the energy of interaction depends very largely on the particular electronic state. According to quantum mechanics there are well defined probabilities that a collision will result in a particular electronic state. This phenomena is illustrated by Hirschfelder, Bird and Spotz (40) for the collision

between two hydrogen atoms. Their view is that the collisions between such molecules is a statistical mixture of two sorts - those with large ε/k and small σ (corresponding to the ground state) and those with small ε/k and large σ (corresponding to an excited state).

The metallic vapours mercury, cadmium and zinc are not valence saturated and therefore it is to be expected that their collisions should be anomalous.

However, whilst it is realised that such molecules may exhibit anomalous behaviour, it is considered that the existing theory can be applied for purposes of estimation, until the theory needed for describing these more complex cases has been developed.

(c) Cigar-shaped Molecules: e.g., n-heptane

If the ratio of the length to the diamter becomes too large, the transport properties are affected. Thus the temperature dependence of the viscosity of n-heptane is greater than would be expected for spherical molecules. Hence estimated values of transport properties such as the diffusion coefficient for n-heptane, based on the existing theory, may be expected to deviate from actual values.

The most complete force constant data for a large number of molecules of the same chemical species has been tabulated by Hirschfelder, Curtiss and Bird (5). To estimate the coefficient of diffusion of a binary mixture, it is necessary to know the potential energy function describing the interaction between pairs of molecules of different species. Hirschfelder, Bird and Spotz (40)(42) demonstrated that the following empirical equations describe with reasonable accuracy the potential energy of interaction between unlike non-polar molecules.

$$\sigma_{12} = \tfrac{1}{2}(\sigma_1 + \sigma_2) \qquad \ldots\ldots 3.15$$

$$\varepsilon_{12} = \sqrt{\varepsilon_1 \varepsilon_2} \qquad \ldots\ldots 3.16$$

Where σ_i and ε_i are the appropriate values for the interaction between like molecules of the ith species. Similar equations were developed by Hirschfelder, Curtiss and Bird (5) for the polar-polar interaction and non-polar-polar interaction.

The coefficient of diffusion can now be estimated once the appropriate force constants are evaluated by the following type of equation first recommended by Hirschfelder, Bird and Spotz (40) and subsequently put into a more convenient form by Hirschfelder, Curtiss and Bird (5).

$$D_{12} = \frac{0.002628 \sqrt{T^3 (M_1 + M_2)/2M_1M_2}}{P \sigma_{12}^2 \Omega_{12}^{(1,1)*}} \quad \ldots\ldots 3.17$$

$$\text{or } D_{12} = \frac{0.002628 \; T^{3/2} \left(\frac{M_1 + M_2}{2M_1M_2}\right)^{\frac{1}{2}}}{P \sigma_{12}^2 \Omega_{12}^{(1,1)*}} \quad \ldots\ldots 3.18$$

This equation is essentially the same as that originally proposed by Hirschfelder, Bird and Spotz (40), although the constant is different because the collision integral $\Omega_{12}^{(1,1)*}$ in the above equation has been assigned differant numerical values. Therefore, this method of estimation of diffusion coefficients is still referred to as the Hirschfelder, Bird and Spotz method. However, as more complete force constant data, including the method of treatment of molecular interactions other than non-polar interaction, is given in the later work by Hirschfelder, Curtiss and Bird (5), the equation proposed by these authors and their notation has been adopted in this review.

The collision integrals $\Omega^{(1,1)*}$ and $\Omega^{(2,2)*}$ are functions of $\frac{kT}{\varepsilon}$. Values of these integrals are tabulated by Hirschfelder, Curtiss and Bird (5).

When the preceeding equation is written for a single component, the coefficient of self-diffusion is obtained

$$D_1 = \frac{0.002628 \quad T^{3/2} \quad M_1^{-\frac{1}{2}}}{p \sigma_1^2 \quad \Omega^{(1,1)*}} \qquad \ldots\ldots 3.19$$

The coefficient of self-diffusion can be measured experimentally by studying the diffusion of radioactive isotopes or ortho and para forms of a single component. Hence if the coefficient of self-diffusion is known, the force constants could be evaluated, which would then allow estimation of the coefficient of diffusion in a binary mixture containing the component being investigated.

The equations given for the coefficient of viscosity, the coefficient of diffusion and the self-diffusion coefficient are the first approximations. Higher approximations are given by Hirschfelder, Curtiss and Bird (5) but for most purposes the first approximations are of sufficient accuracy, particularly as the errors associated with the available experimental data usually render the higher approximations unwarranted.

A simplified graphical correlation procedure based on the Hirschfelder, Bird and Spotz diffusion equation and the theorem of corresponding states has been developed by Fair and Lerner (26). Generalised graphical correlations of the other transport properties, viz. viscosity and thermal conductivity had been developed earlier and as all gas transport properties may be related to essentially the same molecular interactions, it was logical to assume that a graphical correlation with reduced properties could be developed for the diffusion coefficient.

3.14 Comparison of the Methods

Wilke and Lee (128) established the relative accuracy of the various procedures by comparison of calculated results with a body of selected experimental data. These authors selected from reliable sources sixtyfour systems at atmospheric pressure and near room temperature. They considered that the use of this selected data was advisable in view of the uncertainty and lack of precision in many investigations reported in the literature. Also for a large number of the systems chosen, the force constants based on viscosity data were available.

The methods of Arnold and of Hirschfelder, Bird and Spotz gave nearly comparable results, with the latter somewhat better. The method of Gilliland gave poorer agreement for the selected systems. The average and maximum deviations between calculation and experiment as given by Wilke and Lee are summarised in Table 3.1.

TABLE 3.1

COMPARISON OF THE METHODS FOR DIFFUSION COEFFICIENTS WITH SELECTED EXPERIMENTAL DATA

Calculations by Wilke and Lee (128)

Method	Av. Deviation %	Max. % Deviation
Gilliland	20.0	46.8
Arnold	8.4	20.5
Hirschfelder, Bird and Spotz (using force constants from viscosity)	7.0	21.4

The deviations shown in Table 3.1 were for systems at room temperature. Sherwood and Pigford (100) stressed that a major weakness in the Gilliland diffusion coefficient equation was the temperature function $T^{3/2}$, since the coefficient of diffusion is more nearly proportional to T^2. In the

Arnold method the temperature function is $\frac{T^{5/2}}{T + C}$. The Hirschfelder, Bird and Spotz equation has the temperature function $\frac{T^{3/2}}{\Omega(1, 1)^*}$ in which the collision integral is a function of $\frac{kT}{\varepsilon}$. A simple analytical expression is not easily fitted to the relation between $\frac{kT}{\varepsilon}$ and $\Omega^{(1, 1)^*}$, however, Fair and Lerner (26) plotted $\Omega^{(1, 1)^*}$ against $\frac{kT}{\varepsilon}$ and showed that the slope varied from -0.1 to -0.5 over the normal range of engineering calculations. Thus the net dependence of the coefficient of diffusion on temperature for the Hirschfelder, Bird and Spotz equation is of the order $T^{1.6}$ to $T^{2.0}$, which agrees well with experimental evidence.

Wilke and Lee (128) compared the three methods with respect to the effect of temperature. The calculated values of the diffusion coefficient for the system carbon dioxide - air were compared with the experimental values reported by Kilbanova, Pomerantsev and Frank-Kamemetsky (53). The results of the calculations carried out by Wilke and Lee over the temperature range 293 - 1500°K assuming the value at 293°K to be correct, are given in Table 3.2.

TABLE 3.2

EXPERIMENTAL DATA FOR CO_2 - AIR SYSTEM (53)

COMPARISON OF THE METHODS FOR DIFFUSION COEFFICIENTS

Calculations by Wilke and Lee (128)

Temperature °K	Diffusion Coefficient (cm.²/sec.)			
	Expt. Data (smoothed)	Arnold Method Equation 3.3	H.B.S. Method Equation 3.18	Gilliland Method Equation 3.5
293	0.151	—	—	—
400	0.273	0.267	0.266	0.242
600	0.55	0.543	0.523	0.448
800	0.915	0.905	0.883	0.690
1000	1.32	1.28	1.28	0.970
1500	2.45	2.49	2.52	1.77

As expected from the temperature functions of the three methods, the Gilliland equation gives low values of the coefficient of diffusion at high temperatures, whilst the Arnold method and the Hirschfelder, Bird and Spotz method agree closely, probably well within the experimental accuracy of the data.

As a check on the merits of the three methods for estimating the diffusion coefficient of a metallic vapour in a gas, the diffusion coefficient of mercury in air for a total pressure of one atmosphere and a temperature of 341°C was evaluated by equations 3.3, 3.5 and 3.18, and compared with the value experimentally determined by Gilliland (31), as this data was the closest approach to the conditions required for the estimation of the diffusion coefficient of zinc vapour in nitrogen at an elevated temperature. The results of the calculations are shown in Table 3.3.

TABLE 3.3

COMPARISON OF METHODS FOR DIFFUSION COEFFICIENT

MERCURY VAPOUR - AIR (ONE ATMOSPHERE PRESSURE)

Temp. °C	Diffusion Coefficient ($cm.^2/sec.$)			
	Expt. Data (31)	Arnold Method Equation 3.3	H.B.S. Method Equation 3.18	Gilliland Method Equation 3.5
341	0.473	0.563 *	0.502	0.387 *

* The atomic volumes tabulated by Le Bas (58) for Zn and Hg do not appear to be consistent with those calculated from the liquid density at the normal boiling point. Hence the calculated values for Zn and Hg were used.

i.e. $V_{Zn} = 10.05$ cc./g.atom

$V_{Hg} = 15.70$ cc./g.atom

Whereas the Le Bas tabulated data are

$V_{Zn} = 20.4$ cc./g.atom

$V_{Hg} = 19.0$ cc./g.atom

The data of Table 3.3 again show the superiority of the Hirschfelder, Bird and Spotz method. The Arnold method shows a greater deviation than was exhibited in Table 3.2 and the inherent weakness of the Gilliland equation, because of the incorrect temperature function, is emphasised. Thus it would appear that the Hirschfelder, Bird and Spotz method is the best approach for estimating the diffusion coefficients of binary mixtures containing metallic vapours.

3.2 Estimation of the Diffusion Coefficient of Zinc Vapour in Nitrogen

Hirschfelder, Bird and Spotz (40) showed that force constants could not be obtained from experimental viscosity data for the metallic vapours, Hg*, Cd and Zn. For these substances there is no possible choice of ε/k and σ which would lead tothe observed temperature dependence of viscosity.

Therefore viscosity data could not be used to evaluate the force constants of zinc vapour. Strictly speaking the whole concept of the force constants as used by Hirschfelder, Bird and Spotz, cannot be applied to zinc vapour. However, their equation gave a calculated value of the diffusion coefficient of air and mercury, which was very close to the experimentally determined coefficient as shown in Table 3.3. As both mercury and zinc vapour were considered by Hirschfelder, Bird and Spotz to be examples where anomalies may be expected, it would appear that the anomalies are not very serious and that the method may at least be used for giving a fairly reliable estimate, even in such cases.

The estimation of the diffusion coefficient of zinc vapour in nitrogen,

* It is interesting to note, that in a later publication, Hirschfelder, Bird and Curtiss (5) tabulated values of ε/k and σ for mercury vapour, which were said to be derived from viscosity data. These values were used in the calculation of Table 3.3.

using force constants calculated from the empirical equations 3.9 and 3.12 and the method proposed by Hirschfelder, Bird and Spotz was considered the most realiable, and these coefficients were used in the analysis of the zinc absorption in molten lead data obtained in the experimental investigation.

As a check on the accuracy of the empirically determined force constants, the viscosity of zinc vapour at T = 850°K was calculated from equation 3.7 using the empirically calculated force constants. This value was compared with the experimentally determined zinc vapour viscosity (57) at the same temperature. The difference between the two figures was only 15%, part of which can surely be attributed to experimental error. The empirically calculated force constants for zinc vapour, $\varepsilon/k = 1355$ and $\sigma = 2.52$, are therefore considered quite reliable.

The calculated diffusion coefficients of zinc vapour in nitrogen using the force constants discussed and the Hirschfelder, Bird and Spotz equation are shown in Table 3.4.

TABLE 3.4

CALCULATED DIFFUSION COEFFICIENTS

ZINC VAPOUR IN NITROGEN (ONE ATMOSPHERE TOTAL PRESSURE)

Temperature °C	Diffusion Coefficient cm.^{2}/sec.
500	0.918
550	1.033
600	1.143
650	1.260
700	1.390
750	1.520

Besides the diffusion coefficient of zinc vapour in pure nitrogen, the diffusion of zinc vapour in multi-component gases is also considered

of interest, particularly with respect to the multi-component gaseous mixtures associated with the recently developed zinc blast furnace, mentioned in the introduction.

Wilke (130) has recently shown that the effective diffusion coefficient for a gas A in a mixture of gases B, C, D ..... n may be obtained from the expression

$$D_A' = \frac{1 - y_A}{\sum_{i=B}^{n} \frac{y_i}{D_{A-i}}} \qquad \ldots\ldots 3.20$$

where D_A' = effective diffusion coefficient for A in a multi-component system

y = mole fraction in the gas

In equation 3.20 a number of separate binary diffusion coefficients have to be estimated. The direct use of the Hirschfelder, Bird and Spotz method becomes rather involved particularly when a range of temperatures is required. The graphical diffusion coefficient correlation developed by Fair and Lerner (26) based on the Hirschfelder, Bird and Spotz method and the theorem of corresponding states would be of particular value for such cases.

3.3 Nomenclature (c.g.s. units throughout)

(a) Symbols

B	=	constant in Arnold equation (3.1)
C	=	Sutherland constant
D	=	diffusion coefficient in binary mixture
D'	=	effective diffusion coefficient in a multicomponent mixture
k	=	Boltzmann constant
M	=	molecular weight
P	=	total pressure in system
R	=	universal gas constant
r	=	distance between molecules
S	=	distance between centres of two molecules of different species at contact
T	=	absolute temperature
V	=	molecular or atomic volume
y	=	mole fraction in gas phase
η	=	coefficient of viscosity
ε and σ	=	adjustable parameters called force constants, required to describe the potential of approach of two molecules
ε	=	maximum energy of attraction
σ	=	value of r for which the potential energy of interaction is zero
$\Omega^{(1,1)*}$	=	Collision integral for diffusion
$\Omega^{(2,2)*}$	=	Collision integral for viscosity

(b) Subscripts

A.....n	=	components in multicomponent mixture
1, 2	=	components in binary mixture

i	=	ith chemical species in a mixture
c	=	critical point
b	=	normal boiling point
m	=	melting point

CHAPTER 4

DEVELOPMENT OF THE FUNDAMENTAL EQUATION FOR STUDYING ZINC VAPOUR ABSORPTION IN MOLTEN LEAD

4.1 The Additivity of Diffusional Resistances

The most useful approach for analysing the mechanism of an absorption process was introduced by Whitman (129). According to his theory, which is now generally known as the "two-film" or "two-resistance" theory, material is transferred in the bulk of the phases by convection currents and differences in concentration are assumed negligible, except in the vicinity of the interface between the phases. On either side of the phase interface, there is considered to be a thin stagnant film, through which the transfer of material is by molecular diffusion only.

The fluid films adjacent to the phase interface are of hypothetical thickness, as they represent the thickness of stagnant fluid, which offers resistance to mass transfer by molecular diffusion equivalent to the total resistance to mass transfer in the combined process of molecular and eddy diffusion within the phase. In terms of boundary layer theory, the film thickness will be slightly greater than the laminar sub-layer, because it offers a resistance equivalent to the total resistance of the boundary layer.

The film theory assumes that there is no diffusional resistance at the interface and the relationship between the concentrations of diffusing solute in the two phases at the interface is assumed to be the same as in static equilibrium measurements with bulk phases.

The direction of mass transfer across the interface is not determined by the concentration difference,, but the equilibrium relationship, and therefore a very large concentration gradient may exist across the

interface, where equilibrium attainment is assumed because of the absence of any resistance to mass transfer right at the interface.

The factor controlling the rate of absorption is considered to be the rate of diffusion through the two films, in which all the resistance is assumed to lie. The overall diffusional resistance, therefore, comprises the diffusional resistance of the individual fluid films, i.e., the gas and liquid films for a gas absorption process.

The rate of absorption per unit area can be expressed in terms of the driving force for mass transfer across the individual films. Thus a difference in partial pressure of the diffusing component is the driving force in the gas phase and a difference in solute concentration is the potential for mass transfer in the liquid phase. As all the solute diffusing from the gas phase to the interface must also, under steady state conditions, diffuse at the same rate from the interface to the main bulk of the liquid phase, the rate of absorption of component A per unit area, N_A, can be expressed as equation 4.1.

$$N_A = k_g (p_g - p_i) = k_L (c_i - c_L) \qquad \ldots\ldots 4.1$$

Where p_g and p_i represent the partial pressure of component A in the bulk of the gas phase and at the interface, respectively, and c_L and c_i are the concentrations of the component A in the bulk of the liquid phase and at the interface, respectively. According to the two-film theory, p_i and c_i are in equilibrium. The mass transfer coefficients k_g and k_L are known as the gas film coefficient and the liquid film coefficient, respectively.

Equation 4.1 can only be used to calculate the rate of absorption in special circumstances, because the interfacial conditions are not

usually known and cannot in general be measured experimentally. It is therefore convenient to introduce the overall coefficients K_L and K_g, known as the overall liquid phase coefficient and the overall gas phase coefficient, respectively, which are defined by equation 4.2.

$$N_A = K_g (p_g - p_e) = K_L (c_e - c_L) \quad \ldots\ldots 4.2$$

where p_e is the partial pressure of the component A, which is in equilibrium with the liquid phase having a concentration of A equal to c_L, and c_e is the concentration of the component A in the liquid phase, which is in equilibrium with a gas phase containing a partial pressure p_g of the diffusing component.

The relations between the overall mass transfer coefficients and the individual film coefficients are given in equations 4.3 and 4.4.

$$\frac{1}{K_g} = \frac{1}{k_g} + \frac{H}{k_L} \quad \ldots\ldots 4.3$$

$$\frac{1}{K_L} = \frac{1}{k_L} + \frac{1}{Hk_g} \quad \ldots\ldots 4.4$$

where $p_e = Hc$ (H = Henry law constant)

These equations are statements of the concept of the additivity of diffusional resistances in mass transfer between phases. In terms of gas phase compositions, $1/K_g$ represents the overall resistance to mass transfer, $1/k_L$ the liquid phase resistance and H/k_L the liquid phase resistance. In terms of liquid concentrations, $1/K_L$ is the overall resistance to mass transfer, $1/k_L$ the liquid film resistance and $1/Hk_g$ the gas film resistance.

The controlling diffusional resistance in the absorption process can be determined from equation 4.3 or 4.4. Thus for example, for a very soluble gas, the liquid phase resistance becomes very small, because

of the small value of the Henry law constant, and therefore the absorption is said to be a gas phase controlled absorption. Similarly, because of the large Henry law constant for a slightly soluble gas, the absorption in such cases is said to be controlled by the liquid phase.

The assumption made in equations 4.3 and 4.4. is that Henry's law applies to the system (i.e. the equilibrium curve is linear). If the equilibrium curve is not linear, then there is no simple equation relating the overall coefficient with the individual film coefficients.

Although the Whitman two-film theory was postulated in 1923 and has been used extensively ever since in the standard texts dealing with the diffusional mass transfer operations, there was inadequate experimental support for the concept of additive resistances until quite recently.

Several investigators have suspected the existence of a diffusional resistance at the interface under certain conditions.

Emmert and Pigford (23) compared the theoretical and experimental rates of absorption and desorption for oxygen and carbon dioxide, in water, which contained a sulphonate surface-active agent, and which flowed in laminar flow down a wetted wall column. They concluded that there was an interfacial resistance, due to lack of equilibrium at the interface, even with pure water and that the sole effect of the wetting agent was to eliminate rippling. However, later work by Cullen and Davidson (17) suggests that equilibrium does not exist at the surface of pure water, and that the discrepancy, between the theoretical and observed results obtained by Emmert and Pigford, was due to an interfacial resistance caused by the surface active agent.

Cullen and Davidson (17) reviewed the work of several investigators, who had previously reported interfacial resistance effects in liquids containing surface-active high molecular weight solutes. These authors also demonstrated with additions of chemically pure surface-active agents, that there was no resistance to absorption, other than that due to diffusion. However, a solution containing the same pure surface-active agents plus a small amount of impurity or a solution containing a commercial surface-active agent was found to exhibit an interfacial resistance at certain concentrations, which fell to zero at very low and very high concentrations. These authors concluded that an interfacial resistance is caused by the interaction of impurities with the surface-active agents. The mechanism envisaged was not a simple mechanical obstruction, owing to the extreme thinness of the surface film, but to be due to an interaction between the adsorbed film and the diffusing molecules.

However, in normal absorptions, in the absence of surface-active agents, it is now generally agreed, that there is no interfacial resistance and that equilibrium conditions do exist at the phase boundary.

Even though there is no diffusional barrier at the interface, the relationship, between the concentrations in the two phases at the interface, may be expected to be different under dynamic conditions with diffusion taking place, than under conditions of static equilibrium, for which the equilibrium data are compiled. This effect, which would indicate an apparent interfacial resistance varying with the diffusion rate, has been shown by Schrage (93) to be unimportant except at very high mass transfer rates, ordinarily obtainable only at reduced pressures.

Excellent support of the additivity concept of diffusional

resistances was provided by the recent work of Gordon and Sherwood (34) and Goodgame and Sherwood (33). The former workers tested the additivity concepts for mass transfer between two liquid phases and the latter for gas - liquid systems. Goodgame and Sherwood (33) confirmed the additivity concepts by experimental measurements of the transfer coefficients for vaporisation of water into air, and the absorption from air of carbon dioxide, ammonia and acetone by water under conditions of known interfacial area. The results of these workers are of particular interest to this investigation, as they have confirmed, without doubt, the procedure of studying a gas absorption process by evaluating the individual film coefficients.

4.2 The Volumetric Mass Transfer Coefficient, Packed Column Analysis

In most commercial gas absorption equipment it is difficult, if not impossible, to evaluate the interfacial area of the gas and liquid phases. For this reason, the usual procedure is to introduce a new variable "a", which represents the interfacial area per unit volume of the absorber. As both "a" and the mass transfer coefficients depend on the nature of the packing, the type of flow whether wetting or non-wetting and on the flow rates of the liquid and gas streams, they are usually combined as a product, e.g. $K_g a$, which is known as a volumetric mass transfer coefficient, and is a measure of the rate of absorption per unit driving force, **per unit volume of the absorber.**

Sherwood and Pigford (101) and other standard texts, show that the volumetric mass transfer coefficients are related to the height of packing "h" in a packed column by the following equations, which are simplified for application to dilute systems.

$$h = \frac{G_m}{K_g a \quad P} \int_{y_2}^{y_1} \frac{dy}{y - y_e} \qquad \ldots\ldots 4.5$$

$$h = \frac{G_m}{k_g a \quad P} \int_{y_2}^{y_1} \frac{dy}{y - y_i} \qquad \ldots\ldots 4.6$$

$$h = \frac{L_m}{K_L a \; \rho_m} \int_{x_2}^{x_1} \frac{dx}{x_e - x} \qquad \ldots\ldots 4.7$$

$$h = \frac{L_m}{k_L a \; \rho_m} \int_{x_2}^{x_1} \frac{dx}{x_i - x} \qquad \ldots\ldots 4.8$$

In the preceding equations, the volumetric mass transfer coefficients are taken as being constant. However, the overall volumetric coefficients $K_L a$ and $K_g a$ are only constant if the equilibrium curve is linear, i.e. Henry's Law applies. The assumption, that the individual film volumetric coefficients are constant, is quite reasonable for a dilute system operating at almost constant temperature, as the gas and liquid flow rates are affected only very slightly by the absorption in such cases.

When the equilibrium line is curved, the design procedures outlined by Sherwood and Pigford (102) may be used.

4.3 The Concept of the Transfer Unit

The concept of the transfer unit was introduced by Chilton and Colburn (12), as a convenient method for calculating the height of a countercurrent absorption column. Inspection of equations 4.5 to 4.8 shows that the calculation of the height of an absorption column always

requires the evaluation of a definite integral and a second term containing the volumetric mass transfer coefficient.

The value of the definite integral, which is a dimensionless quantity, is a measure of the difficulty of the absorption process. It is an integrated value of the change in composition of the diffusing component, per unit driving force causing the mass transfer. Chilton and Colburn called these definite integrals the "number of transfer units". By definition for dilute systems,

$$N_{OG} = \int_{y_2}^{y_1} \frac{dy}{y - y_e} \qquad \ldots\ldots 4.9$$

$$N_{OL} = \int_{x_2}^{x_1} \frac{dx}{x_e - x} \qquad \ldots\ldots 4.10$$

$$N_G = \int_{y_2}^{y_1} \frac{dy}{y - y_i} \qquad \ldots\ldots 4.11$$

$$N_L = \int_{x_2}^{x_1} \frac{dx}{x_i - x} \qquad \ldots\ldots 4.12$$

The packed height of the absorption column is then given in terms of "the height of a transfer unit". This is a measure of the mass transfer characteristics of the particular packing material and the particular system properties and flow rates being investigated. The height of a transfer unit has the dimensions of length and is usually expressed as feet. The packed height is then related to the number of

transfer units and the height of a transfer unit by equation 4.13.

$$h = N_{OG}\ H_{OG} = N_{OL}\ H_{OL} = N_G\ H_G = N_L\ H_L \qquad \ldots\ldots\ 4.13$$

Comparison of these equations with the equations relating the volumetric coefficients with the packed height, allows the heights of transfer units to be written in terms of the volumetric mass transfer coefficients.

$$H_{OG} = \frac{G_m}{K_g a\ P} \qquad \ldots\ldots\ 4.14$$

$$H_{OL} = \frac{L_m}{K_L a\ \rho_m} \qquad \ldots\ldots\ 4.15$$

$$H_G = \frac{G_m}{k_g a\ P} \qquad \ldots\ldots\ 4.16$$

$$H_L = \frac{L_m}{k_L a\ \rho_m} \qquad \ldots\ldots\ 4.17$$

When the equilibrium curve is linear, the evaluation of the number of transfer units is simplified, as it can be shown (103) for this case that,

$$N_{OG} = \frac{y_1 - y_2}{(y - y_e)_{L.M.}} \qquad \ldots\ldots\ 4.18$$

Analogous expressions can be written for the other evaluations.

The concept of the additivity of diffusional resistances can also be applied to the heights of transfer units (104). If the equilibrium curve is linear, the following equations apply:-

$$H_{OG} = H_G + \frac{m\ G_m}{L_m} H_L \qquad \ldots\ldots\ 4.19$$

$$H_{OL} = H_L + \frac{L_m}{m\ G_m} H_G \qquad \ldots\ldots\ 4.20$$

In equation 4.19, for example, H_{OG} is a measure of the overall resistance to mass transfer, H_G represents the diffusional resistance in the gas phase and $\frac{m\ G_m}{L_m} H_L$ the diffusional resistance in the liquid phase.

4.4 Application of the Two-Resistance Concepts to Zinc Vapour Absorption in Molten Lead

In most conventional gas absorption systems, the equilibrium conditions can be represented either by a single straight line or a single curve.

However, for the absorption of zinc vapour in molten lead, the temperature of the liquid lead changes appreciably as it flows through the absorption column, and the equilibrium conditions alter according to the position in the column. This is because the zinc activity coefficient and the vapour pressure of pure zinc vary greatly with temperature.

As the absorptions of this investigation were carried out in very dilute alloys, Henry's law could be assumed to apply for each temperature level within the absorption column. Hence the equilibrium zinc partial pressure over the alloys formed by absorption, for a particular temperature, are linearly related to the zinc concentration in the liquid lead alloy, i.e. the mole fraction (y_e) of zinc in the gas phase, which is in equilibrium with a zinc mole fraction of (x) in the liquid lead phase can be given by the following equations:-

$$p_{Zn} = x\ \gamma_{Zn}\ p^{o}_{Zn} \qquad \ldots\ldots 4.21$$

$$\therefore\ y_e = \frac{p^{o}_{Zn}\ \gamma_{Zn}}{P_T} \cdot x \qquad \ldots\ldots 4.22$$

i.e. Slope of Equilibrium Line = $\frac{p^{o}_{Zn} \gamma_{Zn}}{P_T}$ 4.23

The equilibrium conditions in a system, in which molten lead is contacted with zinc vapour, can therefore be represented, for the case of dilute alloys, by a series of straight lines of slope $\frac{p^{o}_{Zn} \gamma_{Zn}}{P_T}$, as shown in Fig. 4.1.

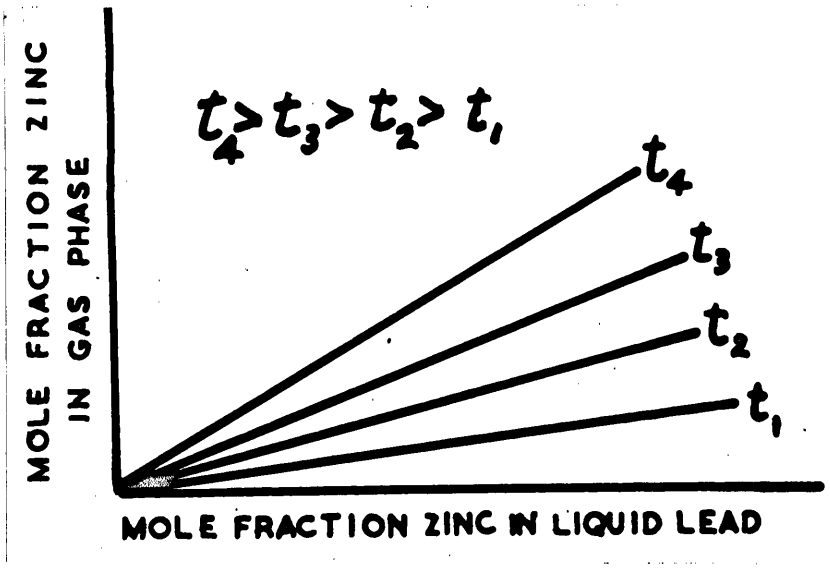

Fig. 4.1 - Equilibrium conditions

If the equilibrium conditions at the various levels in the absorption column are taken as shown in Fig. 4.1, a fundamental equation can be derived, using the additive diffusional resistance concepts, for the absorption of zinc vapour in molten lead. The equation developed is considered to be an original approach, although the derivation is similar to the procedure used by Sherwood and Pigford (102), when these authors analysed an absorption, in which a curved equilibrium relationship existed.

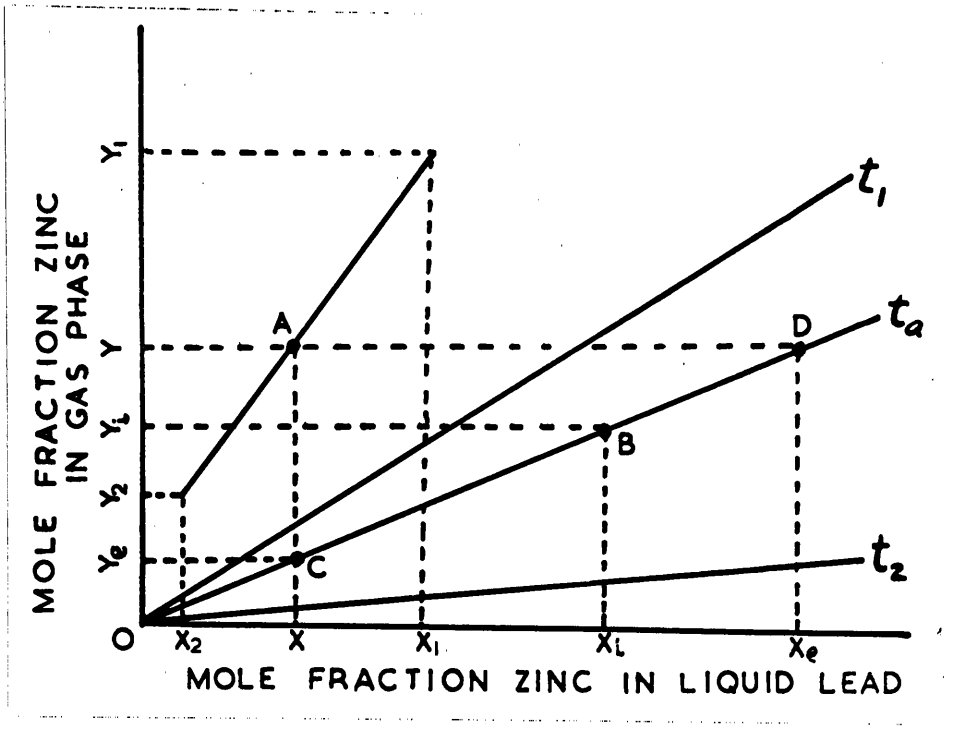

Fig. 4.2 - Graphical representation of the absorption of zinc vapour in molten lead

Consider a zinc absorption process, in which the lead inlet temperature is t_2 and the outlet temperature t_1.

At a point within the column, where the lead temperature is t_a, the bulk zinc mole fractions in the liquid lead and the gas phases are x and y, respectively.

The bulk phase conditions may be represented in Fig. 4.2 by the point A, having co-ordinates (x, y). Point A will be located on the operating line, which for a dilute system, in which the molar gas and liquid flow rates can be considered constant, is a straight line terminated by (x_1, y_1) and (x_2, y_2).

The interfacial conditions can be represented by the point B,

which will be located on the equilibrium line for temperature t_a and will have co-ordinates (x_i, y_i).

The points C and D on the equilibrium line for temperature t_a, have co-ordinates (x, y_e) and (x_e, y) respectively.

From Fig. 4.2,

$$(y - y_e) = (y - y_i) + (y_i - y_e) \qquad \ldots\ldots 4.24$$

Now $\frac{y_i - y_e}{x_i - x}$ = Slope of Equilibrium Line for t_a

$$= \frac{p^{o}_{Zn}\ \gamma_{Zn}}{P_T} \quad \text{(from equation 4.23)}$$

i.e. $$(y_i - y_e) = \frac{p^{o}_{Zn}\ \gamma_{Zn}}{P_T}\ (x_i - x) \qquad \ldots\ldots 4.25$$

Hence from equation 4.24,

$$(y - y_e) = (y - y_i) + \frac{p^{o}_{Zn}\ \gamma_{Zn}}{P_T}\ (x_i - x) \qquad \ldots\ldots 4.26$$

Since $N_A = K_g a\ P(y - y_e) = k_g a\ P(y - y_i) = k_L a\ \rho_m (x_i - x)$

Equation 4.26 may be re-written

$$\frac{N_A}{K_g a\ P} = \frac{N_A}{k_g a\ P} + \frac{N_A}{k_L a\ \rho_m} \cdot \frac{p^{o}_{Zn}\ \gamma_{Zn}}{P_T} \qquad \ldots\ldots 4.27$$

i.e. $$\frac{1}{K_g a\ P} = \frac{1}{k_g a\ P} + \frac{1}{k_L a\ \rho_m} \cdot \frac{p^{o}_{Zn}\ \gamma_{Zn}}{P_T} \qquad \ldots\ldots 4.28$$

Now from equation 4.5

$$h = \frac{G_m}{K_g a\ P} \int_{y_2}^{y_1} \frac{dy}{y - y_e}$$

However, in this case, $K_g a$ is not constant, because as can be seen from equation 4.28

(a) $p^{o}_{Zn}\ \gamma_{Zn}$ varies through the column

(b) $k_g a$ and $k_L a$ may also vary, because of temperature variation in the column

and, hence, the equations similar to equation 4.5 must include the coefficients within the integral.

Now, if both sides of equation 4.28 are multiplied by $\frac{G_m \; dy}{y - y_e}$ and the resulting equation integrated between the limits y_2 to y_1, equation 4.29 is obtained.

$$h = \frac{G_m}{P} \int_{y_2}^{y_1} \frac{dy}{K_g a \;\; (y - y_e)} = \frac{G_m}{P} \int_{y_2}^{y_1} \frac{dy}{k_g a \;\; (y - y_e)} + G_m \int_{y_2}^{y_1} \frac{(p^{o}_{Zn} \;\; \gamma_{Zn}) \; dy}{P_T \; k_L a \; \rho_m (y - y_e)} \qquad \ldots\ldots 4.29$$

However, if the major variation of $K_g a$ is considered to be due to the variation of $(p^{o}_{Zn} \;.\gamma_{Zn})$ and the individual coefficients assumed to be fairly constant equation 4.29 can be simplified,

$$h = \frac{G_m}{K_g a \;\; P} \int_{y_2}^{y_1} \frac{dy}{y - y_e} + \frac{G_m}{k_L a \; \rho_m} \int_{y_2}^{y_1} \frac{p^{o}_{Zn} \;\; \gamma_{Zn}}{P_T} \; \frac{dy}{y - y_e}$$

If each side of equation 4.30 is divided by $\int_{y_2}^{y_1} \frac{dy}{y - y_e} = N_{OG}$

since $h = N_{OG} \cdot H_{OG}$

and $H_G = \frac{G_m}{k_g a \;\; P}$, $H_L = \frac{L_m}{\rho_m \; k_L a}$

Equation 4.30 is transformed into the final form:

$$H_{OG} = H_G + \frac{G_m}{L_m} \; \frac{H_L}{N_{OG}} \int_{y_2}^{y_1} \frac{p^{o}_{Zn} \;\; \gamma_{Zn}}{P_T} \; \frac{dy}{y - y_e} \qquad \ldots\ldots 4.31$$

4.5 Nomenclature

(a) Symbols

a	=	area of interphase contact, $ft.^2/ft.^3$
c	=	solute concentration, $lb.mole./ft.^3$
G_m	=	superficial molar mass velocity of the gas phase, $lb.mole./(hr.)(ft.^2)$
h	=	height of packed section of absorption column, ft.
H	=	Henry's law constant, p_e/c
H_G	=	height of a gas film tansfer unit, ft.
H_{OG}	=	height of an overall gas phase transfer unit, ft.
H_L	=	height of a liquid film transfer unit, ft.
H_{OL}	=	height of an overall liquid phase transfer unit, ft.
k_g	=	gas film transfer coefficient, $lb.mole./(hr.)(ft.^2)(atm.)$
K_g	=	overall gas phase coefficient, $lb.mole./(hr.)(ft.^2)(atm.)$
$k_g a$	=	volumetric gas film coefficient, $lb.mole./(hr.)(ft.^3)(atm.)$
$K_g a$	=	overall volumetric gas phase coefficient, $lb.mole./(hr.)(ft.^3)(atm.)$
k_L	=	liquid film transfer coefficient, $lb.mole./(hr.)(ft.^2)(unit \Delta C)$
K_L	=	overall liquid phase transfer coefficient, $lb.mole./(hr.)(ft.^2)(unit\ \Delta C)$
$k_L a$	=	volumetric liquid film coefficient, $lb.mole./(hr.)(ft.^3)(unit\ \Delta C)$
$K_L a$	=	overall volumetric liquid phase coefficient, $lb.mole./(hr.)(ft.^3)(unit\ \Delta C)$
L_m	=	superficial molar mass velocity of the liquid phase, $lb.mole./(hr.)(ft.^2)$
m	=	slope of equilibrium curve, dy_e/dx
N_A	=	mass transfer rate of the diffusing component A, $lb.mole./(hr.)(ft.^2)$
N_G	=	number of gas film transfer units
N_{OG}	=	number of overall gas phase transfer units

N_L = number of liquid film transfer units

N_{OL} = number of over liquid phase transfer units

p = partial pressure solute, atm.

P = total pressure on system, atm.

p_{Zn} = partial pressure of zinc in gas phase, mm. Hg.

P_T = total pressure on system, mm. Hg.

t = temperature, ^oF

x = mole fraction of diffusing component in liquid phase

y = mole fraction of diffusing component in gas phase

ρ_m = molar density of liquid, lb.mole./ft.^{3}

γ_{Zn} = activity coefficient of zinc in liquid lead - zinc alloy, (standard state pure liquid zinc at the same temperature)

(b) Subscripts

1 = concentrated end of countercurrent system

2 = dilute end of countercurrent system

e = equilibrium value

g = bulk of gas phase

i = gas - liquid interface

L = bulk of liquid phase.

EXPERIMENTAL INVESTIGATION

SECTION A

FUNDAMENTAL STUDIES OF DISC COLUMN PERFORMANCE

CHAPTER 5.

INTRODUCTION TO THE DISC ABSORPTION COLUMN

A new type of laboratory absorption column named a disc column was introduced in 1951 by Stephens and Morris (116). This column was introduced primarily for the determination of liquid phase mass transfer coefficients for systems in which reliable diffusion data is not available. As the results of physical absorption in the disc column are similar to those obtained in a packed tower, Stephens and Morris suggested that, if the relative performance of the disc column and the various commercial packings could be established, the laboratory disc column could be used as a design basis, obviating the need of semi-plant size tests using large quantities of gas and liquid.

The disc column is a development of a simple wetted wall column in which the liquid is allowed to flow over a series of discs arranged in a single vertical row with alternate discs set mutually at right angles. The flow of liquid over the disc assembly is such that the film of liquid is interrupted at each disc intersection during its descent, thereby simulating conditions in a packed column. The differences between the hydrodynamics of packed towers and the disc column and the limitations of the latter as a model of the former have been outlined by Danckwerts (18) and Hoftyzer (45).

The essential features of the Stephens and Morris disc column are shown in Fig. 5.1. The discs forming the absorption element are 1.45 to 1.5 cm. diameter and 0.44 to 0.46 cm. thickness. The discs are cemented to a centrally located supporting wire or rod, which is placed vertically inside a glass tube of 2.5 cm. bore. Taylor and Roberts (122) have

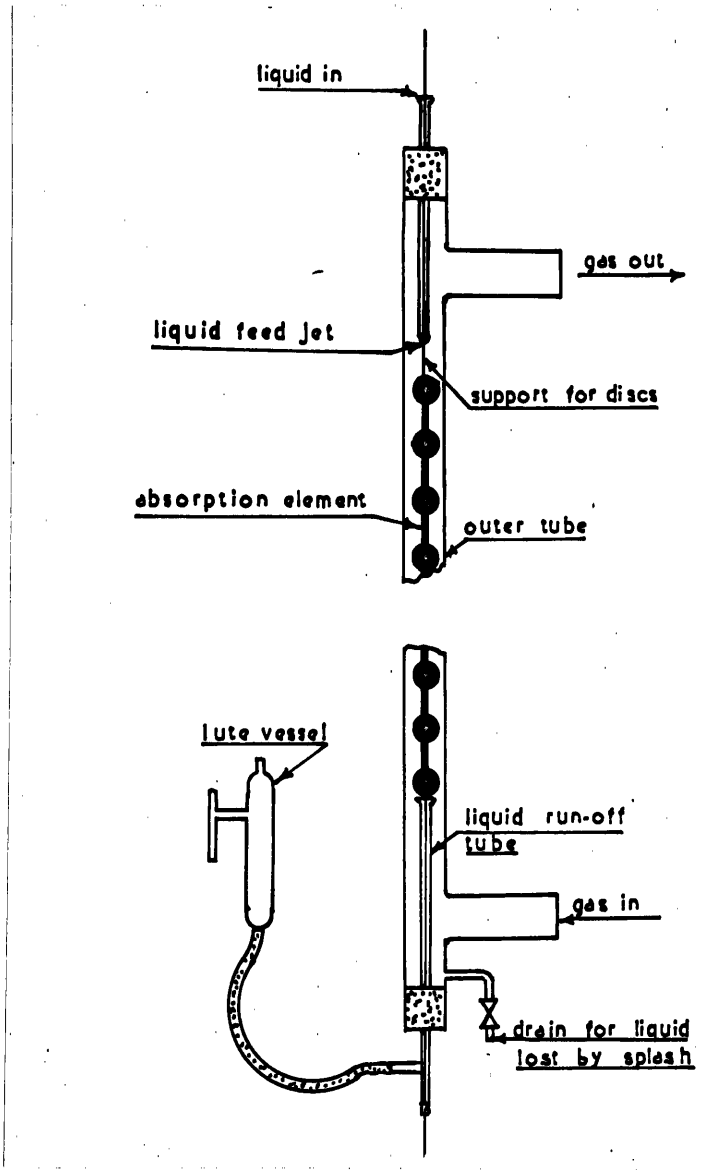

Fig. 5.1 - The Stephens and Morris disc column

shown that the type of disc material used has no effect on the mass transfer characteristics, although better wetting at low flow rates was observed when discs were roughened by a file and kept soaked between runs.

The primary use of the disc column has been for investigations of absorption systems in which the controlling diffusional resistance is located in the liquid phase. Morris and Jackson (77) have outlined a method of predicting liquid film coefficients suitable for use in a packed tower for cases of physical absorption from data obtained on the same system by using a disc column. Furthermore, Roper (90) has shown that the disc column has characteristics similar to those of a packed tower for the more complex case of absorption accompanied by a simultaneous chemical reaction in the liquid phase. As there is no method available at present for predicting liquid film coefficients in a full size commercial packed tower for this process of chemical absorption, it would appear that the use of the disc column in this field would be of particular value.

However, the gas phase mass transfer characteristics of the disc column have received only incidental interest, mainly with the view of calibrating the column with respect to the gas film so that overall mass transfer coefficients, for systems controlled by the liquid film, may be corrected for the gas film resistance.

To establish the characteristics of the column with respect to the gas film, Stephens and Morris (116) and Taylor and Roberts (123) applied a liquid film correction to the overall coefficients obtained for the absorption of ammonia in water from dilute mixtures with air. Roper (89) evaporated water by air to establish the gas film resistance to be taken into account in subsequent liquid film controlled absorptions.

These investigators presented their gas film data in the form of generalised correlations of the type, which had been found applicable to wetted wall columns (30)(50). The use of the generalised correlations, for determination of gas film coefficients in a disc column, is not entirely justified on the basis of the experimental work reported. No data have been published for gas film coefficients in a disc column for any other gas phase except air or dilute air mixtures with air as the diluent.

Therefore, it was considered that, if the disc column is to be used for a system in which a substantial fraction of the total diffusional resistance is located in the gas phase and where the properties of the gas phase are significantly different to those for air at room temperature, further fundamental work must be undertaken to establish the characteristics with respect to the gas film.

The use of a disc column for such applications rather than a simple wetted wall column is justified, because attempts to correlate liquid film coefficients using wetted wall columns have been unsuccessful and the coefficients have been found to depend on the length of the wetted wall column (116). The liquid film coefficients for a disc column, however, are independent of the column length (116)(122) and therefore the correction of a measured overall coefficient for resistance in the liquid film is theoretically justified, as the overall coefficient for a disc column absorption is independent of the column length.

On this basis, the disc column is preferred to the wetted wall column for all laboratory absorption except, perhaps, where there is no liquid film resistance as in the evaporation and condensation of a pure

liquid or where the liquid film resistance is negligible. However, for cases in which the liquid film is known to contribute to the overall resistance to diffusion or where the extent of the liquid film resistance is not known for certain, the disc column is preferred.

The absorption of zinc vapour in molten lead would, on the surface, appear to be an absorption controlled chiefly by diffusion in the gas phase. However, as the contribution of the liquid film diffusional resistance is not known, it was proposed to study this system using a disc column, so as to eliminate any uncertainty with respect to the liquid film. The known surface area of the liquid phase, in either a disc or wetted wall column, has the obvious advantage, that the mechanism of the absorption can be studied more fully, than would be possible if a small packed column was used for the investigation.

There was considerable doubt existing at the onset of the experimental program, as to whether it would be possible to operate a disc column with molten lead as the liquid phase, particularly in view of the lack of success Davey (19) met when, during the course of vacuum dezincing experiments on molten dessilverised lead, a form of wetted wall column was desired but was found impossible to achieve due to the formation of thick rivulets rather than a continuous film, when molten lead flowed over a surface. However, it was considered worthwhile to investigate fully the possibility of using a disc column with molten lead because of the very significant advantages, which a disc column would possess in the analysis of the mechanism of the absorption.

As it was realised, that the information available on the gas phase mass transfer characteristics of the disc column, would not be sufficient to interpret the results of a zinc absorption in molten lead, a collateral

experimental program was instituted to study the fundamental characteristics of the disc column, which would be important in the analysis of a gas film controlled absorption process. This collateral investigation proceeded concurrently with the major project of studying the absorption of zinc vapour in molten lead.

CHAPTER 6

LIQUID FLOW BEHAVIOUR IN THE DISC COLUMN

Taylor and Roberts (122) have reported, that a distinct change in slope occurs at approximately the same liquid rate (Γ = 155 lb./(hr.)(ft.) for water), when plots of gas and liquid film coefficients are made. These authors visually examined the discs over a series of flow rates to see if any differences could be observed above and below the critical flow rate of Γ = 155 lb./(hr.)(ft.). The flow patterns on the face of the discs appeared to remain unchanged, but the flow pattern around the rim of the discs altered at a flow rate of Γ = 155 lb./(hr.)(ft.). Immediately below the critical flow rate, there was transient formation of ripples. Ripple formation on the rims of the discs became permanent above the critical flow rate. It was concluded that this ripple formation was the cause of the break noticed in the mass transfer data. The earlier data of Stephens and Morris (116), who examined the same chemical systems as the former authors, failed to exhibit this break.

There appears to be considerable doubt, as to whether the relative velocity of the gas and liquid streams or the linear velocity of the gas stream, should be used in correlating gas film data. Gilliland (30) concluded from vaporisation experiments with a wetted wall column, that the linear velocity of the gas should be used, because data on co-current and countercurrent flow of liquid and gas gave poorer correlation, when the relative velocity of the gas and liquid streams was used. However, the results of co-current and countercurrent flow of the liquid and gas streams for the absorption of ammonia in water from a dilute ammonia air mixture in a disc column, as reported by Stephens and Morris (116) and Taylor and Roberts (122) indicated that the relative velocity of the gas

and liquid streams is the significant velocity term. The values used for the liquid velocity on the discs were assumed by Stephens and Morris (116) to be equal to two thirds the theoretical value for streamline flow down a flat vertical surface, whereas Taylor and Roberts (122) assumed the theoretical value.

Cooper, Drew and McAdams (15) reviewed the existing experimental data on the isothermal flow of liquid layers on plane surfaces and showed, that the data could be correlated by the conventional Fanning friction factor and the Reynolds number relationship, in which the friction factor (f) and the Reynolds number (Re) are given by:-

$$f = \frac{2\,gm^3\,\rho^2 \sin\alpha}{\Gamma^2}$$

$$= \frac{2\,gm\,\sin\alpha}{v^2}$$

$$Re = \frac{4\,\Gamma}{\mu}$$

$$= \frac{4\,mv\rho}{\mu}$$

For streamline flow with a free surface, hydrodynamic theory predicts the relation between the friction factor and Reynolds number to be:-

$$f = \frac{24}{Re}$$

The agreement of the experimental data reviewed by these authors with the theoretical relationship for the streamline region was very good. These equations neglect any traction effect on the gas liquid interface, due to the flow of gas past the interface. These traction effects would normally be small except at very high gas rates.

As the liquid velocity appears to be an important variable in the

interpretation of disc column absorption data, it was decided to experimentally check the liquid velocities, to see if the theoretical conditions of streamline flow down a flat vertical surface actually apply to the flow of liquid down the disc assembly. It was also considered that such an investigation would reveal any departure from theoretical conditions, when water rates greater than Γ = 155 lb./(hr.)(ft.) are employed.

6.1 Experimental Procedure

The absorption element from a standard disc column, consisting of eighty carbon discs, was mounted vertically, so that the total holdup of liquid on the discs, at any instant, could be determined as a function of the liquid rate. The holdup was measured by collecting all of the liquid, which drained from the disc assembly, when the liquid feed to the top disc was cut off. Appropriate end corrections were applied to the total volume collected, to allow for the holdup of liquid between the bottom disc and the point where the holdup was collected.

The apparatus used for determining the liquid holdup on the disc assembly is shown in Fig. 6.1 and details of the disc assembly in Table 6.1.

TABLE 6.1

DISC DIMENSIONS

Number of Discs	=	80
Average Disc Diameter	=	0.0484 ft.
Average Disc Thickness	=	0.0148 ft.
Surface Area of Disc*	=	0.475 ft.^{2}
Mean Perimeter for Liquid Flow	=	0.122 ft.

*Uncorrected for liquid film thickness or for loss of area at points of contact, but used throughout as an approximation of the true liquid surface area.

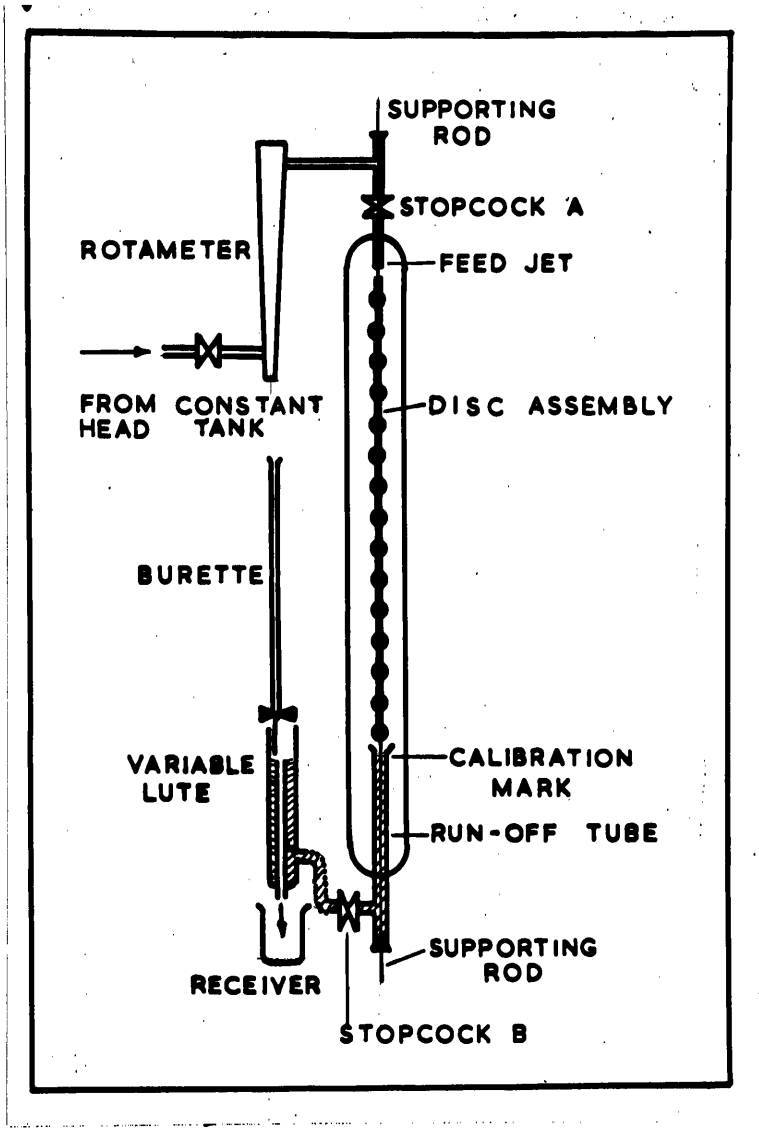

Fig. 6.1 - General layout of apparatus used for measuring the liquid holdup on the disc assembly

The experimental technique used was as follows:-

(a) When steady conditions at the desired liquid flow rate were reached and the variable lute adjusted so that the level of liquid in the run off tube was at the calibration mark, the stopcock A was closed and the receiver was placed simultaneously under the lute discharge.

(b) After allowing sufficient time to elapse to ensure complete

drainage from the disc assembly (five minutes was found to be sufficient), the level in the liquid run off tube, which had fallen when the liquid supply was stopped, was brought back to the calibration mark by raising the adjustable lute.

(c) The stopcock B was then closed and the volume of liquid required to refill the lute until the first drop had overflown into the discharge, was added by a burette (volume A).

(d) A further end correction, due to the volume of water flowing between the overflow weir of the lute and the point where the receiver was placed, was determined by simultaneously closing stopcock B and collecting the liquid which drained from the lute (volume B). No end correction was deemed necessary for the liquid between the first disc and the stopcock A. When stopcock A was closed, the liquid feed jet did not drain but remained full. The holdup on the half inch of supporting rod, between the exit of the liquid feed jet and the first disc, was considered negligible.

(e) To calculate the liquid holdup on the discs, the volume of liquid collected minus the sum of volume A and volume B, was corrected for the small volume of water which does not drain from the column but remains as a thin film over the surface of the discs and at the disc junctions.

(f) The mass of liquid adhering to the discs was found by wiping the surface of the discs with a tared cloth and reweighing the cloth to determine the liquid retained. This technique originally used by Claassen (13) was found to give reproducible results. The mass of liquid retained on the eighty discs was found to be 0.9 gram and hence this small correction was added to all the calculated holdups.

6.2 Experimental and Calculated Results

The experimental data obtained, using the foregoing procedure with water as the irrigating liquid phase, are shown in Table 6.2. Each experimental run shown is the mean of three separate determinations. The results calculated from these data are presented in Table 6.3.

TABLE 6.2

EXPERIMENTAL DATA

Run	Liquid Rate ml./min.	Liquid Temp. °C	Total Volume Collected (ml.)	End Corrections Volume A (ml.)	End Corrections Volume B (ml.)	Liquid Adhering to Discs (ml.)	Total Holdup on Discs (ml.)
1	344	19.4	22.0	2.0	2.1	0.9	18.8
2	300	19.4	20.0	1.0	1.8	0.9	18.1
3	364	19.4	18.3	0.9	1.6	0.9	16.7
4	219	19.4	15.3	0.7	1.4	0.9	14.1
5	176	19.6	13.9	0.4	1.2	0.9	13.2
6	131	19.7	12.4	0.4	1.0	0.9	12.0
7	94	20.1	10.7	0.3	0.8	0.9	10.5
8	62	18.1	9.0	0.3	0.7	0.9	8.9

TABLE 6.3

CALCULATED FRICTION FACTOR DATA

Run	Wetting Rate $\frac{\text{lb./(hr.)}}{\text{(ft.)}}$	Average Film Thickness m (ft.)	Average Liquid Velocity $\frac{v^{*}}{\text{(ft./sec.)}}$	Reynolds Number $\frac{4\Gamma}{\mu}$	Friction Factor (f)
1	372	1.40×10^{-3}	1.19	615	0.0646
2	324	1.34×10^{-3}	1.08	537	0.0756
3	285	1.24×10^{-3}	1.02	472	0.0768
4	237	1.05×10^{-3}	1.00	392	0.0673
5	190	0.98×10^{-3}	0.86	315	0.0853
6	142	0.89×10^{-3}	0.71	234	0.116
7	102	0.78×10^{-3}	0.58	169	0.151
8	67	0.66×10^{-3}	0.45	110	0.212

Average Film Thickness = Volume Held by Discs/ Surface Area of Discs

* Average Liquid Velocity (v) = $\frac{\Gamma}{m \rho}$

Friction factor calculated taking total surface area to be vertical, i.e. sin. α = 1

6.3 Discussion

The calculated friction factor data in Table 6.3 has only limited theoretical significance. The wetting rate on the rim of the discs would be different to the variable rate on the faces. The film thickness and hence the velocity of liquid on the rim of the discs varies from point to point on the rim, depending on the latitude of the particular point taken. The calculations were therefore based on average conditions of wetting rate, film thickness and liquid velocity. A further simplification was made that the total surface area was vertical. The friction factor thus calculated is equivalent to the flow of the liquid over a vertical flat plate with the same average wetting rate as for the discs and, therefore, must be considered as being an artificial figure. The friction factor is plotted against Reynolds number on a log.-log. graph in Fig. 6.2.

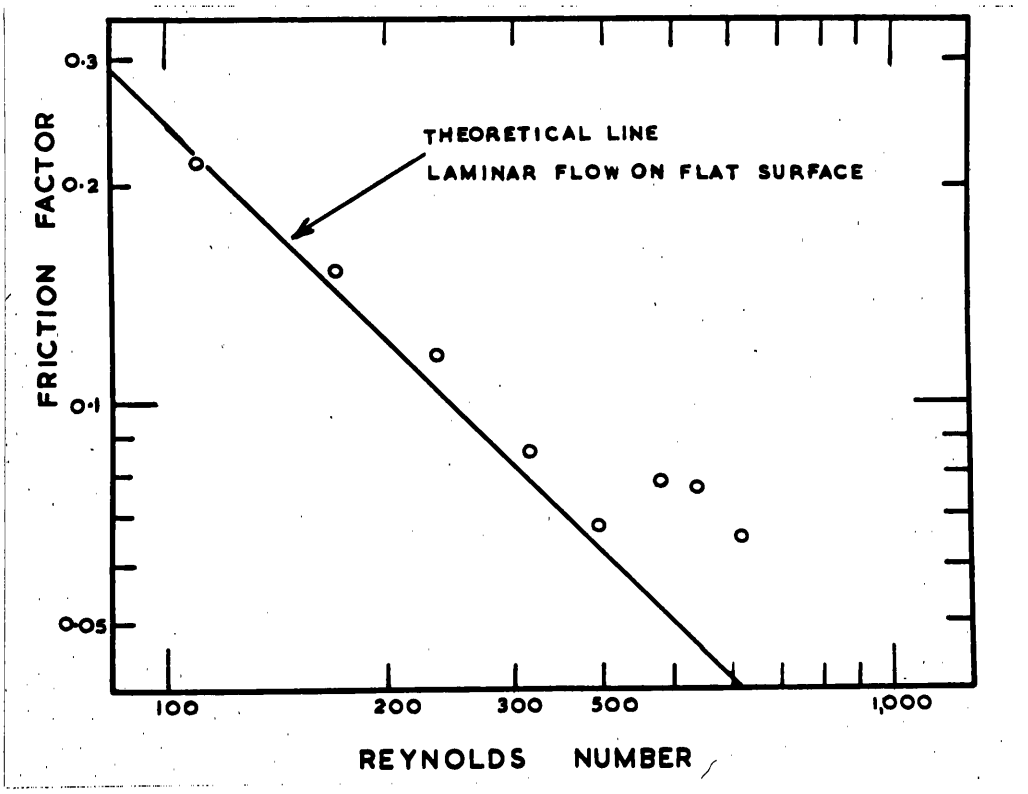

Fig. 6.2 - Friction factor - Reynolds number relationship for liquid flow on the discs

For Re less than 392 the data agrees well with the theoretical equation for laminar flow on a flat vertical surface. Therefore, calculations based on laminar flow over a flat vertical surface at the average disc wetting rate, should give average liquid velocities close to the true conditions. The procedure used by Taylor and Roberts (122), for calculating the liquid velocity on the discs, is therefore justified experimentally for Re less than 392.

A departure from the theoretical equation occurs between Re = 392 and Re = 472 (i.e. between Γ = 237 and Γ = 285 lb./(hr.)(ft.). A plot of liquid velocity versus wetting rate shows a breakpoint, which would indicate that the departure from the theoretical equation to be near Γ = 237 lb./(hr.)(ft.). It is thought that this breakpoint is comparable to the breakpoint observed by Taylor and Roberts (122) in both liquid and gas film mass transfer coefficients, when plotted versus liquid rate, and which was correlated by these authors as being due to the formation of ripples on the rim of the discs at wetting rates greater than 155 lb./(hr.)(ft.).

The same explanation can be applied to the friction factor data, although in this case the breakpoint or departure from theoretical conditions is at a somewhat higher wetting rate. The formation of ripples on the rims of the discs would increase the average film thickness and decrease the average liquid velocity, below that in the absence of ripples. Both these factors will cause the friction factor to be greater than the theoretical, as is shown significantly in Fig. 6.2. Besides the formation of ripples on the rims of the discs, any other cause of increased liquid holdup, such as surface disturbances on the face of the discs, could also explain the behaviour. The exact nature of these liquid surface disturbances could possibly be determined by high speed photography.

6.4 Nomenclature

f	=	friction factor (dimensionless)
g	=	gravitational conversion factor, ft./sec.^{2}
m	=	thickness of liquid layer, ft.
Re	=	Reynolds number (dimensionless)
v	=	mean velocity of liquid, ft./sec.
α	=	angle of flow path to horizontal
ρ	=	density of liquid, lb./ft.^{3}
μ	=	viscosity of liquid, lb./(ft.)(sec.)
Γ	=	liquid rate, lb./(sec.)(ft.) unless otherwise indicated

CHAPTER 7.

GAS FLOW CHARACTERISTICS

Theoretical and experimental developments in the three fields of fluid friction, heat and mass transfer indicate that they are all closely related. It was therefore considered that an investigation of the gas flow characteristics of the disc column would provide data useful in the interpretation of gas phase mass transfer coefficients. It is reasonable to expect comparable changes in mass transfer coefficients, when conditions of the gas flow alter. Stephens and Morris (116) were the first to observe a change in slope of the line obtained, when the gas film coefficients, for a particular liquid rate, were plotted against the relative velocity of the liquid and gas streams. The existence of such a discontinuity or "breakpoint" in the graph is an indication that the gas flow characteristics of the disc column undergo a change at a definite gas velocity.

The gas flow characteristics of the disc column were conveniently studied by measurements of the gas phase pressure drop across the discs of the column. By selecting a range of gases which had extremely different physical properties, it was possible to establish relationships, which showed the positions of the discontinuities observed in the gas flow conditions and enabled the pressure drop measurements to be correlated with the velocity and the physical properties of the gas phase.

As a knowledge of the limiting capacity is useful in the design of experimental work using the disc column, the air velocities at which the column ceased to function, due to entrainment of the liquid phase, were also determined.

7.1 Experimental Procedure and Results

A standard disc column, consisting of twenty seven carbon discs, was modified by locating manometer tappings, for determining the pressure drop across the discs, in the surrounding glass tube a short distance from each end of the disc assembly. The pressure drop was measured using a micromanometer graduated to read to one hundredth of a millimeter water gauge pressure differential. The gas was metered to the column by calibrated orifice plates, whilst a rotameter was used to meter the liquid supply.

The general layout of the apparatus is shown in Fig. 7.1 and the principal dimensions are shown in Table 7.1.

TABLE 7.1

PRINCIPAL DIMENSIONS OF DISC COLUMN

Number of discs	= 27
Disc diameter	= 1.475 cm.
Disc thickness	= 0.45 cm.
Tube diameter	= 2.5 cm.
Mean perimeter for liquid flow	= 0.122 ft.
Equivalent diameter for gas flow	= 0.052 ft.
Free space (dry)	= 89%
Absorption surface (dry)	= 0.1605 sq. ft.

(a) Flooding Characteristics

The maximum air velocities, at which the column could be operated without the water being blown from the discs and the column flooding, were investigated for different water rates. The liquid rate was maintained constant and the gas velocity was slowly increased until the "flooding velocity" was reached.

The "flooding velocity" of the column was determined visually. The first visual appearance of flooding occurred when small drops of water

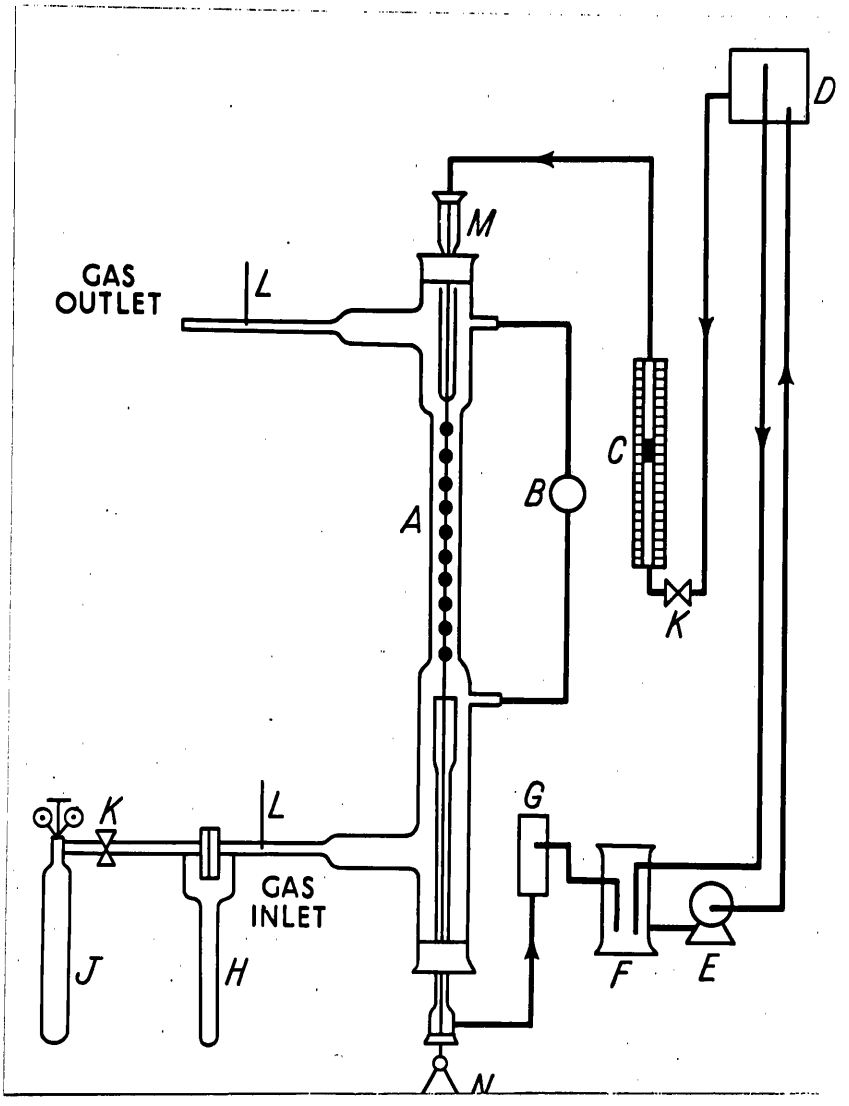

Fig. 7.1 - General arrangement of apparatus used for studying the gas flow characteristics of the column

A - Disc column
B - Micromanometer
C - Liquid rotameter
D - Constant head tank
E - Circulating pump
F - Pump sump
G - Liquid seal arrangement
H - Calibrated orifice plate
J - Compressed gas source
K - Needle control valve
L - Thermometer
M - Liquid flow nozzle
N - Disc supporting weight

were blown off the periphery of the wetted discs. The column became unstable at this point and, as the gas velocity was increased or the liquid rate increased, slugs of liquid were blown off the discs and surged upward through the column.

Due to the unstable nature of the column when the flooding conditions were approached, it was found difficult to determine accurately the exact flooding point. Data based on the visual determination of the air flooding velocity for different water rates are shown in Table 7.2.

TABLE 7.2.

AIR VELOCITIES WHICH INITIATE FLOODING

(FLOODING VISUALLY DETERMINED.)

Liquid Rate lb./(hr.)(ft.)	Air Velocity ft./sec.
101	32.0
141	27.0
188	26.5
234	23.5
281	22.5
325	21.0
368	21.5
408	20.0

(b) Total Pressure Drop across the Column

The total pressure drop across the column was measured for different liquid and gas flow rates for a wide range of gases. The gases studied were hydrogen (mol. wt. = 2), air (mol. wt. = 29), vinyl chloride (mol. wt. = 62.5) and dichlorodifluoromethane (mol. wt. = 121). As the investigation was centred on the gas phase characteristics, the liquid phase flowing over the discs was not varied initially and water was used in these runs. The data for the pressure drop across the whole column are shown in Table 7.3.

Throughout these investigations, all pressure drop data with the discs irrigated were taken as the difference between the micromanometer reading at the given gas and liquid rate and the reading at zero gas flow but at the same liquid rate as in the determination. The manometer reading was found to be dependent on the liquid rate at zero gas flow, presumably because of the liquid feed jet acting as an ejector, thereby lowering the pressure in the gas at the top of the column. This effect at high liquid rates gave manometer deflections as high as 0.006 cm. H_2O. Hence, if the micromanometer zero reading was taken at both zero gas and liquid flow, an appreciable error would have been introduced, as the ejector action of the feed jet would continue irrespective of the gas flow rate.

TABLE 7.3

DATA FOR PRESSURE DROP ACROSS THE COLUMN

Liquid Rate lb./hr.ft.	Gas Velocity ft./sec.	Gas Re	ΔP_t lb./ft.^{2}	Liquid Rate lb./hr.ft.	Gas Velocity ft./sec.	Gas Re	ΔP_t lb./ft.^{2}	Liquid Rate lb./hr.ft.	Gas Velocity ft./sec.	Gas Re	ΔP_t lb./ft.^{2}
	Dichlorodifluoromethane - Water							Hydrogen - Water			
255	3.96	7700	0.1970	131	3.95	7680	0.1640	255	13.6	630	0.0964
255	3.41	6630	0.1620	131	3.25	6320	0.1232	255	15.2	704	0.1087
255	2.76	5370	0.1150	131	2.57	5000	0.0882	255	17.2	795	0.1312
255	2.16	4190	0.0818	131	2.02	3920	0.0613	255	20.5	950	0.1745
255	1.67	3244	0.0594	131	1.46	2840	0.0410	255	23.5	1090	0.2112
255	1.34	2608	0.0432	131	0.87	1690	0.0239	255	26.5	1230	0.2544
255	0.96	1865	0.0328					255	29.5	1365	0.3060
				355	3.93	7640	0.2113	255	16.2	750	0.1250
166.5	3.97	7720	0.1663	355	3.37	6550	0.1725	255	33.0	1530	0.3510
166.5	3.34	6500	0.1393	355	2.82	5480	0.1330	255	38.0	1760	0.4325
166.5	2.78	5400	0.1044	355	2.03	3940	0.0882	255	33.6	1560	0.3670
166.5	2.26	4390	0.0779	355	1.47	2860	0.0575	255	3.65	169	0.0226
166.5	1.82	3540	0.0574	355	1.01	1963	0.0369	255	4.1	190	0.0246
166.5	1.32	2570	0.0410	355	0.665	1293	0.0226	255	4.8	222	0.0308
166.5	0.92	1780	0.0256					255	7.3	338	0.0452
								255	9.3	430	0.0595
								255	12.5	579	0.0881
								255	10.0	463	0.0696
								255	14.0	648	0.1024

TABLE 7.3 (CONTINUED)

Liquid Rate lb./hr.ft.	Gas Velocity ft./sec.	Gas Re	ΔP_t lb./ft.^{2}	Liquid Rate lb./hr.ft.	Gas Velocity ft./sec.	Gas Re	ΔP_t lb./ft.^{2}	Liquid Rate lb./hr.ft.	Gas Velocity ft./sec.	Gas Re	ΔP_t lb./ft.^{2}
	Air - Water				Air - Water				Air - Water		
408	5.13	1650	0.1580	368	4.95	1590	0.1438	281	4.43	1425	0.1187
408	6.90	2210	0.2420	368	6.20	1990	0.1926	281	6.55	2100	0.2032
408	8.35	2680	0.3196	368	7.40	2380	0.2566	281	8.20	2630	0.2870
408	8.83	2835	0.3490	368	8.50	2730	0.3080	281	10.8	3470	0.4372
408	10.8	3470	0.4920	368	11.30	3630	0.4955	281	13.0	4175	0.5930
408	13.6	4370	0.6940	368	12.8	4120	0.6060	281	16.0	5130	0.8322
408	15.6	5000	0.8740	368	13.5	4330	0.6600	281	18.7	6000	1.1100
408	16.6	5290	0.9625	368	14.7	4720	0.7675	281	20.7	6650	1.3350
408	17.7	5680	1.0970	368	17.2	5530	1.0030				
408	20.6	6620	1.4430	368	19.0	6100	1.1690	255	1.05	337	0.0238
				368	19.7	6330	1.2730	255	1.35	433	0.0266
335	1.05	337	0.0226	368	21.1	6780	1.4390	255	1.80	578	0.0328
335	1.28	411	0.0266					255	1.90	611	0.0390
335	1.42	456	0.0308	166.5	0.96	296	0.0144	255	2.40	772	0.0471
335	1.75	562	0.0368	166.5	1.35	433	0.0239	255	3.16	1015	0.0737
335	2.37	761	0.0492	166.5	1.53	491	0.0246	255	4.60	1477	0.1187
335	2.85	916	0.0636	166.5	1.80	577	0.0308	255	6.40	2055	0.1826
335	3.70	1190	0.0944	166.5	2.16	639	0.0369	255	7.10	2280	0.2177
335	4.90	1573	0.1394	166.5	2.70	867	0.0470	255	8.10	2760	0.2784
335	7.35	2360	0.2440	166.5	4.05	1300	0.0881				
335	8.80	2820	0.3078	166.5	5.60	1797	0.1294	378	1.05	337	0.0188
				166.5	6.95	2230	0.1890	378	1.35	433	0.0266
188	4.23	1360	0.1043	166.5	9.04	2900	0.2650	378	1.70	546	0.0350
188	6.30	2020	0.1763					378	2.32	745	0.0492
188	7.40	2380	0.2214	188	18.2	5840	0.9415	378	3.22	1035	0.0782
188	9.40	3020	0.3074	188	20.2	6480	1.1320	378	4.30	1381	0.1169
188	10.7	3430	0.3996	188	21.2	6810	1.2475	378	5.80	1860	0.1725
188	13.0	4175	0.5280	188	22.0	7060	1.3225	378	6.90	2210	0.2210
188	14.4	4620	0.6425					378	8.50	2730	0.2996
188	16.2	5190	0.7560								
	Vinyl Chloride - Water										
255	4.27	5080	0.1457	355	4.22	5020	0.1636				
255	3.93	4680	0.1270	355	3.94	4690	0.1475				
255	3.52	4180	0.1087	355	3.52	4180	0.1250				
255	3.03	3600	0.0862	355	3.00	3570	0.1006				
255	2.70	3210	0.0717	355	2.43	2900	0.0718				
255	2.36	2810	0.0594	355	1.92	2280	0.0512				
255	1.50	1785	0.0369	355	1.29	1537	0.0328				
255	1.16	1605	0.0269								

The data of Table 7.3 are well correlated when ΔP_t is plotted against $v\rho^{0.41}\Gamma^{0.22}$ on a log.-log. scale as shown in Fig. 7.2.

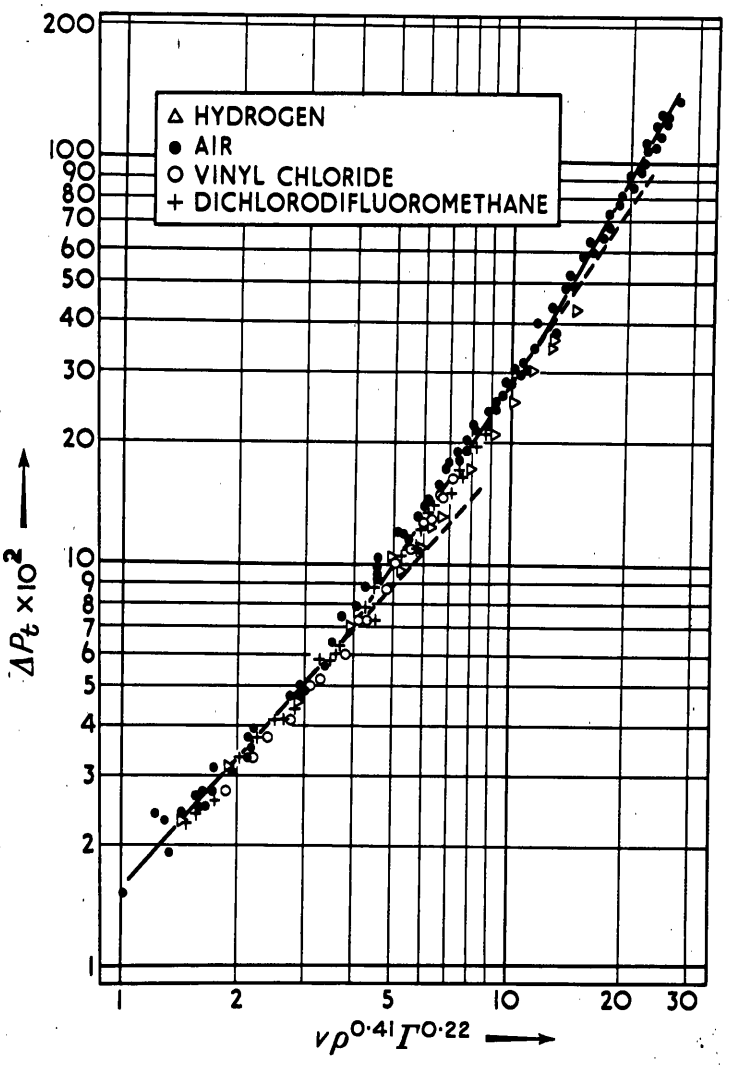

Fig. 7.2 - Pressure drop across the column

The three straight lines of Fig. 7.2 and the location of the "breakpoints" are better illustrated by plotting the dimensional group $\frac{\Delta P_t}{v^2\rho}$ against gas velocity. A comparison of the two methods of plotting is shown in Fig. 7.3, in which ΔP_t and $\frac{\Delta P_t}{v^2\rho}$ are plotted against gas velocity for data of one of the air water runs shown in Table 7.3.

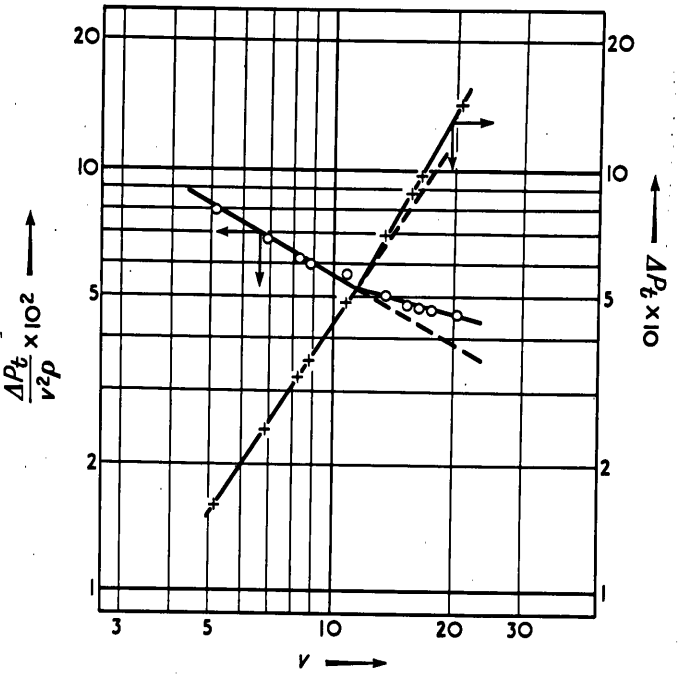

Fig. 7.3 - Comparison of methods of plotting data

$\frac{\Delta P_t}{v^2\rho}$ versus v

ΔP_t versus v

Air - water system (Γ = 408 lb./(hr.)(ft.)

(c) Pressure Drop across Column at Zero Liquid Rate

Flow through the dry column is equivalent to flow through a porous media with a single fluid phase. Such data are best correlated by plotting a friction factor against Reynolds number on a log.-log. graph. However, it is not necessary to use the complete Fanning friction factor for purpose of illustrating the flow characteristics of a particular column. The dimensional group $\frac{\Delta P_t}{v^2\rho}$ (which is directly proportioned to the Fanning friction factor) has been plotted against Re in Fig. 7.4 for data on the pressure drop across the dry column as shown in Table 7.4.

TABLE 7.4

PRESSURE DROP ACROSS THE COLUMN AT ZERO LIQUID RATE

Gas Velocity ft./sec.	Gas Re	ΔP_t lb./ft.^{2}	Gas Velocity ft./sec.	Gas Re	ΔP_t lb./ft.^{2}	Gas Velocity ft./sec.	Gas Re	ΔP_t lb./ft.^{2}
	Air		Vinyl Chloride			Dichlorodifluoromethane		
1.35	417	0.0143	4.17	4960	0.1067	4.03	7850	0.1822
1.67	537	0.0205	3.72	4420	0.0839	3.46	6730	0.1413
4.30	1380	0.0800	3.20	3800	0.0635	3.09	6000	0.1169
5.75	1845	0.1290	2.96	3520	0.0553	2.70	5250	0.0922
7.2	2310	0.1886	2.11	2510	0.0307	2.15	4175	0.0594
9.08	2920	0.2642	1.47	1750	0.0164	1.42	2760	0.0307
2.17	698	0.0286	1.23	1463	0.0123	1.04	2020	0.0185
1.42	457	0.0154	0.68	950	0.0051	0.75	1460	0.0103
1.67	537	0.0184	3.5	4160	0.0822	4.02	7820	0.1887
6.20	1990	0.1683	3.0	3570	0.0656	3.73	7250	0.1620
8.20	2630	0.2420	2.68	3190	0.0513	3.30	6420	0.1313
10.7	3430	0.3852	2.23	2660	0.0369	2.97	5770	0.1067
14.2	4560	0.5980	1.66	1973	0.0226	2.53	4920	0.0800
16.3	5230	0.7155	1.35	1605	0.0143	2.14	4160	0.0615
19.2	6160	0.9665	0.91	1082	0.0082	1.82	3540	0.0452
20.7	6650	1.0975	4.0	4760	0.1064	1.42	2760	0.0287
22.2	7130	1.2310	3.45	4110	0.0821	0.80	1566	0.0123
24.0	7700	1.3975	3.07	3650	0.0635	0.57	1108	0.0072
			2.50	2980	0.0430			
			2.10	2500	0.0307			
			1.78	2120	0.0225			
			1.47	1750	0.0174			
			1.44	1713	0.0164			
			1.56	1855	0.0185			

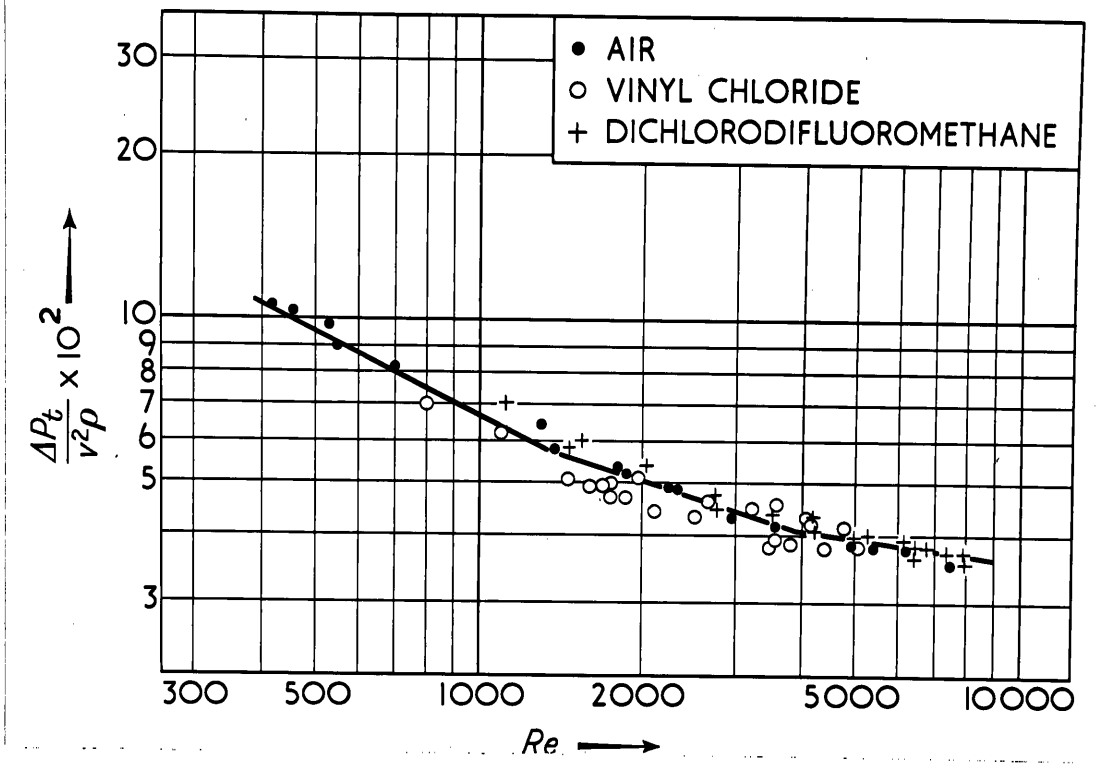

Fig. 7.4 - Pressure drop across column at zero liquid rate

(d) Pressure Drop across the Empty Column

To evaluate the pressure drop due to the disc assembly, the pressure drop due to the glass column itself, without the discs in place, was measured using the same range of gases as in the total pressure drop studies. This pressure drop constituted the skin friction on the column walls and the entrance and exit losses associated with the test length of the column.

Correlation of the data shown in Table 7.5 is obtained by plotting the dimensional group $\frac{\Delta P_e}{v^2\rho}$ against Re on a log.-log. graph as shown in Fig. 7.5.

TABLE 7.5

PRESSURE DROP ACROSS THE EMPTY COLUMN (DISCS REMOVED)

Gas Velocity ft./sec.	Gas Re	ΔP_e lb./ft.^{2}	Gas Velocity ft./sec.	Gas Re	ΔP_e lb./ft.^{2}	Gas Velocity ft./sec.	Gas Re	ΔP_e lb./ft.^{2}
	Hydrogen			Air			Vinyl Chloride	
8.7	402	0.0164	1.73	555	0.0082	1.62	1928	0.0061
11.3	522	0.0205	2.50	803	0.0133	2.30	2737	0.0144
15.8	730	0.0369	2.74	880	0.0154	2.90	3451	0.0164
19.0	880	0.0451	2.55	1140	0.0225	3.35	3987	0.0210
23.0	1065	0.0595	3.95	1268	0.0266	4.10	4879	0.0307
25.2	1165	0.0675	4.70	1509	0.0327	4.00	4760	0.0266
30.3	1400	0.0863	5.85	1878	0.0429	1.46	1737	0.0061
37.0	1710	0.1150	6.95	2230	0.0532	1.84	2190	0.0103
11.5	532	0.0225	7.70	2472	0.0655	2.25	2678	0.0123
12.3	570	0.0266	8.20	2632	0.0820	2.70	3213	0.0164
16.3	755	0.0389	2.50	803	0.0164	3.12	3713	0.0185
17.2	797	0.0410	3.02	969	0.0184	3.62	4311	0.0226
19.7	913	0.0451	3.85	1236	0.0225	3.90	4641	0.0297
23.0	1065	0.0573	4.60	1477	0.0308	4.16	4950	0.0317
25.0	1157	0.0677	5.10	1637	0.0369	4.45	5296	0.0389
30.3	1400	0.0862	6.35	2038	0.0472	4.40	5236	0.0389
36.5	1690	0.1128	7.9	2536	0.0697	1.95	2321	0.0113
13.8	638	0.0287	8.2	2632	0.0800	1.50	1785	0.0061
15.6	722	0.0348	5.9	1895	0.0410			
18.2	843	0.0431	8.1	2600	0.0614			
14.7	680	0.0318	10.6	3400	0.0944	Dichlorodifluoromethane		
17.2	796	0.0410	15.2	4870	0.1907			
19.0	880	0.0451	17.7	5670	0.2560	2.75	5350	0.0246
			19.6	6280	0.2890	0.98	1907	0.0061
	Air		23.5	7540	0.4020	1.50	2920	0.0103
1.77	568	0.0082	5.45	1155	0.0328	2.1	4080	0.0184
2.68	860	0.0144	6.40	2060	0.0431	2.93	5700	0.0328
3.1	995	0.0184	7.40	2380	0.0513			
4.04	1297	0.0267	9.10	2920	0.0717			
5.10	1637	0.0369	11.5	3680	0.1190			
6.10	1958	0.0451	13.2	4230	0.1558			
6.85	2199	0.0553	14.5	4650	0.1865			
7.60	2440	0.0676	18.6	5960	0.2682			
8.30	2664	0.0758	22.3	7150	0.3668			

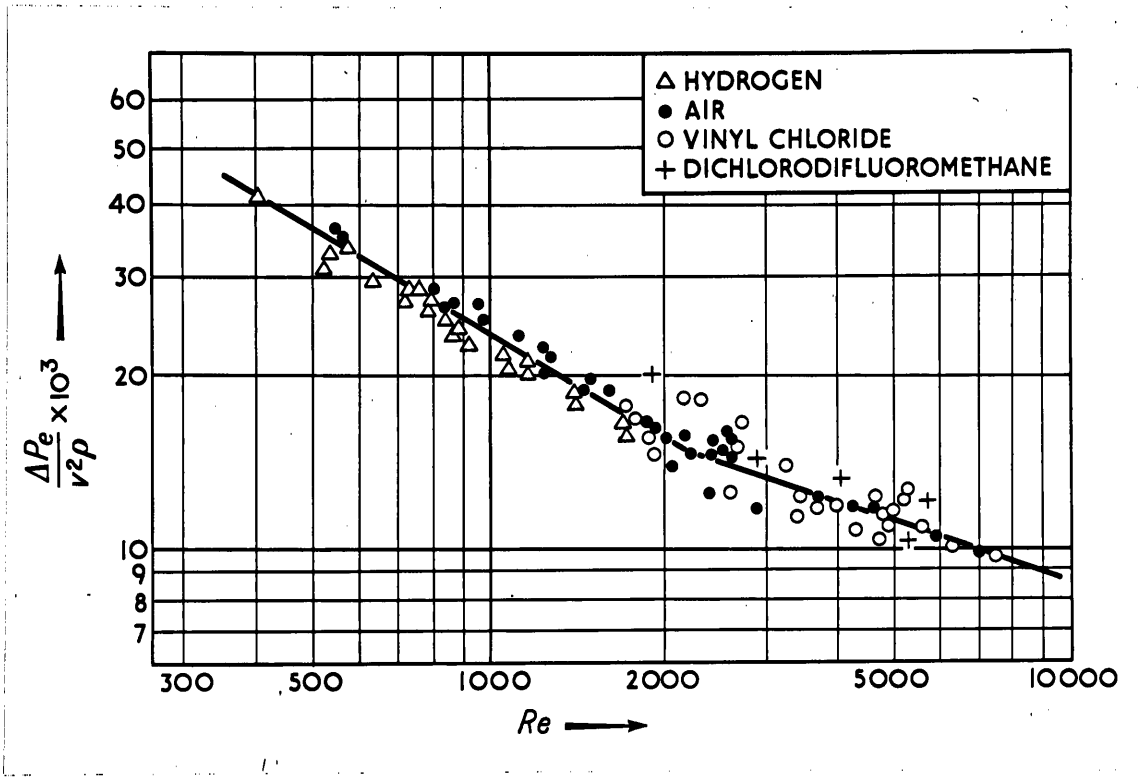

Fig. 7.5 - Pressure drop across the empty column (discs removed)

(e) Estimated Pressure Drop due to Discs

The pressure drop across the column due to the discs was obtained by substracting the pressure drop due to the empty column (as determined from Fig. 7.5) from the pressure drop data due to the assembled column.

An example of the method of calculation used to approximate the pressure drop across a single disc in a disc column is shown in Table 7.6.

The estimated pressure drop ΔP_d due to a single disc is well correlated by plotting ΔP_d against $v \rho^{0.41} \Gamma^{0.22}$ on a log.-log. graph as shown in Fig. 7.6.

The dimensional equations for the correlation are

Let $v \rho^{0.41} \Gamma^{0.22} = \phi$

(a) Above $\phi = 12$

$$\Delta P_d = 9.8 \times 10^{-5} \phi^{1.84} \quad \ldots\ldots 7.1$$

(b) Between $\phi = 12$ and $\phi = 4$

$$\Delta P_d = 2.94 \times 10^{-4} \phi^{1.41} \quad \ldots\ldots 7.2$$

(c) Below $\phi = 4$

$$\Delta P_d = 4.5 \times 10^{-4} \phi^{1.09} \quad \ldots\ldots 7.3$$

TABLE 7.6

DETERMINATION OF PRESSURE DROP ACROSS A DISC

Liquid Rate $\frac{lb.}{(hr.)(ft.)}$	Gas Velocity $\frac{ft.}{sec.}$	Gas Re	ΔP_t lb./ft.^{2}	$\frac{\Delta P_e \text{ lb.}}{ft.^2}$ (from Fig. 7.5)	$\Delta P_t - \Delta P_e$ lb./ft.^{2}	ΔP_d lb./ft.^{2}
368	4.95	1590	0.1438	0.0328	0.1110	0.00411
368	6.20	1990	0.1926	0.0450	0.1476	0.00547
368	7.40	2380	0.2566	0.0597	0.1969	0.00729
368	8.50	2730	0.3080	0.0755	0.2325	0.00853
368	11.3	3630	0.4955	0.1200	0.3755	0.01389
368	12.8	4120	0.6060	0.1482	0.4578	0.01695
368	13.5	4330	0.6600	0.1606	0.4994	0.01851
368	14.7	4720	0.7675	0.1857	0.5818	0.02153
368	17.2	5530	1.0030	0.2400	0.7630	0.02820
368	19.0	6100	1.1690	0.2846	0.8844	0.03272
368	19.7	6330	1.2730	0.3030	0.9700	0.03590
368	21.1	6780	1.4390	0.3388	1.1010	0.04075

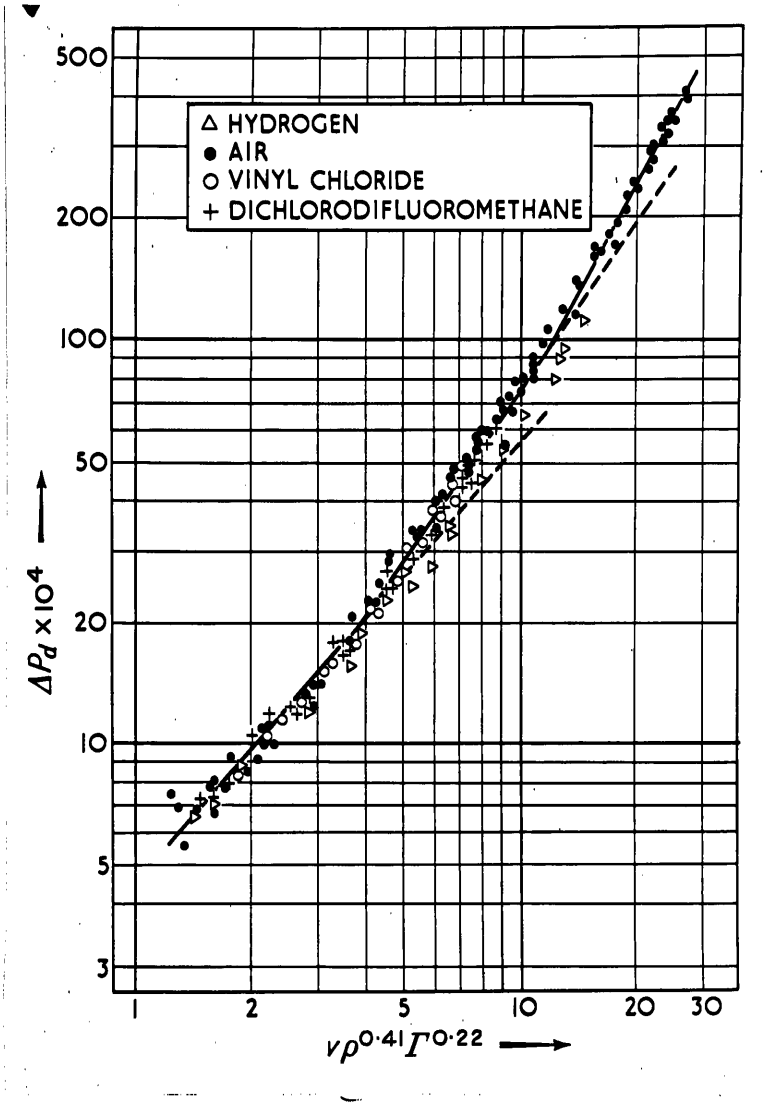

Fig. 7.6 - Pressure drop across a disc

7.2 Discussion

The correlation for pressure drop across a disc in which ΔP_d is plotted against $v \rho^{0.41} \Gamma^{0.22}$ on a log. scale shows that the graph obtained is discontinuous and is characterised by two breakpoints over the range studied. These breakpoints are at $v \rho^{0.41} \Gamma^{0.22} = 4$ and $v \rho^{0.41} \Gamma^{0.22} = 12$. The positions of the breakpoints for a particular system are not fixed exactly by these equations, as they tend to give high

values of the critical velocities for the air runs and low values for the hydrogen and dichlorodifluoromethane runs.

However, they do give an indication of the gas phase velocities, near which changes in the gas flow conditions can be expected.

The existence of these critical points is better illustrated by plotting $\frac{\Delta P_t}{v^2 \rho}$ against gas Reynolds number Re for individual runs with liquid rates as parameters. Such a series of graphs is presented in Fig. 7.7.

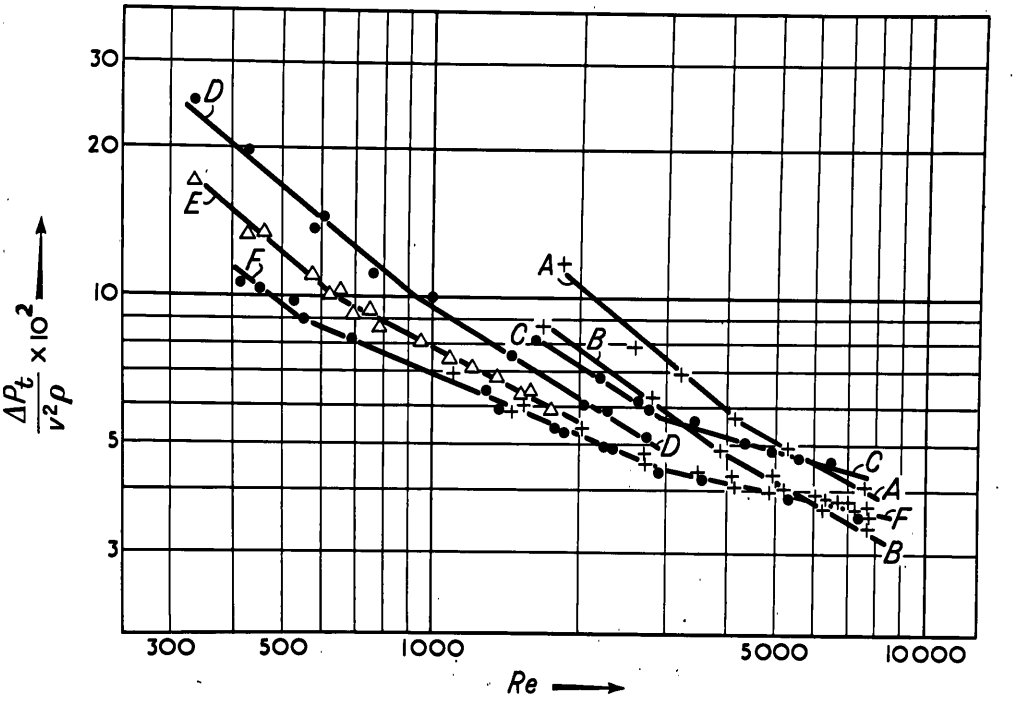

Fig. 7.7 - AA dichlorodifluoromethane-water Γ = 255 lb./(hr.)(ft.)
BB dichlorodifluoromethane-water Γ = 131 lb./(hr.)(ft.)
CC air-water Γ = 408 lb./(hr.)(ft.)
DD air-water Γ = 255 lb./(hr.)(ft.)
EE hydrogen-water Γ = 255 lb./(hr.)(ft.)
FF air and dichlorodifluoromethane Γ = 0 lb./(hr.)(ft.)

Referring to Fig. 7.7 the lines AA and BB are typical of a group of lines obtained for a particular gas phase with different liquid rates, showing the existence of a breakpoint at Reynolds number of approximately 4000. This breakpoint corresponds to the lower breakpoint of the

correlation shown in Fig. 7.2. Lines AA, DD and EE are for different gas phases with the same liquid rate. The breakpoints for these lines are approximately Re = 4000, Re = 950 and Re = 600 respectively. These breakpoints all correspond to the lower breakpoints of the correlation shown in Fig. 7.2. A breakpoint corresponding to the higher breakpoint of the correlation shown in Fig. 7.2 is indicated by the line CC at Re = 3000.

The inclusion in Fig. 7.7 of the data for the dry column shows that the flow conditions can be well correlated by graphing $\frac{\Delta P_t}{v^2 \rho}$ against Re as shown by line FF. However, once the column is operating with liquid flowing over the discs, the gas flow characteristics at a constant liquid rate can no longer be correlated by a Reynolds number alone.

This can be clearly seen from the lines EE, DD and AA, which are for constant liquid rate with different gas phases. Hence, it appears that the use of a gas Reynolds number together with some functions of liquid rate as adopted by Stephens and Morris (116) and Roper (89) for a correlation of gas film mass transfer coefficients, is not sufficient for a general correlation applicable to all gaseous systems.

As can be seen from Fig. 7.7, the line for zero liquid rate is found to intersect the line BB for dichlorodifluoromethane at high Reynolds number and then continues above the low liquid rate line. A similar effect was noticed if the low liquid rates of the air runs were plotted.

The higher pressure drop of the dry column at the high Reynolds number could be attributed to the increase in impact losses on the square edges of the dry discs. The effect of liquid flowing is to round off the discs and thereby reduce the impact pressure losses. However, the liquid flowing over the discs will greatly increase skin friction and hence the

general trend that pressure drop is increased with increased liquid rate.

The fact that breakpoints are observed indicates that flow conditions in the gas phase change at definite critical points. Hence, it is reasonable to expect some comparable change in the gas film coefficient under similar conditions. The data of Roper (89) and Stephens and Morris (116) were critically examined for discontinuity in the gas film coefficient at gas velocities corresponding to the breakpoint indicated by pressure drop measurements.

The bulk of the data reported by Roper (89) on the evaporation of water in a disc column was for air velocities which are below the first breakpoint on the pressure drop relations. However, data for liquid rates of 121 lb./(hr.)(ft.) and 81 lb./(hr.)(ft.) extend on both sides of the first breakpoint observed in the pressure drop relation investigated. These data have been plotted in Fig. 7.8 in which the pressure drop data for a low liquid rate of the air - water system are also shown.

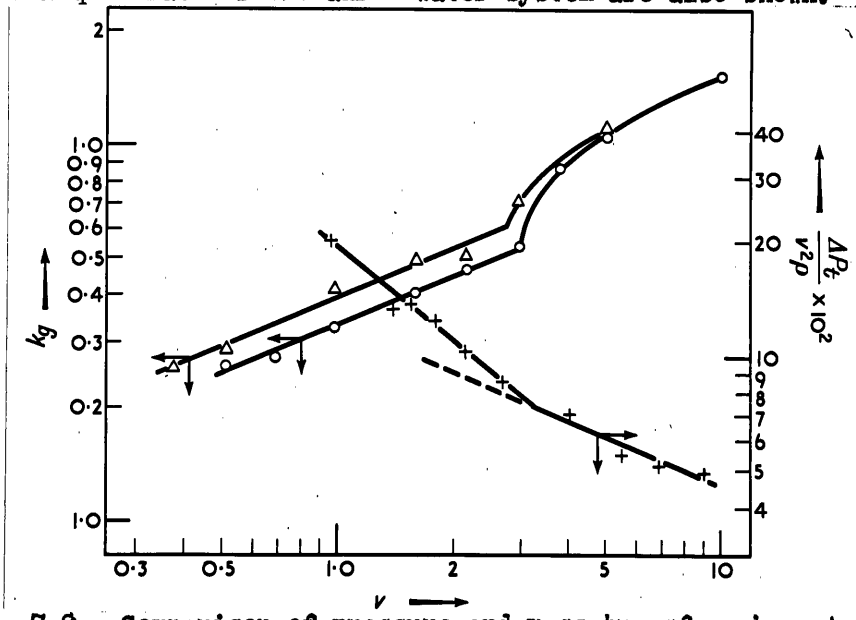

Fig. 7.8 - Comparison of pressure and mass transfer characteristics

Δ	Γ = 121 lb./(hr.)(ft.)	Data of Roper (89)
o	Γ = 81 lb./(hr.)(ft.)	Gas film mass transfer coefficients for the vaporisation of water in air
+	Γ = 166.5 lb./(hr.)(ft.)	Pressure drop data for air-water system

The breakpoint in the gas film mass transfer coefficient graph compares well with the observed breakpoint in the pressure drop data. The data of Stephens and Morris (116) for the gas film coefficient in the absorption of dilute ammonia-air mixtures by water, when plotted in the same manner, also show a breakpoint which is consistent with that observed for pressure drop data. Subsequent to publication of these results, [Warner (125)] Taylor and Roberts (122) reported a breakpoint in their gas film mass transfer data at a point approximated by the equation developed by the author for counterflow conditions.

In the preceding analysis, the velocity term used was the linear velocity of the gas irrespective of the liquid velocity. However, as already indicated, the relative velocity of the liquid and gas stream has been used successfully for correlating countercurrent and co-current absorption data in a disc column. Therefore, a further analysis of the pressure drop data was made, in which the significant velocity term was taken as the relative velocity of the gas and liquid streams.

Fig. 7.7 showed that a friction factor (or its equivalent $\frac{\Delta P_t}{v^2 \rho}$) versus Reynolds number type of plot based on the linear gas velocity was satisfactory for the dry packing but unsuitable for the irrigated packing, as data for a constant liquid rate but different gas phases could not be correlated. The same approach was attempted using the relative velocity of the liquid and gas streams as the velocity term.

Fig. 7.9 is a plot of $\frac{\Delta P_d}{v^2_R \rho}$ (the equivalent of a "relative" friction factor) versus the "relative" Reynolds number $(Re)_R$ for all the data up to and including a liquid rate of 255 lb./(hr.)(ft.). The full line A-A in the diagram is the line of best fit for the pressure drop across one

dry disc with air as the gas phase. The other full line in the diagram represents the low flow rate hydrogen data, which extends into the low Reynolds number region, whilst still maintaining a reasonable pressure drop and is therefore not subject to the errors associated with the low flow air data. This line representing the hydrogen data was drawn with the theoretical slope of -1, as at these low Reynolds numbers, it is considered that laminar flow conditions would exist. The agreement of the hydrogen data with this line of theoretical slope is good for $(Re)_R$ below 500.

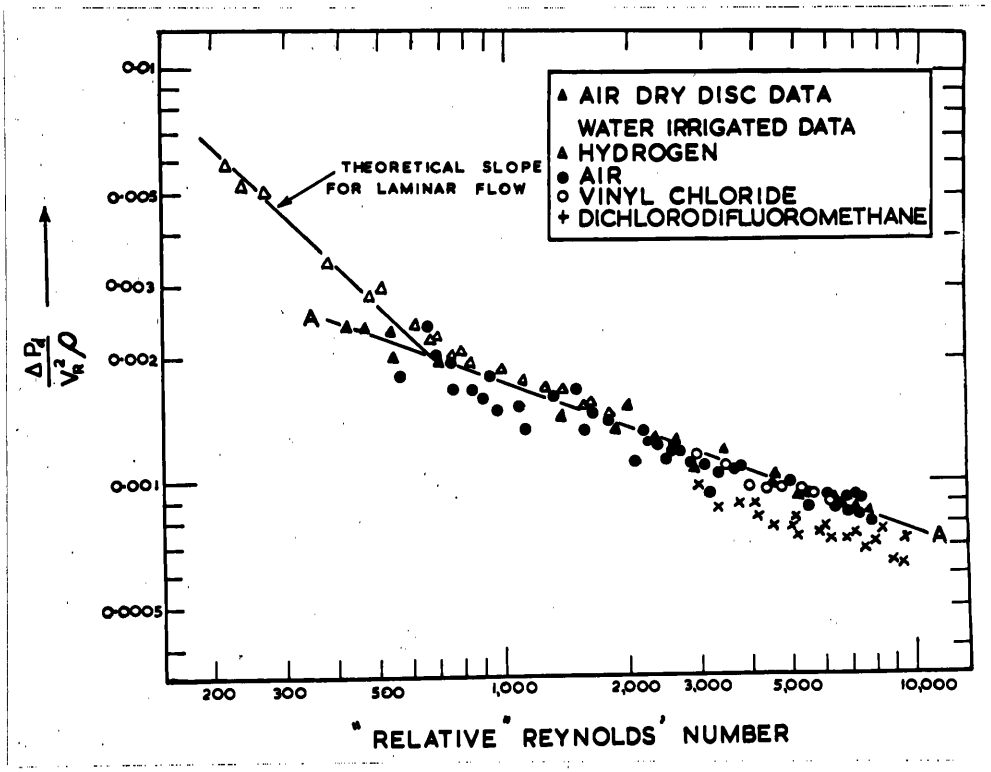

Fig. 7.9 - The equivalent of a "relative friction factor" versus "relative Reynolds number" plot (excluding liquid rates above Γ = 255 lb./(hr.)(ft.)

The significant features of Fig. 7.9 are:-

(1) The irrigated and dry disc data are correlated using a "relative" friction factor plot. This is in marked contrast with the absence of

correlation, when linear gas velocity was used for evaluating the friction factor and the Reynolds number.

(2) The dichlorodifluoromethane and the low velocity air results are significantly below the other data. Due to the large molecular weight of the former gas, high values of $(Re)_R$ can be obtained at lower velocities than the other gases. The total pressure drop across a disc is due to both skin friction and form drag. Form drag results from the eddy currents caused by impact of the gas with the surface and edges of the disc. As form drag involves the dissipation of kinetic energy, the losses are proportional to the square of the velocity. Whilst, however, it is considered that the velocity of the liquid flowing down the disc would contribute to the formation of the eddy currents in the gas phase, the use of the full relative velocity, to account for this effect, is probably not justified. Hence at a given $(Re)_R$, the form drag losses would be less than an analysis based on relative velocity would suggest. This effect would be most noticeable, at a given $(Re)_R$, for data in which the relative and linear gas velocities are markedly different. Thus for a constant liquid rate, the dichlorodifluoromethane data is displaced below the air data at high values of $(Re)_R$ and at low values of $(Re)_R$ the air data is displaced below the hydrogen data.

The data for liquid rates higher than 255 lb./(hr.)(ft.) exhibited behaviour different to the lower liquid rate data. The air data for these high liquid rates are shown in Fig. 7.10, in which the equivalent of the "relative" friction factor is plotted against the "relative" Reynolds number on a log.-log. graph. The air data only was plotted in this graph. The dichlorodifluoromethane data, if plotted on the diagram, would fall consistently below the air data, as was the case for the lower

liquid rate data. The full line A-A is the best fit of the zero liquid rate data for air as the gas phase. The "relative" friction factors for these higher rates are dependent on the liquid rate, although below $(Re)_R$ = 1200 the results could be represented by the line A-A. The departure from the line A-A, as well as the dependency on the liquid rate, increases as $(Re)_R$ is increased beyond $(Re)_R$ = 1200.

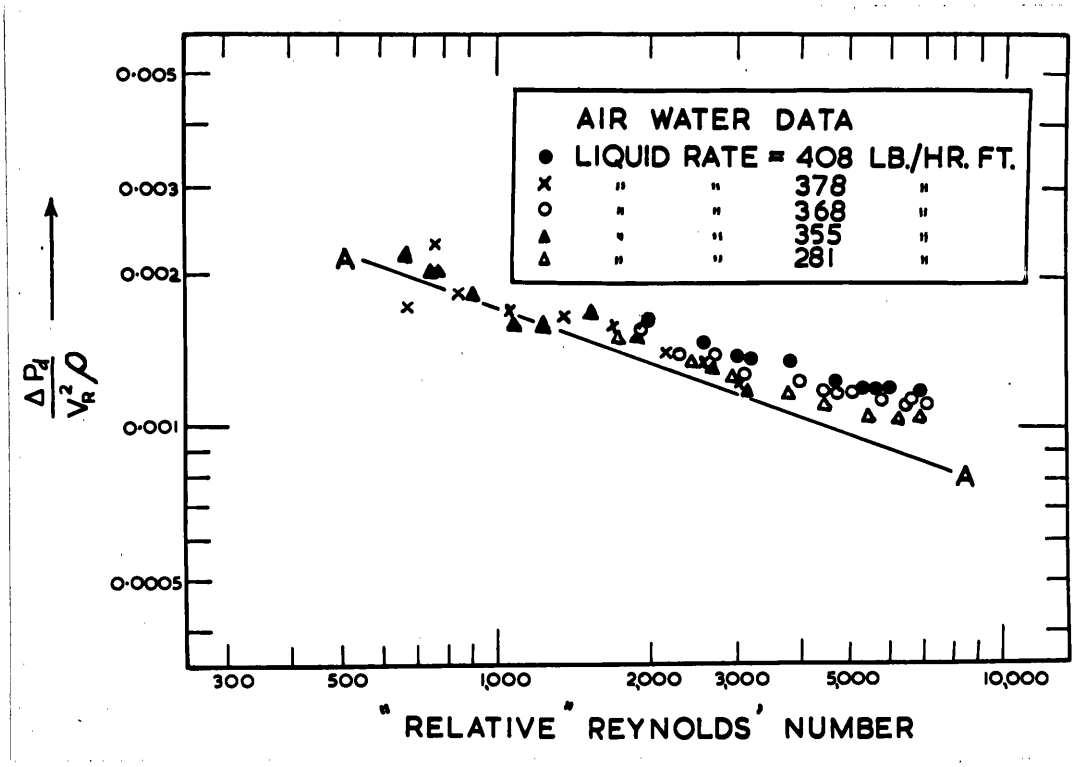

Fig. 7.10 - The equivalent of a "relative friction factor" versus "relative Reynolds number" plot for $\Gamma >$ 255 lb./(hr.)(ft.)

These phenomena are thought to be associated with the behaviour of the liquid flowing over the discs. The results of the experiments outlined in Chapter 6 indicated that the liquid flow characteristics below Γ = 237 lb./(hr.)(ft.) were different to the flows of Γ = 285 lb./(hr.)(ft.) and higher, the difference being attributed to ripples and surface disturbances on the liquid as it flows over the

discs. These surface disturbances, which appear to be non-existent at the lower flow rates, have the effect of roughening the liquid surface.

Therefore, the data, for flow rates below the rate required for the establishment of the surface disturbances, are analogous to friction data for smooth pipes, whereas the data for the higher liquid rates are analogous to friction data for rough pipes. Friction factors for rough pipes can only be correlated by the introduction of the parameter "relative roughness" which is the ratio of the surface irregularities to the diameter of the pipe. The relative roughness has no effect in the laminar region but becomes of increasing importance as the Reynolds number is increased.

These explanations elucidate the essential difference observed in the friction factor plots for high and low liquid rate data, and are consistent with the observations of Taylor and Roberts (122), who reported that disc column gas film mass transfer coefficients, at constant relative velocity, are independent of the liquid rate at low liquid rates but affected by liquid rate at higher liquid flows.

As a further check on the use of the relative velocity of the gas and liquid streams for comparing pressure drop data, the pressure drops with air as the gas phase were measured for a number of liquid phases with markedly different physical properties and flow rates. The liquids used and the relative physical properties are shown in Table 7.7.

The experimental and calculated results are shown in Tables 7.8 and 7.9, which are appended to this chapter rather than included in the bulk of the text so as to retain the continuity of the discussion.

The pressure drop data is well correlated by a log.-log. plot of ΔP_d versus relative velocity, whereas it is not correlated by the gas phase velocity alone as shown in Fig. 7.11.

TABLE 7.7

PROPERTIES OF LIQUID PHASES

Liquid Phase	Rate lb./(hr.)(ft.)	Viscosity centipoise	Density g./cc.	Liquid Velocity ft./sec. *
Aq. Sucrose	272	8.9	1.21	0.51
Toluene	14 163	0.6	0.87	0.20 1.01
n-Heptane	15 113	0.41	0.68	0.25 0.96

* Calculated assuming $f = \frac{24}{Re}$

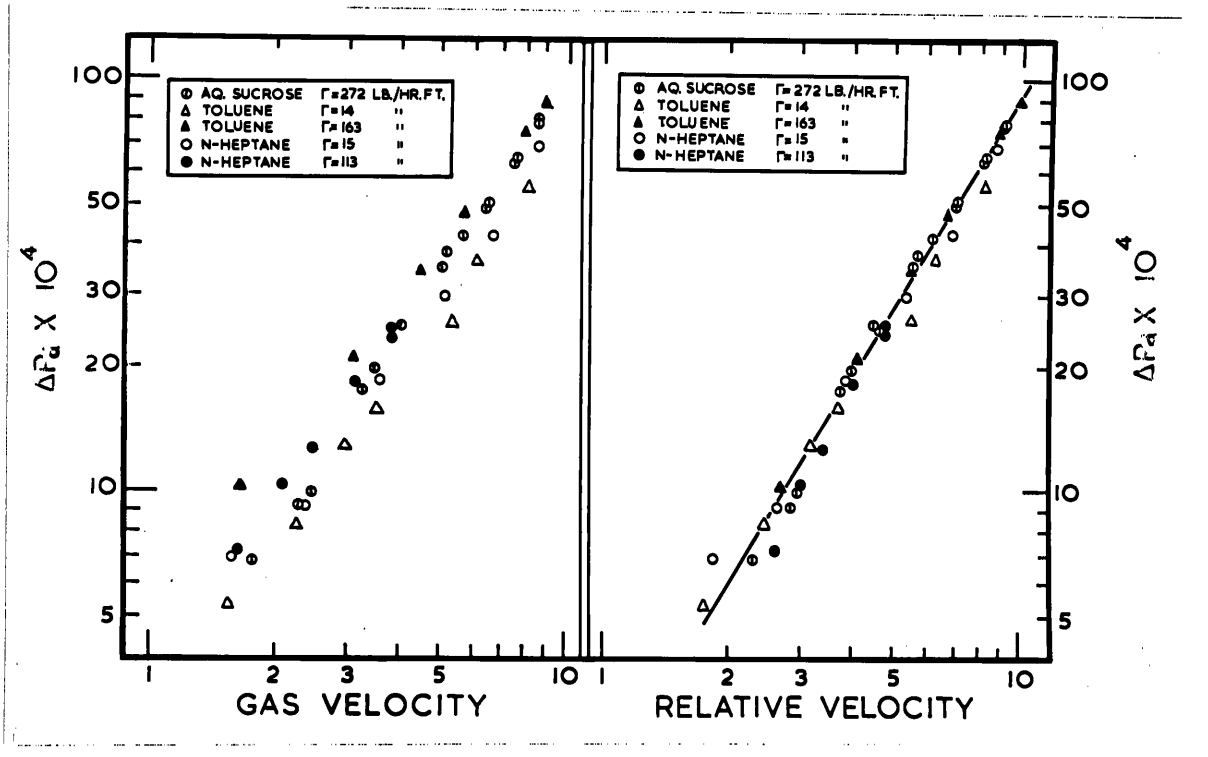

Fig. 7.11 - Comparison of gas velocity and relative velocity for correlating pressure drop data

As the variable liquid phase experimental results add further bias towards the adoption of the relative velocity of the liquid and gaseous streams, the data presented in Fig. 7.8, showing the existence of a "breakpoint" in the pressure drop characteristics at the same gas velocity as a mass transfer coefficient discontinuity, was replotted in Fig. 7.12 using the relative velocity as the significant velocity term. This figure indicated that the "breakpoint" in the pressure drop data is no longer present. The discontinuity in the mass transfer data, whilst still existing, is less well defined compared to the previous method of plotting the data.

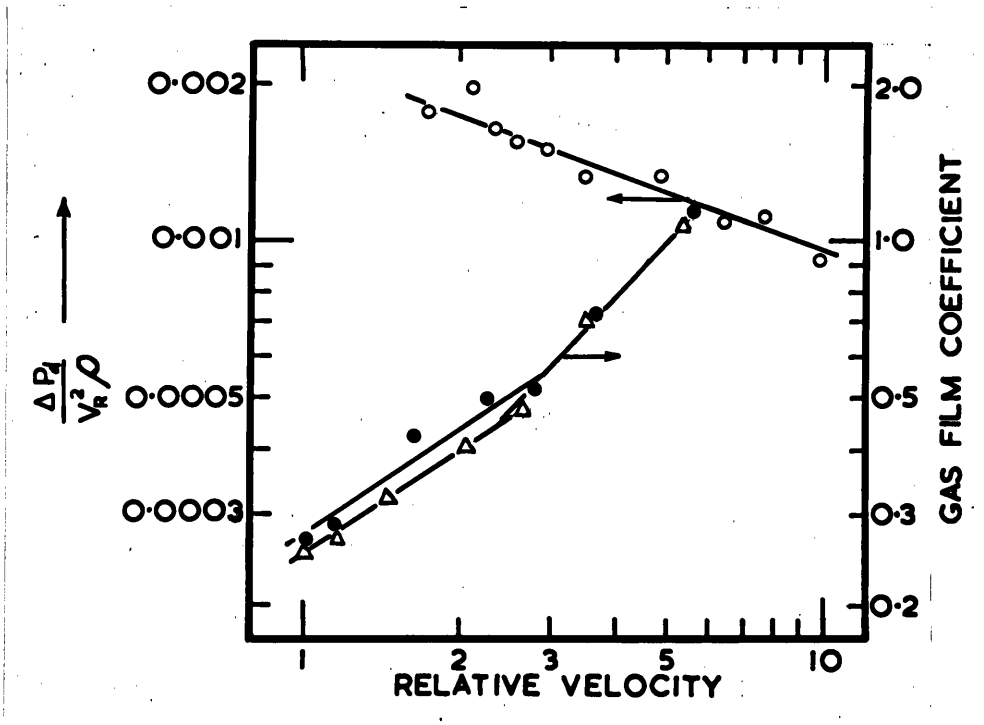

Fig. 7.12 - Comparison of pressure and mass transfer characteristics using the relative velocity

- ● Γ = 121 lb./(hr.)(ft.) Data of Roper (89)
- Δ Γ = 81 lb./(hr.)(ft.) Gas film mass transfer coefficients for the vaporisation of water in air
- o Γ = 166.5 lb./(hr.)(ft.) Pressure drop data for air-water system

Therefore the "breakpoints" observed, when the gas velocity is used for plotting pressure drop data, would appear to have no real physical significance, but are due to the method of presentation of the data. This suggests that, if the relative velocity is used, the existence of "breakpoints" would be less clearly defined and may even be absent.

However, for the gas systems studied, the use of the gas velocity resulted in empirical equations, which represented all the experimental data with only a very slight scatter, compared with the scatter observed, when the relative velocity is used. Therefore their use is justified for calculating pressure drops within the range and systems studied. Any extension to other systems or other gas or liquid velocity ranges would be unwise, because of the apparent absence of physical significance, which can be attached to the "breakpoints".

If extrapolation to other systems is required, the "relative friction factor" versus the "relative Reynolds number" type of correlation is considered more reliable.

TABLE 7.8

EXPERIMENTAL AND CALCULATED DATA

AIR - AQUEOUS SUCROSE SYSTEM

% Sucrose = 45.6
Temperature of Liquid = 23.1°C
Viscosity = 8.9 Centipoise
Density = 1.21 g./c.c.

Gas Velocity ft./sec.	Γ lb./(hr.)(ft.)	Liquid Re	Liquid Velocity ft./sec.	Relative Velocity ft./sec.	ΔP_t cm.H_2O	ΔP_e cm.H_2O	ΔP_d lb./ft.^{2}
2.33	272	50.5	0.51	2.84	0.016	0.004	0.00091
3.46	272	50.5	0.51	3.97	0.034	0.008	0.00197
4.00	272	50.5	0.51	4.51	0.042	0.009	0.00251
5.04	272	50.5	0.51	5.55	0.059	0.013	0.00349
6.52	272	50.5	0.51	7.03	0.086	0.019	0.00508
7.58	272	50.5	0.51	8.09	0.109	0.023	0.00652
8.57	272	50.5	0.51	9.08	0.131	0.028	0.00782
1.78	272	50.5	0.51	2.29	0.012	0.003	0.00068
2.47	272	50.5	0.51	2.98	0.018	0.005	0.00099
3.22	272	50.5	0.51	3.73	0.030	0.007	0.00175
4.05	272	50.5	0.51	4.56	0.043	0.010	0.00250
5.62	272	50.5	0.51	6.13	0.070	0.015	0.00418
5.18	272	50.5	0.51	5.69	0.063	0.013	0.00380
6.41	272	50.5	0.51	6.92	0.082	0.018	0.00485
7.55	272	50.5	0.51	8.06	0.105	0.023	0.00623
8.43	272	50.5	0.51	8.94	0.128	0.027	0.00767

TABLE 7.9

EXPERIMENTAL AND CALCULATED DATA

AIR - TOLUENE SYSTEM

Gas Velocity ft./sec.	Γ lb./(hr.)(ft.)	Liquid Re	Liquid Velocity ft./sec.	Relative Velocity ft./sec.	ΔP_t cm.H_2O	ΔP_e cm.H_2O	ΔP_d lb./ft.^{2}
1.54	14	38.6	0.20	1.74	0.009	0.002	0.000531
2.26	14	38.6	0.20	2.46	0.015	0.004	0.000835
2.95	14	38.6	0.20	3.15	0.023	0.006	0.00129
3.50	14	38.6	0.20	3.70	0.029	0.008	0.00159
5.38	14	38.6	0.20	5.58	0.049	0.015	0.00258
6.10	14	38.6	0.20	6.30	0.065	0.017	0.00364
8.13	14	38.6	0.20	8.33	0.099	0.026	0.00554
8.93	163	450	1.01	9.94	0.146	0.029	0.00883
7.90	163	450	1.01	8.91	0.123	0.025	0.00745
5.70	163	450	1.01	6.71	0.078	0.016	0.00474
4.46	163	450	1.01	5.47	0.056	0.011	0.00342
3.09	163	450	1.01	4.10	0.034	0.006	0.00210
1.65	163	450	1.01	2.66	0.016	0.003	0.00102
		AIR - n-HEPTANE SYSTEM					
1.58	15	60	0.25	1.83	0.011	0.002	0.00068
2.40	15	60	0.25	2.65	0.017	0.005	0.00091
3.60	15	60	0.25	2.85	0.032	0.008	0.00182
5.15	15	60	0.25	5.40	0.052	0.013	0.00296
6.65	15	60	0.25	6.90	0.075	0.020	0.00418
8.58	15	60	0.25	8.83	0.118	0.028	0.00684
1.65	113	450	0.96	2.61	0.012	0.003	0.00071
2.47	113	450	0.96	3.43	0.021	0.005	0.00124
3.84	113	450	0.96	4.80	0.040	0.009	0.00237
3.84	113	450	0.96	4.80	0.041	0.009	0.00245
3.09	113	450	0.96	4.05	0.030	0.006	0.00180
2.09	113	450	0.96	3.05	0.017	0.004	0.00102

7.3 Nomenclature

f	=	Fanning friction factor (dimensionless)
g	=	gravitational conversion factor, ft./sec.^{2}
kg	=	gas film mass transfer coefficient, $\frac{\text{lb.mole}}{(\text{hr.})(\text{ft.}^2)(\text{atm.})}$
ΔP_t	=	pressure drop across whole column, lb./ft.^{2}
ΔP_d	=	pressure drop across a disc (corrected for the column shell), lb./ft.^{2}
ΔP_e	=	pressure drop across the empty column (discs removed), lb./ft.^{2}
Re	=	Reynolds number (dimensionless)
$(Re)_R$	=	"relative Reynolds number" based on the relative velocity of the gas and liquid streams
v	=	average gas velocity, ft./sec.
v_R	=	relative velocity of the gas and liquid streams, ft./sec.
ρ	=	density of the gas, lb./ft.^{3}
μ	=	viscosity of the gas, lb./(ft.)(sec.)
Γ	=	liquid or wetting rate, lb./(hr.)(ft.)
ϕ	=	$v \rho^{0.41} \Gamma^{0.22}$

CHAPTER 8

GAS PHASE MASS TRANSFER

Previous data reported for gas phase mass transfer in a disc column has been determined with air at room temperature as the gas phase (116)(122)(89). To develop a generalised correlation applicable to any gaseous system, further investigation was necessary to establish the effects of the fluid properties on the gas phase transfer process. An experimental program was therefore initiated so that a reliable correlation of gas phase data could be obtained for the disc column. Such a generalised correlation would have been required in the analysis of the zinc absorption in molten lead data, had the disc column proved satisfactory for this application.

The most convenient method of measuring a gas film mass transfer coefficient is to study the rate of vaporisation of a pure liquid in a series of gas phases. As there is no diffusional resistance in the liquid phase in this case, the measured overall mass transfer coefficient is equal to the gas film coefficient.

The rates of vaporisation of water in hydrogen, air, carbon dioxide and dichlorodifluoromethane were studied. The effect of changing the diffusing species was determined by studying the vaporisation of n-heptane in air.

The gas film mass transfer data, thus obtained, was analysed to see if the conventional methods of correlation could be applied to the results and the relation between the gas phase pressure drop and the gas film coefficient was investigated. Any changes in mass transfer characteristics were compared with similar changes in the gas and liquid flow behaviour.

8.1 Apparatus

The apparatus used for this investigation was basically the same as used to determine the gas flow characteristics. The same disc column was used for both studies. Provision was made for withdrawal of samples of inlet and exit gas for analysis. To measure the exit liquid temperature from the discs at low liquid flow rates, where an error would be introduced if the temperature was measured external to the column, as is the usual practice, a copper constantan thermocouple, with cold junction at 0°C, was installed inside the column in the liquid run-off tube just below the last disc.

A general view of the experimental apparatus together with the gas analysis and calibrating system is shown in Fig. 8.1.

8.2 Gas Analysis

The analysis of the exit gas for the concentration of the diffusing component was achieved continuously using a calibrated gas analysis cell operating on the difference of thermal conductivity between the diffusing vapour and the carrier gas. The inlet gas to the column was analysed at the beginning and end of each series of runs, the change in the inlet concentration being too small to warrant continuous analysis.

The principles and electric circuits relating to thermal conductivity gas analysis cells have been outlined by Hamilton (37). The particular cell used for these studies was constructed from portion of an aircraft fuel mixture indicator and was suitably modified so that small partial pressures of the diffusing component could be measured accurately. When thus modified, the cell became extremely sensitive to factors, which for the normal application of thermal conductivity gas analysis, are considered unimportant.

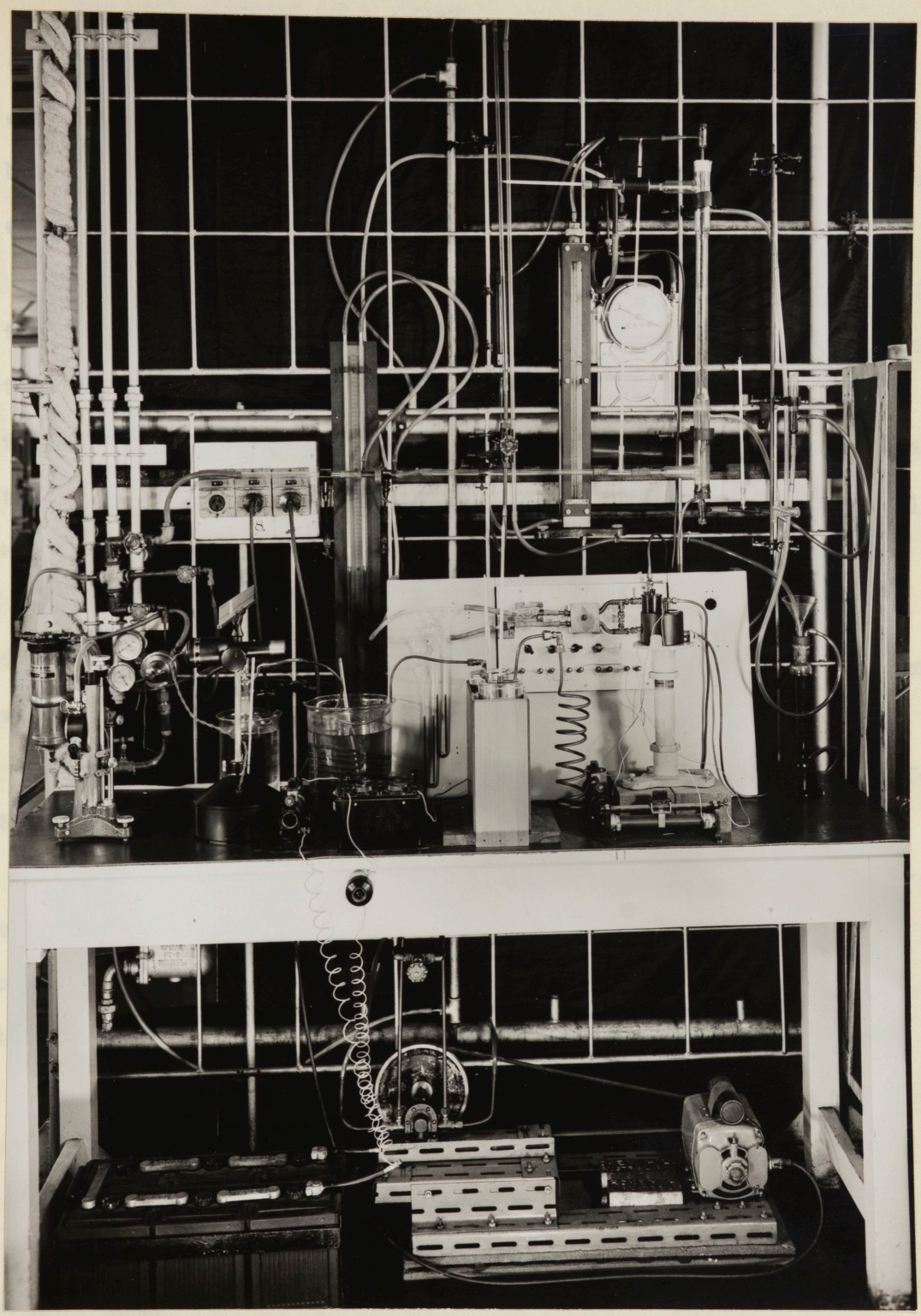

Fig. 8.1 - General view of the apparatus used in the gas phase mass transfer studies

The cell elements were located in a solid brass cube so that any changes in ambient temperature would affect each element to the same extent. Two of the four elements constituting the thermal conductivity bridge operated in an atmosphere of vapour free carrier gas, whilst the other two contained the gas mixture being analysed.

Although there was no direct flow of gas through the elements of the cell, the transport of the gas to the elements being by diffusion through short arms at right angles to the gas flow lines through the cell, the out of balance of the Wheatstone bridge was found to be dependent on the gas flow rate through the cell. This effect, which has apparently not been previously reported, is thought to be due to either:-

(a) Flow past the entrance of the cell elements creating a disturbance which is transmitted in the form of eddies into the element space, thereby altering the boundary conditions.

(b) Flow determining the back pressure in the cell, thereby affecting the heat transfer properties of the gas surrounding the element.

These effects were counteracted by installing two identical orifice meters on the outlets of both the gas streams passing through the cell unit, and maintaining flow of each stream at the same predetermined level throughout the analysis and subsequent calibration.

The gas analysis cell was calibrated by supplying the cell with gas with a known vapour content. The out of balance of the bridge, as indicated by the galvanometer, was found to be linear with the concentration of the vapour at the small concentration levels encountered in this work.

The supply of gas with known vapour contents required for the cell calibration was obtained by saturating the gas with the vapour over a

range of temperatures. The saturation train used is shown in Fig. 8.2.

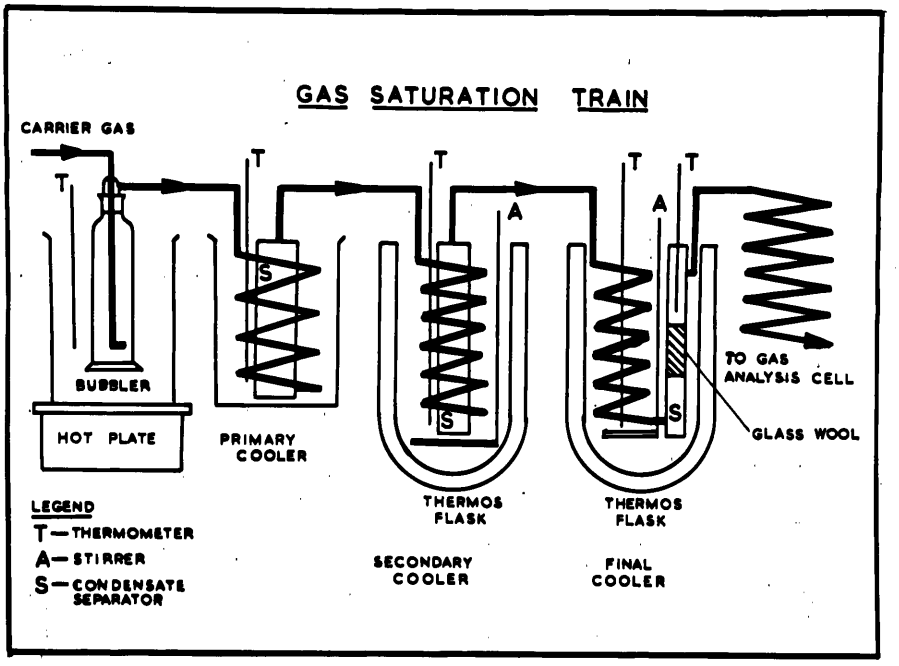

Fig. 8.2 - Gas saturation apparatus used for calibrating thermal conductivity cell

The essential features of this apparatus are summarised:-

(a) The carrier gas was bubbled through a warm bath of the liquid whose vapour is being analysed.

(b) The gas stream was then cooled in three stages by passing through water cooled condensers consisting of coils of copper tubing terminated in condensate separators. These three units were named primary, secondary and final coolers.

(c) The temperature of the water in the primary cooler was maintained between 5° and 10°C below the desired exit gas temperature. The bulk of the condensation load was located in this cooler. The condensate separator of the unit was made larger than those in the later stages, to ensure complete gas-liquid disengagement before passing to the secondary cooler.

(d) In the secondary and final coolers, the condenser units were

placed inside "Thermos" vacuum flasks. The water in these flasks was agitated intermittently with a hand stirrer, to ensure temperature uniformity.

(e) The temperatures of the cooling water in these last stages of condensation were maintained within 1°C of each other, with the final cooler at the lowest temperature of the cooling train. The gas entering the final cooler under these conditions would be very close to the water temperature of the secondary cooler and hence the condensation load on the final cooler would be very small, cooling in this stage being no more than 1°C. This stage-wise condensation followed by separators, plus the slow approach to the final saturation level, was considered necessary to reduce the possibility of mist formation in the gas phase. A plug of glass wool was placed in the separator of the final cooler as a final precaution against carry over liquid droplets or mist into the exit gas stream.

(f) The temperature of the gas emerging from the final cooler was measured with a thermometer. The temperature of the exit gas was rarely more than 0.1°C higher than the water temperature. Under these conditions, errors in the measurement of the true gas temperature due to radiation between the thermometer bulb and the copper wall would be negligible. The gas was considered saturated at the temperature of the exit gas from the final cooler.

(g) To bring the gas stream back to ambient temperature, a copper coil was interposed in the line between the final cooler and the analysis cell.

The gas saturation procedure was checked for the air-water vapour system by gravimetric analysis. The air-water vapour mixture from the

saturation train was passed through three "Nesbitt" absorption bulbs in series. The solid absorbants used were "anhydrone" in the first bulb, followed by phosphorus pentoxide. The volume of air passed through the absorption tubes was measured with a "Boys Bell" wet gas meter. The results of the check and the relevant experimental data are shown in Table 8.1 for three difference water vapour partial pressures.

TABLE 8.1

GRAVIMETRIC CHECK ON SATURATION PROCEDURE

Test	1	2	3
Saturation Train			
Bubbler Temp. (°C)	39.2	36.5	33.5
Primary Cooler Temp. (°C)	23.6	16.0	12.5
Secondary Cooler Temp. (°C)	21.4	13.3	4.9
Final Cooler Temp. (°C)	20.7	12.8	4.3
Exit Air Temp. (°C)	20.8	12.90	4.4
p Saturation (mm. Hg)	18.40	11.16	6.27
Gravimetric Analysis			
Vol. of Air Passed ($ft.^3$)	1/6	1/6	1/6
Time taken to pass Air (min.)	12.5	8	5
Temp. of Air at Meter	26.5	27.0	27.0
Increase in Nesbitt Bulbs wt. (g.)	0.079	0.049	0.027
p Gravimetric (mm. Hg)	17.5	10.8	6.18
% Difference $= \frac{\text{p sat'n} - \text{p grav.}}{\text{p grav.}}$	+5.1%	+3.3%	+1.5%

An example of a calibration graph, obtained for the gas analysis cell using the saturation calibration technique, is shown for mixtures of water vapour and air in Fig. 8.3. All the calibration graphs obtained for the various gaseous mixtures were found to be linear at these low concentration levels.

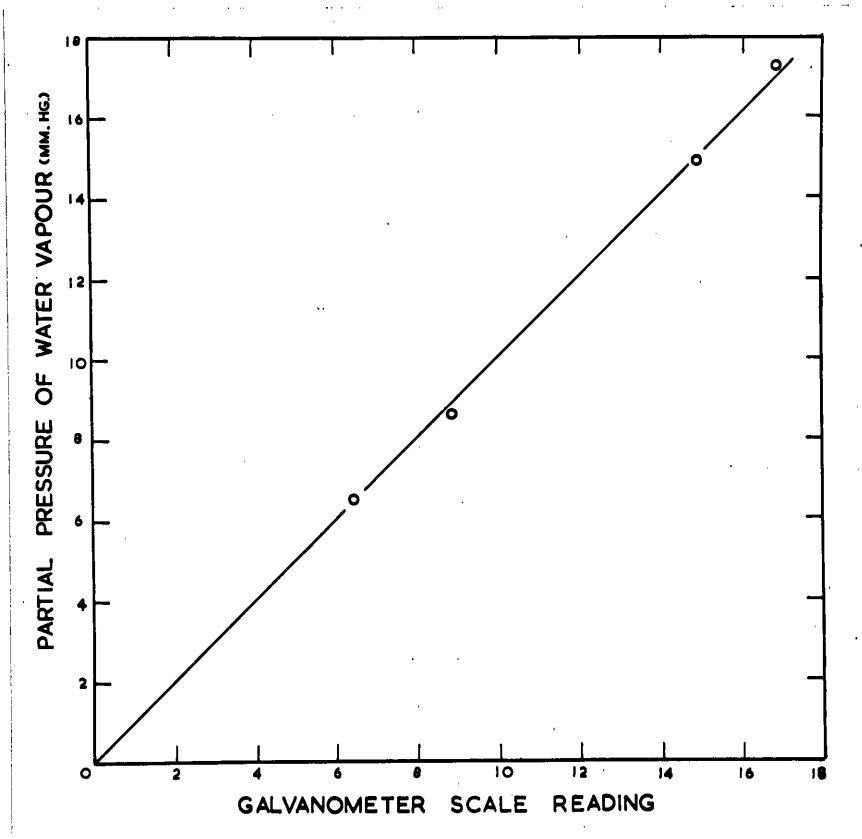

Fig. 8.3 - Typical calibration graph for air-water system

8.3 Experimental Results

The experimental data obtained by studying the countercurrent vaporisation of water in hydrogen, air, carbon dioxide and dichlorodifluoromethane and the data for the vaporisation of n-heptane in air are shown in Tables 8.2, 8.3, 8.4, 8.5 and 8.6.

TABLE 8.2

VAPORISATION OF WATER WITH HYDROGEN

Run	Liquid Rate $\frac{lb.}{(hr.)(ft.)}$	Gas Rate $\frac{ft^3}{min.}$	Partial Pressure of Diffusing Component (mm. Hg.)		Temperatures (°C)			
			Inlet	Outlet	Liquid Inlet	Liquid Outlet	Gas Inlet	Gas Outlet
1A	325	1.50	0.4	13.8	25.4	24.4	26.3	25.9
2A	325	2.75	0.5	11.4	25.4	23.8	26.2	25.6
3A	325	3.55	0.5	10.7	25.4	23.5	26.2	25.5
4A	325	4.25	0.6	10.1	25.4	23.1	25.9	25.3
5A	325	4.95	0.7	9.5	25.4	22.8	25.4	25.2
1B	325	2.40	0.4	11.5	25.1	23.6	25.9	25.2
2B	325	3.75	0.4	10.1	25.1	23.0	26.0	25.0
3B	325	4.30	0.5	9.8	25.1	22.8	26.2	25.0
4B	325	6.30	0.5	9.0	25.1	22.0	26.0	24.7
5B	325	7.80	0.6	8.5	25.1	21.5	25.0	24.2
6B	325	5.65	0.6	9.2	25.1	22.0	23.8	24.0
7B	325	4.55	0.7	9.8	25.0	22.5	23.6	24.2
8B	325	2.95	0.7	11.3	25.0	23.1	24.0	24.6
9B	325	1.62	0.7	13.4	25.0	23.8	24.8	25.1

TABLE 8.3

VAPORISATION OF WATER WITH AIR

Run	Liquid Rate $\frac{lb.}{(hr.)(ft.)}$	Gas Rate $\frac{ft.^3}{min.}$	Partial Pressure of Diffusing Component (mm. Hg.)		Temperatures (°C)			
			Inlet	Outlet	Liquid Inlet	Liquid Outlet	Gas Inlet	Gas Outlet
1C	325	2.40	2.6	11.8	24.0	22.6	23.5	23.6
2C	325	2.10	2.6	12.3	24.0	22.8	23.5	23.7
3C	325	1.80	2.6	12.5	24.0	22.9	23.6	23.7
4C	325	1.45	2.6	13.4	24.0	23.0	23.6	23.8
5C	325	1.12	2.6	14.3	24.0	23.1	23.6	23.8
6C	325	0.78	2.6	14.8	23.9	23.2	23.5	23.7
7C	325	0.56	2.6	16.4	23.9	23.3	23.4	23.7
8C	325	0.36	2.6	18.6	23.8	23.4	23.1	23.5
1D	298	0.50	2.8	18.9	26.2	25.6	24.9	25.2
2D	240	0.50	2.8	18.6	26.1	25.4	24.6	24.9
3D	149	0.50	2.8	18.1	25.8	24.8	24.0	24.3
4D	64	0.50	2.8	16.5	25.3	23.6	23.9	24.0
1E	298	0.70	2.8	15.2	23.5	22.8	21.6	22.2
2E	240	0.70	2.8	15.0	23.5	22.6	21.9	22.3
3E	149	0.70	2.8	14.2	23.2	22.1	21.9	22.2
4E	64	0.70	2.8	13.2	22.8	21.0	21.6	21.8
5E	298	1.10	2.6	12.9	22.7	21.8	21.1	21.5
6E	240	1.10	2.6	12.7	22.9	21.9	21.1	21.6
7E	149	1.10	2.6	12.1	22.7	21.3	21.1	21.4
8E	64	1.10	2.6	11.3	22.2	19.8	20.7	20.7
1F	298	1.40	2.8	12.1	22.8	21.8	21.0	21.8
2F	240	1.40	2.8	11.8	22.8	21.6	21.3	22.1
3F	149	1.40	2.8	11.5	22.9	21.4	21.5	22.2
4F	64	1.40	2.8	10.7	22.7	20.1	21.8	22.0
5F	298	1.73	2.8	11.7	23.0	22.0	22.2	22.6
6F	240	1.73	2.8	11.1	23.0	21.8	22.3	22.6
7F	149	1.73	2.8	10.6	23.0	21.3	22.4	22.5
8F	64	1.73	2.8	10.2	23.0	20.0	22.4	22.3

TABLE 8.4

VAPORISATION OF WATER WITH CARBON DIOXIDE

Run	Liquid Rate $\frac{lb.}{(hr.)(ft.)}$	Gas Rate $\frac{ft.^3}{min.}$	Partial Pressure of Diffusing Component (mm. Hg.)		Temperatures (°C)			
			Inlet	Outlet	Liquid Inlet	Liquid Outlet	Gas Inlet	Gas Outlet
1G	325	0.44	1.6	18.8	26.7	26.2	29.4	29.4
2G	325	0.53	1.7	18.4	26.9	26.3	29.1	29.2
3G	325	0.60	1.9	16.7	26.9	26.3	29.0	29.3
4G	325	1.07	2.3	14.2	26.9	26.0	26.7	28.6
5G	325	0.82	2.5	16.4	27.0	26.2	27.5	29.2
6G	325	0.72	2.7	17.1	27.0	26.4	28.3	29.7
7G	325	0.61	2.8	17.5	27.0	26.5	29.0	30.0
8G	325	0.48	2.9	18.4	27.0	26.6	29.9	30.5
9G	325	0.32	3.1	19.8	27.1	26.8	31.0	31.0
10G	325	0.26	3.2	21.5	27.1	26.9	31.0	31.2

TABLE 8.5

VAPORISATION OF WATER WITH DICHLORODIFLUOROMETHANE

Run	Liquid Rate $\frac{lb.}{(hr)(ft.)}$	Gas Rate $\frac{ft.^3}{min.}$	Partial Pressure of Diffusing Component (mm. Hg.)		Temperatures (°C)			
			Inlet	Outlet	Liquid Inlet	Liquid Outlet	Gas Inlet	Gas Outlet
1H	325	0.18	0	15.8	23.1	22.8	20.8	21.2
2H	325	0.27	0	13.7	23.1	22.8	20.5	21.3
3H	325	0.33	0	13.4	23.1	22.7	20.3	21.4
4H	325	0.32	0	13.6	23.1	22.6	20.5	21.3
5H	325	0.45	0	12.5	23.1	22.5	20.2	21.3
6H	325	0.24	0	15.1	23.1	22.7	20.2	21.3
7H	325	0.23	0	14.4	23.1	22.7	20.2	21.3

TABLE 8.6

VAPORISATION OF n-HEPTANE WITH AIR

Run	Liquid Rate $\frac{lb.}{(hr.)(ft.)}$	Gas Rate $\frac{ft.^3}{min.}$	Partial Pressure of Diffusing Component (mm. Hg.)		Temperatures (°C)			
			Inlet	Outlet	Liquid Inlet	Liquid Outlet	Gas Inlet	Gas Outlet
1J	113	0.48	0	28.5	30.0	26.7	27.0	28.0
2J	113	0.72	0	22.0	28.5	24.9	26.8	26.9
3J	113	1.12	0	16.7	27.2	23.0	26.6	25.8
4J	113	1.12	0	17.5	27.7	23.4	25.7	25.8
5J	113	0.90	0	17.3	26.1	22.5	25.1	24.7
6J	113	0.61	0	20.4	25.0	22.2	24.5	24.0
1K	89	0.72	0	20.0	27.9	23.9	26.7	26.4
2K	89	1.12	0	15.5	26.9	22.4	26.6	25.6
3K	89	1.42	0	13.6	26.5	21.5	26.3	25.0
4K	89	1.12	0	17.8	29.6	24.5	26.0	26.7
5K	89	0.90	0	16.0	25.6	21.5	24.9	24.2
6K	89	0.61	0	18.4	24.7	21.6	24.4	23.9
1L	50	0.62	0	12.6	19.6	15.0*	17.0	17.2
2L	50	0.86	0	10.3	18.7	13.2*	16.5	16.2
3L	50	1.18	0	9.0	18.7	12.5*	16.1	16.0
4L	50	1.45	0	8.1	18.5	11.5*	16.0	15.6
5L	50	1.77	0	7.4	18.2	10.7*	15.5	15.0
6L	50	2.14	0	6.8	18.3	10.3*	15.4	14.8
1M	15	0.46	0	8.0	13.7	7.5*	12.8	12.3
2M	15	0.70	0	6.1	13.1	5.5*	12.5	11.0
3M	15	1.05	0	4.8	12.7	4.0*	12.2	10.0
4M	15	1.50	0	4.2	12.3	3.0*	11.3	9.2
5M	15	1.94	0	3.8	12.2	3.2*	11.7	9.3
6M	15	2.50	0	3.2	12.4	3.2*	11.7	9.0

* These temperatures measured close to the last disc by Copper-Constantan thermocouple with cold junction at 0°C.

8.4 The True Mean Driving Force

To compute the gas film mass transfer coefficient from the vaporisation experiments, the true driving force for mass transfer in the column under the actual conditions of the particular vaporisation run, must be established. This means that the gas-liquid interfacial temperature must be known as a function of the amount of the liquid vaporised in the column. If the relationship is available or can be calculated, the true mean driving force can be obtained by graphical integration of a plot of driving force versus amount of material transferred.

The technique of making the liquid enter the system at the wet bulb temperature has been used by several investigators studying vaporisation in wetted wall columns. In this case, the temperature of the liquid remains constant throughout the column, the heat required for vaporisation being just balanced by the supply of sensible heat from the gas and hence there is no flow of heat into or from the bulk of the liquid and therefore no temperature gradient in the liquid phase. The consequence of this is that the gas-liquid interfacial temperature is known and constant and, therefore, the relation between driving force and material vaporised in the column is linear. This linear relationship, between the quantity transferred and the driving force, allows direct use of the log. mean of the terminal driving forces, as the true mean driving force for the whole column.

The use of the log. mean terminal driving force in cases, where the driving force is not linear with the amount transferred, is not theoretically correct. However, in many cases, the coefficient so obtained varies only slightly from the true coefficient based on the

true mean driving force. Before the log. mean driving force is used, the more complicated procedure of evaluating the true mean driving force must be resorted to, so that the extent of the error introduced by using the log. mean of the terminal driving forces, can be ascertained.

8.4.1 Simultaneous Heat and Mass Transfer

Simultaneous heat and mass transfer occurs when a liquid is evaporated in a gas stream. The theoretical aspects of this subject have been adequately covered by Sherwood and Pigford (99) and other standard texts on mass transfer.

The heat being conducted away from the gas-liquid interface, by the vapour molecules diffusing into the bulk of the gas phase, may be neglected for the case of the dilute systems studied in this investigation, without the introduction of any appreciable error. Making this assumption, it is possible to consider the processes of heat and mass transfer as being independent of each other. Under steady state conditions, the simultaneous heat and mass transfer processes occurring at any point within the column can be represented by diagrams such as Figs. 8.4 and 8.5.

These two diagrams indicate the most common states existing in the vaporisation studies reported in this investigation.

At the top of the column the liquid is at a higher temperature than the gas leaving the column. Hence as shown in Fig. 8.4, latent heat and sensible heat are gained by the gas phase. This heat is supplied by the sensible heat of the liquid. The heat balance is represented by equation 8.1.

$$h_L(t_L - ti) - hg\ (ti - tg) = kgM_A\lambda\ (pi - pg) \qquad \ldots\ldots\ 8.1$$

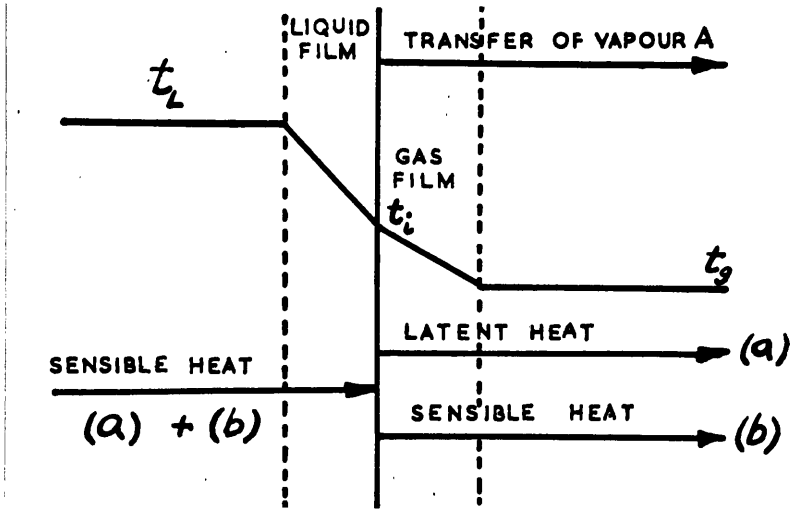

Fig. 8.4 - Conditions at top of column

As the liquid passes through the column, the temperature drops until the liquid temperature is below the gas temperature. Thereafter, sensible heat is transferred to the liquid interface from the gas phase. Sensible heat is also transferred from the bulk of the liquid to the interface. Hence conditions at the bottom of the column would be as illustrated in Fig. 8.5.

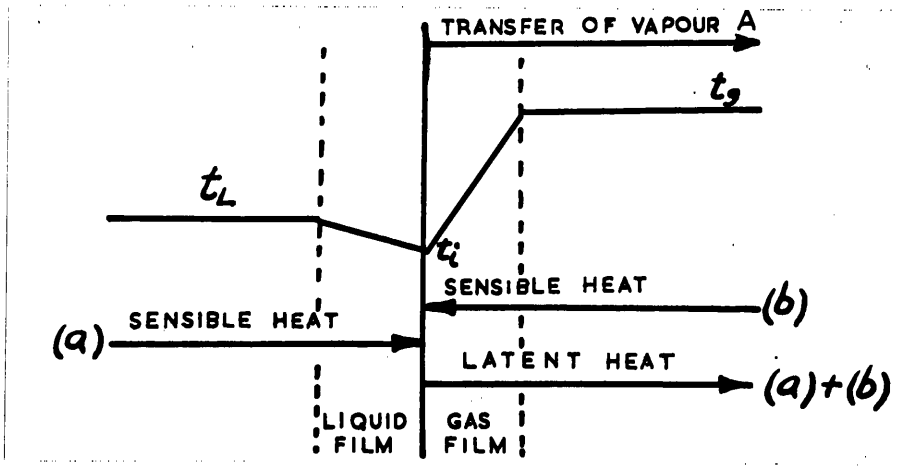

Fig. 8.5 - Conditions at bottom of column

The heat balance for the condition at the bottom of the column can be represented by equation 8.2.

$$h_L (t_L - t_i) + h_g (t_g - t_i) = k_g M_A \lambda (p_i - p_g) \quad \ldots\ldots 8.2$$

Other possibilities exist, as, for example, the liquid may be cooled down to the wet bulb temperature, in which case, the sensible heat supplied to the interface from the gas phase is just sufficient to account for the heat required for vaporisation. In this case, the heat balance becomes

$$h_g (t_g - t_i) = k_g M_A \lambda (p_i - p_g) \quad \ldots\ldots 8.3$$

Depending on the temperature of the gas and liquid phases, it is also possible to have conditions at the bottom of the column as shown in Fig. 8.4, or when the liquid feed to the column is colder than the gas exit temperature, conditions as shown by Fig. 8.5 will exist at the top of the column.

To determine the true mean driving force, it is necessary that the variation of driving force with the amount transferred be known.

The amount of mass transferred is related directly to the partial pressure of the diffusing component p_g. The driving force, at any point in the column, is the difference $(p_g - p_i)$ and hence provided the temperature at the interface is known and assuming equilibrium at the interface, the desired relationship between the amount transferred and the driving force can be evaluated, if the relation of p_g and t_i or p_g and p_i can be calculated (p_i and t_i are fixed by the equilibrium conditions for the system).

For a particular point in the column, at which the bulk temperatures of the gas and liquid phases and the partial pressure of the diffusing component p_g are known or can be calculated, and if the mass and heat

transfer coefficients can be estimated, the temperature t_i and the equilibrium partial pressure of the diffusing component can be calculated by application of equations 8.1 or 8.2, depending on the temperature of the liquid with respect to the gas temperature.

8.4.2 Estimation of Film Heat Transfer Coefficients

Gas and liquid film heat transfer coefficients in a disc column have not been determined experimentally. However, to interpret the vaporisation data, knowledge is required of the interfacial temperature of the evaporating liquid. To estimate this interfacial temperature, a knowledge of the liquid and gas film heat transfer coefficients is required.

Chilton and Colburn (11) have suggested an equality between the heat transfer factor j_H and the mass transfer factor j_D, which are defined by

$$j_H = \frac{h}{Cp \rho v} \left(\frac{Cp \mu}{k} \right)^{2/3} = \tfrac{1}{2} f \qquad \ldots\ldots 8.4$$

$$j_D = \frac{k_c \, PBM}{v \quad P} \left(\frac{\mu}{\rho D} \right)^{2/3} = \tfrac{1}{2} f \qquad \ldots\ldots 8.5$$

The equality of j_D, j_H and $\frac{1}{2} f$ has been shown experimentally for turbulent flow through tubes and across plane surfaces. However, for turbulent flow around a cylinder

$$j_D = j_H < f/2 \qquad \ldots\ldots 8.6$$

This difference is because of "form drag" as distinct from skin friction. However, theequality of $j_D = j_H$ is usually considered to hold irrespective of the departure from $f/2$.

The bulk of the experimental verification of the use of the j_D and j_H factors has been for "gas film" transfer, for which the range of the Schmidt number has been in the order of 0.5 - 2.5. However, there have

been two recent sets of data, which have extended the range of the Schmidt number, by studying "liquid film" data for the case of mass transfer inside a pipe.

Linton and Sherwood (60), in 1950, studied the dissolution by water of tubes constructed from cinnamic acid, benzoic acid and β naphthol. The Schmidt number in this investigation ranged from 1000 to 3000. Although the spread of j_D values was considerable, the results agreed moderately well with predicted values based on the equality $j_D = j_H = f/2$ for smooth pipes.

The dissolution of a zinc tube, by the forced convection flow of mercury through the tube, was reported by Dunn, Bonilla, Ferstenberg and Gross (20) in 1956. The value of the Schmidt number in this case was in the order of 83. Values of j_D compared well with the classic Chilton-Colburn equation for heat transfer when modified for mass transfer.

In the light of these two experimental investigations, it would appear that the j-factor equations, as proposed by Chilton and Colburn, are not restricted to Schmidt numbers in the range in which earlier investigations had been made.

(a) Estimation of the Liquid Film Heat Transfer Coefficient

The most recent data for liquid film mass transfer in a disc column were reported by Taylor and Roberts (122). Although this data was different to that reported earlier by Stephens and Morris (116), it is considered that the former data may be more precise. Taylor and Roberts observed a distinct change in slope when the liquid film coefficient was plotted versus the liquid rate. This breakpoint in liquid film mass transfer data occurs at approximately the same liquid rate, as

the departure from theoretical streamline flow behaviour, as observed by the author.

Because of the consistency existing between the author's experiments and the data reported by Taylor and Roberts, the estimation of h_L was based on the data given by these authors.

TABLE 8.7

(i) VALUES OF h_L FOR WATER FLOWING OVER DISCS

CALCULATED ASSUMING $j_D = j_H$

BASED ON MASS TRANSFER DATA OF TAYLOR AND ROBERTS

Liquid Rate lb./(hr.)(ft.)	k_L lb./(hr.)(ft.^{2})(lb./ft.^{3}) CO_2 Absorption in Water	h_L (Calculated) Liquid Film Heat Transfer Coefficient B.T.U./(hr.)(ft.^{2})(^oF)
50	0.60	720
100	0.78	936
200	1.10	1320
400	2.20	2640

(ii) h_L CALCULATED FOR n-HEPTANE FLOWING OVER

DISCS AT Γ = 15 lb./(hr.)(ft.)

$$h_L = 262 \text{ B.T.U./(hr.)(ft.}^2\text{)(}^oF\text{)}$$

(b) Estimation of the Gas Film Heat Transfer Coefficient

The gas film heat transfer coefficient can be calculated, to a first approximation, by assuming $j_D = j_H$. The value of j_D is obtained using the uncorrected gas film mass transfer coefficient. This uncorrected coefficient is the experimentally determined coefficient based on a driving force, which is assumed to be equal to the log. mean driving force of the terminal conditions, and further assuming the bulk liquid temperature to be the same as the temperature at the gas - liquid interface.

$$j_D = \frac{k_g \, p_{BM}}{G_m} \left(\frac{\mu}{\rho D}\right)^{2/3} \qquad \ldots\ldots 8.7$$

$$j_H = \frac{h_g}{C_p \rho v} \left(\frac{C_p \mu}{k}\right)^{2/3} \qquad \ldots\ldots 8.8$$

Whence if system is very dilute ($p_{BM} = 1$) and $j_D = j_H$

$$h_g = k_g M_B C_p \left\{\frac{\frac{\mu}{\rho D}}{\frac{C_p \mu}{k}}\right\}^{2/3} \qquad \ldots\ldots 8.9$$

The value h_g, so obtained, can then be used in conjunction with the liquid film heat transfer coefficient and the uncorrected gas film mass transfer coefficient, to determine the true gas-liquid interfacial temperatures throughout the column and hence the true driving force can then be established. The mass transfer coefficient based on this true driving force can then be used as a better approximation for evaluating the gas film heat transfer coefficient and the calculations then repeated to enable a better estimate to be made of the gas film mass transfer coefficient.

8.4.3 Calculation of the True Mean Driving Force

The most serious error introduced by using the log. mean of the terminal driving forces, based on bulk liquid temperatures, rather than the true mean driving force, will occur under the following conditions:-

i) When the liquid film heat transfer coefficient is small.

ii) When the temperature difference between liquid in and liquid out of the column is large.

Both these factors are aggravated at very low liquid rates. Therefore, it was decided to analyse the data for the evaporation of n-heptane, which was carried out at an extremely low liquid rate compared to the other vaporisation data, to see to what extent error is introduced, if the more simple log. mean driving force is used rather

the laborious evaluation of the true mean driving force.

A complete analysis of two of the n-heptane vaporisation runs, one at a low and one at high gas throughput, is presented to indicate the approach used. The physical properties of n-heptane used in the calculations are listed in Table 8.8.

TABLE 8.8

PHYSICAL PROPERTIES OF n-HEPTANE

	Source
Viscosity at 68°F = 0.41 centipoise	Spiers (114)
Specific Gravity = 0.68	Perry (85)
Molecular Weight = 100	
Latent Heat at 57°F = 160 B.T.U./lb.	McAdams (71)
Specific Heat at 57°F = 0.55 B.T.U./(lb.)(°F)	Spiers (114)
Prandtl Number at 57°F = 5.8	McAdams (72)
Vapour Pressures interpolated by log. p versus $\frac{1}{T}$ from the following data:-	
Vapour Pressure (mm. Hg) / Temperature °C	Stull (117)
10 / -2.1	
20 / 9.5	
40 / 22.3	
60 / 30.6	

CASE 1.

VAPORISATION OF n-HEPTANE AT LOW LIQUID RATE AND LOW GAS THROUGHPUT

(a) Experimental Data:

Liquid Rate	=	14.7 lb./(hr.)(ft.) ≡ 1.8 lb./hr.
Air Rate	=	0.46 ft.^{3}/min. ≡ 2.07 lb./hr.
Liquid Inlet Temp.	=	56.7 °F
Liquid Outlet Temp.	=	45.5 °F
Gas Inlet Temp.	=	55.0 °F
Gas Outlet Temp.	=	54.1 °F
Partial Pressure of n-heptane in Outlet Gas	=	8.0 mm. Hg

(b) Calculated Data:

Vaporisation Rate	=	0.75 x 10^{-3} lb.moles./hr.
Log. Mean Driving Force	=	17.65 mm. Hg
Uncorrected Gas Film Mass Transfer Coefficient	=	0.200 lb.moles./(hr.)(ft.^{2})(atm.)
Gas Film Heat Transfer Coefficient	=	2.74 B.T.U./(hr.)(ft.^{2})(°F)
Liquid Film Heat Transfer Coefficient	=	262 B.T.U./(hr.)(ft.^{2})(°F)
Overall Heat Balance (Neglecting Radiation from Surroundings) Expressed as % of heat required for vaporisation	=	92.5%

(c) Estimation of Interfacial Temperatures

(1) Conditions at Top of Column

Sensible heat from the liquid must supply the sensible heat transferred to the gas and the latent heat required for the vaporisation. Therefore, equation 8.1 will apply:-

$$h_L (t_L - t_i) = h_g (t_i - t_g) + k_g M_A \lambda (p_i - p_g)$$

Assume t_i = 56.4, $\therefore$ p_i = 25.2 mm. Hg

L.H.S. = 262 (56.7 - 56.4)
= 78.6

R.H.S. = 2.74 (56.4 - 54.1) + $\frac{0.200 \times 100 \times 160}{760}$ (25.2 - 8)
= 6.3 + 71.5
= 77.8

$\therefore$ Interface Temperature at Top = 56.4°F

(2) Conditions at Bottom of Column

The latent heat required for vaporisation is derived from the sensible heat of the gas and the liquid. Therefore, equation 8.2 will apply:-

$$h_L (t_L - t_i) + h_g (t_g - t_i) = k_g M_A \lambda (p_i - p_g)$$

Assume t_i = 45.3, $\therefore$ p_i = 17.7 mm. Hg.

L.H.S. = 262 (45.5 - 45.3) + 2.74 (55 - 45.3)
= 52.3 + 26.5
= 78.8

R.H.S. = $\frac{0.200 \times 100 \times 160}{760}$ (17.7 - 0)
= 74.5

$\therefore$ Interface Temperature at Bottom of Column = 45.3°F

(d) Error Introduced by Assuming Bulk Liquid Temperature = Interface Temperature

(i) Log. Mean of Terminal Driving Forces based on Bulk Liquid Temperatures

= 17.65 mm. Hg.

(ii) Log. Mean of Terminal Driving Forces based on Interface Temperatures

= 17.45 mm. Hg.

$\therefore$ Percent Error Based on (ii) = 1.15%

Hence the use of bulk liquid temperatures rather than calculated interfacial temperatures, for this run, introduced an error, which is insignificant considering the experimental error associated with the data. Therefore, for the sake of simplification of calculations, the bulk liquid temperatures have been used to evaluate the true mean driving force in the next calculation.

(e) Calculation of the Variation of Liquid Temperature with the Amount Vaporised

The liquid temperature at any point within the column, corresponding to a known amount of

vaporisation, can be calculated by a trial and error stepwise procedure, starting at the bottom of the column, where the amount transferred is zero or starting at the top of the column, where the amount transferred is 100%. The vaporisation is considered to take place in a definite number of equal steps. By analysing the direction of the sensible heat transfer terms, depending on the relative gas and liquid temperatures, a heat balance can be established over each of these vaporisation steps. Trial and error calculations are made on each step until the assumed liquid temperature balances the heat terms. The heat transferred to the liquid by radiation from the surroundings is small compared to the other heat terms and is therefore neglected in these calculations.

Vaporisation Rate = 0.75×10^{-3} lb.moles/hr.

Consider the vaporisation in five steps each of 0.15×10^{-3} lb.moles/hr. The column is then considered in five steps A, B, C, D, E shown in the diagram:-

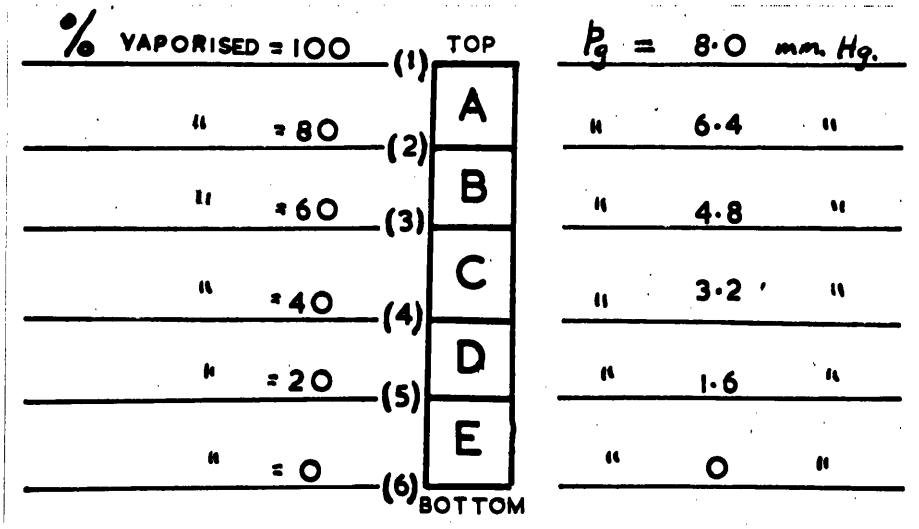

Example

Calculation of $(t_L)_5$

Consider Step E

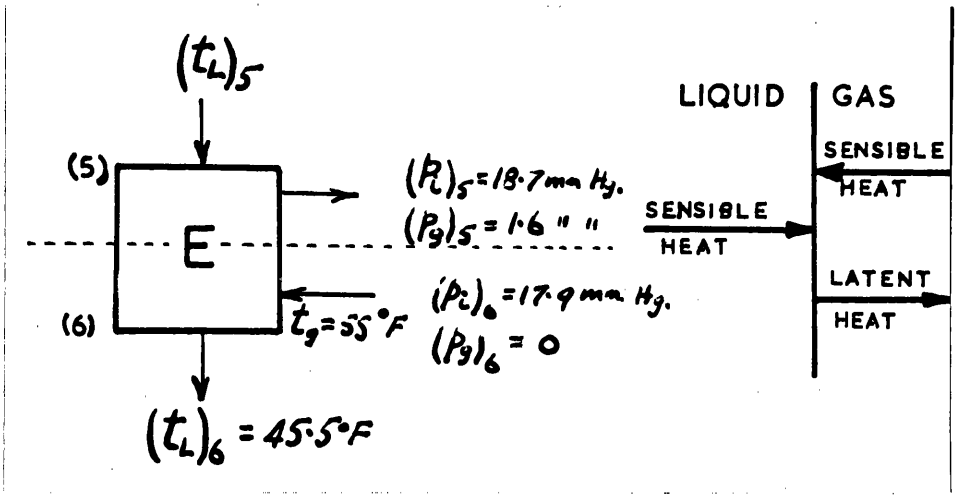

An estimate of $(t_L)_5$ can be obtained by considering the percentage of the total heat to be transferred, which is being contributed by loss of sensible heat of the liquid under the known conditions at (6). This has been evaluated previously when the interfacial temperature at (6) was calculated.

$$\text{At (6)} \quad \frac{\text{Heat Transferred from Liquid}}{\text{Heat Transferred from Gas + Heat Transferred by Liquid}} = \frac{52.3}{26.5 + 52.3} = 66.5\%$$

Heat Required to Evaporate 0.15×10^{-3} lb.moles./hr.
$= 0.15 \times 10^{-3} \times 100 \times 160$ B.T.U./hr.
$= 2.4$ B.T.U./hr.

$\therefore$ Loss of Sensible Heat of Liquid between (5) and (6)

$$\doteq 2.4 \times \frac{66.5}{100} = 1.6 \text{ B.T.U./hr.}$$

$$= m_L s_L \left[(t_L)_5 - (t_L)_6\right]$$

$$= 1.8 \times 0.55 \left[(t_L)_5 - 45.5\right]$$

$\therefore$ $(t_L)_5 \doteq 47.1$ °F

$\therefore$ As first approximation assume $(t_L)_5 = 47.1$ °F

Mean Driving Force for Vaporisation across E

$(p_i)_5 = 18.7$
$(p_g)_5 = 1.6$ Driving Force at (5) = 17.1

$(p_i)_6 = 17.9$
$(p_g)_6 = 0$ Driving Force at (6) = 17.9

$\therefore$ Mean Driving Force = 17.5 mm. Hg.

Calculation of Area E

$$N_A = k_g A (\Delta p)_m$$
$$\therefore 0.15 \times 10^{-3} = 0.20 \times A \times \frac{17.5}{760}$$
$$\therefore A = 0.0325 \text{ ft.}^2$$

Sensible Heat Transferred from Gas over this Area

$$\text{Sensible Heat Transferred} = h_g A (\Delta t)_m = m_g s_g \left[(t_g)_6 - (t_g)_5\right]$$

$$(\Delta t)_m = \frac{(t_g)_6 - (t_L)_6 + (t_g)_5 - (t_L)_5}{2} = \frac{55.0 - 45.5 + (t_g)_5 - 47.1}{2}$$

$$\therefore \frac{27.4 \times 0.0325}{2}\left[(t_g)_5 - 37.6\right] = 2.07 \times 0.24 \times \left[55.0 - (t_g)_5\right]$$

$$\therefore (t_g)_5 = 53.5 \text{ }^{\circ}\text{F}$$

$\therefore$ Sensible Heat Supplied by Gas = 2.07 x 0.24 x (55 - 53.5)
= 0.745 B.T.U./hr.

Sensible Heat Supplied by Liquid

By Heat Balance:- (Basis One Hour)
Heat Required for Vaporisation = Sensible Heat Supplied by Gas + Sensible Heat Supplied by Liquid

i.e. 2.4 = 0.745 + Sensible Heat Supplied by Liquid

$\therefore$ Sensible Heat Supplied by Liquid = 1.65 B.T.U./hr.

Temperature of Liquid at (5)

Sensible Heat Supplied by Liquid = $m_L \; s_L \left[(t_L)_5 - (t_L)_6 \right]$

$\therefore \; 1.65 = 1.8 \times 0.55 \left[(t_L)_5 - 45.5 \right]$

$\therefore \; (t_L)_5 = 47.2 \; ^oF$

Original assumption of $(t_L)_5 = 47.1 \; ^oF$

The procedure could then be repeated using assumption $(t_L)_5 = 47.2^oF$ However, as the assumed original value and the calculated value are so close, further calculation is unnecessary.

$\therefore$ Temperature of Liquid at (5) = 47.2 ^oF

(f) Evaluation of the True Mean Driving Force

The trial and error procedure, illustrated for the calculation of the liquid temperature at position (5) in the column, is repeated stepwise throughout the column. The results of these calculations are shown in Table 8.9, in which the true driving force is shown as a function of the mass transferred. The bulk liquid temperatures were used, as it has been shown earlier, that the error introduced by not calculating the interface temperatures is negligible.

TABLE 8.9

TRUE DRIVING FORCE VARIATION WITH % TRANSFERRED

CASE 1. EVAPORATION OF n-HEPTANE WITH AIR LOW LIQUID RATE, LOW GAS THROUGHPUT

% of Total Transfer	Liquid Temp. (^oF)	P_i (mm. Hg.)	P_g (mm. Hg.)	True Driving Force (mm. Hg.)
0	45.5	17.9	0	17.9
20	47.2*	18.8	1.6	17.2
40	49.2*	20.0	3.2	16.8
60	51.4*	21.4	4.8	16.6
80	54.1*	23.4	6.4	17.0
100	56.7	25.4	8.0	17.4

(* Calculated Liquid Temperatures)

The true mean driving force is obtained by the graphical integration of a plot of driving force versus the amount transferred. Such a plot is shown in Fig. 8.6.

From the graphical integration of this diagram, the true mean driving force for Case 1 equals 17.01 mm. Hg.

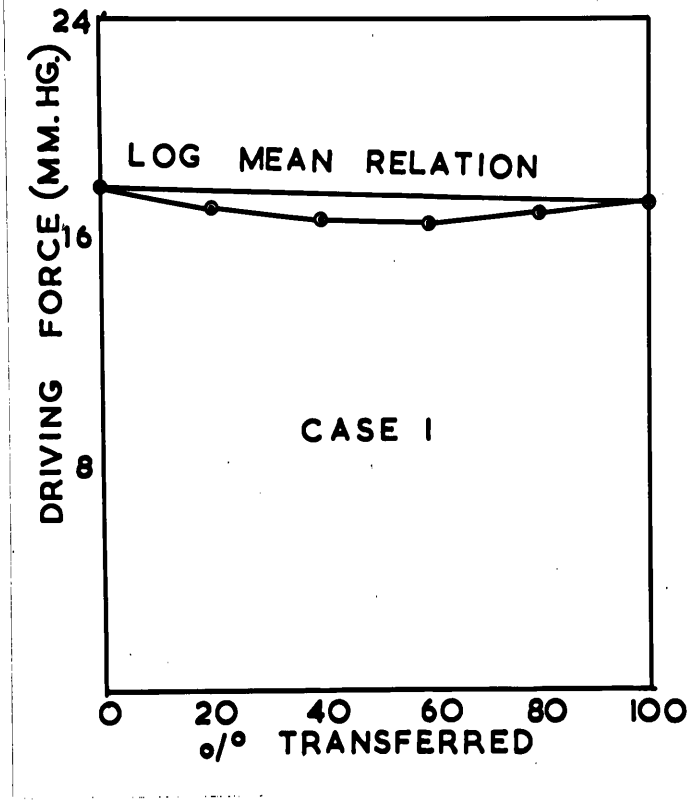

Fig. 8.6 - Graphical determination of the true mean driving force

CASE 2.

VAPORISATION OF n-HEPTANE AT LOW LIQUID RATE AND HIGH GAS THROUGHPUT

(a) Experimental Data:

Liquid Rate	=	14.7 lb./(hr.)(ft.) ≡ 1.8 lb./hr.
Air Rate	=	2.5 $ft.^3$/min. ≡ 11.23 lb./hr.
Liquid Inlet Temp.	=	54.3 °F
Liquid Outlet Temp.	=	37.8 °F
Gas Inlet Temp.	=	53.0 °F
Gas Outlet Temp.	=	48.2 °F
Partial Pressure of n-heptane in Outlet Gas	=	3.2 mm. Hg.

(b) Calculated Data:

Vaporisation Rate	=	1.62×10^{-3} lb.moles./hr.
Log. Mean Driving Force	=	16.90 mm. Hg.
Uncorrected Gas Film Mass Transfer Coefficient	=	0.448 lb.moles./(hr.)$(ft.^2)$(atm.)
Gas Film Heat Transfer Coefficient	=	6.15 B.T.U./(hr.)$(ft.^2)$(°F)
Liquid Film Heat Transfer Coefficient	=	262 B.T.U./(hr.)$(ft.^2)$(°F)
Overall Heat Balance (Neglected Radiation from Surroundings) Expressed as % of Heat Required for Vaporisation	=	112%

(c) Estimation of Interfacial Temperatures

(1) Conditions of Top of Column

Sensible heat from the liquid must supply the sensible heat transferred to the gas and the latent heat required for the vaporisation. Therefore, equation 8.1 will apply:-

$$h_L (t_L - t_i) = h_g (t_i - t_g) + k_g M_A \lambda (p_i - p_g)$$

Assume t_i = 53.4, $\therefore$ p_i = 22.8 mm. Hg

L.H.S. = 262 (54.3 - 53.4)

= 236

R.H.S. = $6.15 (53.4 - 48.2) + \frac{0.448 \times 100 \times 160}{760} (22.8 - 3.2)$

= 32 + 185

= 217

$\therefore$ Interface Temperature at Top of Column = 53.4 °F

(2) Conditions at Bottom of Column

The latent heat required for vaporisation is derived from the sensible heat of the gas and liquid. Therefore, equation 8.2 will apply:-

$$h_L (t_L - t_i) + h_g (t_g - t_i) = k_g M_A \lambda (p_i - p_g)$$

Assume $t_i = 37.6$, $\therefore p_i = 13.8$

L.H.S. $= 262 (37.8 - 37.6) + 6.15 (53.0 - 37.6)$

$= 52.3 + 94.6$

$= 146.9$

R.H.S. $= \frac{0.448 \times 100 \times 160}{760} (13.8 - 0)$

$= 130.5$

$\therefore$ Interface Temperature at Bottom of Column = 37.6 °F

(d) Error Introduced by Assuming Bulk Liquid Temperature = Interface Temperature

(i) Log. Mean of Terminal Driving Forces based on Bulk Liquid Temperatures

= 16.90 mm. Hg.

(ii) Log. Mean of Terminal Driving Forces based on Interfacial Temperatures

= 16.52 mm. Hg.

$\therefore$ Percentage Error based on (ii) = 2.3%

This error, although larger than the comparable error in Case 1, is not sufficiently large to warrant the use of interfacial temperatures rather than the more easily calculated bulk liquid temperatures. Therefore, for ease of calculation, the true mean driving force was evaluated using bulk liquid temperatures.

(e) Evaluation of the True Mean Driving Force

The results of the stepwise trial and error calculations for determining the liquid temperature as a function of the amount transferred are shown in Table 8.10.

TABLE 8.10

TRUE DRIVING FORCE VARIATION WITH % TRANSFERRED

CASE 2. EVAPORATION OF n-HEPTANE WITH AIR, LOW LIQUID RATE, HIGH GAS THROUGHPUT

% of Total Transfer	Liquid Temp. (°F)	P_i (mm. Hg.)	P_g (mm. Hg.)	True Driving Force (mm. Hg.)
0	37.8	13.9	0	13.9
25	40.3*	15.0	0.8	14.2
50	44.8*	17.5	1.6	15.9
75	50.2*	20.6	2.4	18.2
100	54.3	23.5	3.2	20.3

(* Calculated Liquid Temperatures)

The true mean driving force calculated by graphical integration of Fig. 8.7 equals 16.3 mm. Hg.

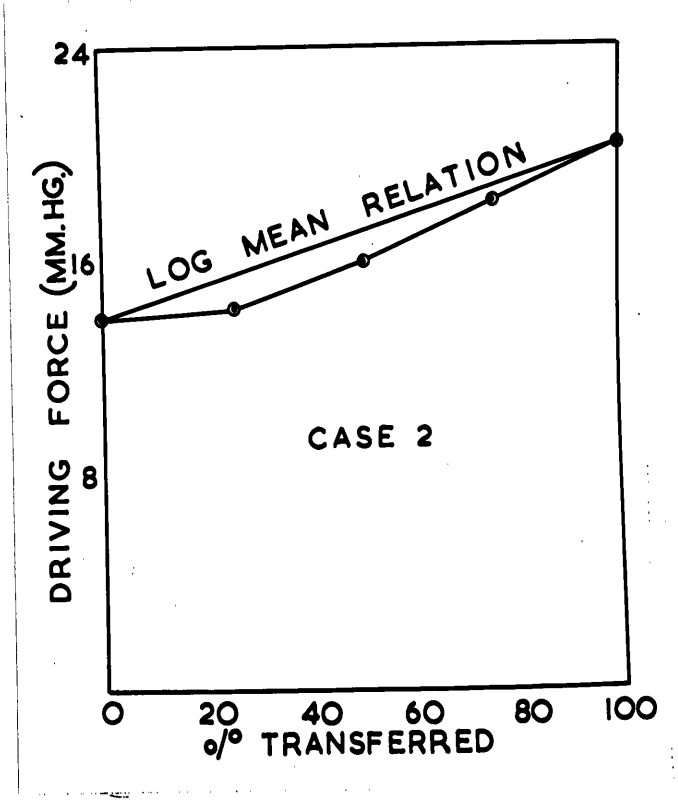

Fig. 8.7 - Graphical determination of the true mean driving force

8.4.4 Comparison of True Mean and Log. Mean Driving Force

As already indicated, the low liquid rate heptane evaporation runs should exhibit the greatest departure from log. mean driving force conditions. The potential or driving force must be linear with the amount transferred if the log. mean is to have theoretical significance.

The evaporation of water in these experiments was carried out at very much higher liquid rates. The liquid film heat transfer coefficients, at these high liquid rates, are very considerably higher than those for the low liquid rate heptane data and therefore, the difference between the bulk liquid temperature and the interface temperature for the water evaporation runs, would be even smaller than that calculated for the heptane data.

The high flow rates used in the water evaporation experiments result in only relatively small temperature drops between liquid inlet and outlet, compared to the significant cooling of the liquid in the heptane evaporation experiments.

Therefore any error introduced by using the log. mean of the terminal driving forces, based on bulk liquid temperatures, would be considerably less in the water evaporation data than it would be for the heptane evaporation data. Table 8.11 shows the error introduced when log. mean is used in place of the true mean driving force.

TABLE 8.11

COMPARISON OF TRUE AND LOG. MEAN DRIVING FORCE

	Case 1	Case 2
Liquid Phase	n-heptane	n-heptane
Gas Phase	Air	Air
Liquid Rate	1.8 lb./hr.	1.8 lb./hr.
Gas Rate	2.07 lb./hr.	11.23 lb./hr.
Liquid Temp. In	56.7 °F	54.3 °F
Liquid Temp. Out	45.5 °F	37.8 °F
True Mean Driving Force (Based on Bulk Liquid Temperatures)	17.01 mm. Hg.	16.30 mm. Hg.
Log. Mean Driving Force	17.65 mm. Hg.	16.90 mm. Hg.
Error % True Mean (Based on Bulk Liquid Temperatures)	+ 3.8%	+ 3.7%
Error due to Use of Bulk Liquid Temperature instead of Interfacial Temperature	+ 1.2%	+ 2.3%
Overall Error Introduced by Using Log. Mean Driving Force Based on Bulk Liquid Temperature	+ 5.0%	+ 6.0%

8.5 Calculation of Gas Phase Transfer Data

The log. mean of the terminal driving forces was used in all cases, except the low liquid rate heptane data, for evaluating the gas film mass transfer coefficient. For the low liquid rate heptane data, the calculated true mean driving force was used, as the error introduced by using the log. mean was considered high enough to be significant.

The equilibrium vapour pressures were obtained from the extensive tables compiled by Stull (117). Interpolation of the data was achieved by plot of log. p versus $\frac{1}{T}$.

The calculated gas film mass transfer coefficients together with other relevant results for the systems studied are shown in Tables 8.12, 8.13, 8.14, 8.15 and 8.16.

TABLE 8.12

VAPORISATION OF WATER WITH HYDROGEN

Run	$\frac{lb.}{(hr.)(ft.)}$ Γ	Gas Velocity $\frac{ft.}{sec.}$	Liquid Velocity $\frac{ft.}{sec.}$	Relative Velocity $\frac{ft.}{sec.}$	Vaporisation Rate x 10^3 $\frac{lb.mole.}{(hr.)(ft.)^2}$	Log.Mean Driving Force x 10^2 (atm.)	Gas Film Mass Transfer Coefficient $\frac{lb.mole.}{(hr.)(ft^2)(atm.)}$
1A	325	5.15	1.08	6.23	25.45	2.073	1.23
2A	325	9.44	1.08	10.52	37.95	2.226	1.70
3A	325	12.19	1.08	13.27	45.84	2.257	2.03
4A	325	14.59	1.08	15.67	51.12	2.263	2.26
5A	325	16.99	1.08	18.07	55.15	2.279	2.42
1B	325	8.24	1.08	9.32	33.73	2.172	1.55
2B	325	12.87	1.08	13.95	46.06	2.242	2.05
3B	325	14.76	1.08	15.84	50.63	2.240	2.26
4B	325	21.63	1.08	22.71	67.79	2.243	3.02
5B	325	26.78	1.08	27.86	78.01	2.227	3.50
6B	325	19.40	1.08	20.48	61.51	2.226	2.76
7B	325	15.62	1.08	16.70	52.43	2.193	2.39
8B	325	10.13	1.08	11.21	39.59	2.130	1.86
9B	325	5.56	1.08	6.64	26.04	2.011	1.29

TABLE 8.13

VAPORISATION OF WATER WITH AIR

Run	$\frac{\text{lb.}}{(\text{hr.})(\text{ft.})}$ Γ	Gas Velocity $\frac{\text{ft.}}{\text{sec.}}$	Liquid Velocity $\frac{\text{ft.}}{\text{sec.}}$	Relative Velocity $\frac{\text{ft.}}{\text{sec.}}$	Vaporisation Rate x 10^3 $\frac{\text{lb.mole.}}{(\text{hr.})(\text{ft.})^2}$	Log. Mean Driving Force x 10^2 (atm.)	Gas Film Mass Transfer Coefficient $\frac{\text{lb.mole.}}{(\text{hr.})(\text{ft.}^2)(\text{atm})}$
1C	325	8.24	1.08	9.32	27.95	1.841	1.52
2C	325	7.21	1.08	8.29	25.79	1.813	1.42
3C	325	6.18	1.08	7.26	22.56	1.800	1.25
4C	325	4.98	1.08	6.06	19.83	1.738	1.14
5C	325	3.84	1.08	4.92	16.58	1.663	1.00
6C	325	2.68	1.08	3.76	12.05	1.608	0.75
7C	325	1.92	1.08	3.00	9.79	1.461	0.67
8C	325	1.22	1.08	2.30	7.19	1.205	0.60
1D	298	1.70	1.04	2.74	10.09	1.674	0.60
2D	240	1.70	1.00	2.70	9.90	1.679	0.59
3D	149	1.70	0.74	2.44	9.58	1.643	0.58
4D	64	1.70	0.43	2.13	8.58	1.646	0.52
1E	298	2.40	1.04	3.44	10.99	1.480	0.74
2E	240	2.40	1.00	3.40	10.80	1.485	0.73
3E	149	2.40	0.74	3.14	10.06	1.490	0.68
4E	64	2.40	0.43	2.83	9.20	1.473	0.62
5E	298	3.78	1.04	4.82	14.95	1.543	0.97
6E	240	3.78	1.00	4.78	14.05	1.590	0.89
7E	149	3.78	0.74	4.52	13.23	1.580	0.84
8E	64	3.78	0.43	4.21	12.10	1.510	0.80
1F	298	4.81	1.04	5.85	16.48	1.622	1.02
2F	240	4.81	1.00	5.81	15.95	1.632	0.98
3F	149	4.81	0.74	5.55	15.42	1.651	0.93
4F	64	4.81	0.43	5.24	14.00	1.611	0.87
5F	298	5.94	1.04	6.98	19.50	1.689	1.16
6F	240	5.94	1.00	6.94	18.18	1.728	1.05
7F	149	5.94	0.74	6.68	17.09	1.629	1.01
8F	64	5.94	0.43	6.37	16.20	1.672	0.97

TABLE 8.14

VAPORISATION OF WATER WITH CARBON DIOXIDE

Run	Γ $\frac{\text{lb.}}{(\text{hr.})(\text{ft.})}$	Gas Velocity $\frac{\text{ft.}}{\text{sec.}}$	Liquid Velocity $\frac{\text{ft.}}{\text{sec.}}$	Relative Velocity $\frac{\text{ft.}}{\text{sec.}}$	Vaporisation Rate $\times 10^3$ $\frac{\text{lb.mole.}}{(\text{hr.})(\text{ft.})^2}$	Log.Mean Driving Force $\times 10^2$ (atm.)	Gas Film Mass Transfer Coefficient $\frac{\text{lb.mole.}}{(\text{hr.})(\text{ft}^2)(\text{atm.})}$
1G	325	1.51	1.08	2.59	9.58	1.86	0.52
2G	325	1.82	1.08	2.90	11.21	1.93	0.58
3G	325	2.06	1.08	3.14	11.25	2.09	0.54
4G	325	3.67	1.08	4.75	16.12	2.25	0.72
5G	325	2.82	1.08	3.90	14.43	2.09	0.69
6G	325	2.47	1.08	3.55	13.13	2.02	0.65
7G	325	2.09	1.08	3.17	11.35	1.99	0.57
8G	325	1.65	1.08	2.73	9.42	1.90	0.50
9G	325	1.08	1.08	2.16	6.68	1.81	0.37
10G	325	0.88	1.08	1.96	5.95	1.61	0.37

TABLE 8.15

VAPORISATION OF WATER WITH DICHLORODIFLUOROMETHANE

Run	Γ $\frac{\text{lb.}}{(\text{hr.})(\text{ft.})}$	Gas Velocity $\frac{\text{ft.}}{\text{sec.}}$	Liquid Velocity $\frac{\text{ft.}}{\text{sec.}}$	Relative Velocity $\frac{\text{ft.}}{\text{sec.}}$	Vaporisation Rate $\times 10^3$ $\frac{\text{lb.mole.}}{(\text{hr.})(\text{ft.})^2}$	Log.Mean Driving Force $\times 10^2$ (atm.)	Gas Film Mass Transfer Coefficient $\frac{\text{lb.mole.}}{(\text{hr.})(\text{ft}^2)(\text{atm.})}$
1H	325	0.61	1.08	1.69	3.56	1.475	0.24
2H	325	0.93	1.08	2.01	4.68	1.685	0.28
3H	325	1.14	1.08	2.22	5.64	1.707	0.33
4H	325	1.11	1.08	2.19	5.55	1.693	0.33
5H	325	1.56	1.08	2.64	7.18	1.685	0.43
6H	325	0.84	1.08	1.92	4.65	1.458	0.32
7H	325	0.79	1.08	1.87	4.19	1.622	0.26

TABLE 8.16

VAPORISATION OF n-HEPTANE WITH AIR

Run	Γ $\frac{\text{lb.}}{(\text{hr.})(\text{ft.})}$	Gas Velocity $\frac{\text{ft.}}{\text{sec.}}$	Liquid Velocity $\frac{\text{ft.}}{\text{sec.}}$	Relative Velocity $\frac{\text{ft.}}{\text{sec.}}$	Vaporisation Rate x 10^3 $\frac{\text{lb.mole}}{(\text{hr.})(\text{ft.})^2}$	Log. Mean Driving Force x 10^2 (atm.)	Gas Film Mass Transfer Coefficient $\frac{\text{lb.mole.}}{(\text{hr.})(\text{ft.})(\text{atm.})}$
1J	113	1.65	0.96	2.61	17.33	5.118	0.34
2J	113	2.47	0.96	3.43	20.06	5.066	0.40
3J	113	3.84	0.96	4.80	23.68	4.947	0.48
4J	113	3.84	0.96	4.80	24.82	5.039	0.49
5J	113	3.09	0.96	4.05	19.70	4.671	0.42
6J	113	2.09	0.96	3.05	15.75	4.211	0.37
1K	89	2.47	0.81	3.28	18.24	4.961	0.37
2K	89	3.84	0.81	4.65	21.98	4.934	0.45
3K	89	4.87	0.81	5.68	24.45	4.868	0.50
4K	89	3.84	0.81	4.65	25.24	5.513	0.46
5K	89	3.09	0.81	3.90	18.22	4.553	0.40
6K	89	2.09	0.81	2.90	14.20	4.250	0.33
1L	50	2.13	0.56	2.69	9.88	3.25	0.30
2L	50	2.95	0.56	3.51	12.23	3.14	0.36
3L	50	4.05	0.56	4.61	13.42	3.16	0.43
4L	50	4.97	0.56	5.53	14.88	3.11	0.48
5L	50	6.07	0.56	6.63	16.60	3.05	0.54
6L	50	7.33	0.56	7.89	18.40	3.07	0.60
1M	15	1.58	0.25	1.83	4.66	2.33	0.21*
2M	15	2.40	0.25	2.65	5.40	2.27	0.25*
3M	15	3.60	0.25	2.85	6.38	2.22	0.30*
4M	15	5.15	0.25	5.40	7.98	2.17	0.39*
5M	15	6.65	0.25	6.90	9.33	2.20	0.45*
6M	15	8.58	0.25	8.83	10.10	2.25	0.48*

* Corrected for True Mean Driving Force

8.6 Correlation and Discussion of Results

The correlation of the mass transfer data obtained in these disc column experiments has revealed some very interesting aspects of gas phase mass transfer, which are considered to be of general application and, which are extended in the later chapters of this thesis to an analysis of the data obtained, when zinc vapour was absorbed in molten lead using a packed column.

To preserve the continuity of the discussion, which is presented in three sections, tables of the calculated valuesused in the correlations are not placed in the text but appended to the discussion.

The diffusion coefficients for the water systems were taken from the table of selected experimental data compiled by Wilke and Lee (198) and the diffusion coefficient for the air - n-heptane system was obtained from the measurements of Schlinger et.al. (99).

The relevant diffusion data is shown in Table 8.17.

TABLE 8.17

PUBLISHED DIFFUSION DATA

System	Temp. (°C)	Diffusion Coefficient $cm.^2/sec.$	Schmidt Number
H_2 - H_2O	20	0.850	1.25
Air - H_2O	25	0.260	0.60
CO_2 - H_2O	25	0.164	0.48
CCl_2F_2 - H_2O	25	0.105	0.25
Air - n-heptane	21	0.073	2.05

8.6.1 Correlation by Dimensional Analysis

Dimensional analysis applied to forced convection mass transfer indicates that the group $\frac{k_c L}{D}$, which is analogous to the Nusselt number for heat transfer, is a function of the Schmidt number (Sc. = $\frac{\mu}{\rho D}$) and the Reynolds number (Re = $\frac{Lv\rho}{\mu}$)

i.e. $$\frac{k_c L}{D} = \psi\left[\left(\frac{Lv\rho}{\mu}\right), \left(\frac{\mu}{\rho D}\right)\right] \quad \ldots\ldots 8.10$$

Usually a power function is assumed:-

$$\frac{k_c L}{D} = \alpha\left(\frac{Lv\rho}{\mu}\right)^m \left(\frac{\mu}{\rho D}\right)^n \quad \ldots\ldots 8.11$$

If both sides of equation 8.11 are divided the product $\frac{Lv\rho}{\mu} \cdot \frac{\mu}{\rho D}$ the resulting equation is obtained:-

$$\frac{k_c}{v} = \alpha\left(\frac{Lv\rho}{\mu}\right)^{m-1} \left(\frac{\mu}{\rho D}\right)^{n-1} \quad \ldots\ldots 8.12$$

The term $\frac{p_{BM}}{P}$ was introduced into this equation and the exponent on the Schmidt number was made equal to 2/3 by analogy with the corresponding heat transfer equation, by Chilton and Colburn (11), to define a new dimensionless factor known as j-factor.

$$j_D = \frac{k_c}{v} \frac{p_{BM}}{P} \left(\frac{\mu}{\rho D}\right)^{2/3} \quad \ldots\ldots 8.13$$

The corresponding heat transfer equation is:-

$$j_H = \frac{h}{C_p \rho v} \left(\frac{C_p \mu}{k}\right)^{2/3} \quad \ldots\ldots 8.14$$

Chilton and Colburn (11) extended Reynolds (88) analogy between heat transfer and fluid friction to mass transfer and proposed the relation

$$j_D = j_H = \frac{f}{2} \quad \ldots\ldots 8.15$$

The limitations of this analogy are discussed more fully when the relation between ΔP_d and k_g is discussed.

The expression of mass transfer data in the form of the j_D factor is convenient, as this factor can then be correlated with Reynolds number.

For gas phase mass transfer, the j_D equation can be expressed in terms of the coefficient k_g.

Since $k_c = \frac{P}{\rho_m} \cdot k_g = RT\, k_g$ 8.16

$$j_D = \frac{k_g\ p_{BM}}{v\ \rho_m} \left(\frac{\mu}{\rho D}\right)^{2/3} = \frac{k_g\ p_{BM}}{G_m} \left(\frac{\mu}{\rho D}\right)^{2/3} \quad \text{..... 8.17}$$

The j_D factor has been extensively used for correlating gas film mass transfer data in absorption equipment. However, the j_D factor does not recognise any effect, which a relative interfacial velocity would have on the mass transfer process. As the relative velocity of the gas and liquid phases was found to exhibit a very significant bearing on the disc column pressure drops as described in Chapter 7, and as the author has found that the use of a "relative friction factor" and a "relative Reynolds number" allowed correlation of the irrigated pressure drop data, it is considered, that the significant velocity term, in the original dimensional analysis of the mass transfer process, should have been the relative interfacial velocity.

i.e. $\frac{k_c L}{D} = \gamma_1 \left[\left(\frac{Lv_R \rho}{\mu}\right), \left(\frac{\mu}{\rho D}\right)\right]$ 8.18

A "relative j_D" factor can then be defined:-

Relative $j_D = (j_D)_R = \frac{k_c}{v_R} \frac{p_{BM}}{P} \left(\frac{\mu}{\rho D}\right)^{2/3}$ 8.19

$$= \frac{k_g}{v_R} \frac{p_{BM}}{\rho_m} \left(\frac{\mu}{\rho D}\right)^{2/3} \quad \text{..... 8.20}$$

It is proposed that the "relative j_D factor" should be a function of the "relative Reynolds number " $\frac{Lv_R \rho}{\mu}$

It would be preferable to have these relative terms based on the relative interfacial velocity, but the actual velocity of the liquid interface is not readily measured, although, if a semi-parabolic velocity distribution in the liquid is assumed, the interfacial velocity may be calculated from the average velocity as outlined by Potter (86).

In a disc column or packed column, the liquid velocity alters from point to point, and hence any rigorous analysis of the interfacial liquid velocity would appear to be unjustified. However, the relative velocity of the gas and liquid phases, based on the average linear velocity of the streams, should be suitable for experimental correlation of data.

The effect of the relative velocity on the gas phase mass transfer process can be seen from a comparison of Figs. 8.8 and 8.9, in which both the linear gas velocity and the relative velocity are used to compare the gas film coefficients for the vaporisation of water in air.

When the linear gas velocity is used, the gas film coefficients are clearly dependent on the liquid rate. The pressure drop characteristics would suggest that a breakpoint occurs in the data. However, these results failed to exhibit this breakpoint, except possibly the data for Γ = 325 lb./(hr.)(ft.), which does exhibit a break shown by the dotted line on the graph.

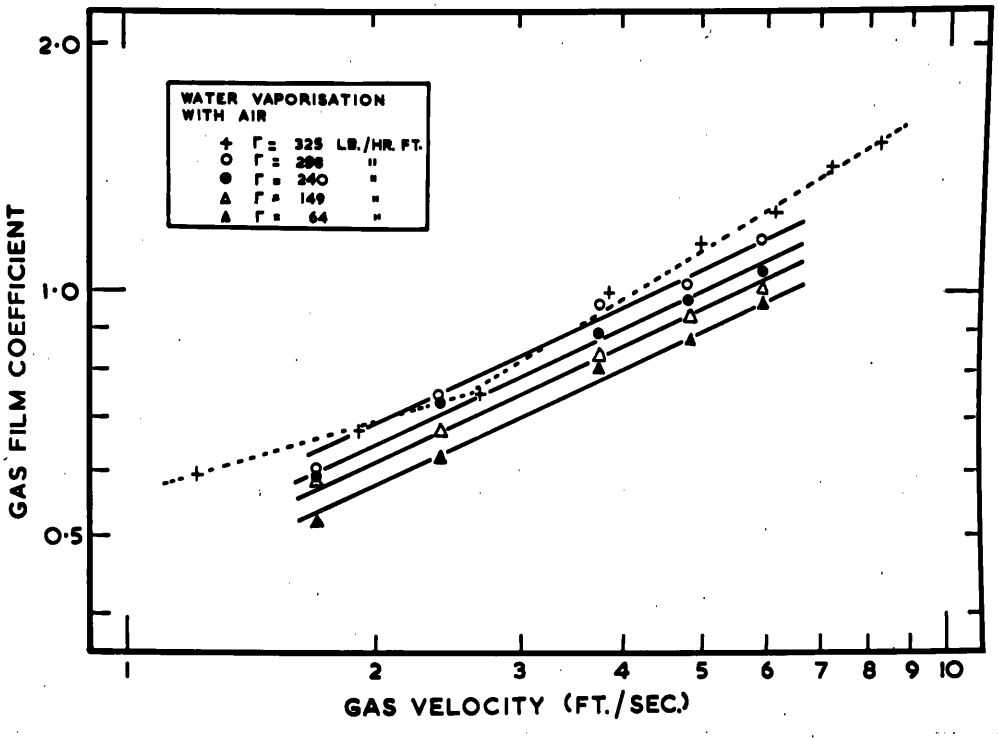

Fig. 8.8 - The effect of gas velocity on the gas film mass transfer coefficient k_g for various liquid rates

The use of the relative velocity in Fig. 8.9 shows that k_g is independent of liquid rate at the lower velocities, but at the high velocities, for liquid rates above Γ = 240 lb./(hr.)(ft.), a dependency on liquid rate is observed. This behaviour is the same as observed when the relative velocity was used to compare "relative friction factor" data and the same explanation as presented in Chapter 7 is thought to apply. The surface disturbances at the higher liquid rates affect the mass transfer process only at high Reynolds numbers in the same way, as "relative roughness" only affects pipe friction as the turbulence is increased and has no effect in the streamline region. This departure at high liquid and gas rates could

be considered as a discontinuity in the data, and therefore, a breakpoint, as observed by Stephens and Morris (116) and Taylor and Roberts (122), may be represented by the dotted line in the diagram, although it appears very unlikely that a breakpoint would exist at lower liquid rates and is therefore consistent with the conclusions reached, when the liquid and gas flow characteristics of the column were studied.

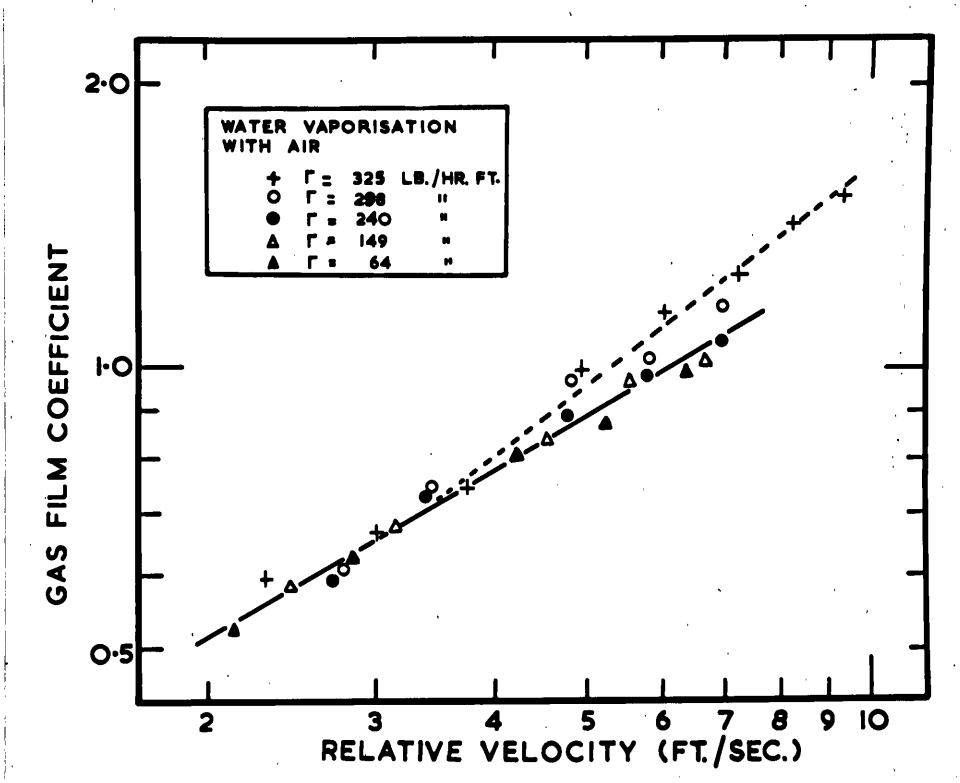

Fig. 8.9 - The effect of relative velocity on the gas film mass transfer coefficient k_g for various liquid rates

As the results of this investigation and the earlier data of Stephens and Morris (116) and Taylor and Roberts (122), all indicate that the relative velocity of the gas and liquid streams is significant in gas phase mass transfer, the newly defined "relative j_D factor" type of correlation and the conventional j_D correlation were applied to the experimental data for all systems.

Fig. 8.10 is a comparison of the two methods of correlation of the data. Of the n-heptane results only the 15 lb./(hr.)(ft.) data are treated, as the higher liquid rate data are considered unreliable, as outlined fully when the relation between k_g and ΔP_d is treated in the next section of the discussion. The "relative j_D" correlation includes data for all liquid rates. The j_D correlation includes data for only the constant liquid rate of 325 lb./(hr.)(ft.).

The conventional j_D type of correlation shows the hydrogen data as being displaced below the air data, particularly at low Reynolds numbers, where the effects of relative velocity for the air data are greatest. The difference between the air and hydrogen data decreases with increased Re. This is to be expected, if the relative velocity is the significant velocity term in the mass transfer process, as at these higher values of Re, the influence of the liquid velocity has a much smaller effect on both the hydrogen and air data, because of the higher gas velocities. The dichlorodifluoromethane data, however, do not exhibit the same trend, as to be consistent these results should be displaced above the air data, whereas they are also displaced below the air data.

The newly proposed "relative j_D" versus "relative Re" plot correlates all the data irrespective of the liquid rate, with the exception of the dichlorodifluoromethane results. These data are displaced well below the line correlating the remainder of the points. A similar discrepancy is observed for the two low velocity carbon dioxide points, which are also displaced significantly below the other data. These two CO_2 points and the bulk of the CCl_2F_2 data are cases,

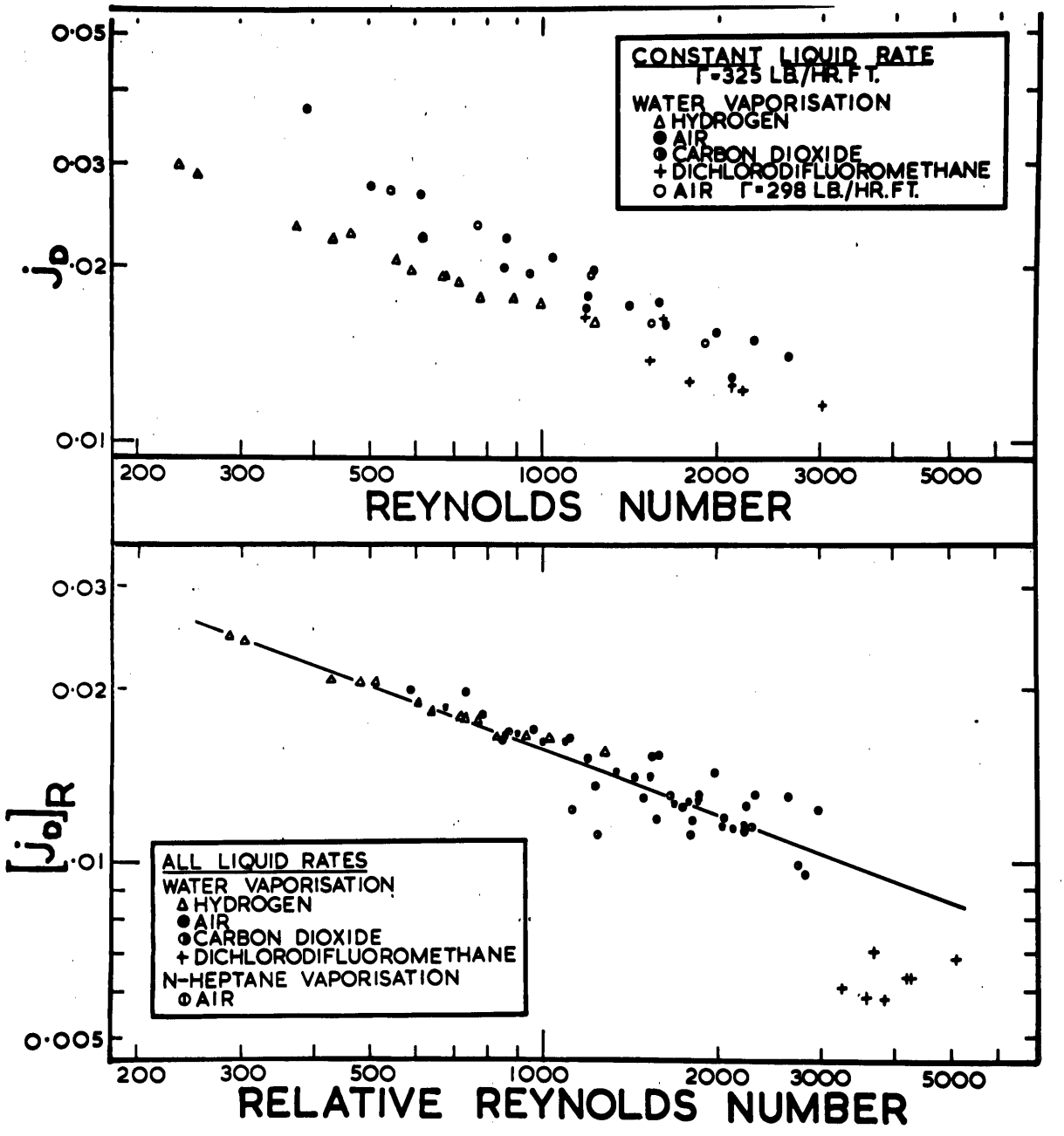

Fig. 8.10 - Comparison of the j_D and $(j_D)_R$ methods of correlation

in which the liquid velocity is greater than the gas velocity. In these cases, the correction of the gas velocity to allow for the liquid velocity has a very marked effect.

The "relative friction factor" versus "relative Re" correlation of Chapter 7 also showed the dichlorodifluoromethane data as being displaced well below the other data, and therefore it is considered, that the same explanation can apply to the mass transfer data. A significant contribution to the total mass transfer rate, at high Reynolds numbers, is by the process of eddy diffusion. Whereas the liquid flowing over the discs is considered to contribute to the formation of eddies in the gas phase, it is doubtful if the full relative velocity should be used to account for this effect.

However, as most gas phase mass transfer operations are carried out at gas velocities higher than the liquid velocity, the use of new "relative j_D" versus "relative Reynolds number" type of correlation is considered to have general application. For cases in which the liquid velocity is greater than the gas velocity, further experimental work would have to be undertaken, to determine the exact effect the velocity of the liquid has on the transfer process.

The experimental results reported by Stephens and Morris (116) and Taylor and Roberts (122) for the co-current and countercurrent absorption of ammonia in water from dilute ammonia - air mixtures, and the part of the water vaporisation in air data reported by Roper (89), have been recalculated using the author's method of correlation and compared in Fig. 8.11 to the results of this investigation for the vaporisation of water in air at similar liquid rates.

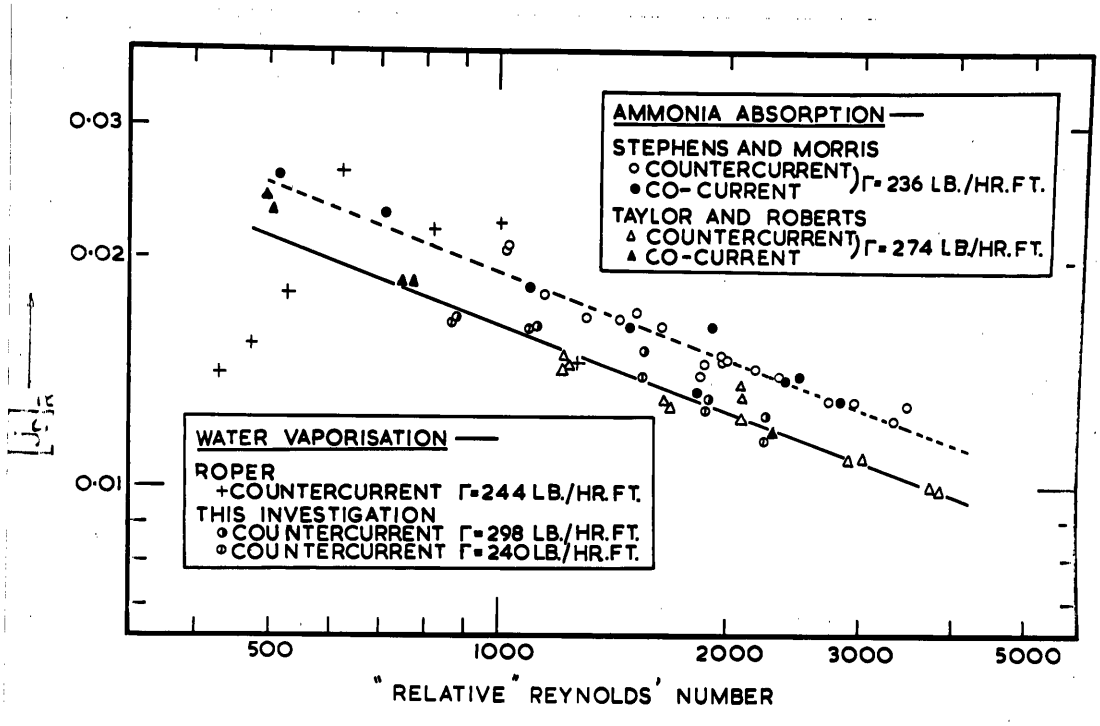

Fig. 8.11 - Comparison with previous investigations

The full line in the diagram is the line representing the best fit of the author's air - water vaporisation data. Very close agreement exists between the author's vaporisation data and the ammonia absorption results reported by Taylor and Roberts (122). The data of Stephens and Morris (116) are displaced above these data and can be well represented by the dotted line drawn parallel to the full line in the diagram. The data of Roper (89) scatter on both sides of the full and dotted lines. The three points displaced well beneath the other data were for gas velocities less than the liquid velocity and therefore may add further evidence to the inherent weakness of the "relative j_D factor" type of correlation, for cases, in which the liquid velocity exceeds the gas velocity. However, Roper's low air velocity data are of doubtful accuracy, because of the close approach to equilibrium

conditions in the exit gas stream, as in these three runs the relative humidity was 96 - 99% and therefore considerable error is likely to be introduced.

Similar anomalies to those observed in this investigation, when the liquid velocity exceeded the gas velocity, were reported by Cooper, Christl and Peery (16) and Beattie (4). Although these authors studied vastly different systems to those of this investigation , their results are considered to support the conclusions reached in this work with respect to gas velocities below the liquid velocity.

Cooper, Christl and Peery (16) studied the absorption of carbon dioxide in water in a packed tower, under such conditions that the linear velocities of the liquid were greater than the gas velocities. The heights of liquid phase transfer units, which were calculated assuming counterflow conditions, were higher than those for gas velocities exceeding the liquid velocity. These authors attributed this to the gas being carried downward by the liquid, the reverse flow tending to mix the gas vertically in the tower and thereby destroying the countercurrent action. The results of this longitudinal mixing within the tower meant that the true driving force could not be evaluated, unless complete mixing was assumed, in which case the concentration of the diffusing component in the gas phase would be the same at both top and bottom of the tower.

These observations support the low mass transfer coefficients, evaluated assuming no longitudinal mixing, observed in this investigation for the data, in which the liquid velocity exceeded the gas velocity. The other important aspect is that the gas is entrained by the liquid at the low gas velocities and therefore the relative interfacial velocity

cannot be readily computed from the gas and liquid velocities under such conditions.

Additional evidence that longitudinal mixing can be expected at low fluid velocities in a disc column, was reported by Beattie (4). During the course of liquid - liquid extraction experiments with a disc column, in which water was passed down the column at a very slow rate and butanol up the column on the discs, a dye was injected into the aqueous phase. Longitudinal mixing in the aqueous phase was visually observed. Hence it is also reasonable to expect a similar degree of longitudinal mixing for low gas rates in a disc column.

8.6.2 Implications of the "Relative j_D" Correlation

The effect of the diffusivity on the rate of gas phase mass transfer has for many years been the subject of conflicting reports and apparent anomalies.

Several investigators have reported results, which suggest, that the exponent on the Schmidt number is different to the $^2/_3$ exponent proposed by Chilton and Colburn (11) from analogy with the known Prandtl number effect in heat transfer. Gilliland (30) correlated data on the vaporisation of organic liquids and water by air in a wetted wall column and found the gas film coefficient to be proportional to $D^{0.56}$ rather than $D^{2/3}$. Yoshida (132) and Lynch and Wilke (63) evaporated water with a series of gases in a packed column and found the transfer rate, at a given Reynolds number, to be proportional to $D^{0.77}$ and $D^{0.90}$ respectively. Two sets of data obtained by vaporising organic liquids and water by air in a packed column, reported by Mehta and Parekh (74) and Surosky and Dodge (118), indicate the gas phase transfer rates to be proportional to $D^{0.17}$ and $D^{0.15}$ respectively.

However, the experimental investigations in support of the $^{2}/_{3}$ exponent are very extensive, as shown by the numerous cases quoted by Sherwood and Pigford (105). Thus, for example, the mass transfer data obtained by Powell (87) and Lorisch (61), for the evaporation and absorption of water from non-irrigated cylinders placed normal to air flow (Sc. = 0.60) and the data of Linton (60), for the dissolution in water of cast cylinders of benzoic and cinnamic acid (Sc. = 1000 to 3000), are well correlated using the conventional j_D factor with the $^{2}/_{3}$ exponent on the Schmidt number. Furthermore, the data of Schulman and DeGouff (108), for the vaporisation of napthalene raschig rings in a packed column, and the data of Taecker and Hougen (121), for the vaporisation of water by air from prewetted but non-irrigated raschig rings in a packed column, were well correlated using the $^{2}/_{3}$ exponent on the Schmidt number. The data of Hobson and Thodos (43), for the transfer from non-irrigated prewetted packing, supported the $^{2}/_{3}$ exponent. The recently reported data by Schulman and Margolis (109), for the vaporisation of napthalene Berl saddles in a series of gases, were also correlated using the $^{2}/_{3}$ exponent on the Schmidt number.

The newly proposed "relative j_D factor" is thought to have considerable bearing on the anomalies existing in this field. An analysis of the investigations, showing significant departure from the $^{2}/_{3}$ exponent, shows that the irrigation of the surface is the significant factor in determining the exponent. The non-irrigated data supports the $^{2}/_{3}$ exponent, whereas, in the irrigated data, the range of exponents is from 0.15 to 0.90.

Dodge and Surosky (118) commented that their low exponent of 0.15 could be due to differences in interfacial area masking the true

effect of the diffusivity, as these areas could be different for organic liquids and water. Schulman et.al. (111) later showed that differences in the effective interfacial areas could account for the discrepancy.

The data reported by Lynch and Wilke (63), in which the one liquid phase was used, and in which the exponent at constant Reynolds number was found to be 0.9, cannot be explained by differences in effective interfacial areas. These authors commented that the observed effect of the diffusivity seemed unrealistic and, tentatively proposed, that the Reynolds number should not be used for correlating gas film mass transfer in packed columns, and that data should be compared at equal values of the gas inertia $v^2\rho$. Using the gas inertia as the correlating modulus, the exponent on the Schmidt number was found to be 0.47.

It is proposed that the true effect of diffusivity in the studies of Yoshida (130) and Lynch and Wilke (63) is masked by the relative velocity of the gas and liquid streams. The effect of relative velocity would be greater in the data of Lynch and Wilke, because the use, of dichlorodifluoromethane as a gas phase, results in low gas velocities, which are therefore seriously affected by correction to relative velocity. Yoshida used carbon dioxide as his densest gas phase. Therefore, if the relative velocity is significant in determining the departure from the $^2/_3$ exponent, Yoshida's exponent should be closer to the $^2/_3$ exponent than the exponent of Lynch and Wilke. This is consistent with the reported value of 0.77 and 0.9 for the exponents of Yoshida and Lynch and Wilke, respectively.

To illustrate the extent, which the relative velocity could mask the true effect of diffusivity on the mass transfer process, selected values of the data tabulated by Lynch and Wilke (63), covering the range of the investigation but keeping below the observed loading points, have been recalculated and correlated using the new "relative j_D" type of correlation. The relative velocities were calculated using a linear liquid velocity of 0.1 ft./sec. This value was chosen to make the data have the $^2/_3$ exponent on the Schmidt number and is therefore not presented as proof of the $^2/_3$ exponent, but merely to indicate the effect, which even a small liquid velocity of 0.1 ft./sec. could have on the interpretation of the data. The figure chosen, however, is not an unrealistic value, as liquid velocities of this order could be expected in a packed column. The gas velocities used were the true gas velocities calculated using a void fraction of 0.726 for 1" raschig rings, as reported by Schulman et.al. (111).

The selected recalculated data is plotted as the product $a(j_D)_R$ versus $\frac{v_R \rho}{\mu}$ on a log.-log. scale in Fig. 8.12.

The correlation of the data in Fig. 8.12 is extremely good and shows very clearly the marked effect, which the small liquid velocity correction of 0.1 ft./sec., has on the data. This is due mainly to the very low dichlorodifluoromethane gas velocities of 0.25 to 1.49 ft./sec. for the points plotted. The exponent on the Schmidt number in this correlation is $^2/_3$ compared to the exponent of 0.9 obtained using the conventional j_D type of correlation.

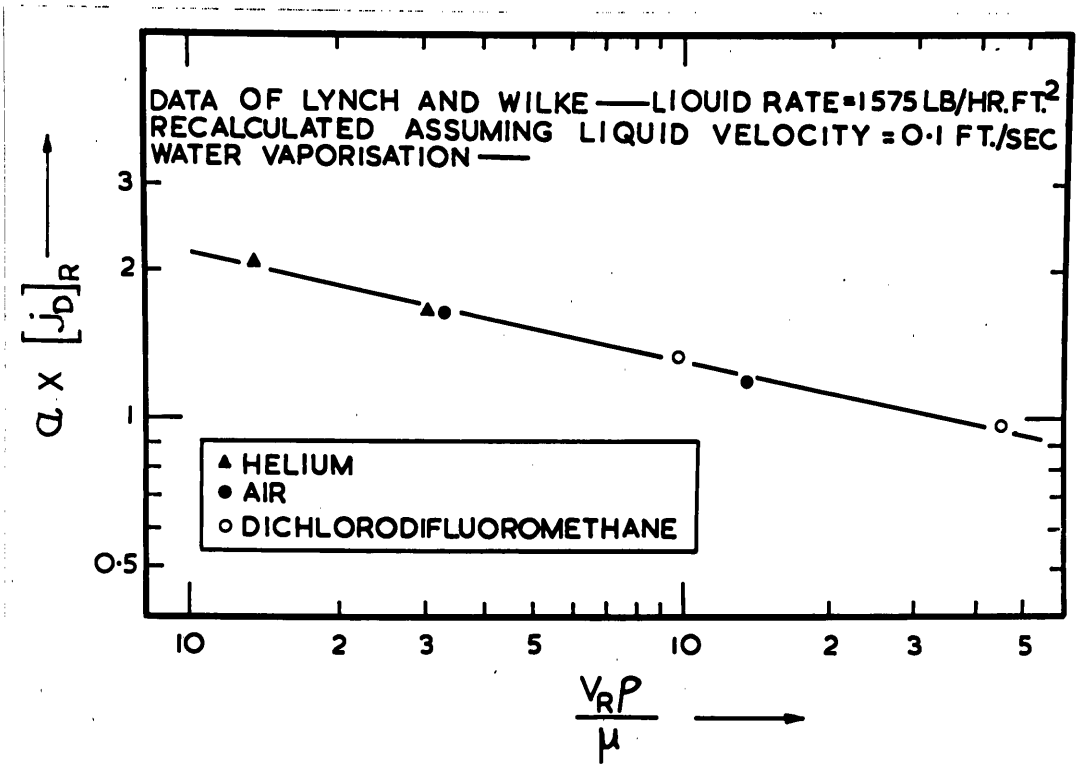

Fig. 8.12 - Correlation of Lynch and Wilke (63) data using "relative j_D" factor and "relative Reynolds" number.
Conventional j_D correlation masks the true effect of diffusivity.

It is also considered, that a similar treatment of the data of Gilliland (30), in which the observed exponent on the Schmidt number was less than $^2/_3$, may also result in the $^2/_3$ exponent. The data of Gilliland, in which air was the only gas phase, falls into two groups: the water data with a low Schmidt number and the organic data with higher Schmidt numbers. At a constant liquid rate in lb./(hr.)(ft.), organics have usually higher liquid velocities, as can be seen by substitution into the theoretical equation for laminar flow down a vertical surface. Therefore, if relative velocity is masking the true effect of the diffusivity, the exponent on the Schmidt number should be less than $^2/_3$, when organics are compared with water vaporisation studies

in air. This is consistent with the reported exponent of 0.56 by Gilliland.

A further implication, arising from the introduction of the "relative j_D factor", is that the true gas velocity, rather than the superficial gas or mass velocity, should be used in the analysis of gas phase mass transfer, as the correction of a superficial gas velocity for liquid velocity effects would have no significance. Therefore, the actual free space available for gas flow under operating conditions of liquid flow must be measured, if this type of correlation is to be used, and also an estimate of the average linear velocity of the liquid phase must be made.

If the "relative j_D factor" rather than the conventional j_D factor is introduced, the method of correlation of mass transfer data by using the concept of Height of a Transfer Unit (H.T.U.), introduced by Chilton and Colburn (12), is no longer applicable, as this also would have to be modified for relative velocity effects. This aspect is discussed in detail when the analysis of the zinc absorption in molten lead data is made.

8.6.3 Relation between k_g and ΔP_d

In 1952, Ergun (25) reviewed the analogy between pressure loss and mass transfer. The original Reynolds analogy (88) between heat transfer and resistance to fluid flow by friction, and the subsequent extension and modification of this analogy by Colburn (14) and Chilton and Colburn (11) to mass transfer, are discussed and further developed to mass transfer in a packed column. Ergun showed that his extension on the analogy applied to data on mass transfer between solid

particles and liquid streams in a packed column. However, the application of the analogy to gas streams was unsuccessful. This was in part attributed to the "deficiency and uncertainty of the published data for gas phase mass transfer", as no consistent data, including all the pertinent variable required for the analysis, were available. The data of this investigation could also not be correlated by the equations proposed by Ergun.

The failure of formal analogies between fluid friction and heat and mass transfer are usually attributed to the effects of form drag. Sherwood and Pigford (106) suggest, that the analogies would be successful, if the skin friction only is considered. Thus, for example, the Chilton and Colburn (11) j-factor analogy of $j_D = j_H = \frac{f}{2}$ is found to well represent the experimental data for fluid friction, heat and mass transfer inside pipes or across flat plates. In these cases, the measured pressure drop is due entirely to skin friction as form drag is not present.

If the j-factor analogy is to be used to compare data, in which the total drag or pressure drop is due to both skin friction and form drag, the effects of form drag must be substracted from the measured total drag.

The form drag correction, which would have to be applied to the disc column pressure drop data, does not lend itself to rigorous calculation, because of the complex nature of the solid surface, and could only be determined by carrying out a pressure traverse around the periphery of the discs. Such an investigation would be extremely difficult.

Although a formal theoretical analogy between the measured pressure

drop and the observed mass transfer coefficients in this investigation is not possible, because of the unknown contribution of form drag to the measured total pressure drop, it is considered that a relation between the pressure drop and the mass transfer coefficient, could be an extremely useful experimental tool for studying gas phase controlled absorptions. An entirely empirical approach was therefore used to see if any consistent relationship existed.

At a constant gas velocity, the pressure drop across the discs and the gas film mass transfer coefficient, increase with increases in liquid rate. It seemed reasonable to assume, that the same mechanism is involved in the increase of both these phenomena and, therefore, a plot of k_g versus ΔP_d for a particular system, but with different liquid rates, was constructed. Fig. 8.13 shows that all the air - water data, irrespective of liquid or gas rate, are well correlated by plotting k_g versus ΔP_d on a log.-log. graph.

Any breakpoints in the gas film data, which may have been observed, when the gas or relative velocity was used for comparing the data, are no longer present, because the gas film coefficients and the pressure drops are equally affected by any change in the flow characteristics.

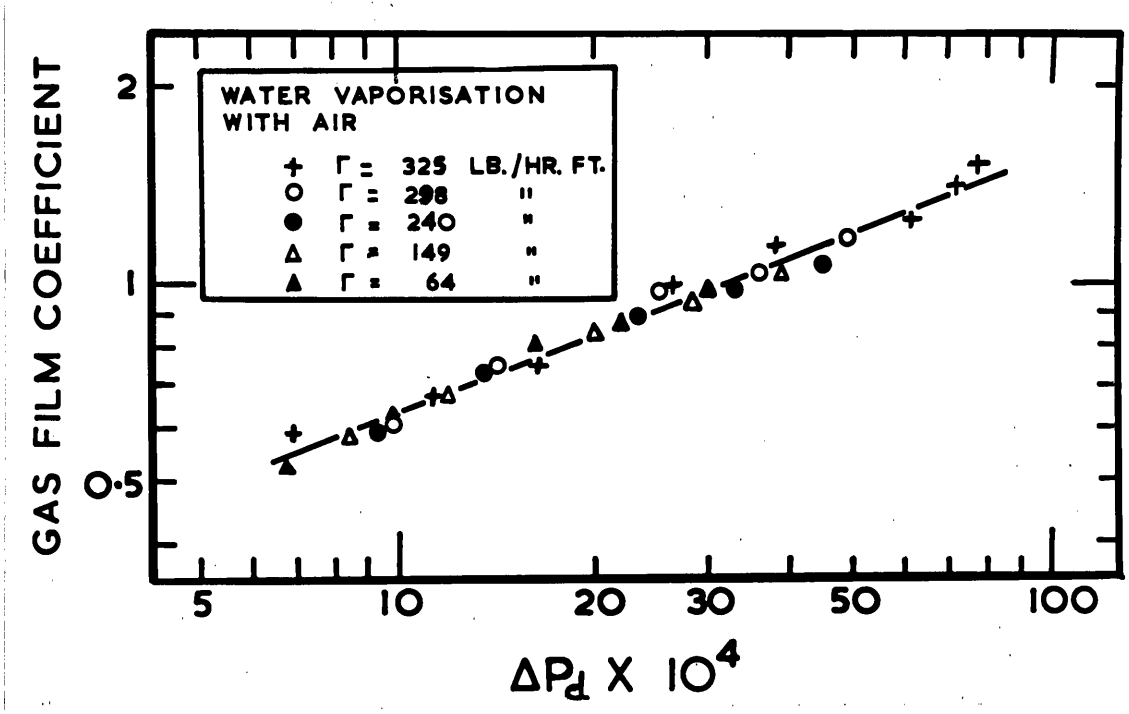

Fig. 8.13 - The relation between pressure drop and the gas film mass transfer coefficient k_g for the air - water system

When the same approach was applied to the n-heptahe vaporisation data, it was found that the gas film coefficients were not correlated by the pressure drop alone, but were also dependent on the liquid rate as shown in Fig. 8.14.

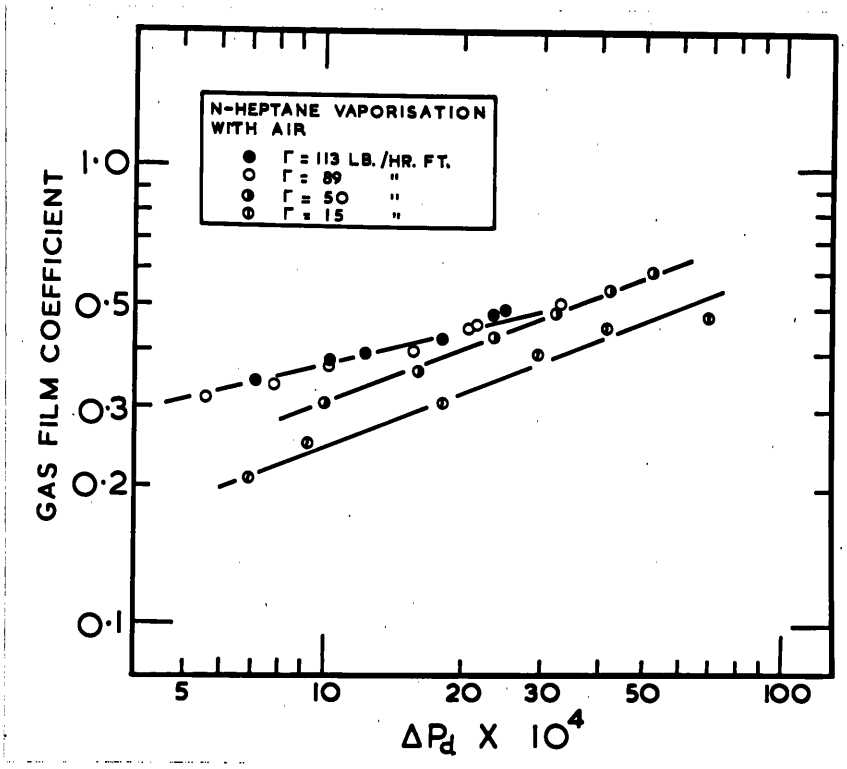

Fig. 8.14 - The relation between pressure drop and the gas film mass transfer coefficient k_g for the air - n-heptane system

The line representing the higher liquid rate data is displaced above the low liquid rate data and also exhibits a different slope. The rate of increase of k_g with increase in ΔP_d, for the high liquid rate data, is less than at lower liquid rates. This departure from the corresponding behaviour observed for the water vaporisation, was originally thought to be due to improper calculation of the mean driving force. The low liquid rate data being characterised by severe temperature drop as the liquid flows down the column. If this was the reason for the discrepancy, the high and low liquid rate data should depart further at increased gas rates (i.e. increased ΔP_d), because of the very pronounced cooling of the liquid phase at high gas rates. The observed difference, however,

is decreased at the higher gas rates.

The possibility of some physical cause of this behaviour was, therefore, investigated. A visual examination of the flow of n-heptane over the discs, in the absence of air flow, was made under such conditions that the liquid was cooled to below the ambient temperature before admission to the column. In this way, condensation on the wall of the column was prevented and only mechanically entrained liquid could reach the column wall. After circulating the n-heptane over the discs for several minutes, at a temperature just slightly below the ambient temperature to reduce re-evaporation of entrained liquid, blotches consisting of very fine liquid droplets were observed on the column wall at all liquid rates in excess of 15 lb./(hr.)(ft.). These blotches were clearly an indication, that the n-heptane tended to spray or splash at the higher liquid rates.

Similar experiments carried out with toluene and dioxane as the liquid phase, indicated splashing at all but very low liquid rates. Therefore, any mass transfer data at rates barely above that required to completely wet the discs, when an organic liquid is used as the liquid phase, would not be reliable because of the unknown contribution the splash would make to the measured rate of vaporisation. A conclusion, which may be reached, is that the technique of vaporising organic liquids to obtain mass transfer data in other types of equipment, such as packed columns, would be subject to the same error.

When the same visual examination was undertaken with water as the irrigating liquid, there was no apparent spray of the liquid onto the column wall. When the liquid temperature was allowed to rise above the ambient temperature, the column wall became fogged up due to condensation,

which is not to be confused with mechanical entrainment.

This splash behaviour of n-heptane, at all but extremely low liquid rates, explains why the high liquid rate data in Fig. 8.14 are displaced above the data for the 15 lb./(hr.)(ft.) and also explains the difference in slope. The contribution to the total vaporisation due to the splashing would most probably be unaffected by the gas rate, as the entire splash would flash when gas is being circulated through the column. Therefore, the largest effect of the splashing would be observed at low gas rates, where the total vaporisation rate is small. Hence, the observed decrease in the difference between the high and low liquid rate data, as the pressure drop (i.e. the gas rate also) is increased.

The only reliable n-heptane mass transfer data are, therefore, the results of the 15 lb./(hr.)(ft.) vaporisations. The other data were rejected and not included in any subsequent treatment.

For a particular system, it is apparent, that the gas film mass transfer coefficient can be correlated in terms of the measured pressure drop across a disc. This method of correlation is very attractive, particularly as the uncertain effects of liquid flowing over the discs are eliminated, as the mass transfer coefficient and the pressure drop are both affected to the same extent by these uncertain effects.

The application of this type of correlation to all the systems studied can be seen in Fig. 8.15, which is a plot of log. k_g versus log. ΔP_d.

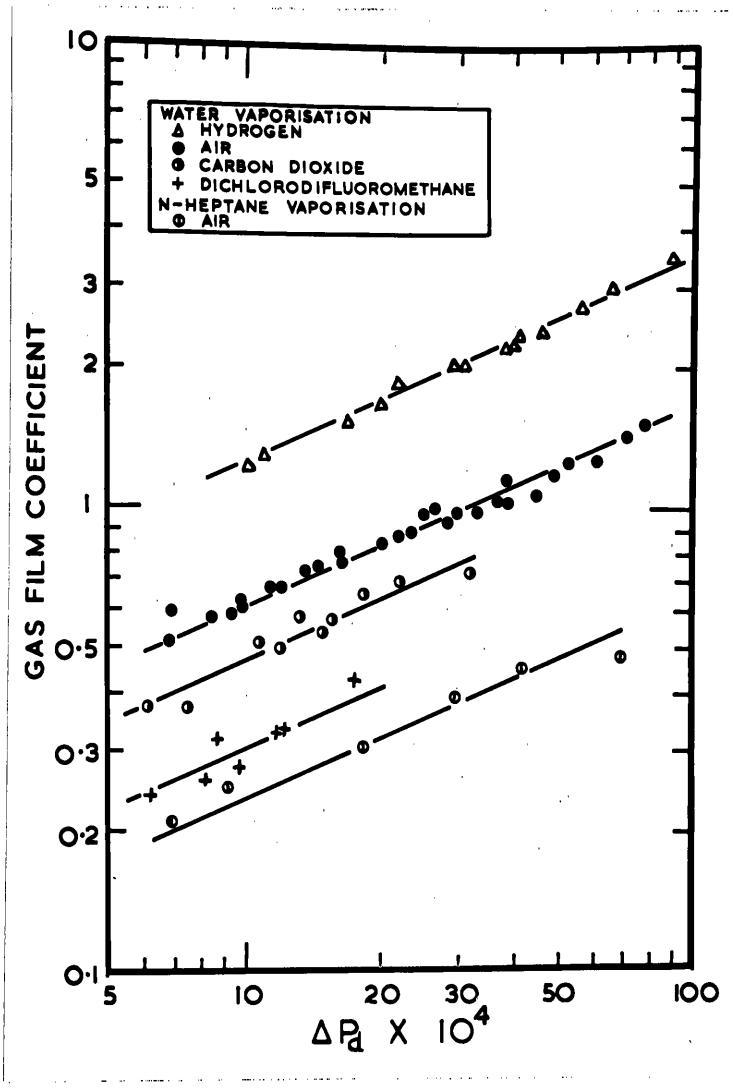

Fig. 8.15 - The relation between k_g and ΔP_d for all systems

Fig. 8.15 shows that all the data can be represented by a series of parallel lines and, hence to develop a generalised correlation, the factors, considered to be cause of the displacement of the different systems, were analysed. It seemed reasonable to expect the differences in the diffusion coefficients of the systems, to be the cause of the displacement. Therefore, a cross plot at constant ΔP_d was made, as shown in Fig. 8.16, in which k_g is graphed against the diffusion coefficient D on a log.-log. scale.

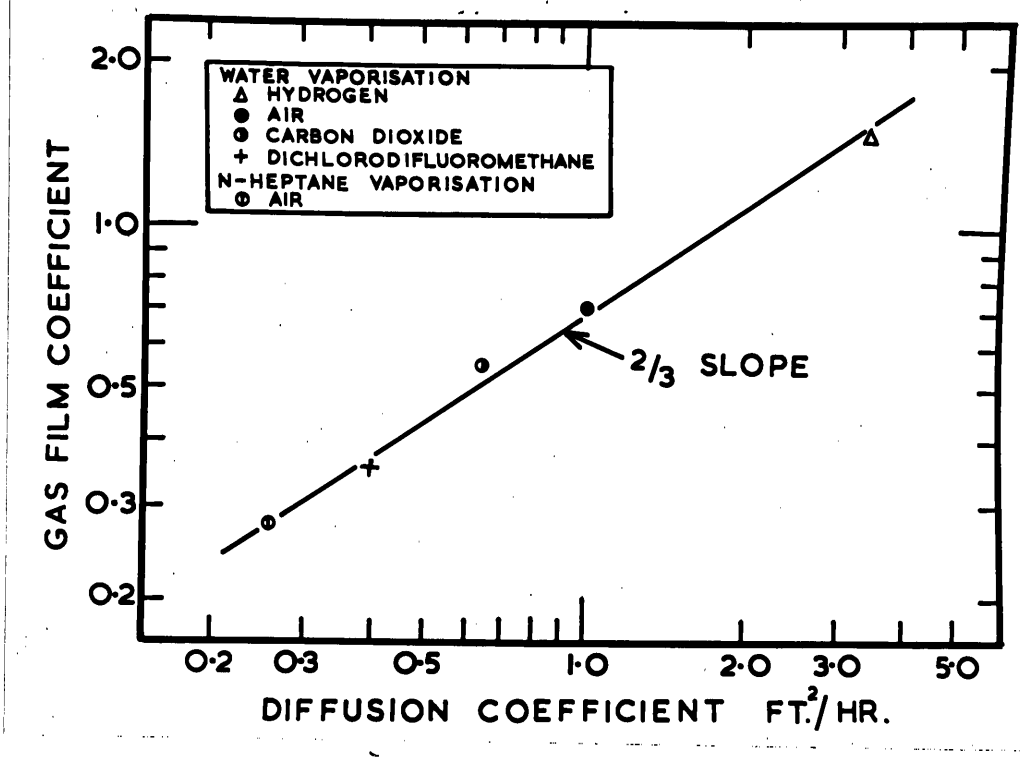

Fig. 8.16 - The effect of diffusivity on the gas film mass transfer coefficient k_g.
Constant $\Delta P_d = 15 \times 10^{-4}$ lb./ft.²

The diffusion coefficients were evaluated at the arithmetic mean film temperature. The diffusion data given in Table 8.17 was extended to the mean film temperature assuming $D \propto T^2$. This is in accordance with the simple procedure recommended by Sherwood and Pigford (107), and is considered of sufficient accuracy, as the differences in temperatures involved in the extrapolations were at the most only 10°C. Had the differences in temperature been greater, the extrapolation would have been carried out by the method of Hirchfelder, Bird and Spotz (40).

As can be seen from Fig. 8.16, a line with a slope of $^2/_3$ represents the data very well. This $^2/_3$ exponent on the diffusivity is considered to lend excellent support to the use of this exponent for correlating gas phase mass transfer data, as the uncertain effects of liquid velocity

associated with the other published irrigated data, as discussed in the previous section of this discussion, are eliminated in this approach.

A recent mathematical paper by Potter (86), for mass transfer between co-current streams, based on boundary layer solutions for Schmidt numbers greater than unity, suggests that the exponent Λ depends on the relative interfacial velocity. Although a similar analysis was not developed for countercurrent flow, it would appear that a mathematical analysis, based on boundary layer theory, would also predict a similar variation of the exponent on the Schmidt number, with changes in relative interfacial velocity for countercurrent flow. These experimental results suggest that this is not the case, although the possibility does exist, that the range of relative velocities covered in this investigation (0.04 to 1.77 expressed as the ratio of liquid velocity to gas velocity) is outside the range, in which a variation of the exponent on the Schmidt number occurs. However, this seems extremely unlikely, as, for co-current flow, Potter's mathematical analysis (86) over the same range of relative interfacial velocities, would predict a change in the exponent from $^{2}/_{3}$ to 0.45. These exponents are one minus the exponents given by Potter, as this author chose to derive his equations in the form of the dimensionless Nusselt number $\left(\frac{k_c L}{D}\right)$.

All the mass transfer results of this investigation can be well correlated by a log.-log. plot of $k_g D^{-2/3}$ versus ΔP_d, as shown in Fig. 8.17. This type of correlation of gas film data has not been previously reported.

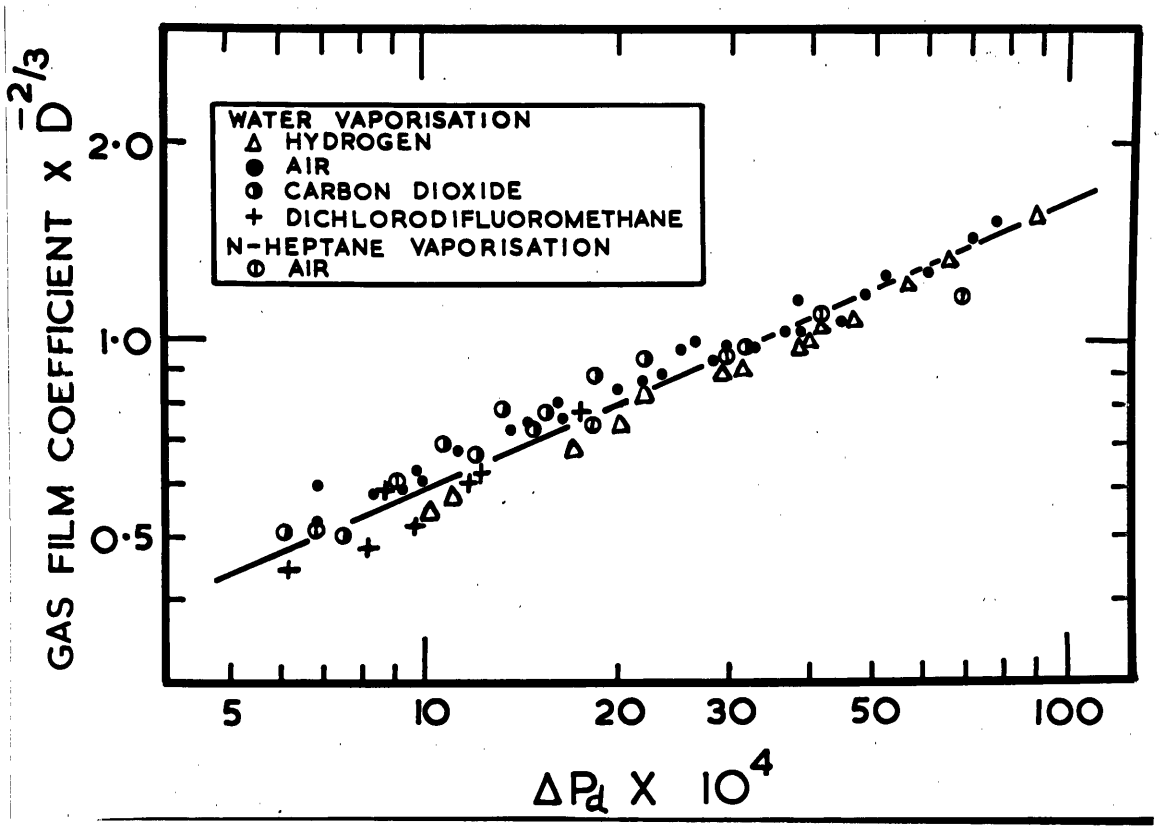

Fig. 8.17 - Generalised correlation of gas film mass transfer coefficients in terms of the diffusivity and the pressure drop

The use of the gas phase mass transfer coefficient k_g in the correlation shown in Fig. 8.17 was a matter of convenience. A more fundamental method of expressing mass transfer coefficients is to use the coefficient k_c, which is defined as "the molar rate of transfer of material per unit area per unit molar concentration difference" (99). As the coefficients k_g and k_c are simply related ($k_c = k_g RT$), the data have not been replotted using k_c rather than k_g.

However, if this type of correlation is to be used at higher temperatures, as would have been the case in the absorption of zinc vapour in molten lead, the correct form is considered to be a correlation using k_c rather than k_g.

The new correlation was developed from data on dilute systems only. For more concentrated systems, further experimental work would be required to establish the inclusion of further terms in the correlation.

The fact, that the mass transfer coefficient can be simply related to the pressure drop and the diffusivity only, is considered very significant and could well be an extremely useful approach for both theoretical and experimental advances in the field of mass transfer.

8.6.4 Calculated Values used in the Correlations

Tables 8.18 to 8.22 contain the calculated values used in the correlations discussed. The pressure drops for the water data were obtained from the experimentally determined equations 7.1, 7.2 and 7.3. The n-heptane pressure drop data was measured during the actual vaporisation run and then corrected for the pressure drop due to the empty column.

TABLE 8.18

VAPORISATION OF WATER WITH HYDROGEN

Run	Γ $\frac{\text{lb.}}{(\text{hr.})(\text{ft.})}$	k_g $\frac{\text{lb. moles.}}{(\text{hr.})(\text{ft.})(\text{atm.})}$	ΔP_d x 10^4 $\frac{\text{lb.}}{\text{ft.}^2}$	Re	$(Re)_R$	j_D	$(j_D)_R$
1A	325	1.23	10.2	328	288	0.0297	0.0246
2A	325	1.70	19.8	437	487	0.0224	0.0205
3A	325	2.03	29.4	564	613	0.0206	0.0190
4A	325	2.26	38.0	675	723	0.0194	0.0180
5A	325	2.42	46.5	786	835	0.0178	0.0166
1B	325	1.55	17.0	381	432	0.0234	0.0207
2B	325	2.05	31.0	595	644	0.0198	0.0183
3B	325	2.26	39.5	683	732	0.0190	0.0178
4B	325	3.02	66.0	1000	1050	0.0174	0.0165
5B	325	3.50	90.0	1239	1290	0.0162	0.0157
6B	325	2.76	56.5	897	947	0.0178	0.0168
7B	325	2.39	41.4	722	722	0.0190	0.0178
8B	325	1.86	22.0	469	518	0.0229	0.0206
9B	325	1.29	11.0	257	307	0.0288	0.0241

TABLE 8.19

VAPORISATION OF WATER WITH AIR

Run	Γ $\frac{\text{lb.}}{(\text{hr.})(\text{ft.})}$	k_g $\frac{\text{lb.moles.}}{(\text{hr.})(\text{ft.}^2)(\text{atm.})}$	$\Delta P_d \times 10^4$ $\frac{\text{lb.}}{\text{ft.}^2}$	Re	$(Re)_R$	j_D	$(j_D)_R$
1C	325	1.52	78.0	2645	2990	0.0141	0.0125
2C	325	1.42	65.0	2314	2660	0.0150	0.0131
3C	325	1.25	52.5	1984	2330	0.0154	0.0132
4C	325	1.14	38.2	1599	1980	0.0174	0.0144
5C	325	1.00	26.5	1233	1580	0.0198	0.0155
6C	325	0.75	16.4	860	1205	0.0199	0.0152
7C	325	0.67	11.3	616	962	0.0266	0.0171
8C	325	0.60	6.9	392	738	0.0372	0.0198
1D	298	0.60	9.8	548	878	0.0270	0.0168
2D	240	0.59	9.3	548	866	0.0264	0.0167
3D	149	0.58	8.4	548	783	0.0261	0.0182
4D	64	0.52	6.8	548	683	0.0233	0.0187
1E	298	0.74	14.2	770	1105	0.0236	0.0165
2E	240	0.73	13.5	770	1090	0.0231	0.0164
3E	149	0.68	12.0	770	1010	0.0215	0.0164
4E	64	0.62	9.9	770	908	0.0198	0.0168
5E	298	0.97	25.2	1213	1550	0.0196	0.0153
6E	240	0.89	23.5	1213	1535	0.0179	0.0142
7E	149	0.84	20.0	1213	1450	0.0169	0.0142
8E	64	0.80	16.2	1213	1350	0.0161	0.0145
1F	298	1.02	36.0	1544	1880	0.0161	0.0132
2F	240	0.98	33.0	1544	1865	0.0155	0.0128
3F	149	0.93	28.5	1544	1780	0.0148	0.0129
4F	64	0.87	22.0	1544	1685	0.0138	0.0127
5F	298	1.16	49.0	1907	2240	0.0148	0.0126
6F	240	1.05	45.0	1907	2230	0.0135	0.0116
7F	149	1.01	39.0	1907	2150	0.0129	0.0115
8F	64	0.97	30.0	1907	2050	0.0124	0.0116

TABLE 8.20

VAPORISATION OF WATER WITH CARBON DIOXIDE

Run	Γ $\frac{\text{lb.}}{(\text{hr.})(\text{ft.})}$	k_g $\frac{\text{lb.moles.}}{(\text{hr.})(\text{ft.2})(\text{atm.})}$	ΔP_d x 10^4 $\frac{\text{lb.}}{\text{ft.}^2}$	Re	$(Re)_R$	j_D	$(j_D)_R$
1G	325	0.52	10.7	867	1490	0.0224	0.0130
2G	325	0.58	13.1	1045	1665	0.0209	0.0131
3G	325	0.54	15.0	1182	1800	0.0171	0.0112
4G	325	0.72	31.8	2107	2730	0.0128	0.0098
5G	325	0.69	22.0	1619	2240	0.0160	0.0116
6G	325	0.65	18.2	1418	2040	0.0172	0.0120
7G	325	0.57	15.3	1200	1820	0.0179	0.0118
8G	325	0.50	11.7	947	1570	0.0196	0.0119
9G	325	0.37	7.4	620	1240	0.0223	0.0112
10G	325	0.37	6.0	506	1125	0.0274	0.0123

TABLE 8.21

VAPORISATION OF WATER WITH DICHLORODIFLUOROMETHANE

Run	Γ $\frac{\text{lb.}}{(\text{hr.})(\text{ft.})}$	k_g $\frac{\text{lb.moles.}}{(\text{hr.})(\text{ft.})(\text{atm.})}$	ΔP_d x 10^4 $\frac{\text{lb.}}{\text{ft.}^2}$	Re	$(Re)_R$	j_D	$(j_D)_R$
1H	325	0.24	6.2	1186	3280	0.0167	0.0061
2H	325	0.28	9.8	1800	3900	0.0128	0.0059
3H	325	0.33	12.3	2210	4300	0.0123	0.0063
4H	325	0.33	11.8	2148	4250	0.0126	0.0064
5H	325	0.43	17.5	3030	5120	0.0116	0.0069
6H	325	0.32	8.8	1620	3720	0.0162	0.0071
7H	325	0.26	8.2	1532	3620	0.0138	0.0059

TABLE 8.22

VAPORISATION OF n-HEPTANE WITH AIR

Run	Γ $\frac{\text{lb.}}{(\text{hr.})(\text{ft.})}$	k_g $\frac{\text{lb.moles.}}{(\text{hr.})(\text{ft.}^2)(\text{atm.})}$	$\Delta P_d \times 10^4$ $\frac{\text{lb.}}{\text{ft.}^2}$	$(Re)_R$	$(j_D)_R$
1M	15	0.21	6.8	587	0.0199
2M	15	0.25	9.1	850	0.0163
3M	15	0.30	18.2	1235	0.0136
4M	15	0.39	29.6	1730	0.0125
5M	15	0.45	41.8	2220	0.0114
6M	15	0.48	68.4	2830	0.0096
1J	113	0.34	7.1		
2J	113	0.40	12.4		
3J	113	0.48	23.7		
4J	113	0.49	24.5		
5J	113	0.42	18.0		
6J	113	0.37	10.2		
1K	89	0.37	10.2		
2K	89	0.50	20.7		
3K	89	0.50	32.6		
4K	89	0.46	21.4		
5K	89	0.40	15.7		
6K	89	0.33	7.8		
1L	50	0.30	9.9		
2L	50	0.36	16.0		
3L	50	0.43	23.6		
4L	50	0.48	32.0		
5L	50	0.54	41.8		
6L	50	0.60	51.7		

8.7 Nomenclature

(a) Symbols

A = gas - liquid interfacial area, ft.^{2}

a = gas - liquid interfacial area in a packed column, ft.^{2}/ft.^{3}

C_p = specific heat of fluid, B.T.U./(lb.)($^\circ$F)

D = diffusion coefficient or diffusivity, ft.^{2}/hr.

f = Fanning friction factor (dimensionless)

G_m = molar mass velocity, lb.mole./(hr.)(ft.^{2})

G = mass velocity, lb./(hr.)(ft.^{2})

h = heat transfer coefficient, B.T.U./(hr.)(ft.^{2})($^\circ$F)

h_L = liquid film heat transfer coefficient, B.T.U./(hr.)(ft.^{2})($^\circ$F)

h_g = gas film heat transfer coefficient, B.T.U./(hr.)(ft.^{2})($^\circ$F)

$j_D = \frac{k_c}{v} \cdot \frac{p_{BM}}{P} \cdot \left(\frac{\mu}{\rho D}\right)^{2/3} = \frac{k_c \, p_{BM}}{G_m} \left(\frac{\mu}{\rho D}\right)^{2/3}$

$(j_D)_R = \frac{k_c}{v_R} \cdot \frac{p_{BM}}{P} \cdot \left(\frac{\mu}{\rho D}\right)^{2/3} = \frac{k_g \, p_{BM}}{v_R \, \rho_m} \left(\frac{\mu}{\rho D}\right)^{2/3}$

$j_H = \frac{h}{C_p \rho v} \left(\frac{C_p \mu}{k}\right)^{2/3} = \frac{h}{C_p \, G} \left(\frac{C_p \mu}{k}\right)^{2/3}$

k = thermal conductivity of fluid, B.T.U./(hr.)(ft.^{2})($^\circ$F/ft.)

k_c = mass transfer coefficient, lb.mole./(hr.)(ft.^{2})(lb.mole./ft.^{3})

k_g = gas film mass transfer coefficient, lb.mole./(hr.)(ft.^{2})(atm.)

L = characteristic dimension, ft.

M = molecular weight

m = mass of fluid, lb.

N_A = mass transfer rate, lb.mole./(hr.)

N_u = Nusself number $\frac{k_c L}{D}$ (dimensionless)

p = partial pressure of diffusing species, mm. Hg.

P = total pressure, atm.

p_{BM} = logarithmic mean of the partial pressure of the non-diffusing component at the phase boundary and in the bulk of the fluid, atm.

$(\Delta p)_m$ = mean driving force for mass transfer, atm.

ΔP_d = pressure drop across a disc, lb./ft.^{2}

R = universal gas constant

Re = Reynolds number $\frac{L v \rho}{\mu}$ (dimensionless)

$(Re)_R$ = "relative Reynolds number", based on the relative velocity of the gas and liquid streams $\frac{L v_R \rho}{\mu}$ (dimensionless)

s = mean specific heat, B.T.U./(lb.)($^\circ$F)

Sc = Schmidt number $\frac{\mu}{\rho D}$ (dimensionless)

t = fluid temperature, $^\circ$F

T = absolute fluid temperature, $^\circ$R

v = average gas velocity, ft./sec.

v_R = relative velocity of the gas and liquid streams, ft./sec.

ρ = fluid density, lb./ft.^{3}

ρ_m = molar density, lb.mole./ft.^{3}

μ = fluid viscosity, lb./(ft.)(sec.)

λ = latent heat of vaporisation, B.T.U./lb.

Γ = liquid or wetting rate, lb./(hr.)(ft.)

(b) Subscripts

A = diffusing component

B = non-diffusing component

L = liquid phase

g = gas phase

i = gas - liquid interface

1 .... 6 = positions in the column.

SECTION B

INVESTIGATION OF THE ABSORPTION OF ZINC VAPOUR IN MOLTEN LEAD

CHAPTER 9

DISC COLUMN EXPERIMENTS AND DEVELOPMENT OF AUXILLIARY EQUIPMENT

To study the absorption of zinc vapour in molten lead, an experimental system having a known gas - liquid interfacial area was considered preferrable.

Two laboratory absorption columns having known surface areas are the wetted wall column and the disc column. The advantages of the disc column have been discussed in the previous section. Therefore it was decided that a disc column should be used for the investigation.

The application of a Stephens and Morris disc column to a mass transfer investigation, relies for its effectiveness on a knowledge of the exact surface area of liquid in contact with the gas containing the component to be absorbed. To be effective, the molten lead would have to completely cover the disc assembly without splashing. Serious doubts of achieving this aim, existed at the onset of the experimental program. The experiments by Davey (19), who attempted to use a form of wetted wall column during vacuum dezincing experiments on desilverised bullion, were discouraging, as, instead of obtaining a continuous film of lead, a number of small rivulets of lead flowed down the surface.

As the knowledge of the interfacial area would have been extremely useful in analysing the mechanism of zinc vapour absorption in molten lead, the disc column could not be rejected without ample experimentation. The failure of the wetted wall type of column used by Davey (19) was attributed to non-wetting conditions. Experiments on a stainless steel

disc assembly showed, that disc column operation under non-wetting conditions, was impossible. The stainless steel discs were coated with paraffin wax and then irrigated with water. At low water rates, thick rivulets flowed over the central portions of the discs. At higher water rates, the thick rivulets became unstable and splashed off the discs. The same disc assembly was also irrigated with mercury. At all liquid rates, the mercury splashed off the discs. Experiments with a carbon disc assembly using water as the liquid phase, indicated that the discs could not be covered at low liquid rates, because of non-wetting effects, but at higher liquid rates, the discs were covered by the water. As a result of these preliminary checks, it was considered that disc column may function, if the liquid lead could be made to wet the disc surface.

As the auxilliary equipment required for the liquid lead, gas circulation and gas analysis systems, would be the same irrespective of the type of absorption column used, it was decided to proceed with the design and installation of the units with a view of determining the feasibility of using a disc column for the investigation.

Although the disc column finally had to be rejected, the time spent in attempting to make the disc column function was not a complete waste, as it was during these attempts that suitable apparatus and techniques were developed for operating the somewhat difficult ancillary systems associated with the project.

The following discussions are therefore presented for the dual purpose of showing the development of the auxilliary equipment to the modified forms finally used in the investigations and also as a record of the actual experimentation with the disc column.

9.1 The Absorption Column

An absorption column was constructed, having the same principal dimensions as the Stephens and Morris disc column, but of materials to withstand the high temperature service required. The original column shell was a silica tube with clear Vitreosil windows welded into the tube to enable observation of the flow inside the tube. The silica tube was clamped between stainless steel end cover plates and the disc assembly was supported between the end cover plates. The liquid feed jet and the liquid seal were located in the top and bottom end cover plates, respectively.

The silica tube was unsatisfactory, as once the column had been heated, the asbestos gasket material, sealing the tube to the end cover plates, hardened and leakage of gas became excessive. Therefore, a stainless steel column with mica sight windows was fabricated and installed to replace the silica tube. The column could then be sealed more effectively without fear of breakage. The expansion of the stainless steel column was taken up by inserting inconel springs on the studs used for clamping the cover plates to the column shell.

The column assembly was surrounded by a steel casing containing "vermiculite" insulation. The three pairs of mica windows in the column shell were connected to the steel casing by half inch pipes. The mica windows were placed flush with the column shell to prevent condensation of zinc on the windows obscuring the vision. Observation of the discs inside the column was possible by illuminating the three back windows with 32 volt lamps, and viewing through the front three windows, which were directly opposite the illuminated windows.

Because of the desire to observe the flow over the discs, the column

could not be enclosed in a tube furnace. Therefore, to reduce the heat losses, two 1000 watt "calrod" elements were bent into U shape and placed around the absorption column on a 3" square pitch in the "vermiculite" insulation. To prevent the "calrods" from overheating, thermocouples were brazed onto the elements and the power input adjusted.

The original discs were machined from stainless steel rod. The stainless steel disc assembly was sprayed with nickel and after fluxing, was dipped into a bath of molten lead. The lead coating thus obtained was unsatisfactory and portion of the sprayed nickel tended to peel off. Therefore, a new disc assembly was fabricated from pure nickel. This disc assembly was coated with lead by application of a $NH_4Cl - ZnCl_2$ flux and wire brushing molten lead onto the surface of the hot discs. The coating of lead obtained was quite satisfactory and very strongly adherent.

Nickel was used as the surface for lead coating, because the results of Fox (27) and Bailey (3) indicated that molten lead would wet a nickel surface, whereas non-wetting was observed when a steel surface was used. Nickel is slightly soluble in lead at the proposed temperatures of operation (3) and therefore, the original nickel sprayed discs had the advantage that the nickel surface could be readily replaced on depletion. As an adherent coating was not possible on the sprayed discs, it was considered that the life of the pure nickel discs would suffice to establish the feasibility of using the disc column.

The lead coated nickel discs possessed the desired properties, as under static conditions the lead would wet the discs. Whether or not the liquid lead would flow over the discs without excessive splashing, could only be determined by experiment.

Accurate temperature measurement of the liquid lead flowing on the discs was essential, due to the large temperature dependence of the activity of zinc in the lead - zinc alloy formed on absorption. Heat transfer between the lead stream and the hot gas stream would have seriously affected the accuracy, had measurements been made of the column inlet and outlet lead temperatures, rather than the actual temperature on the discs. The use of sheathed thermocouples on the face of the discs was precluded because of the lack of space. As severe alloying with liquid lead occurs with all the standard thermocouples (66), a bare thermocouple could not be located on the face of the discs. The possibility of coating the thermocouple tip with a heat resisting enamel was investigated. Initial coating trials on a sand blasted chromel-alumel thermocouple, fired at 920°C with a heat resisting enamel, were promising, although better results may have been obtained, had the couple been suitably pickled before coating. However, this approach was discontinued, when a more elegant method of measuring the lead temperature was devised.

As the discs would be at the same temperature as the bulk temperature of the lead flowing over them, it was considered simpler to measure the disc temperatures rather than attempt to measure the flowing lead temperatures. This was achieved by mounting the discs on a 3.5 mm. O.D. stainless steel tube, down which two separate 30 gauge iron - constantan, glass - asbestos insulated thermocouples could be inserted from the top of the assembly. The lead temperature could then be measured on the first and last disc or any intermediate disc if required, without fear of alloying of the couple or bad contact of the thermocouple junction with the disc surface. The iron - constantan duplex wire was the only available in Sydney, which was small enough to suit the application, and although iron - constantan

thermocouples are not usually recommended for temperatures as high as those to be measured, the wire was maintained in an inert atmosphere of nitrogen and was readily replaceable without dismantling the apparatus.

The other problem of temperature measurement in the column was the measurement of the gas temperatures. As the gas velocities in the column were high, the errors, associated with radiation between the thermocouple placed in the gas stream and the column wall, were considered negligible. Bare chromel-alumel thermocouples were therefore inserted directly into the gas stream. These couples were set in twin hole silica insulators, which fitted into stainless steel branch tubes welded to the side of the column shell. To reduce diffusion of zinc vapour along the branch tubes and the subsequent alloying of the wires when the zinc condensed, a small stream of nitrogen was bled from the cold end of the branch tubes back into the column to oppose the diffusion.

The lead supply to the discs was through the liquid feed jet, which was designed, so that the disc assembly was located centrally around six liquid lead feed ports, placed on a hexagonal pitch to ensure uniform lead supply to all parts of the top disc.

The lead discharge from the column was originally through a U bend of 3/8" stainless steel tube, which served as a liquid seal accommodating column pressures up to 12.5 p.s.i.g. This type of liquid seal later proved unsatisfactory, as indicated in a later section of this chapter.

The discharge from the liquid seal passed into a vessel sheathed by a tube furnace, which was to be used for measuring the lead flow rate. This flow calibrating vessel was provided with a self-acting syphon to facilitate intermittent drainage of the lead from the vessel. Electrical

contacts were located inside the vessel to record the time taken to fill a known volume of the vessel after a syphonic discharge, and thereby record the lead flow rate. This system, however, was discarded early in the experimental program, when it was realised that considerable difficulty was to be experienced in making even the less complex units operate. Therefore, rather than persist with a contingent source of experimental difficulty, the more simple procedure, of directly casting the lead discharge from the liquid seal and weighing the ingots was adopted.

A line diagram showing the essential features of the disc absorption column developed for the investigation is shown in Fig. 9.1.

1. Introduction
2. Definitions
3. Scope of Regulations
4. Application for Licence
5. Licence Fees
6. Licence Period
7. Licence Not Transferable
8. Licence Must Be Displayed
9. Licence Must Be Produced on Demand
10. Licence May Be Suspended or Revoked
11. Licence Must Be Returned on Suspension or Revocation
12. Licence May Be Reissued
13. Licence Must Be Returned on Change of Address
14. Licence Must Be Returned on Change of Vehicle
15. Licence Must Be Returned on Change of Ownership
16. Licence Must Be Returned on Change of Name
17. Licence Must Be Returned on Change of Address
18. Licence Must Be Returned on Change of Vehicle
19. Licence Must Be Returned on Change of Ownership
20. Licence Must Be Returned on Change of Name

L E G E N D

A. Disc Assembly

B. Column Shell

C. Top Cover Plate

D. Bottom Cover Plate

E. Top Sealing Ring

F. Bottom Sealing Ring

G. Liquid Feed Nozzle

H. Disc Assembly Bottom Support

J. Inconel Spring

K. 1000 W. "Calrod" Element

L. Mica Window

M. Window Viewing Tube

N. Lead Inlet Tube

O. Provision for Lead Outlet to Liquid Seal

P. Provision for Gas Inlet

Q. Provision for Gas Outlet

R. Water Jacket

S. Gas Inlet Temperature Probe

T. Gas Inlet Temperature Probe

U. Disc Supporting Tube

V. Asbestos Gasket

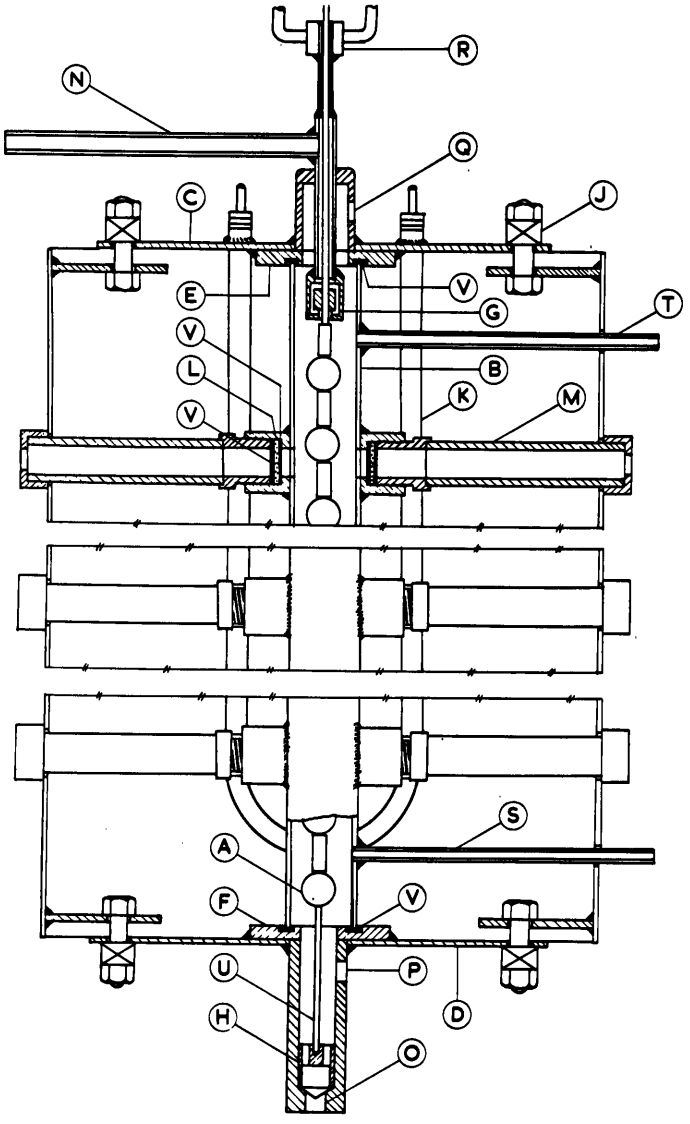

SECTIONAL ELEVATION

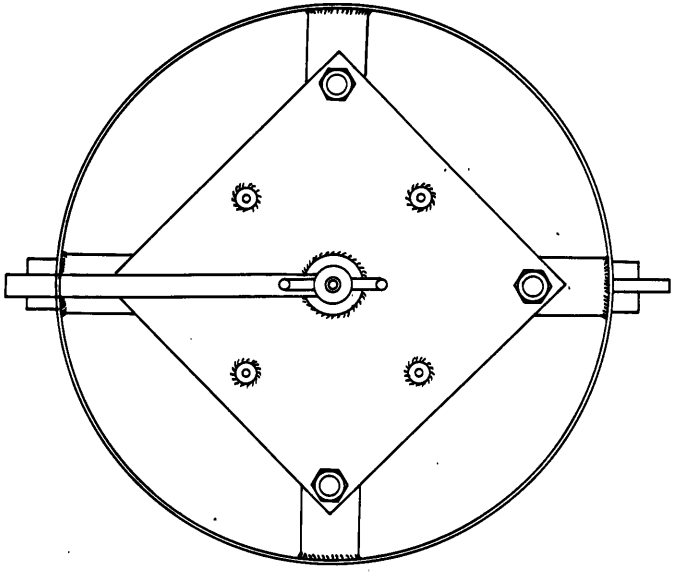

PLAN

Fig. 9.1 - Disc Column - Zinc Absorption Studies

9.2 Liquid Lead System

The systems investigated for the molten lead flow arrangement included the following:-

(a) Gravity feed from lead tank with submerged valve for flow control

(b) Static pressure system with submerged valve for control of flow

(c) Submerged centrifugal pump and valve.

All the above systems, with the exception of the static pressure system, in which pressure inside the tank is used to elevate the lead to the apparatus, were amenable to a reduction in the size of a lead storage tank below that required for a whole run of the apparatus. However, subsequent charging of solid ingots to the tank would have been necessary. Charging of ingots under the maximum lead flow rate of 400 lb./hr. would have required a heat input of 14,000 B.T.U./hr. to bring the solid lead to the temperature of the tank.

To overcome the temperature fluctuations that such a charge would have caused to the main tank, it would have been necessary to melt the charge in a separate tank, bring it up to the desired temperature and then transfer it to the main tank. Such a procedure would have needed attention over a prolonged period and also would have required very high power inputs.

The only real advantage of intermittent charging was that the size of melting and storage tank would have been reduced and hence the total weight of the assembly would have been decreased. This, however, was only critical if the tank was to be elevated to provide gravity feed to the column. As the location of a storage tank above the apparatus was not considered advisable, the use of intermittent charging was eliminated.

The heat requirements to keep a large insulated tank containing all the lead for a six hour run at the operating temperature of 350°C were

calculated to be 2000 B.T.U./hr. (i,e. once the charge had been brought up to temperature).

From a consideration of the characteristics required, it was decided to use a large storage tank capable of supplying the need of a six hour run at the rate of 3 gallons per hour, and to elevate the lead to the column by a small submerged centrifugal pump. The melting tank was placed inside another steel tank so that 6" of slag wool insulation surrounded the unit.

Such an installation was constructed outside the laboratory on a concrete platform, thereby reducing hazards associated with the project to a minimum.

The lead flow rate was adjusted by a remote controlled needle valve, submerged in the lead melting tank. Intermittent checks on the lead discharge rate into a casting wheel, located at the bottom of the absorption column, served as a means of keeping the lead flow rate at the desired level.

The lead tank, pump assembly and valve were enclosed in an inert atmosphere of nitrogen and 2" of granulated charcoal was added to the top of the lead to reduce oxidation.

The lead temperature in the supply tank was maintained at 350°C. by a Cambridge Regulator. The lead was used in the absorption column at temperatures up to 700°C. If the lead was stored at this temperature, extreme measures for the prevention of oxidation would have been required. Also a temperature of 700°C. would have precluded the use of mild steel and cast iron, in construction of the tank, centrifugal pump and valve.

The method used was to melt the lead in a mild steel tank by 2 x 1000 watt "calrod" immersion elements, controlling the temperature

at 350°C. The lead was then pumped at this temperature by a small mild steel and cast iron centrifugal pump designed for the project.

The 2½" diameter cast iron impeller and bowl of the centrifugal pump were standard parts from a small pump manufactured to supply cutting compound to lathes. The impeller was mounted vertically on a ¾" bright mild steel shaft, which extended to two adapter type ball bearings located on the top fange assembly. The vee pulley for driving the shaft at 3000 R.P.M. was located between the two bearings. The whole unit was mounted on a cover plate which allowed easy removal of the pump from the lead tank. The needle valve was built into the top of the impeller housing. As the unit was totally submerged, glands were not required on the shaft entrance to the bowl of the pump or on the needle control valve. The valve spindle terminated above the top cover plate and was positioned in a yoke driven through bevel gears by a shaft, the handle of which was located beside the absorption column inside the laboratory. Provision was made for water cooling the shaft between the bearings, but this was not found necessary.

To maintain the inert atmosphere of nitrogen in the tank, the pump shaft, the valve spindle and the lead discharge pipe were supplied with stuffing boxes on the top cover plate.

The lead was charged to the tank through a removeable gasketed cover plate located on top of the tank. The charge was made the evening before the apparatus was to be run and the power switched on. By the following morning the charge had reached the controlled temperature of 350°C.

The lead dischargedfrom the pump into a 3/8" O.D. 18 gauge stainless steel tube which carried the molten lead through the wall of the building into the apparatus located inside. The lead was heated to the desired

temperature as it passed through this tube by passing a heavy electrical current through the pipe and its contents. Approximately 350 amp. were required to heat the lead to the column operating temperature. The heavy current source used was a 1000 amp., 12.5 volt Selenium Rectifier Plating Unit. The passage of heavy current through the tube also served to preheat the tube to above the melting point of lead, before the lead pump was switched on.

The original method of sealing the lead discharge pipe from the pump to the top cover plate by a stuffing box was found to be unsatisfactory. As the heavy current circuit extended from the surface of the molten lead back along the discharge pipe through the insulated stuffing box, severe overheating of the pipe occurred in the stuffing box, as the asbestos sealing rings also served as heat insulators. This was overcome by locating the discharge pipe in a larger pipe welded onto the top cover of the tank and welded below the surface of the lead in the tank onto the lead discharge line. The bottom end of this larger diameter pipe was sealed and thus there was no chance of nitrogen leakage from the tank. The electrical circuit was still maintained as the discharge pipe was insulated from the larger shielding pipe by a silica tube. The heavy current was introduced into the discharge pipe at the surface of the lead inside the tank and hence the whole length of the discharge pipe above the lead level was evenly heated.

A line diagram of the lead melting tank and the centrifugal pump assembly is shown in Fig. 9.2. Photographs of the installation are shown in Figs. 9.3, 9.4 and 9.5.

L E G E N D

A. Lead Melting Tank (22" O.D. x 24" High x 5/16" Wall)

B. Centrifugal Pump

C. 1000 W. "Calrod" Element

D. "Calrod" Terminal Box

E. Lead Discharge Pipe

F. Shield Pipe for Lead Discharge Line

G. Silica Insulating Tube

H. Needle Valve Body

J. Extended Valve Spindle

K. Extended Pump Shaft

L. Adapter Type Ball Bearing

M. Double Vee Pulley

N. Stuffing Box on Pump Shaft

O. Stuffing Box on Valve Spindle

P. Pump Assembly Cover Plate

Q. Lead Charging Port

R. Copper Busbar for Heavy Current Entry

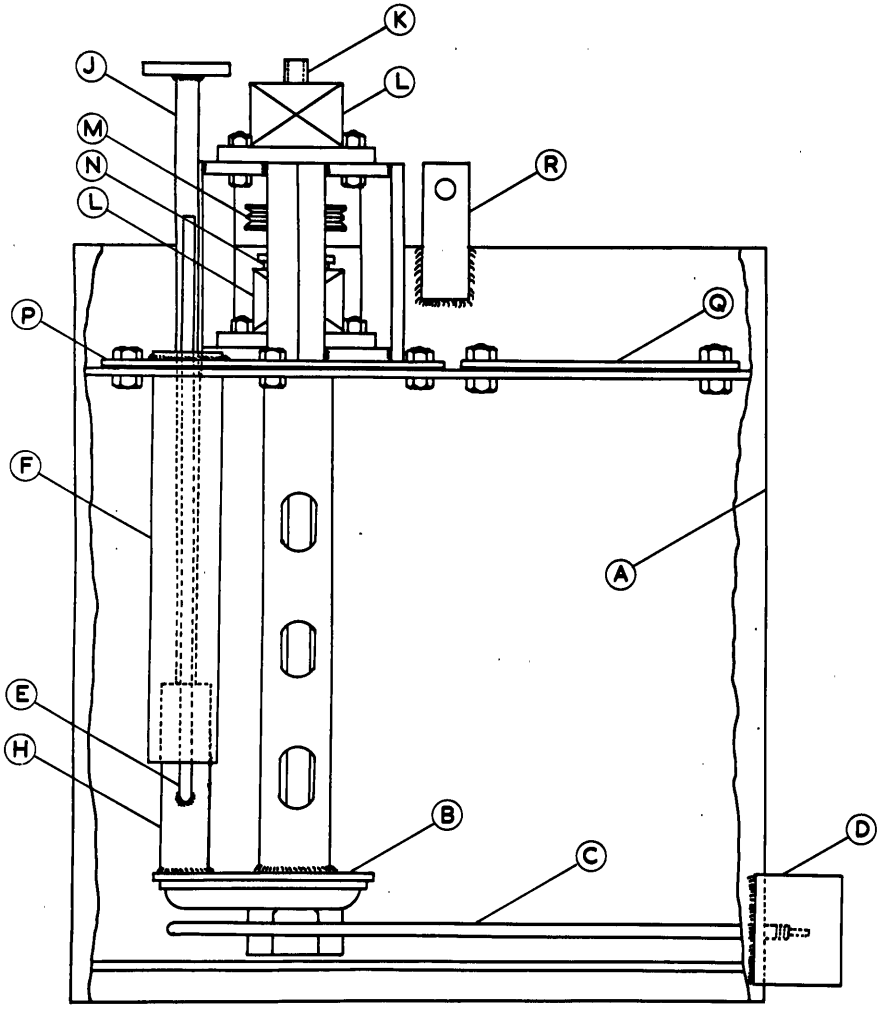

ELEVATION

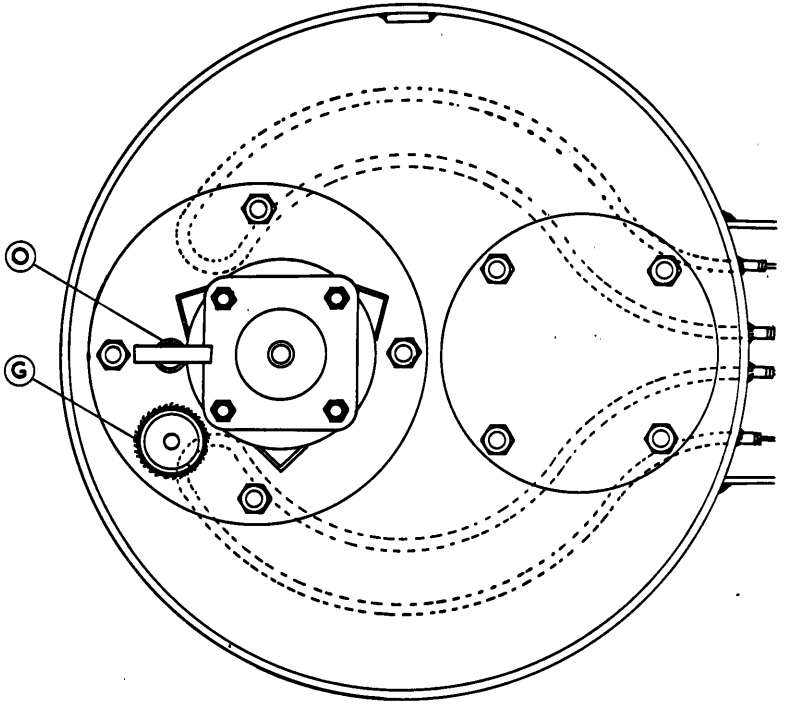

PLAN

Fig. 9.2 - Lead Melting Tank and Centrifugal Pump

Fig. 9.3 - General View of Lead Melting Tank

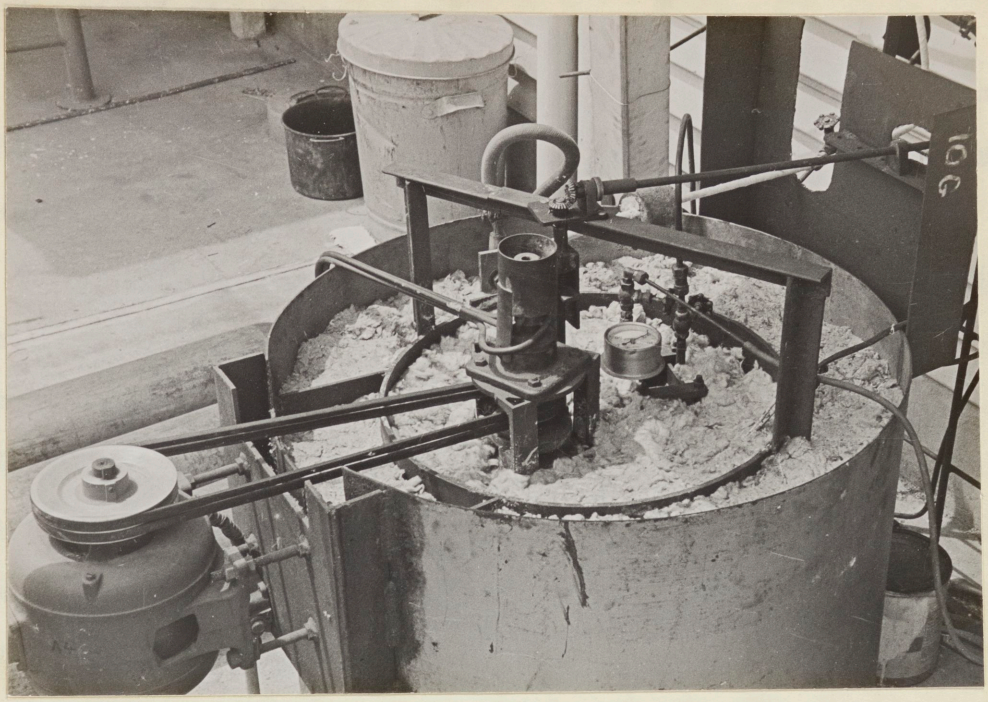

Figs. 9.4 and 9.5 - Close-up Views of Lead Melting Tank and Submerged Centrifugal Pump Assembly

9.3 Gas Circulating System

Dry nitrogen was used as carrier gas for the vaporised zinc in the experimental apparatus. Nitrogen was chosen because of its inertness and its availability.

The nitrogen was circulated through the apparatus at rates between 0.5 and 4.0 ft.^{3}/min. (measured at 60°F. and 1 atm.). The gas circuit operated on a closed system with two sliding vane rotary blowers in parallel providing the necessary boosting for recirculation. A wet gasholder was connected to the suction side of the boosters to maintain a positive pressure of 2" w.g. on the suction side of the system. This was to prevent the infiltration of air into the system through any leaks. The gasholder was filled with a light oil to eliminate water vapour which would otherwise have been present, if water was used as the liquid seal in the gasholder.

To preheat the nitrogen to a temperature of approximately 600°C a heater was designed. The heater consisted essentially of a cylindrical resistance furnace made from nichrome winding on a silica former. Inside the furnace were six passes each 2'6" long of 3/8" O.D. stainless steel tube. At the gas rates required, this preheater was found satisfactory.

The hot nitrogen was then introduced into a second resistance furnace containing a cylindrical stainless steel sheath. Inside this sheath carbon boats containing rods of zinc were placed. This furnace acted as the zinc vaporisation furnace and the temperature was controlled to give the desired concentration of zinc in the gas phase.

To ensure that there was no condensation of zinc in the gas line between the vaporising section and the absorption column, a superheating

section to bring the gas temperature to 700 - 800°C., before it entered the absorption column, was installed. On a calculated figure for the heat transfer coefficient of 100 B.T.U./(hr.)(ft.^{2})(°F) for the mass flow rates required, the necessary superheating was obtained in a four foot length of 3/8" O.D. stainless steel tube at 850°C set in between the vaporising section and the absorption column. A current of approximately 250 amp. was passed through this tube, using the same heavy current source as for the lead system, to maintain the superheater tube at the required temperature.

The nitrogen plus zinc vapour then passed up the absorption column, in which it was brought into contact with the lead flowing down the column.

The gas leaving the column, containing still some vaporised zinc and a small amount of mechanically entrained lead droplets, was piped to a filter unit by a 3/8" O.D. stainless steel tube, heated by passage of heavy current to prevent zinc condensation. The gas was then filtered to remove the zinc dust, formed on cooling, by passing through a tower packed with glass wool.

The zinc - free gas stream was then cooled in two single pass shell and tube water coolers, passed through another filter packed with cotton wool and through a 700 ft.^{3}/hr. dry gas meter. This meter was modified by the manufacturers to enable readings to the nearest one cubic foot to be made. The gas meter gave the integrated gas flow for the period of a test run. Also the reading of the meter established if there were any major leaks in the system, by comparing the flow rate with that calculated from a venturi installed in the high pressure side of the gas flow system. The venturi located just before the nitrogen preheater served as a flow indicator throughout the progress of a test run, whereas the gas meter was used for the subsequent establishment of a zinc mass balance on the

apparatus.

The nitrogen was then recycled through the system by the two blowers in parallel. The flow rate of nitrogen was controlled by a globe valve on a by-pass across the boosters.

Any leaks in the system were made up by supply of nitrogen from the gas holder. The nitrogen supply to the gasholder was by an automatic solenoid operated valve from a compressed nitrogen cylinder.

9.4 Gas Phase Zinc Analysis System

The nitrogen containing zinc vapour was analysed for its zinc content before and after leaving the absorption column. Samples of gas were drawn off from the inlet and outlet gas streams by piping sample lines to the suction side of the gas boosters. Originally the samples of nitrogen containing the zinc vapour were withdrawn from the main gas circuit by means of tee connections, the short arm of the tee leading into the analysis furnace. Difficulty in keeping this short length at the correct temperature, without causing severe overheating of the main gas line, necessitated the modification.

The sample of gas for analysis on the inlet side of the absorption column was therefore taken from a manifold located inside the zinc vaporisation furnace. The sample of gas for outlet zinc analysis was taken directly from the top cover plate of the absorption column. Both inlet and outlet sample lines were of 3/8" O.D. stainless steel tube connected electrically together in series. The lines formed the circuit for the passage of the heavy current (approximately 250 amp.) used for keeping them above the dew point of the zinc vapour. Temperature control of the lines was by insertion of the required resistance in series with the circuit.

The sample lines were connected to removeable stainless steel headers inside resistance furnaces also maintained well above the dew point of the zinc vapour. Connected to the headers and protruding out of the analysis furnaces were detachable ¼" O.D. stainless steel tubes, each containing a small glass wool filter unit for collecting the condensed zinc formed, as the gas cooled inside these ¼" tubes. At the conclusion of the experimental run on the apparatus, these tubes were removed, the zinc leached out with hot 5N. HNO_3 and determined volumetrically using sodium versenate. Provision was made in the construction of the analysis headers for installing seven tubes in both the inlet and outlet analysis headers. After the gas had its zinc content removed in the analysis tube, it was cooled, filtered through a glass wool column, measured in two 30 $ft.^3/hr.$ gas meters (one each for outlet and inlet analysis) and returned to the system at the suction side of the gas boosters.

To reduce diffusion of zinc into the analysis tubes whilst samples were not being taken, a stream of nitrogen was bled back into the system in the reverse direction through the analysis tubes. The bleeding of a stream of nitrogen back into the system was also used in other parts of the gas system where it was desired to reduce diffusion of zinc vapour and subsequent condensation. For example, such places as manometer pressure tappings and thermowells had a very slight stream of nitrogen bled back into the system to prevent blockage of the tubes by zinc condensation. These bleed streams were controlled at one point with visual flow indicators in the form of bubblers on each stream.

A material balance or zinc mass balance was to be established on the absorption column, based on the total gas flow, total lead flow, zinc

analysis on the lead in and out of the column and the zinc analysis of the gas in and out of the column.

9.5 Liquid Lead System Trials and Modifications

Considerable difficulties were experienced in getting the lead system into operation. Initial pumping trials were unsuccessful.

The first motor installed was a ½ H.P. 1440 R.P.M. squirrel cage single phase capacitance start induction motor. The current drawn by this motor when driving the pump at various speeds is shown in Table 9.1.

TABLE 9.1

Pump Speed	Current drawn by Motor
1425 R.P.M.	2.3 amp.
1900 R.P.M.	2.5 amp.
	Motor Rating = 3.38 amp.
3000 R.P.M.	14.0 amp.

As can be seen from Table 9.1, the motor was grossly overloaded when driving the pump at 3000 R.P.M., and hence a trial at this speed was impossible. The lower speeds (up to 2000 R.P.M.) did not result in motor overload and the pump did elevate the lead inside the delivery pipe as was seen by the increased current drawn by the pipe heating system. At the time, it was thought that the lower pump speeds did not develop sufficient head and hence no delivery. Because of this, it was decided to change the motor to a 2 H.P. 1440 R.P.M., 3 phase squirrel cage induction motor, to drive the pump at 3000 R.P.M., and to reduce the total head to be pumped by lowering the whole apparatus inside the laboratory by approximately three feet.

On the basis of later tests with the pump, it is now considered that the ½ H.P. motor driving the pump at 2000 R.P.M. could have achieved the desired head and capacity, without the need for the time consuming process of installation of the new motor drive and complete reassembly of the whole apparatus to reduce the pumping head. The chief factor causing the difficulties in early pumping trials was the presence of cold spots in the liquid flow path. As the flow rates were very small and as lead has such a low specific heat, it was found necessary to ensure that the whole pipe length was well above the melting point of lead before the pump was turned on. The freezing of lead in the pipe around a cold spot was also the cause of pipe failure, in which the part not full of lead became excessively hot due to the increased current flowing through the circuit.

The method of introducing the heavy current into the pipes was initially unsatisfactory, due to the formation of cold spots where the cable clamp was fastened to the pipe. To overcome this, it was decided to introduce the current through a connection of higher electrical resistance than the main pipe, so that the connection itself was hotter than the rest of the pipe. This was achieved by clamping to the lead pipe (3/8" O.D. stainless steel) a small laboratory bosshead to which was brazed a length of 5/16" O.D. stainless steel tube, at the other end of which the conventional cable clamp joined the copper cable to the tube. This system gave the desired "hot" junction where the current was introduced to the main pipe. However, when such a system was used for a pumping trial, the increased temperature of the pipe and its subsequent oxidation, provided only a limited current contact, which resulted in an arc causing puncture of the lead pipe. For this reason, mechanical

clamping of current connections was discarded, and the "hot" current junction was welded directly onto the main pipe. This meant permanent positions for current inlet along the pipe, compared to the readily adjustable mechanical clamping method. However, current adjustment in the pipe section was possible by increasing the length of the 5/16" stainless steel connecting tube and having the sliding cable clamp on this tube to give the desired electrical resistance in series with the main circuit. The net result was good current control and a method of introducing the current without setting up a cold spot or bad contact causing arcing.

Another source of cold spots in the liquid flow path were the pipe couplings. It was necessary to construct 250 watt (32 volt) resistance furnaces wound on silica tubes, to cover all pipe couplings in the lead lines.

With the modifications decribed, the lead pump driven at 3000 R.P.M. was found to have a delivery and head far in excess of what was required for the experiment. The initial procedure of throttling the main discharge from the pump was found to give very poor control of flow, in fact whilst endeavouring to cut down the flow, the needle valve was screwed down too far and the bottom casing of the pump cracked off.

To obtain the desired flow rates of 1 - 4 gallons/hour, the bulk of the lead was by-passed from the pump bowl through three 3/8" diameter ports in the pump discharge assembly. Control of lead flow in the modified system was by a needle valve which throttled the by-pass stream rather than the main discharge stream.

The best method of pumping was to heat all pipes, etc., well above the metling point of lead before staring the pump. On turning the pump

off, the heavy current had to continue to pass through the lines until the current dropped to that corresponding to empty lines. The time taken for drainage of the lead back to the tank was generally less than two minutes. If, however, the current was turned off before drainage was complete, slugs of lead froze in the line and made starting up impossible, unless these slugs were located by measuring the potential drop over a fixed small length of the line and melted by a blow torch with full current flowing through the lines to allow the slugs to drain back into the tank.

9.6 Full Scale Equipment Trials and Modifications

Considerable delay in the experimental program was caused when the first full scale trial run of the apparatus was attempted. Prior to this trial both the gas system involving the vaporisation of the zinc charge and the liquid lead circulating system had been run separately and had operated quite satisfactorily.

It was considered that the first trial on the disc column should be made with the zinc vapour passing over the discs before the lead flow was introduced.

When the lead pump was turned on, the delivery of lead to the column was far in excess of that required, even though the control valve on the pump had been previously set on the required flow rate. The result was that the absorption column immediately filled up with liquid lead and vision through the mica windows, set in the column, was completely obscured. It is difficult to tell, whether this initial mishap also caused the subsequent filling up of all the gaslines and sample lines with liquid lead or, whether later events were the actual cause.

It was only a matter of seconds that the pump was turned on, before it was realised that the flow rate was very excessive. The pump was turned off, the valve adjusted and then the trial recommenced. However, the interior of the column could no longer be seen, which made observation of how the lead was flowing over the discs impossible. On turning the pump on again, there was no delivery from the liquid seal of the apparatus. It was noted that the current flowing in the lines increased as the pump was turned on, as expected once the lead fills the tube forming the electrical circuit. Because of the non-delivery, it was thought, that a slug of lead had frozen in the line. Previous experience with such slugs had indicated that continually turning the pump on and off could sometimes free such a slug. This procedure was adopted but still the lead did not discharge from the apparatus. At this stage, it was decided to discontinue the trial.

Subsequent dismantling of the apparatus revealed, that lead had travelled back through the zinc vapour superheating tube into the zinc vapour analysis headers and tubes and had finally filled up the zinc vaporisation chamber containing the zinc in carbon boats. The actual cause of this could have been either of the following factors:-

(a) The high flow rate, when the pump was initially turned on, may have been of such magnitude that the liquid seal (3/8" O.D. tube) was of too small diameter to cope with the large flow and hence the lead level built up inside the column and discharged into the gas circulating system.

(b) The non-delivery of lead when the pump was turned on for the second time could have been due to either a blockage of dross or a slug of solid lead in the liquid seal of the apparatus. Thus the continual switching on

and off of the pump, to clear the supposed slug of lead in the tube feeding the apparatus, could actually have been filling the system instead of discharging from the liquid seal. The clouding over of the mica sight windows caused initially did not permit visual observation of the flow of lead inside the column.

As a result of this first full scale trial of the apparatus the following modifications were made to the experimental system:

(1) Liquid Seal

The former liquid seal on the absorption column, which consisted of a U shaped 3/8" O.D. stainless steel tube, was replaced by a lute consisting of 5/8" O.D. stainless steel tube immersed in a reservoir of lead with suitable overflow from the reservior into the casting wheel. This reservoir of lead was contained in a 1½" O.D. stainless steel tube with a 5/8" O.D. stainless steel overflow pipe.

Whereas the former liquid seal was heated by passing a heavy current through the pipe, the replacement unit was of such design that it could be readily heated by a wire wound resistance furnace sheathed around the unit. A 1.5 K.W. 240 volt furnace was constructed for this purpose.

This design of liquid seal reduced chance of blockage on the lead discharge side of the apparatus. The former liquid seal could have induced blockage by either of the following means:-

(a) A small slug of lead in the empty tube, caused by blowing over the contents of the seal, could have frozen due to insufficient current flowing because of the relatively high resistance of the empty tube.

(b) The small cross sectional area of the 3/8" tube could have readily become blocked with dross. The cross sectional area of the modified liquid

seal was increased three fold.

(2) Gas Line from Column

The modified liquid seal, relying on the submergence of the discharge in a reservoir of lead, would permit the column pressures between atmospheric pressure and 5 p.s.i.g. The upper limit of 5 p.s.i.g. had to be fixed, as major alteration to the whole assembly would have been required to fit in a seal, which would accomodate pressures up to 12.5 p.s.i.g., which previously were permissable with the former liquid seal. Because of this, the operating pressure inside the column had to be reduced. An analysis of pressure drops through the various components between the absorption column and the gas boosters (maintained at atmospheric pressure), indicated that the replacement of the 3/8" O.D. stainless steel line from the column to the glass wool filter unit, by a shorter length of 5/8" O.D. stainless steel tube, would cut down friction losses sufficiently to allow the desired flow rates, whilst still keeping the column pressure below 5 p.s.i.g.

Previously this 3/8" line had been heated by passing a heavy current through the pipe to keep the temperature above the dew point of the zinc vapour. The installation of the 5/8" line necessitated resistance heating by wire winding around the insulated tube. Whereas the former arrangement had a 2 ft. length of the 3/8" line between the column and the filter, the modified unit consisted of an eight inch length of 5/8" line delivering into a two inch pipe welded at right angles to the smaller line. This two inch pipe was water jacketed and served as a primary zinc condensation unit and trap for entrained lead. Connection between the primary condenser and the filter was by a flexible $\frac{1}{2}$ inch metallic tube. The weight of the primary condenser which was, in effect, cantilevered on

the 5/8" line from the column, was taken by a spring balance to prevent creep of the hot 5/8" line.

(3) Gas Analysis Tubes

The reduced operating pressure of the absorption column necessitated modifications to the zinc vapour analysis tubes. Initially these tubes were packed at the cold end with plugs of glass wool approximately one inch in length. To achieve the desired gas sampling rates with the lower column pressures, the $\frac{1}{4}$ in. O.D. stainless steel tubes were welded into larger diameter filter units. Fourteen of these filter units were constructed, each being $\frac{1}{2}$ inch internal diameter and packed with $1\frac{1}{2}$ inch length of glass wool held in position with stainless steel wire mesh supports. The pressure drop through these modified units enabled the desired gas sampling rates to be achieved when operating on the reduced column pressures.

(4) Interlocking Relay on Lead Pump

To prevent liquid lead from flowing back into the gas circulation system in the case of a blockage in the lead discharge from the column, a relay device was installed in the absorption column to interlock lead level in the column to the centrifugal pump. Once the lead inside the column built up to a dangerous level, the lead pump was automatically cut off. A 32 volt probe was located inside the absorption column. Once contact was made between the insulated probe and the wall of the column by liquid lead, a change-over type electromagnetic relay denergised the coil of an electromagnetic contactor, which cut off the supply of current to the motor driving the pump. The contactor was also arranged with thermal overload protection for the motor.

In the first trial run on the apparatus incorporating the modifications outlined, the newly installed automatic cut-out on the lead pump gave trouble. The pump cut off every time the lead was introduced into the absorption column. This was caused by lead splashing into the probe tube. Therefore, the lead level probe tube was modified by shielding the tip of the probe from any possibility of contact with spray or droplets of lead.

A further two trial runs were then made. These two runs could be considered as the first complete tests on the unit. All ancillary equipment appeared to be working satisfactorily. The automatic cut-off on the lead pump was not actuated until, at one stage, the lead supply to the unit exceeded its capacity. The behaviour of lead flowing over the discs was observed through the mica sight windows. The vision of the process was obscured by small amounts of lead splashing onto the windows. There appeared to be a considerable amount of lead splashing off the discs and falling through the free column space. However, observation was difficult and the lead flow rate fluctuated badly.

The tendency for the lead flow rate to fluctuate, was due to movement of the needle control valve, presumably by the force of the lead in the discharge from the pump. The valve vibrated badly and in doing so was capable of turning sufficiently to cause fluctuation in the flow rate. Because of these fluctuations in flow rate, it was considered that these trials were not a fair indication of the flow of lead over the discs.

The needle valve on the lead by-pass from the pump was modified. A have spring was inserted in the valve spindle to stop the valve lifting on its own accord. The slack in the coupling between the valve and the extension spindle was taken up to prevent any slight rotation or chatter of the valve spindle.

The apparatus was then run with the lead pump on for a duration of three hours. During this period, lead and gas flow rates were varied over a wide range. The conclusion reached at the termination of this trial was that some of the lead was flowing over the discs and some of the lead was just falling through the free space. By visual observation through the mica sight windows, it was not possible to estimate what fraction of the lead was flowing over the discs.

Initially it was thought that the operation of the column could be satisfactorily ascertained by the visual observation of the lead flowing over the discs. In practice, it was discovered that visual observation through the sight windows was not sufficient to determine exactly how the lead was behaving inside the column.

As the uncertainty of whether or not the bulk of the lead was flowing over the discs was present, it was considered that the establishment of experimental results on the system could not be justified, until the flow distribution of the lead inside the column was known exactly.

Therefore the column assembly was dismantled at this stage and the following further modifications were made:-

(1) Liquid Seal

The liquid seal was replaced with a unit, which would separate the flow of lead on the discs to that which was splashing off. This was achieved by having in effect two separate liquid seals both capable of holding column pressures up to 5 p.s.i.g., built into the one unit. The discharge of the lead from two separate overflows would then allow exact determination of the fraction of the lead flowing on the discs. The new liquid seal was enclosed in a 1.5 K.W., 240 volt silica former resistance furnace.

A line diagram illustrating the essential features of the new liquid seal is shown in Fig. 9.6.

(2) Column Shell

Previous trials had indicated that a certain amount of lead was entrained in the gas phase and deposited in the trap on the gas line from the column. This entrainment was due to splashing of the lead and subsequent carry over by the gas stream. Because of this tendency the column shell was enlarged around the lead flow nozzle to cut down the gas velocity at this point.

The splashing of lead due to entrainment around the flow nozzle can be seen in Fig. 9.7 which was taken after the column was dismantled but before the column shell was enlarged around the flow nozzle to reduce this tendency.

A photograph of the modified apparatus after reassembly is shown in Fig. 9.8. An experimental trial on the modified system indicated, by weighing the two lead streams emerging from the liquid seal, that 25% to 20% of the lead flowed over the discs, whilst the remainder fell freely down the column, after having splashed off the disc assembly.

These results were so poor that further work, on the use of the disc column for investigating the absorption of zinc vapour in molten lead, was abandoned.

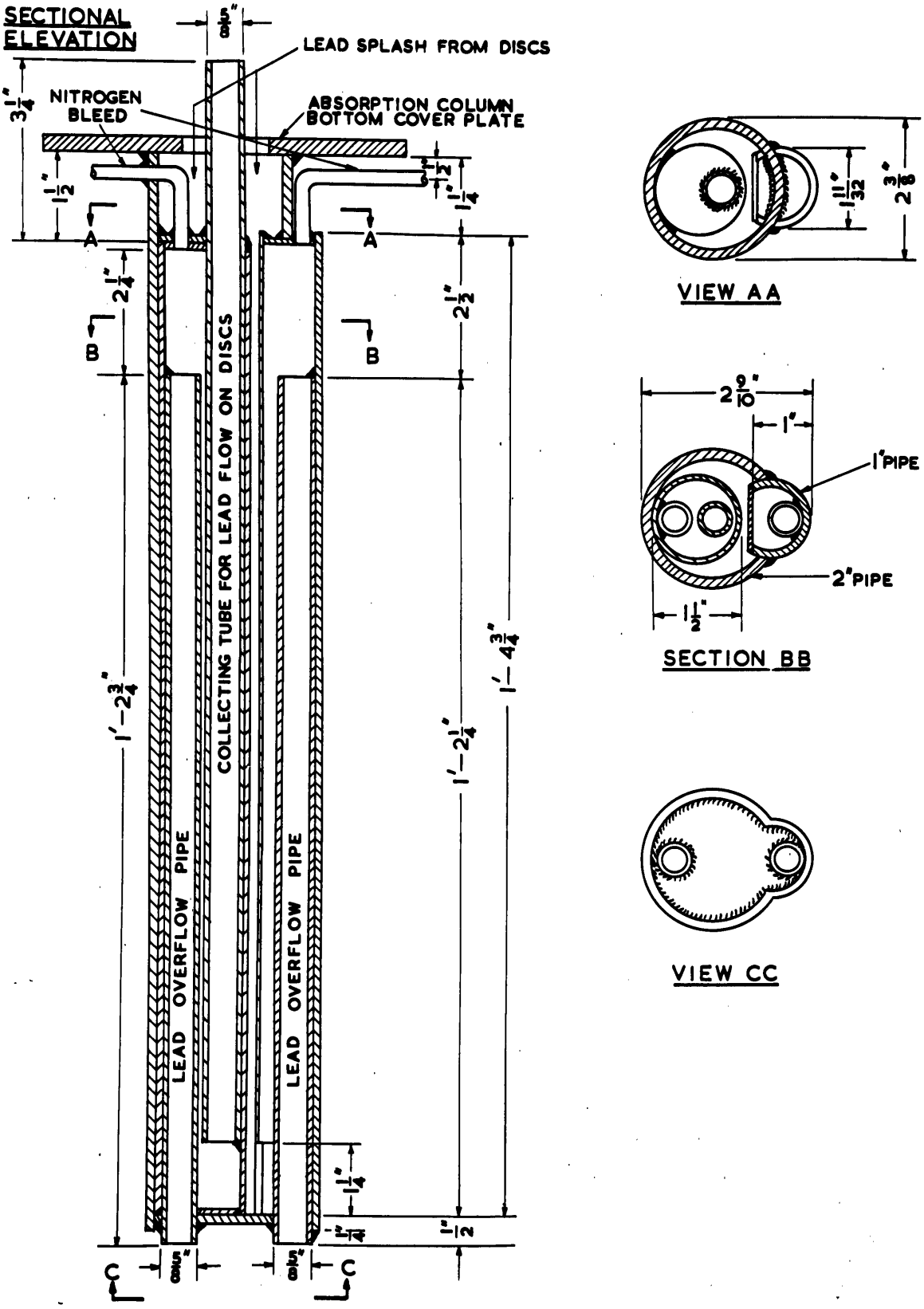

Fig. 9.6 - Liquid Seal for Disc Column

Fig. 9.7 - Photograph of Discs and Top Cover Plate showing Lead Splash around the Liquid Feed Nozzle

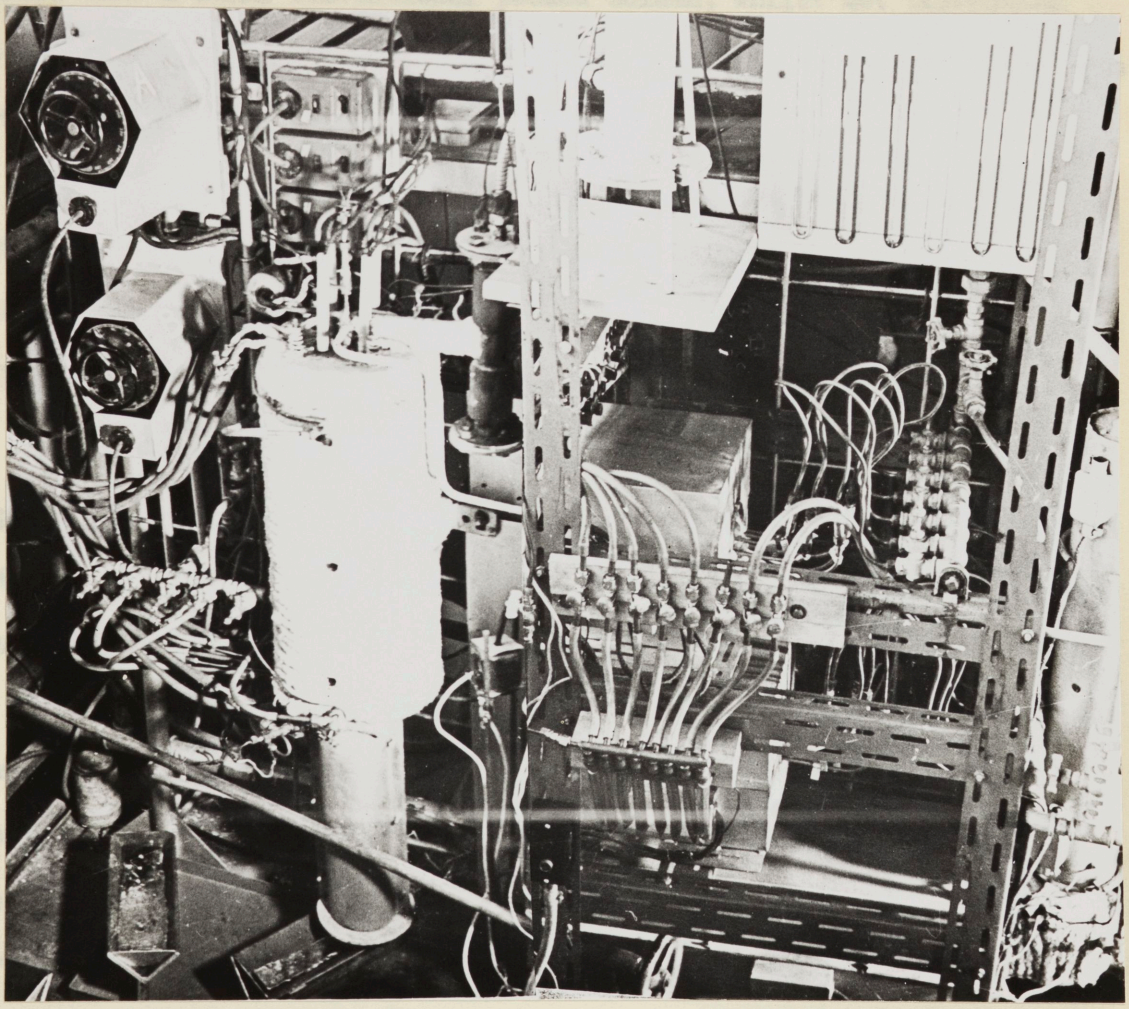

Fig. 9.8 - General View of Disc Absorption Column and Auxilliary Apparatus

CHAPTER 10

PACKED COLUMN ABSORPTION STUDIES

As the disc column proved unsuitable for the investigation, it was decided that a small conventional packed column, whilst not possessing the advantages of known interfacial area, could provide useful information on the absorption of zinc vapour in molten lead.

A column was therefore designed so that, as far as possible, the ancillary systems developed for the disc column experiments could be used with only the minimum modification.

10.1 Apparatus

As the ancillary systems have already been outlined in the previous chapter, descriptions of only the new units and the required modifications of the existing units are presented in this chapter. The "starting-up" troubles associated with the disc column experiments were not present in the packed column studies, as most of the techniques had been fully developed in the earlier experiments. Only slight modification of the new packed column system was required, before the apparatus was in a condition to yield the desired experimental results. The units described are therefore those, which were finally used in the investigation. Any minor modifications made during the course of later experiments are included in the original descriptions.

10.1.1 The Packed Absorption Column

The shell of the absorption column was fabricated from a 2" O.D. 10 gauge stainless steel tube. Details of the shell construction are shown in Fig. 10.1.

Lead and gas temperature probe tubes were welded to the bottom section

L E G E N D

A. Packed Bed ¼" M.S. Raschig Rings

B. Column Shell

C. Column Furnace

D. Packing Support

E. Lead Temperature Probe

F. Lead Collecting Reservoir

G. Lead Inlet Nozzle

H. Lead Inlet from Pump

J. Gas Inlet Temperature Probe

K. Gas Outlet Temperature Probe

L. Gas Inlet Superheater

M. Inlet Gas Distributor

N. Liquid Seal

O. Gas Outlet from Column

P. Outlet Gas Sampling Line

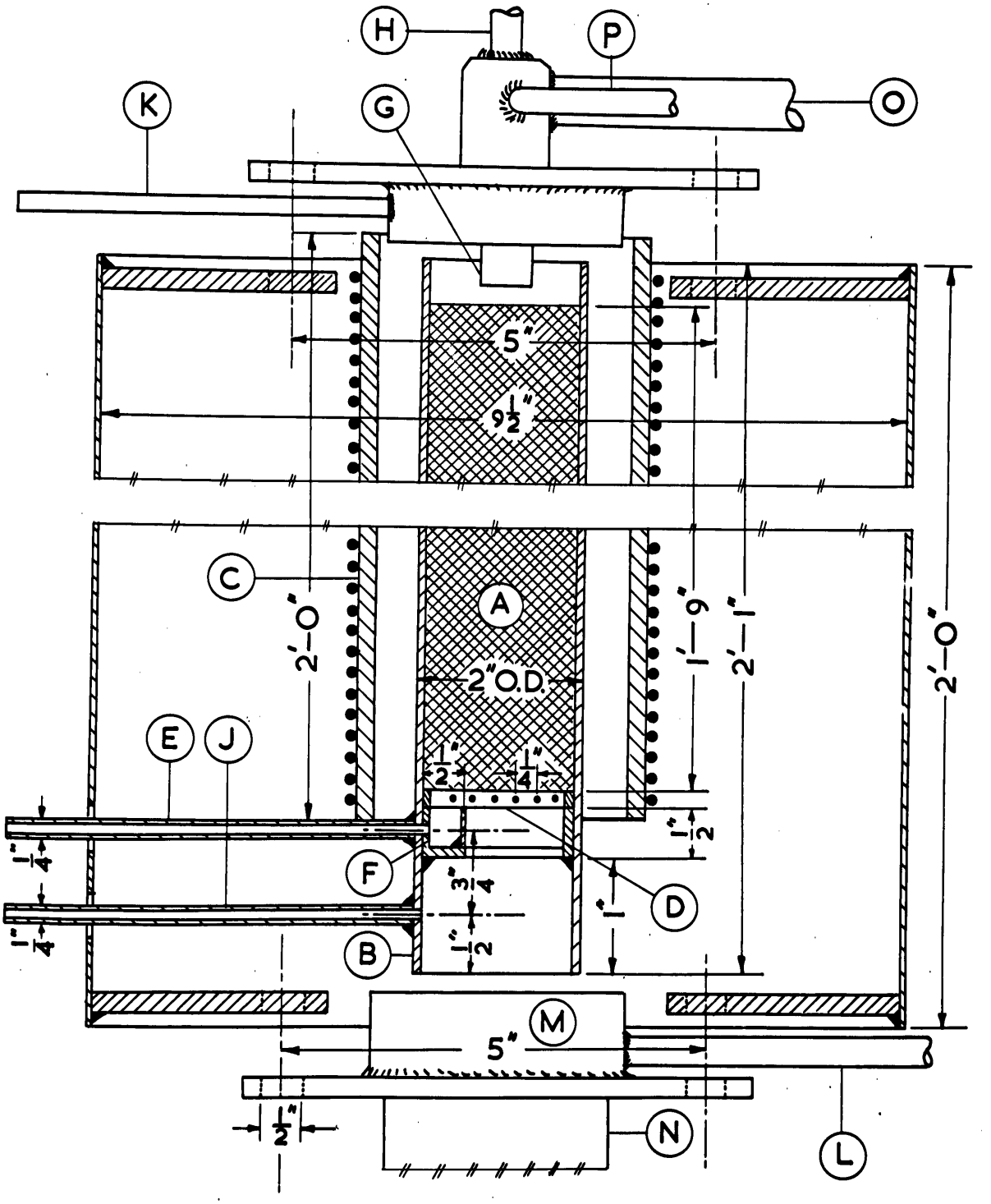

Fig. 10.1 - The Packed Absorption Column

of the shell. Through these probe tubes, stainless steel thermowells made from 3.5 mm. O.D. stainless steel tube were inserted into the lead and gas streams. The thermowells projected out 3/8" from the column shell. The lead thermowell was located in a small reservoir, which was placed directly under the packing support. Portion of the lead flowing down the column was therefore collected in this reservoir, thus enabling its temperature to be measured. The gas temperature thermowell was located directly beneath the reservoir and therefore contact with lead flowing in the column was precluded. The thermowells were sealed into the probe tubes at the cold end using brass "ermeto" tee couplings, fastened to the probe tubes in the normal fashion at one end but packed with graphited cord at the other end to obtain the desired seal. Through the short arm of the "ermeto" tees a bleed of nitrogen was passed to reduce zinc diffusion and subsequent condensation preventing the removal of the thermowells.

A manometer pressure tapping was located beside the gas temperature probe at the bottom of this column. The pressure tapping was also shielded from the lead flow by placing it directly underneath the reservoir used for measuring the lead temperature.

No connections were made to the top section of the column shell. This was to allow installation of a 2 K.W. (240 V) nichrome resistance furnace on a 3" silica tube around the column shell to balance the heat loss from the walls of the column.

The top gas temperature probe and the manometer pressure tapping were located in the sealing ring welded to the top cover plate of the column. The top lead temperature was measured by a thermowell located in the liquid

feed nozzle, which was the same unit as used in the disc column experiments. The connection of these thermowells was the same as outlined for the corresponding units located in the bottom of the column shell.

The tower was packed to a height of 1.75 feet with ¼" mild steel raschig rings. The raschig rings were machined by parting off ¼" lengths of ¼" O.D. 20 gauge mild steel tube. The weight of rings added to the column was recorded to allow calculation of the bed porosity.

Originally it was proposed to clamp this column shell between sealing rings welded to the top and bottom cover plates in the same way as was used for the disc column. However, due to the gasket material becoming hard on heating, the leakage rate around the sealing rings was excessive and therefore the column shell was welded into the sealing rings. This was a drastic step to take, because it meant that the column could not be readily dismantled. However, it was considered more important to eliminate leaks and to face the problem of dismantling, if and when it was necessary.

The top cover plate of the column contained the lead inlet tube, the gas outlet tube, to which was welded the combined primary zinc condenser and entrained lead trap used in the disc column experiments and the outlet gas analysis sampling line. The top sealing ring, containing the temperature probe and the manometer pressure tapping, was also welded to the top cover plate. Details of this top cover plate are shown in Fig. 10.2.

When the disc column was dismantled, a substantial deposit of zinc was found in the 5/8" stainless steel line from the column, where it joined into the combined primary zinc condenser and entrained lead trap.

litre by addition of water in a standard flask and subjected to the following volumetric analysis procedure:-

(a) 100 ml. aliquot for inlet analysis
(500 ml. aliquot for outlet analysis

(b) Neutralised with 20% NaOH solution and then made just acid by dropwise addition of 2N. HCl.

(c) Total volume of inlet solution made up to approximately 250 ml.

(d) Solutions boiled on hot plate in fume cupboard and the following additions made with stirring:-

(i) 2 g. ascorbic acid (reduces Fe^{3+} to Fe^{2+})
(ii) 4 g. mannitol (prevents precipitation of Pb)
(iii) 20 ml. 10% KCN (complexes Zn, Cd, Cu, Ni, Fe^{2+})

(e) 60 ml. NH_4Cl - NH_4OH buffer added to inlet.
120 ml. NH_4Cl - NH_4OH buffer added to outlet.
The addition of buffer was to bring the solution to pH = 10.

(f) Eriochrome Black T indicator powder mixture added to give pink colouration.

(g) Solution titrated with $^{M}/_{20}$ sodium versenate until the indicator changed to blue with complete absence of the original reddish colour. (This titre represented the lead in solution.)

(h) 15 ml. 10% formaldehyde solution added and solution IMMEDIATELY titrated with $^{M}/_{20}$ sodium versenate until the blue end point with the complete absence of the reddish colour was reached. (The formaldehyde discharged the zinc from the cyanide complex making it available for titration with sodium versenate.) This titre represented the zinc present.

For each series of experimental runs, a complete blank analysis was carried out on the No. 7 analysis tube of both the inlet and outlet assemblies. These No. 7 tubes were subjected to the same treatment as the other tubes, with respect to the high temperature service and the possibility of zinc diffusing into the tube followed by subsequent condensation at the cold end. The only difference being that no sample of gas was drawn through them. The zinc titre of the No. 7 tubes was usually in the range of 0.5 to 1.0 ml. compared to zinc titres usually in the

unit in the end of the analysis tube and by squeezing the flexible plastic connection several times, any air pocket in the filter unit or analysis tube was either released to atmosphere through the open end of the header assembly or was trapped in the glass bulb. This procedure was followed in the leaching of all the analysis tubes, as it was considered, that unless the precautions stated were observed, improper contact with the acid, due to the occlusion of an air pocket or bubbles, could lead to erroneous results.

Sufficient hot 5N. HNO_3 was added to the burette so that the level of acid in the assembly was approximately two inches below the manifold, to which all the tubes were welded. In this way, complete contact of the acid with any condensed zinc was ensured because there could be no condensation of zinc in the upper manifold, as during the gas sampling this manifold was maintained well above the zinc dew point temperature. By keeping the liquid level two inches below the manifold, the possibility of the leach solution from one tube spilling into the manifold and the other tubes was eliminated. As described in 10.1.4 any "air-lift" action caused by hydrogen evolution was destroyed, because of the enlarged section connecting the manifold to the smaller diameter analysis tube.

After allowing at least ten minutes contact time, the acid leach solution was drained from the unit and a fresh volume of hot 5N. HNO_3 was added and another ten minutes allowed for solution of any remaining zinc. After this second extract was drained, the tubes were washed three times with hot water to ensure recovery of the zinc solution.

This procedure was repeated in turn for each of the seven analysis tubes in the inlet and outlet header assemblies. The leach solution together with the wash solution for each tube was then made up to one

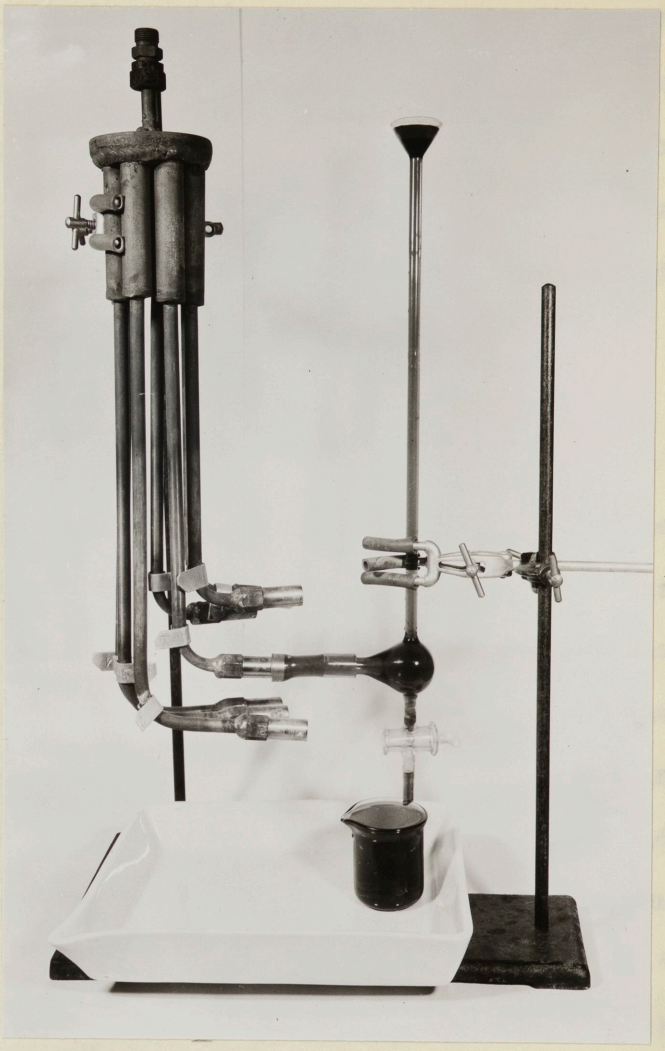

Fig. 10.11 - Analysis header assembled for leaching

The enlarged bulbular section of the glass burette served as a liquid reservior and also as a trap for air caught when the acid was added to the unit. Any air pockets trapped in the filter unit would prevent the desired contact with the acid and therefore incomplete zinc recovery would result. By ensuring that the top of the bulb was higher than the filter

blue end point with complete absence of the reddish colour was reached. (The formaldehyde discharged the zinc from the cyanide complex making it available for titration with sodium versenate. Cadmium also discharged if present, but this may be masked by addition of sodium diethyl dithiocarbamate (55)). This titre represented the zinc present.

10.2.2 Gas Phase Zinc Analysis

The mechanical design feature of the gas phase zinc analysis system, including the method of sampling the inlet and outlet gas from the absorption column, have been treated in 10.1.4. Only the actual chemical analysis procedure involving the leaching of the condensed zinc from the analysis tubes and the subsequent zinc determination is described in this section.

After removal of the stainless steel analysis header units from the analysis furnaces at the conclusion of an experimental run, the condensed zinc in the analysis tubes was leached from the tubes by treatment with hot 5N. HNO_3. Fig. 10.11 is a photograph of one of the analysis header units as assembled during the leaching operation.

The glass burette was connected to the particular analysis tube being leached by a flexible P.V.C. plastic tube, so that the analysis tube and the glass burette formed the equivalent of a vertical "U" tube, one arm being the analysis tube, with the burette forming the other arm. The glass burette was provided with a funnel shaped section at the top to facilitate addition of the acid and wash water. The bottom of the glass burette contained a glass plug cock to enable the leach solution to be drained from the assembly.

10.2.1 Determination of Zinc in Lead

(a) 150 g. Pb. sample, 200 ml. 15N.HNO_3, 750ml. distilled water in a 2 litre beaker heated on a hot plate in a fume cupboard until all the Pb. dissolved.

(b) 150 ml. 1 : 1 H_2SO_4 added slowly with stirring to the boiling solution and then allowed to cool.

(c) $PbSO_4$ precipitate washed by decantation three times with hot water, finally filtered on a Buchner funnel and washed with hot water three times. Precipitate discarded.

(d) Filtrate and washings added to 5 litre beaker and evaporated down almost to dryness in a fume cupboard.

(e) 50 ml. distilled water added to the residue in 5 litre beaker and warmed with stirring on a hot plate. Solution then transferred to 400 ml. beaker and the 5 litre beaker washed thoroughly.

(f) Washings and solution in 400 ml. beaker evaporated down to approximately 50 ml. Solution then allowed to cool.

(g) $PbSO_4$ precipitate washed by decantation with 1 : 10 H_2SO_4 three times, filtered and then washed twice with distilled water. Precipitate discarded.

(h) Filtrate and washings made up to approximately 200 ml. by addition of distilled water after neutralisation of excess acid with 20% NaOH solution.

(i) Solution made just slightly acid by dropwise addition of 2N.HCl and then heated to boiling on hot plate.

(j) 2 g. ascorbic acid, 4 g. mannitol, 20 ml. 10% KCN solution added in this order to the boiling solution whilst stirring in a fume cupboard. (Ascorbic acid reduced Fe^{3+} to Fe^{2+}, mannitol prevents precipitation of Pb, KCN complexes Zn, Cd, Cu, Ni, Fe^{2+}.)

(k) 60 ml. NH_4Cl - NH_4OH buffer added to solution given pH = 10 and cooled to room temperature.

(l) Eriochrome Black T indicator powder mixture added to give pink colouration.

(m) Solution titrated with $^{M}/_{20}$ sodium versenate until the indicator changed to blue with complete absence of the original reddish colour. (This titre represented the lead in solution.)

(n) 15 ml. 10% formaldehyde solution added and the solution IMMEDIATELY titrated with $^{M}/_{20}$ sodium versenate until the

amount of iron present in the usual analytical reagents can interfere with the indicator. When the iron was present as Fe^{2+}, the interfering effects were removed because of the stable cyanide complex formed when potassium cyanide was added.

Initially another source of trouble was that NH_4OH was added to neutralise excess acid after precipitation of $PbSO_4$. The presence of the ammonium salts in the solution interferred with the buffer action, so that pH 10 was not being reached before titration and very poor end points were obtained. Therefore, the neutralisation was achieved by addition of 20% NaOH solution.

A primary separation of lead and zinc was not required in the gas phase zinc analysis. Because of the low lead partial pressures, the zinc collected in the analysis tubes was only slightly contaminated with lead and hence it was possible to titrate this lead directly, whilst the zinc was in the cyanide complex, before releasing the zinc for titration.

The volumetric analysis procedure developed for determining the zinc composition of the lead and the gas phase composition are summarised in 10.2.1 and 10.2.2, respectively. The same major reagents used for both determinations are listed below:-

(a) $^{M}/_{20}$ Sodium Versenate Solution

Standardised with a zinc solution prepared by nitric acid dissolution of A.R. granulated zinc.

(b) Buffer Solution

13.4 g. NH_4Cl + 88 ml. conc. NH_4OH dissolved in water and made up to 250 ml.

(c) Indicator

Eriochrome Black T mixed with dry NaCl. (1 : 400)

Before application of the volumetric procedure, a primary separation of the lead and zinc had to be made. This was achieved by a two stage precipitation of $PbSO_4$. The precipitations of $PbSO_4$ were carried out at the boiling point by the slow addition with stirring of H_2SO_4 (1 : 1) and the precipitate washed by decantation three times followed by filtration and final washing with warm water. These precautions were taken to reduce zinc loss by occlusion and adhesion. The filtrate and washings from the first precipitation were evaporated almost to dryness, a small volume of water added, the precipitate washed three times by decantation, filtered and then washed. The final filtrate and washings, still containing a small amount of lead together with the zinc, were then analysed volumetrically.

Zinc ions can be masked by complex cyanide formation (54)(55)(27). Potassium cyanide was used to complex the zinc in the filtrate obtained after the primary separation of the lead and zinc. The small amount of lead remaining in the filtrate was titrated with sodium versenate, using Eriochrome Black T as indicator, in a solution buffered to pH = 10. Once the lead end point was reached, the addition of formaldehyde solution destroyed the zinc cyanide complex (54)(55)(27), rendering the zinc ion available for titration with sodium versenate.

The method outlined was checked with synthetic mixtures of lead nitrate containing small known amounts of zinc. The method was found very reliable. For example, a mixture containing 0.03% Zn was determined with an error of less than 2½%.

However, even in the analysis of a synthetic mixture, ascorbic acid had to be added to reduce Fe^{3+} to Fe^{2+}. It appears that even the slight

10.2 Chemical Analysis

The chelation of divalent cations with ethylene diamine tetra-acetic acid was originally described by Schwarzenbach (95)(96), who indicated the application of the reagent, now known as "versene", E.D.T.A., "komplexon" or "sequestrol", to volumetric analysis of divalent cations. The theory of such titrations was reviewed by Martell and Calvin (67).

The titration of zinc using the disodium salt of ethylene diamine tetra-acetic acid (sodium versenate) has been the subject of numerous papers over the past few years. However, of particular interest to this investigation were the publications of Kinnunen and Merikanto (54) and Kinnunen and Wennerstrand (55), who reviewed the application of the method for metallurgical control analysis and also the paper by Flaschka (27) on the specific titration of zinc and cadmium. The method finally adopted was based on these three works, suitably modified to suit the particular application. Previous investigators (54)(55)(27) were mainly concerned with determining zinc when present in relatively large amounts. However, in this investigation a method of analysing very small quantities of zinc in a large excess of lead was required. Although lead in small amounts can be masked by complex formation with sodium diethyl dithiocarbamate together with mannitol retaining the lead in solution, such a method could not be used in presence of a large excess of lead.

Even in the presence of small amounts of lead, experiments, carried out during the course of the development of the final technique used, indicated difficulty in observing the end point of the titration, presumably because the lead complex formed with sodium diethyl dithiocarbamate was only slightly more stable than the versenate complex. Therefore it was decided to avoid the use of a reagent to mask lead.

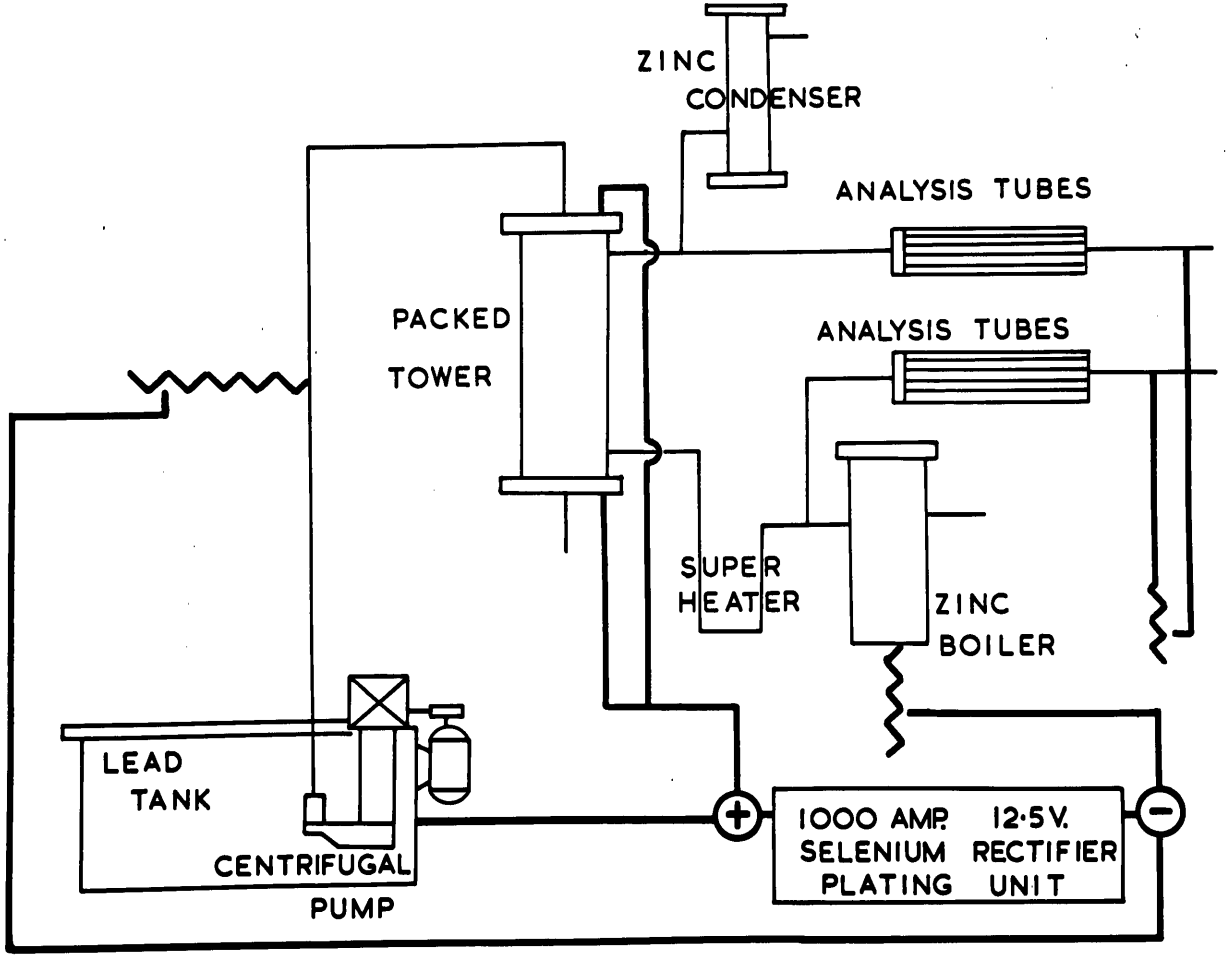

Fig. 10.10 - Low Voltage, Heavy Current
Electrical Circuit

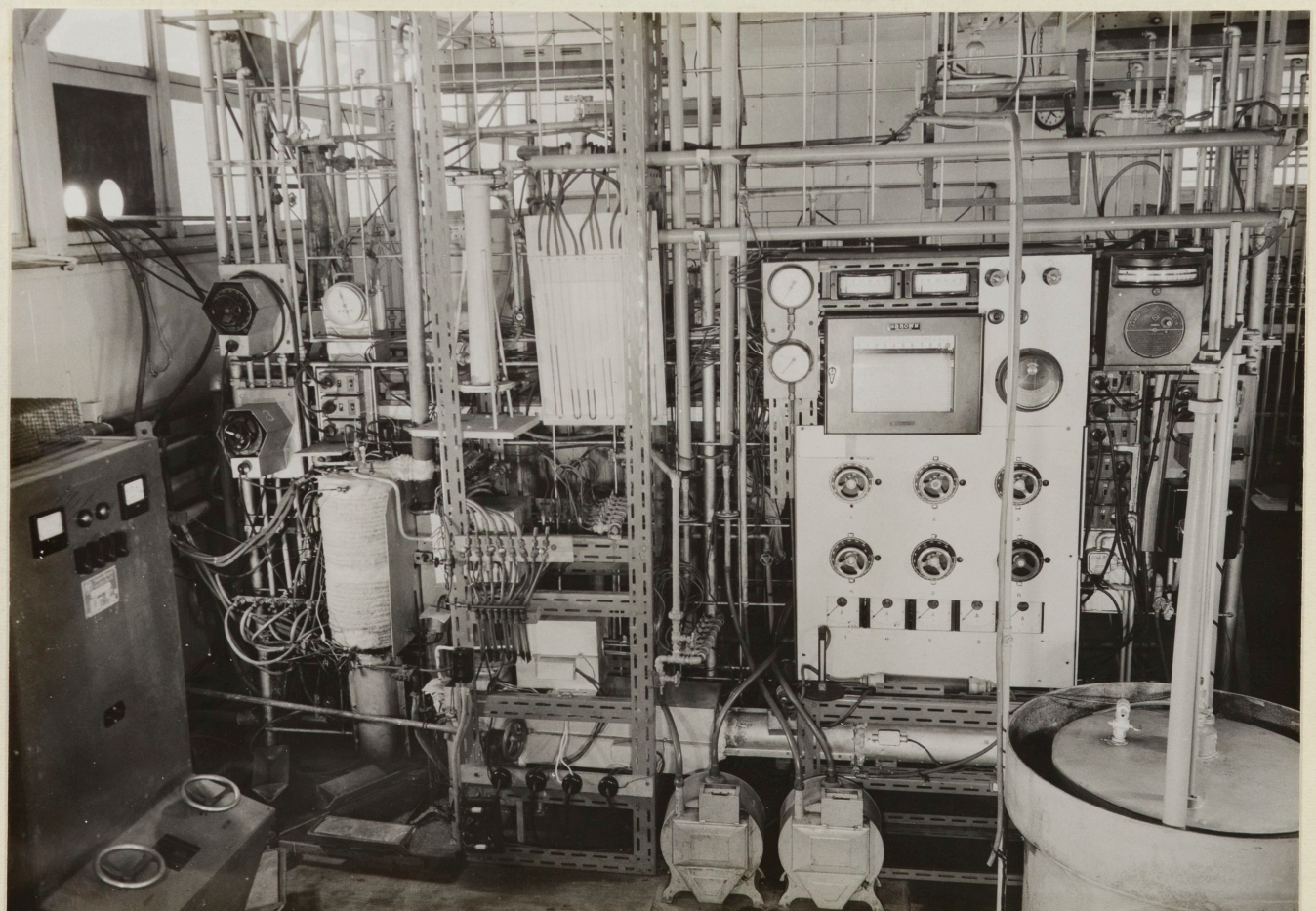

Fig. 10.9 - General View of Packed Absorption Column and Auxilliary Apparatus

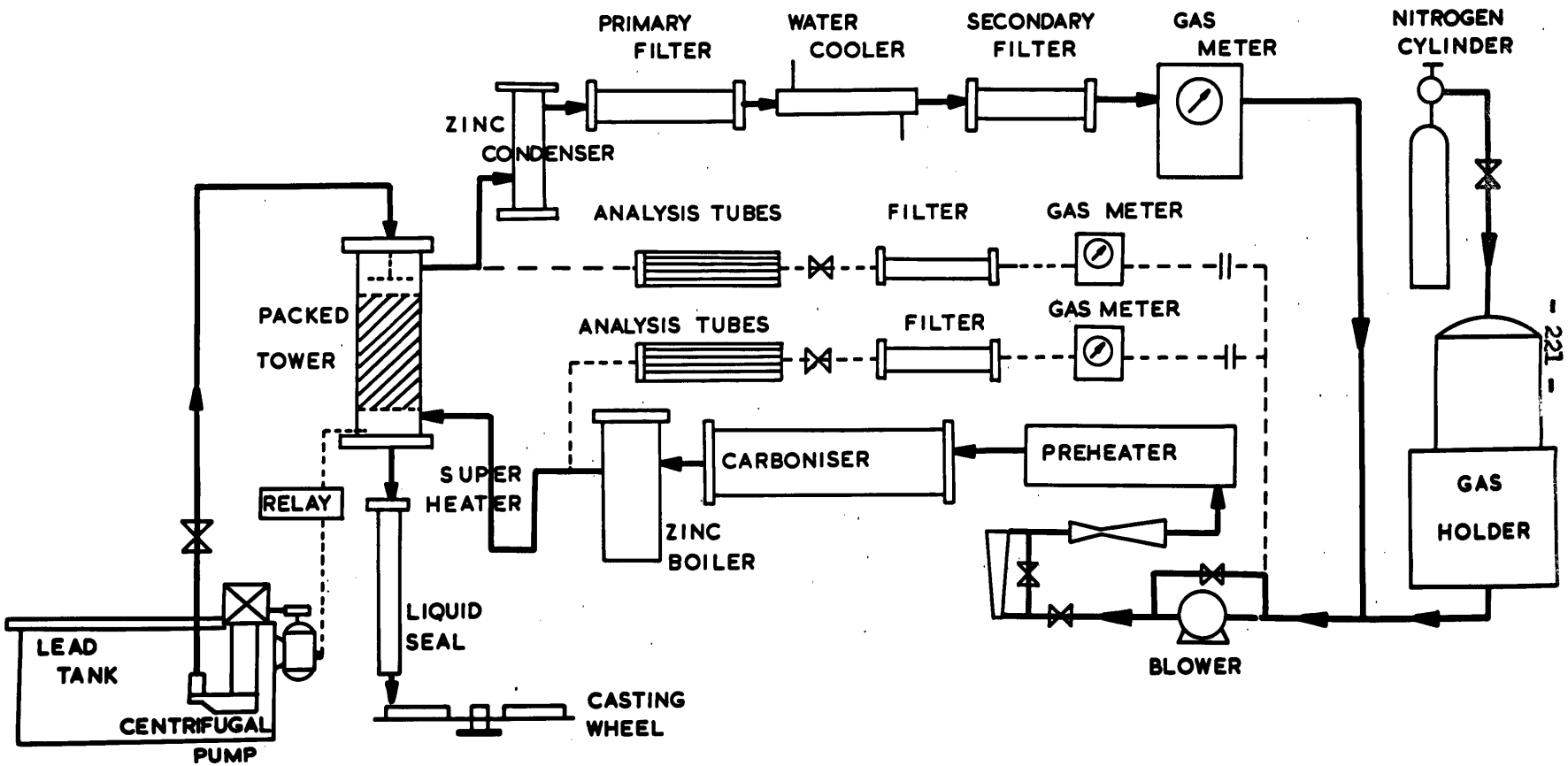

Fig. 10.8 - Flow Sheet of Zinc Absorption in Molten Lead Apparatus

A photograph of the apparatus is shown in Fig. 10.9. The lead melting tank, containing the submerged centrifugal pump and the remote controlled needle valve, were located outside the laboratory on a concrete slab. Photographs and line diagrams of these units were included in the previous chapter (Figs. 9.2, 9.3, 9.4 and 9.5).

The low voltage, heavy current circuit used to heat the liquid lead pipes and the gas circulation lines is shown diagramatically in Fig. 10.10.

.....

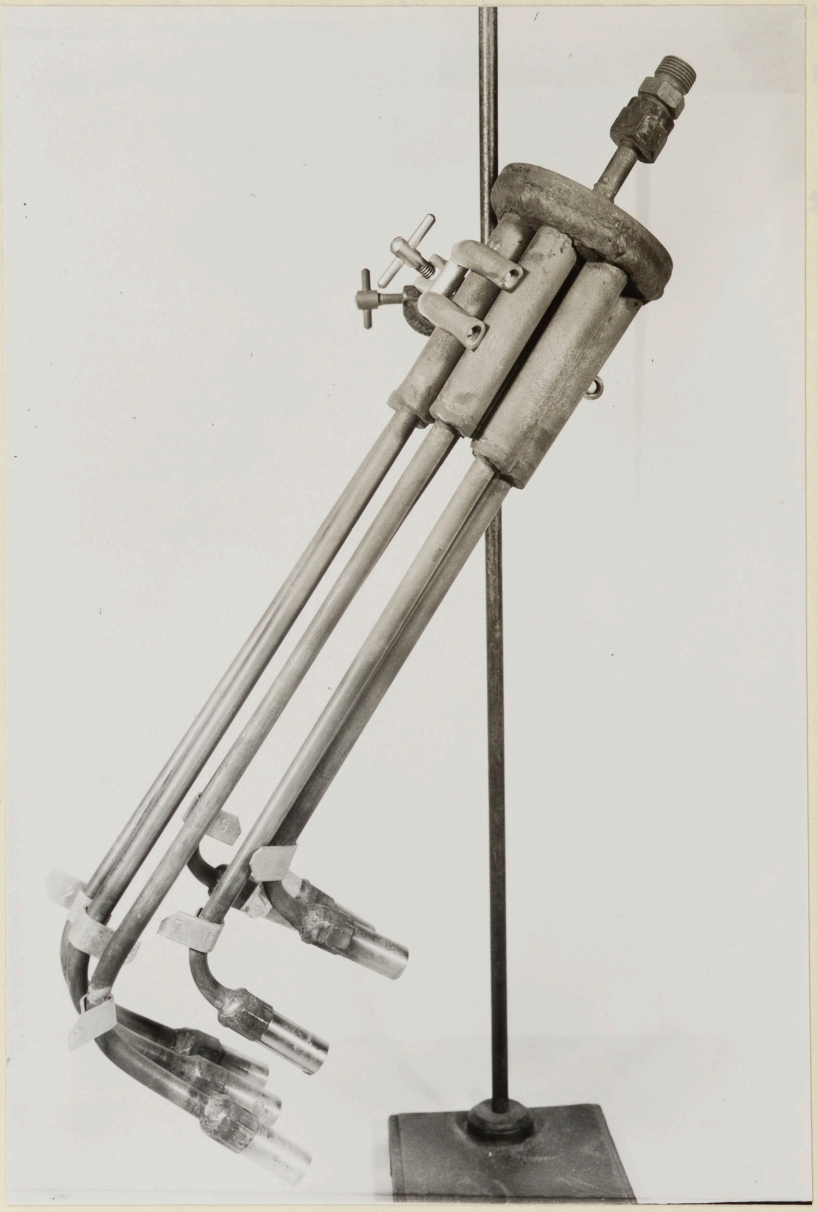

Fig. 10.7 - Stainless Steel Gas Analysis Header

drawn through the desired analysis tube. The manifold was connected to the suction side of the blower. Interposed between the manifold and the blower were 30 ft.^{3}/hr. wet gas meters on both the inlet and outlet analysis systems. These meters were filled with oil instead of the usual water seal, to prevent water vapour from entering the gas circulation system and were provided with glass wool filters on the inlet side, as a precaution against damage due to possible zinc dust entrainment. Orifice meters were located on the outlet of the gas meters to enable the rate of sampling during a run to be observed and controlled at the desired rate.

The inlet and outlet analysis headers were identical. Stainless steel all welded construction was used throughout, to enable the tubes to be leached with nitric acid and to prevent undue oxidation at the high temperatures used. (The analysis furnaces were controlled at approximately 650°C.) A photograph of one of the redesigned analysis header units is shown in Fig. 10.7.

10.1.5 Gas Flow Measurement

The gas flow rates for the packed column were less than the flow rates used for the disc column, because of the tendency towards flooding of the packed column at high gas flows. The gas metering equipment used in the disc column experiments was therefore substituted with units of lower capacity. The 700 ft.^{3}/hr. meter was replaced by a 100 ft.^{3}/hr. dry gas meter. The venturi on the high pressure side of the gas circulation system.was joined in series with a rotameter of lower capacity.

10.1.6 Apparatus Layout

The general arrangement of the experimental apparatus used in the packed column zinc vapour absorption studies is shown in Fig. 10.8.

header and was required so that the header assembly could be removed at the end of the run to allow subsequent analysis.

The reason why the original design of header had detachable analysis tubes, was to prevent carry-over of acid (and therefore zinc) into the header during the leaching operation. An initial study of a glass tube, having the same dimensions as the original analysis tubes, and in which a piece of zinc was placed to simulate the acid leaching, revealed that the hydrogen evolved created an "air-lift" action in the tube, with the result, that the leach solution perked out of the end of the tube, where the analysis header would be in the actual assembly. The conclusion reached from this initial test was that the tubes would have to be detached from the header before leaching.

However, following difficulties which arose when the tubes had to be detached from the header at the end of each run, a further series of tests on glass models of the analysis tubes were conducted, to see if the "air-lift" action on leaching could be eliminated, thereby allowing each tube to be leached independently without detaching from the analysis header.

The desired goal was reached by using 3/8" O.D. analysis tubes terminated into 4" lengths of $\frac{3}{4}$" O.D. tubes welded to the analysis header. Even under extreme conditions of hydrogen evolution, the "air-lift" action was destroyed by the enlargement of the analysis tube to the $\frac{3}{4}$" diameter. The glass wool filter units of the original assembly were welded to the other ends of the 3/8" analysis tubes, which projected out of the analysis furnace and which were below the dew point of the zinc - nitrogen mixture. These filter units were connected by detachable $\frac{1}{4}$" O.D. copper tubes to a manifold provided with a plug cock for each tube, allowing a sample to be

temperatures of operation had deleterious effects on the metal.

The carboniser tube, together with the "ermeto" couplings connecting the unit with the preheater and the zinc boiler, was installed in a 2 K.W., 240 V. nichrome wound silica tube furnace operated at a temperature of 1000°C.

10.1.4 Gas Analysis Headers

The original design of the gas analysis headers, used in the disc column experiments, consisted of detachable ¼" O.D. stainless steel tubes connected to a manifold, to which was attached the gas analysis sample line. These headers were maintained above the dew point of the nitrogen - zinc vapour mixture by enclosing them inside resistance furnaces (nichrome wound on 4" silica tube rated 1.5 K.W. at 240V.).

Difficulties arose when the sample tubes were to be removed from the headers, to enable the condensed zinc to be leached out. The ¼" stainless steel "ermeto" couplings, joining the sample tubes to the headers, tended to seize after prolonged heating in the analysis header furnaces. As both the inlet and outlet analysis headers each contained seven ¼" couplings, which had to be disconnected at the end of each run for analysis, and as usually three or four of these couplings seized after each run, necessitating stripping of the threads on the coupling to remove the tubes, the use of tubes detachable from the header was discarded and a new analysis header designed.

In the new design, each analysis header contained only one "ermeto" coupling, which was subjected to the high temperature of the analysis furnace. This coupling was used to join the 3/8" O.D. sample line to the

10.1.3 Carboniser

The nitrogen used in these investigations was the ordinary grade of commercial nitrogen supplied by Commonwealth Industrial Gases Pty. Ltd. As commercial grade nitrogen is contaminated with oxygen (approx. 0.5%), provision was made for the removal of this oxygen from the nitrogen before entry into the zinc boiler.

As the nitrogen was recycled, the problem of oxygen contamination would have been eliminated, if there were no leaks in the gas circulation system, because the removal of oxygen would have been substantially complete by gaseous oxidation of the zinc after one pass through the zinc boiler.

However, the nitrogen make-up to the system because of leaks, would be contaminated with oxygen and therefore a unit was designed, so that the oxygen content of the nitrogen was converted to carbon monoxide before passage to the zinc boiler. This was achieved by interposing in the line between the preheater and the zinc boiler, a tube packed with carbon granules.

This unit was designated the carboniser. The carboniser was fabricated from 1" inconel tube with the inlet and outlet connection by stainless steel "ermeto" couplings welded to the inconel tube. The carbon granules were retained inside the inconel tube by discs of stainless steel gauze. Several of these stainless steel gauze discs were placed together at both ends of the fixed carbon bed. Initially only one gauze disc was used at each end of the bed. The life of the gauze was short, therefore four discs were placed at each end, as it appeared that the contact of the stainless steel with the carbon at the high-

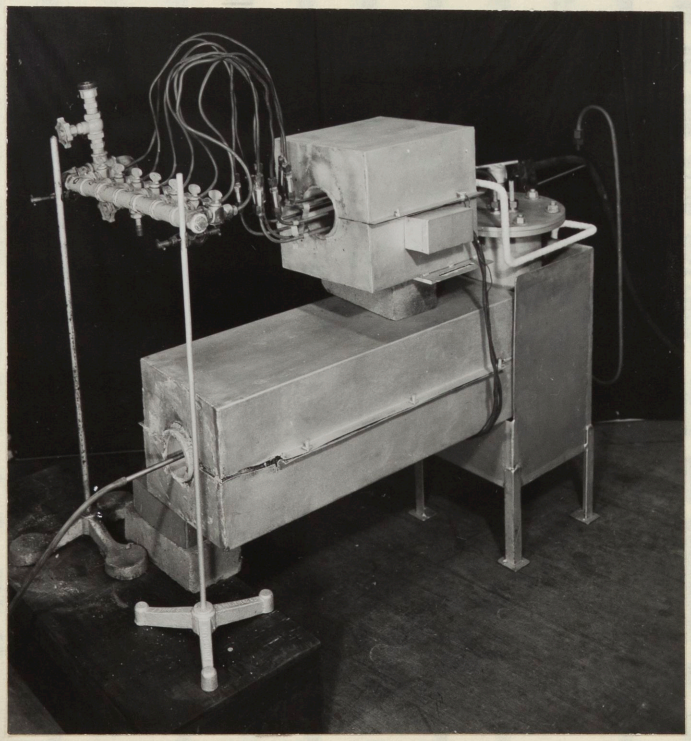

(a) Inlet Zinc Analysis System and Carboniser Connections to Zinc Boiler

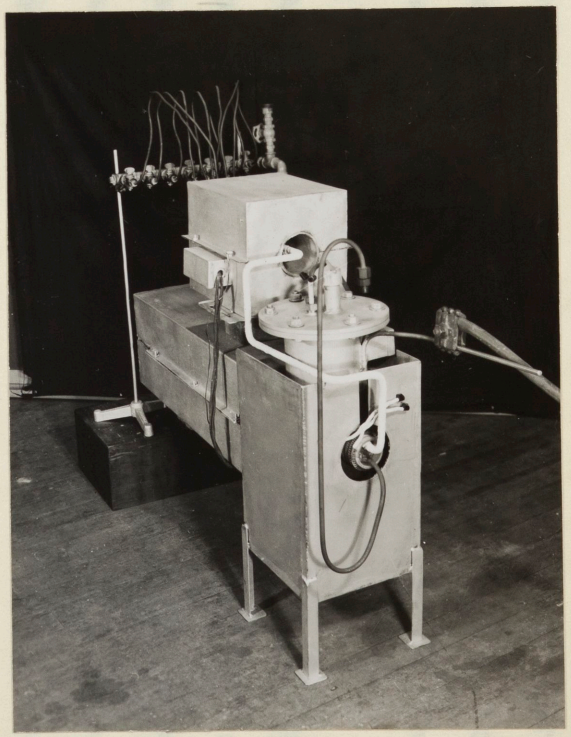

(b) Showing Gas Manifold from Boiler, Inlet Analysis Sampling Line, Superheater Element, Heavy Current Connection

Fig. 10.6 - Preassembled Views of Zinc Boiler and Connecting Units

(a) Pot Furnace Located inside the Boiler

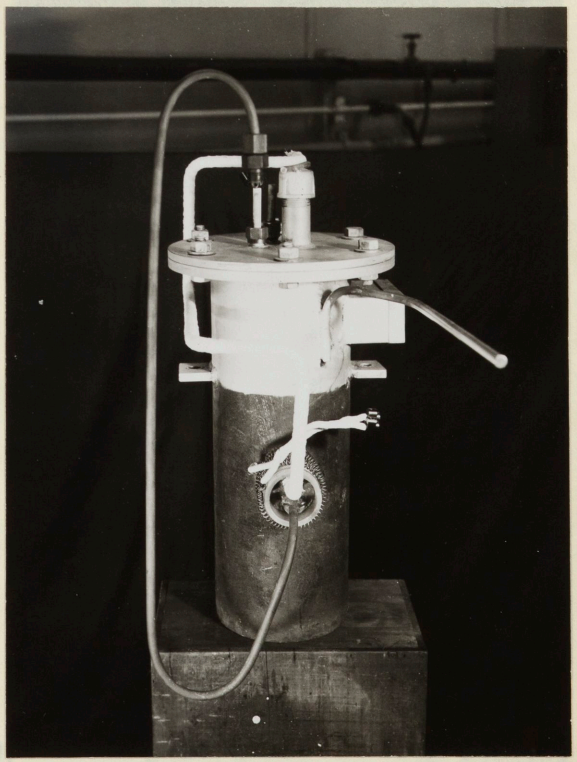

(b) External Steel Vessel

Fig. 10.5 - Zinc Boiler Components

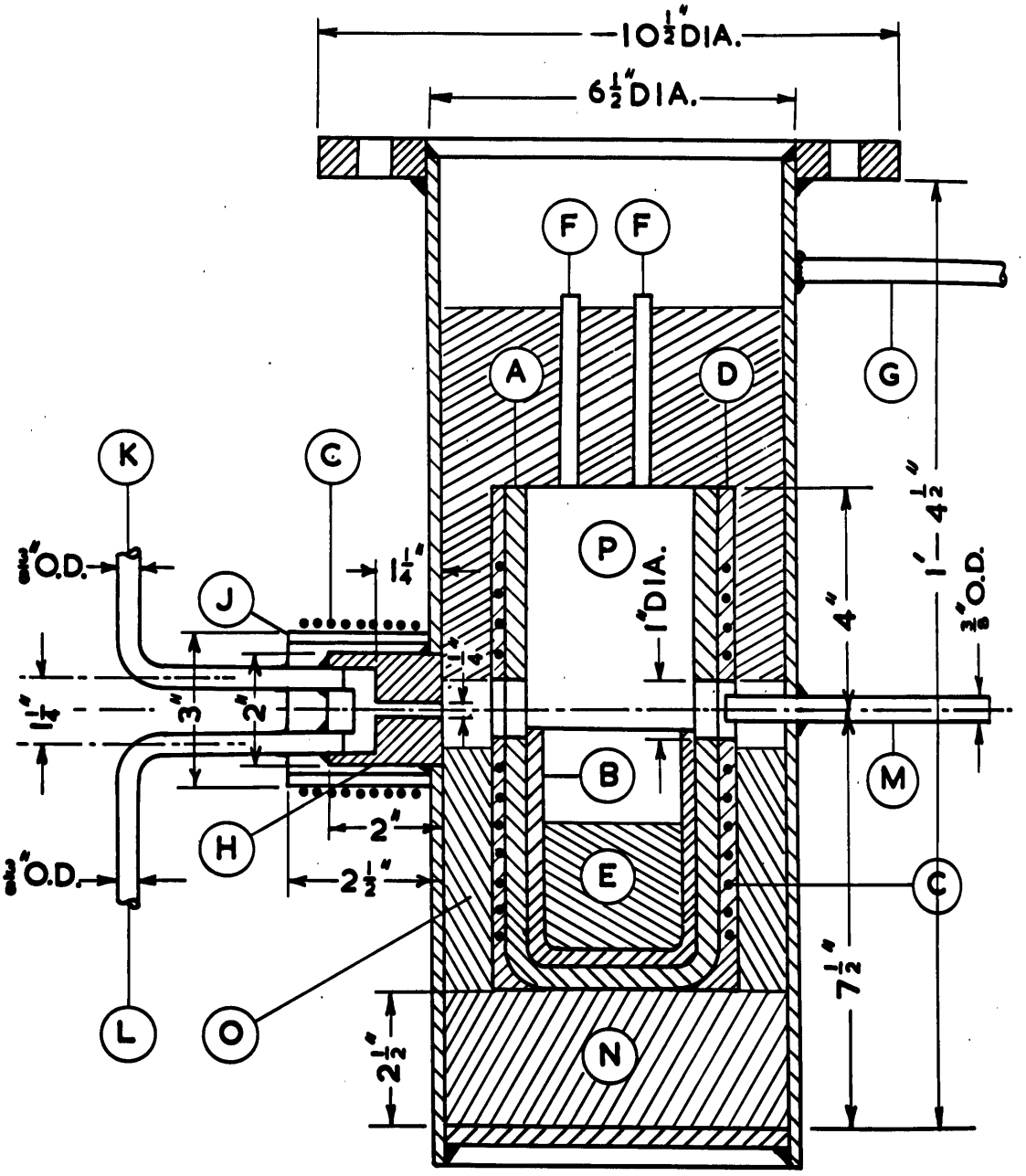

Fig. 10.4 - The Zinc Boiler

Fig. 10.4

LEGEND

A. Morgan Sillimanite Crucible N3907

B. Morgan Sillimanite Crucible N1938

C. Kanthal Resistance Winding

D. Aluminous Cement

E. Zinc Charge

F. Power Input Protection Tubes

G. Heavy Current Connection

H. Outlet Gas Manifold

J. Silica Tube

K. Inlet Gas Sampling Line

L. Superheater

M. Gas Inlet from Carboniser

N. Insulating Brick

O. Vermiculite Insulation

P. Steel Wool

To provide entry for the heavy current, required to heat the tubes welded to the zinc boiler to temperatures above the dew point of the zinc vapour - nitrogen mixture, a 3/8" stainless steel rod was welded to the side of the steel vessel. On this rod a cable clamp was positioned, according to the heavy current required for heating the gas superheater and the gas analysis lines. The superheater and the gas analysis lines constituted a parallel electric circuit. The higher resistance of the longer analysis lines was compensated by lagging the analysis lines with two thicknesses of ½" asbestos tape. The superheater tube required no thermal insulation.

A line drawing of the zinc boiler is shown in Fig. 10.4 and photographs of the components of the boiler and preassembled views of the boiler with its connecting units are shown in Fig. 10.5 (a), (b) and Fig. 10.6 (a), (b), respectively.

The current lead wires were sheathed in mullite tubes, which were cemented into the alumina covering the winding before firing. The open end of the mullite tubes projected into the top section of the metal containing vessel, where the temperature was approximately 200°C, and therefore, the exposed section of the wires was in a zinc free atmosphere.

The top section of the unit was insulated from the high temperature zone by four inches of steel wool packed on top of the furnace. This steel wool served the dual purpose of heat insulation and condensation surface required for the zinc as the temperature decreased above the furnace.

The 240 volt supply to the furnace was through two suitably modified spark plugs located in a protecting box welded to the wall of the vessel near the flanged top. The voltage applied to the furnace was regulated by a 2 K.V.A. variac. Initial trials indicated the approximate voltage required to obtain the desired zinc boil-up.

The top cover plate of the steel vessel contained provision for changing the crucible with rods of zinc without dismantling. This was achieved by having a one inch nominal pipe with a screwed cap extending from above top cover plate to the top of the crucible, in which zinc rods could be inserted from the top by simply unscrewing the cap. The top cover plate also contained glands through which a 3/8" O.D. aluminous porcelain tube and thermowell could be inserted into the crucible. The tube connection to the crucible was provided to allow a bleed of nitrogen to be bubbled through the liquid zinc bath as an alternative method of obtaining the desired zinc vapour concentration in the exit gas stream, without actually boiling the zinc. However, as the boiling method gave satisfactory results, the alternative procedure was never used.

inside the steel vessel, the crucible containing the boiling zinc and the furnace were placed.

The furnace was made by winding with "Kanthal" resistance wire a Morgan sillimanite crucible type number N3907. The furnace winding was in two sections. A lower section which provided the heat required for boiling the zinc and an upper winding which kept the temperature above the dew point of the nitrogen plus zinc vapour mixture formed. The total power input at 240 volts to the furnace was 2 K.W. Two one inch holes were drilled in this crucible between the windings to allow inlet and exit of the nitrogen stream. These holes were on the same centre line as the gas inlet from the carboniser and the gas off-take manifold.

The space between the furnace and the steel vessel was filled with vermiculite insulation up to the level of the gas off-take manifold. Above this manifold steel wool was packed on top of a plate inside the furnace and between the furnace and the wall of the steel pipe.

The boiling zinc was contained in a Morgan sillimanite crucible type number N1938 which fitted neatly into the furnace.

The principal problem, associated with this type of design, was the prevention of zinc condensation on the furnace lead wires, as zinc condensation would have severely attacked nichrome or "Kanthal" resistance wire.

The effect of zinc vapour on the heating elements was unknown, although it was considered that dilute zinc vapour corrosion would not be as severe as liquid zinc corrosion. However, as a precaution against possible zinc vapour attack on the wires, the furnace winding was sealed with alumina cement, prefired to 1000°C before installation into the unit.

temperature drops associated with the heat flow path. The zinc boiler had to be contained in a metal vessel, because the operating pressures of (5 p.s.i.g. approx.) would have resulted in excessive leakage, if a ceramic material were used, because of the difficulty of connection with the other metallic components of the gas circulation system.

The solution to these considerations was to build the furnace inside the metal containing vessel and to insulate the space between the furnace and the metal walls so that the metal wall temperature was below 600°C. This meant that the electric resistance furnace was operated in the zinc containing atmosphere and was under the pressure of the unit. The unit designed was fabricated from a 1 - 6" length of 6" nominal steel pipe, which was flanged at the top with a cover plate bolted to the flange using a rubberised asbestos gasket. A ½" thick steel plate was welded into the bottom of the pipe.

A mild steel gas off-take manifold was welded to the pipe 8" from the bottom of the unit. This manifold contained a 1¼" long x ¼" diameter hole, which lead from the unit and then branched into two 3/8" diameter exits, to which the superheater element of the main gas circulation system and the inlet gas anlaysis line were welded. Turbulence existed in the ¼" diameter off-take and therefore the gas stream was well mixed before a sample was withdrawn for analysis. This gas off-take manifold was sheathed by a silica tube containing a nichrome wound 32 volt resistance furnace, to prevent zinc condensation.

Directly opposite the gas off-take manifold, the 3/8" stainless steel line from the carboniser was welded into the steel pipe. This tube projected inside the steel pipe so that the gas entrance was inside the furnace containing the crucible of boiling zinc. Centrally located

The principal properties of the packed column are summarised in Table 10.1.

TABLE 10.1

PROPERTIES OF THE PACKED COLUMN

Internal diameter	=	1.74"
Empty cross sectional area	=	0.01654 ft. ^{2}
Packing material	=	¼" x ¼" x 20 gauge steel raschig rings
Packed height	=	1.75 ft.
Bed Porosity (before irrigation)	=	0.72

10.1.2 Zinc Boiler

The method of vaporising the zinc used in the disc column experiments was found to be unsatisfactory when applied to the packed column system. The higher gas rates in the disc column were such that turbulent conditions existed in the stainless steel sheath housing the carbon boats containing the zinc. However, at the lower gas rates, which the packed column required, laminar flow existed in the unit. Under the new conditions, the desired zinc partial pressure could not be obtained without over-heating the stainless steel sheath. A new unit was therefore designed.

The new unit operated at the zinc boiling point (906°C at 760 mm. Hg.). The power imput to the boiler determined the rate of vaporisation to give the desired partial pressure of zinc in the nitrogen stream. Because of the high temperature required in the zinc boiler, heating a metal boiler externally was precluded, as the boiling zinc had to be contained in a ceramic crucible because of the extreme corrosive nature of liquid zinc at these temperatures. Therefore, if this crucible was to be located in a metal sheath, which was heated externally, temperatures in excess of 1000°C would have been required in the metal container, allowing for the

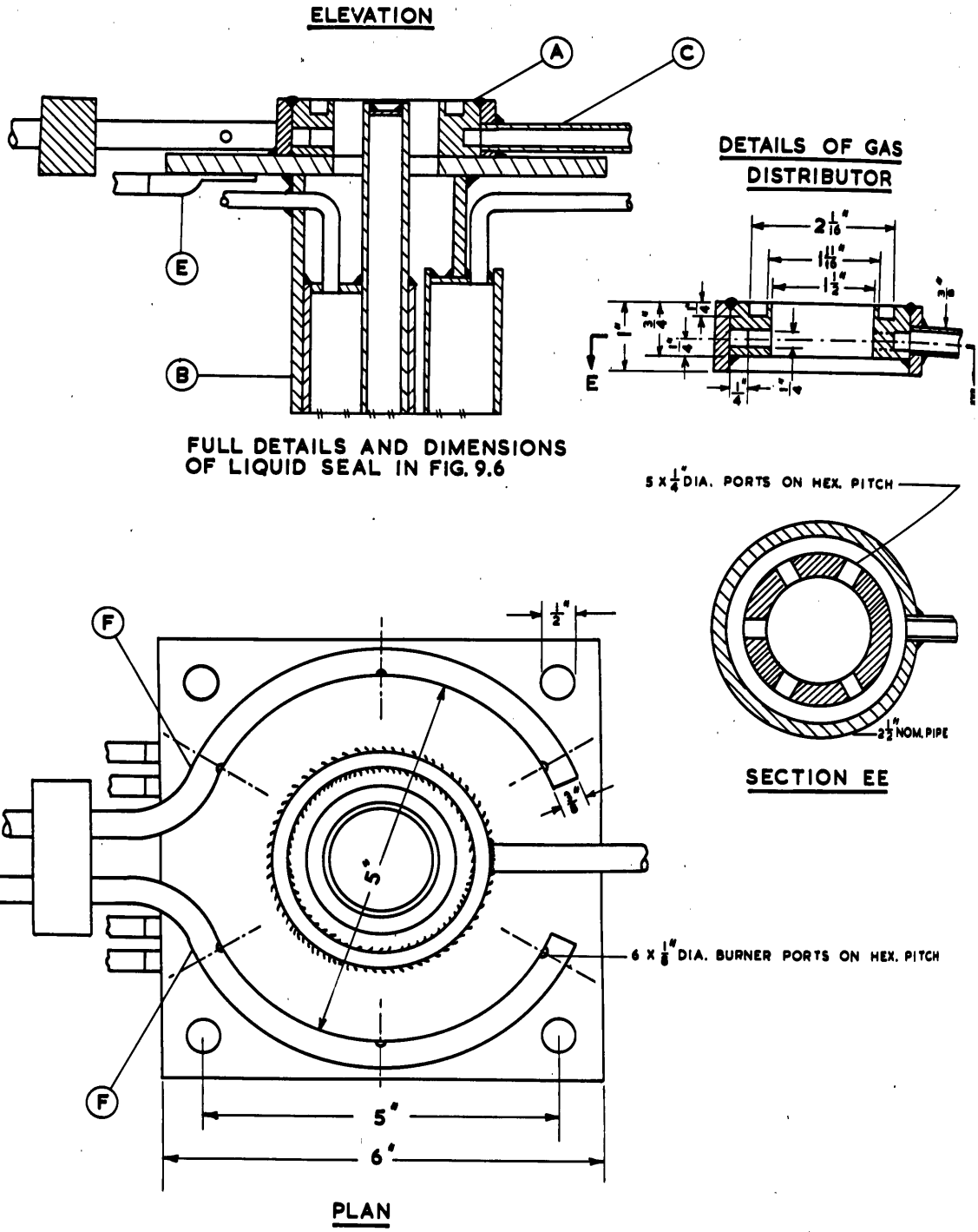

Fig. 10.3 - Bottom Cover Plate of Absorption Column

L E G E N D

A. Inlet Gas Distributor and Bottom Sealing Ring

B. Liquid Seal

C. Gas Superheater Tube

E. Heavy Current Connection

F. Coal Gas Burner

The collar of zinc formed at this point was considered a contingent source of blockage.

A ½" nominal steel pipe was therefore welded into the trap directly opposite the point, where the gas line from the column entered the unit as shown in Fig. 10.2. A gate valve was located at the cold end of this ½" nominal steel pipe. In this way, it was possible to free any accumulated zinc by pushing a rod along the branch pipe to the obstruction, whilst the column was still hot. The presence of a restriction to flow caused by the condensation zinc at this point in the apparatus, was readily detected by observing the back pressure on the absorption column at a given flow rate.

The bottom cover plate of the column contained the gas inlet distributor. The gas distribution to the bottom of the column was through 5 x ¼" diameter ports. The details of the bottom cover plate are shown in Fig. 10.3.

The liquid seal for the column was the same unit as finally used in the disc column experiments, but with the tube, which was to collect the lead flowing over the discs, cut off below to the gas distributor and welded up. The seal was therefore a single unit rather than the dual seal used to separate the lead streams in the earlier disc column experiments. The unit was enclosed in the original 1.5 K.W. 240 volt silica former resistance furnace.

To prevent zinc condensation, additional heating was provided around the gas distributor at the bottom of the column by a coal gas burner formed in two semicircular sections so that the circumference of the distributor was evenly heated. A gas burner was also provided on the top cover plate.

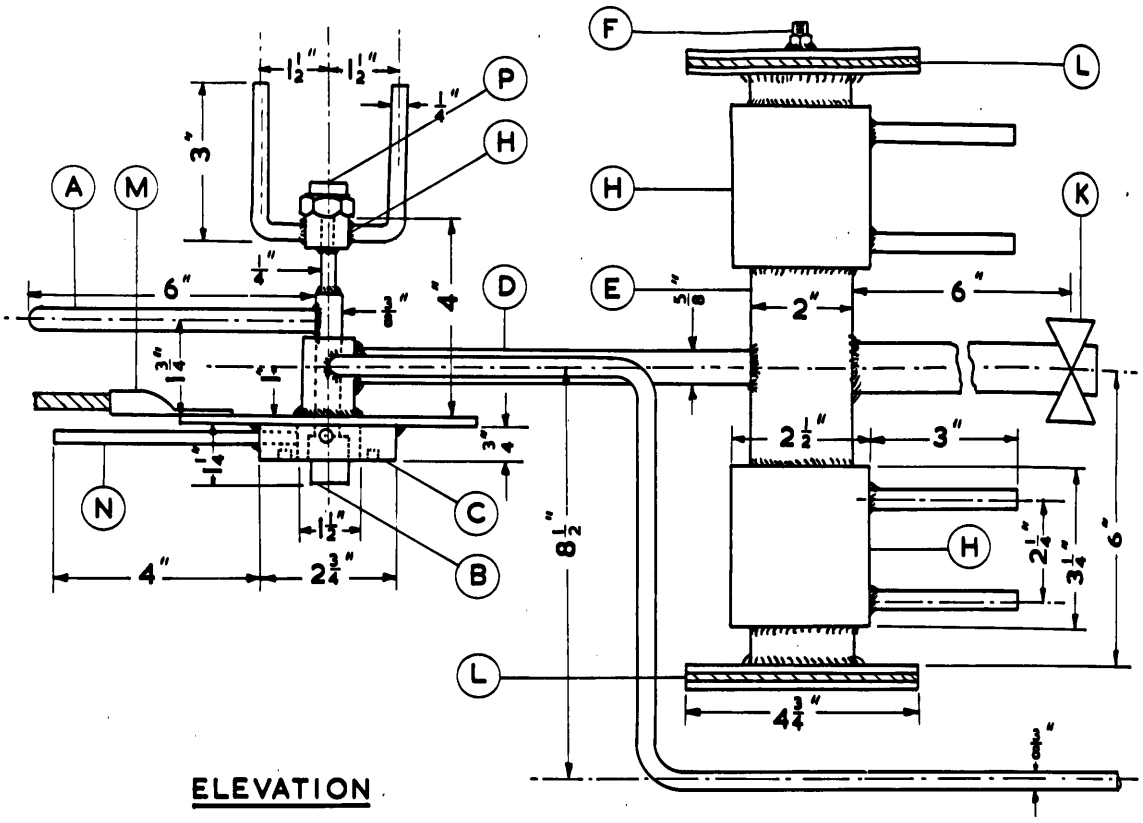

Fig. 10.2 - Top Cover Plate of Absorption Column

L E G E N D

A. Lead Inlet Line from Pump

B. Lead Feed Distributor

C. Top Sealing Ring of Column

D. Gas Outlet Line from Column

E. Primary Zinc Condenser and Entrained Lead Trap

F. Provision for Flexible Gas Outlet to Filter

G. Outlet Gas Analysis Line

H. Water Jacket

J. Branch Line for clearing Blockages

K. Gate Valve

L. Asbestos Gasket

M. Heavy Current Connection

N. Gas Outlet Temperature Probe

O. Manometer Pressure Tapping

P. Provision for Insertion of Lead Inlet Temperature Thermowell

[illegible]

1. Load Inlet Line from Pump
2. Feed Load Distributor
3. Top Secondary Bay of Column
4. Gas Outlet Line from Column
5. Primary Line Condenser and Reduced Load Pump
6. Isolation for Flushing Gas Outlet to Chiller
7. Outlet Gas Analyzer Line
8. Water Jacket
9. Branch Line for Electric Discharge
10. Gate Valve
11. Adsorber Outlet
12. Temporary Connection
13. Gas Outlet Thermometer Line
14. Micrometer Pressure Gauging
15. Provision for Prevention of Load Inlet Temperature Fluctuations

order of 2.0 to 20 ml. This blank was substracted from all the observed zinc analysis titres.

10.3 Operating Procedure

The evening before a schedules series of runs on the apparatus, lead was charged into the lead melting tank and the automatic temperature controller set at 350°C. By the following morning the contents of the tank were at the desired temperature.

The power to the numerous furnaces in the gas circulation system and the furnaces on the couplings in the lead lines was switched on. The automatic nitrogen supply valve was connected to the gas holder, the by-pass valve on the gas blower was opened fully and then the blower was started. The by-pass valve on the blower was opened before switching on the blower, to prevent manometers being blown over, and the gas holder was charged to prevent the oil in the gasholder being sucked into the system when the blower was started.

The system was purged by opening a cock in the gas circulation system with the blower on and allowing the gas to excape from the system at a rate such that the supply to the gas holder was sufficient to maintain the pressure on the suction side of the blower above atmospheric pressure, as observed by an absolute manometer. A modified Orsat type of apparatus was used to analyse the nitrogen for oxygen, by absorption in alkaline pyrogallol. This apparatus was capable of detecting oxygen down to 0.1%. When the oxygen concentration was below 0.5% the purge cock was closed.

Complete oxygen removal at this stage was considered unnecessary, as also was the use of special oxygen-free nitrogen. As the nitrogen in the

system was recycled, the final removal of oxygen from the system relied on the reaction with the hot charcoal bed in the carboniser and also with reaction of any CO_2 or O_2 with the zinc vapour formed later when the zinc boiler had reached operating temperature. The gas in the system, under the final operating conditions, was therefore considered to be oxygen free, as the only make-up to the system was to allow for leaks and this small make-up passed through the carboniser before entering the zinc boiler and the absorption column.

Any major leaks in the gas circulation system were readily detected by observation of the absolute manometer connected to the suction side of the blower. When the system was gas-tight, this manometer indicated a positive pressure of approximately $2\frac{1}{2}$" water gauge. Leaks in the system reduced this positive pressure depending on their magnitude.

When the charge in the zinc boiler had reached the melting point, the heavy current source, used for heating the gas and lead circulation lines, was switched on. This was to prevent condensation of zinc in the cold lines once the partial pressure of the zinc became appreciable. The loading on the Selenium rectifier plating unit, used as the heavy current, low voltage source, was approximately 650 - 750 amp. at 12.5 V. depending on the particular setting of the resistances placed in series with the individual circuits. This loading represented the current drawn before the lead pump was switched on and therefore the lead circulation lines would be free of lead. With the lead pump turned on and the lead circulation lines full of lead, the load on the rectifier increased approximately to 950 - 1000 amp. at 12.5 V.

The power input to the various furnaces was controlled by 2 K.V.A. variacs to enable temperatures in the ranges shown in Table 10.2 to be

obtained, depending on the particular conditions required for the run. The zinc boiler was either operated at the boiling point or slightly below, depending on the desired zinc partial pressure.

TABLE 10.2

OPERATING FURNACE TEMPERATURES

240 Volt Furnaces

Preheater Furnace	950°C - 1000°C
Carboniser Furnace	950°C - 1000°C
Zinc Boiler	875°C - 920°C
Absorption Column Furnace	700°C - 750°C
Inlet Analysis Furnace	650°C - 700°C
Outlet Analysis Furnace	650°C - 700°C
Liquid Seal Furnace	550°C - 650°C

32 Volt Furnaces

Gas Manifold on Zinc Boiler	650°C - 750°C
Gas Line from Column to Primary Condenser	650°C - 750°C
Ermeto Coupling Furnaces:	
(a) Gas Circulation System	650°C - 750°C
(b) Lead Circulation System	550°C - 600°C

Approximately three to four hours, from the time of initially switching the furnaces on, were required for the system to reach steady state conditions, before an actual run could be made.

The steps taken during the actual experimental runs are summarised:

(a) The lead pump was turned on, with the by-pass on the lead pump wide open. The valve was slowly closed, observing the ammeter on the rectifier supplying the current for the lines. The current increased as the valve was closed due to increased supply of lead filling the empty lines. The lead flow rate was set at the desired rate.

(b) After about 10 minutes of pumping the column temperatures became fairly steady and the run was commenced.

(c) For a period of 10 to 20 minutes depending on the lead flow rate:-

(i) All the lead was collected and weighed.

(ii) The total gas flow over the test period was read from the gas meter.

(iii) The inlet and outlet analysis samples were drawn through the appropriate analysis tubes, tagged for the particular run and the sample volumes noted by reading the gas meters before and after sampling.

(iv) The rate of sample withdrawal was noted by observing the orifice meters on both the inlet and outlet analysis systems.

(v) The pressure at the base of the column was read. For the lower gas throughputs, it was sometimes necessary to increase the column pressure by slightly closing a valve on the gas line before the meter, to allow analysis samples to be drawn off at the desired rate.

(vi) The rotameter reading and pressure at the blower were noted.

(vii) The pressure drop across the packed column was measured.

(viii) Samples of lead were obtained by directly collecting the discharge from the liquid seal in a steel crucible approximately $1\frac{1}{4}$" high x $\frac{3}{4}$" diameter. Usually six samples were obtained evenly spread over the test period.

(ix) The total time of the test period was noted and the duration of the run marked on the chart of the sixteen point temperature recorder, which recorded all relevant temperatures used in the final interpretation of the run.

Although the gas analysis system was designed to allow seven runs on the apparatus before removal of the analysis headers for zinc analysis, it was found that only three runs could be made during a complete day's operation of the apparatus. The usual procedure was to allow the gas

system to cool down overnight, with the nitrogen still connected to the gasholder, after the completion of three runs and to repeat the procedure the following day for the remaining three runs, before dismantling the gas anlysis headers for analysis. The remaining gas analysis tube in the inlet and outlet assemblies, not used in the series of runs, served as a blank in the zinc analysis.

At the conclusion of each series of runs the analysis gas meters were calibrated against a standard meter. The calibration of the analysis meters was found to be dependent on the flow rate. The reason for this behaviour is not clear, but it was considered, that the replacement of the usual water seal in the meters with oil may have had a bearing on their performance. However, as the flow rate through the meters was noted during the test periods by observation of the orifice meters on the sampling lines, the analysis volumes recorded during the test could then be corrected by the calibration factor for the particular sampling rate.

10.4 Experimental and Calculated Results

The experimental data obtained using the foregoing procedures are tabulated in Table 10.3. Runs 4B, 4C and 4D were discarded because a leak was discovered at the conclusion of the experiments in the inlet analysis tube No. 4. This leak was not present in Run 4A, as the analysis tubes used in the A series of runs were replaced at the conclusion of this series to enable easier dismantling, as discussed in a previous section. Run 1D was discarded because the automatic cut-off on the lead pump was actuated during this run and therefore a complete series of data was not obtained.

TABLE 10.3

EXPERIMENT RESULTS - COUNTERCURRENT ABSORPTION OF ZINC VAPOUR IN MOLTEN LEAD

Run	Temperature (°C)				Flow Rate (mole/hr.)		Mole Fraction Zn in Pb		Gaseous Zinc Mole Fraction		Total Pressure In Column (mm.Hg.)	Inlet Zinc Partial Pressure (mm.Hg.)	Pressure Drop Across Column (cm.H_2O)
	Gas In	Gas Out	Lead In	Lead Out	Lead	Gas	Inlet x_2	Outlet x_1	Inlet y_1	Outlet y_2			
Series A 1A	620	590	510	620	3.04	0.158	0.000049	0.000923	0.01816	0.000355	841	15.3	15.4
2A	645	570	530	715	1.73	0.089	0.000049	0.000968	0.01887	0.0000658	800	15.1	6.9
3A	700	550	460	665	1.86	0.138	0.000049	0.000795	0.01082	0.000118	836	9.0	14.0
4A	655	525	425	565	2.92	0.132	0.000049	0.000653	0.01263	0.000175	836	10.6	16.0
5A	620	505	400	495	5.65	0.132	0.000049	0.000383	0.01658	0.000147	841	13.9	27.7
6A	655	510	450	595	2.03	0.138	0.000049	0.001280	0.01903	0.000129	836	15.9	14.5
Series B 1B	730	550	460	675	1.75	0.268	0.000049	0.000186	0.00100	0.000209	887	0.98	50.1
2B	710	510	445	635	2.29	0.253	0.000049	0.000198	0.00146	0.000114	892	1.30	48.3
3B	725	520	455	650	1.91	0.204	0.000049	0.000390	0.00327	0.000081	876	2.86	31.0
5B	685	525	480	605	1.46	0.0219	0.000055	0.000293	0.01610	0.000154	826	13.30	1.9
6B	665	510	460	565	2.31	0.0438	0.000055	0.000353	0.01580	0.000100	841	13.30	4.2
Series C 1C	760	685	650	765	2.30	0.147	0.000105	0.000125	0.000553	0.000224	863	0.48	20.7
2C	720	630	560	660	4.26	0.145	0.000105	0.000119	0.000545	0.000123	873	0.48	36.2
3C	735	670	720	735	0.83	0.148	0.000105	0.000192	0.000671	0.000183	863	0.58	17.2
5C	740	640	610	715	2.45	0.0577	0.000105	0.000113	0.000464	0.000115	842	0.39	7.2
6C	750	635	550	705	3.90	0.0598	0.000105	0.000112	0.000588	0.000108	842	0.50	-
Series D 2D	740	650	610	760	2.62	0.147	0.000058	0.000439	0.00745	0.000650	910	6.78	20.8
3D	700	600	515	635	4.92	0.140	0.000058	0.000294	0.00900	0.000705	930	8.37	50.0
5D	700	610	530	640	4.42	0.0496	0.000058	0.000162	0.00955	0.000256	868	8.30	6.6
6D	700	625	635	710	1.77	0.0450	0.000058	0.000259	0.00815	0.000231	878	7.16	4.4

For Series A, the gas inlet zinc mole fraction was calculated from the experimentally determined gas outlet and lead analyses, assuming a zinc balance of 100%. For Series B, C and D, the gas inlet mole fraction was obtained by actual analysis. The reason for this difference was that in Series A, the first set of runs on the apparatus, the experimental procedure was different to the later runs, in that the inlet gas was not analysed during the test period, but measured directly after the test. This procedure was later considered unwise, as operating conditions tended to alter and therefore the early procedure did not give a true indication of conditions during the test period.

The outlet lead was analysed for zinc in Series A and B. This enabled a check to be made on the accuracy of the analytical procedures and the gas and lead flow systems, by calculating zinc mass balances for these runs. A zinc balance could not be established on Runs 1A and 2A, because initial experimental difficulties in these two runs prevented samples of the inlet gas being taken.

Run 1A was terminated immediately after the test period, as condensation of zinc on the terminals of the zinc boiler short circuited the power supply and the circuit breaker was thrown. Under the original operating procedure used in Series A only, the inlet gas analysis sample was to have been taken after the test period.

An inlet gas sample could also not be taken in Run 2A. After the test period, condensation of zinc in the line leading from the column to the zinc condenser caused a partial blockage, thereby preventing the same gas flow rate after the test period as during the test, without exceeding the pressure limitation of the liquid seal on the absorption column. A repetition of this was prevented by locating a branch pipe in the condenser

directly opposite the line from the column, enabling blockages to be cleared, as indicated in the description of the apparatus.

The details of the zinc mass balances for Series A and B are shown in Table 10.4. These results clearly indicate the reliability of the experimental data, particularly when the experimental difficulties associated with the investigation are considered.

As a result of the excellent zinc mass balances obtained, the time consuming zinc analysis of the outlet lead was not undertaken for Series C and D. In these series, the inlet zinc concentration in the lead and the inlet and outlet gas phase zinc compositions were determined experimentally. The zinc in the outlet lead was calculated assuming a zinc mass balance of 100%. Although the outlet lead was analysed in series B, the values tabulated in Table 10.3 were also calculated assuming 100% zinc balance, as the gas phase analyses were considered more reliable than the determinations of zinc in the outlet lead.

.....

TABLE 10.4

ZINC MASS BALANCE DETAILS

Run Number	3A	4A	5A	6A
Inlet Lead				
Sample Wt.	151.7	151.7	151.7	151.7
Titre of E.D.T.A. (ml.)	0.8	0.8	0.8	0.8
Outlet Lead				
Sample Wt.	150.7	150.7	150.3	150.3
Titre of E.D.T.A. (ml.)	12.9	9.2	5.4	20.7
Total Lead Flow (lbs.)	101	107.5	142.8	114.5
Increase in Zinc Equivalent (ml. E.D.T.A.)	3690	2700	2330	6900
Inlet Gas				
Uncorrected Sample Volume ($ft.^3$)	0.88	0.37	0.65	0.99
Sampling Rate ($min./(ft.^3)$)	9.0	7.5	11	10
Meter Calibration Factor	0.86	0.88	0.83	0.85
Corrected Sample Volume ($ft.^3$)	0.76	0.33	0.54	0.84
Titre for Sample Volume (ml. E.D.T.A.)	235	113	213	450
Outlet Gas				
Uncorrected Sample Volume ($ft.^3$)	2.66	1.53	1.07	3.06
Sampling Rate ($min./(ft.)^3$)	6	7.5	7.0	5.33
Meter Calibration Factor	0.98	0.94	0.95	0.98
Corrected Sample Volume ($ft.^3$)	2.61	1.43	1.02	3.00
Titre for Sample Volume (ml. E.D.T.A.)	7.7	6.3	3.7	9.8
Total Gas Flow				
Flow through Meter ($ft.^3$)	12.0	8.0	5.5	12.0
Outlet Sample Volume ($ft.^3$)	2.6	1.43	1.02	3.0
Total Gas Flow through Column ($ft.^3$)	14.6	9.43	6.52	15.0
Decrease in Zinc Equivalent (ml. E.D.T.A.)	4480	3230	2606	7971
Zinc Mass Balance				
$\frac{\text{Increase in Zinc Equivalent of Lead}}{\text{Decrease in Zinc Equivalent of Gas}} \times 100$	82%	84%	90%	87%

TABLE 10.4
(CONTINUED)

ZINC MASS BALANCE DETAILS

Run Number	1B	2B	3B	5B	6B
Inlet Lead					
Sample Wt.	152.3	152.3	152.3	153.0	153.0
Titre of E.D.T.A. (ml.)	0.8	0.8	0.8	0.9	0.9
Outlet Lead					
Sample Wt.	152.5	151.7	151.7	152.0	150.7
Titre of E.D.T.A. (ml.)	3.0	3.2	5.9	4.8	5.3
Total Lead Flow (lbs.)	78.4	110.5	105.4	105.0	142.0
Increase in Zinc Equivalent (ml. E.D.T.A.)	513	795	1610	1225	1880
Inlet Gas					
Uncorrected Sample Volume ($ft.^3$)	0.28	0.34	0.85	0.49	0.42
Sampling Rate $(min./ft.)^3$	50	44	21.2	45.0	45.0
Meter Calibration Factor	0.77	0.80	0.90	0.79	0.79
Corrected Sample Volume ($ft.^3$)	0.22	0.27	0.77	0.39	0.33
Titre for Sample Volume (ml. E.D.T.A.)	6.0	10.0	63.0	157.0	132.0
Outlet Gas					
Uncorrected Sample Volume ($ft.^3$)	2.22	2.74	2.91	2.87	2.74
Sampling Rate $(min./ft.)^3$	6.3	5.1	5.5	7.3	6.7
Meter Calibration Factor	1.00	1.01	1.01	1.01	1.00
Corrected Sample Volume ($ft.^3$)	2.22	2.75	2.92	2.89	2.74
Titre for Sample Volume (ml. E.D.T.A.)	11.7	7.9	5.9	12.8	6.9
Total Gas Flow					
Flow through Meter ($ft.^3$)	20	21.0	19.0	0.17	2.5
Outlet Sample Volume ($ft.^3$)	2.22	2.75	2.92	2.89	2.74
Total Gas Flow ($ft.^3$) through Column	22.22	23.75	21.92	3.06	5.24
Decrease in Zinc Equivalent (ml. E.D.T.A.)	500	804	1755	1229	2071
Zinc Mass Balance					
Increase in Zinc Equivalent of Lead / Decrease in Zinc Equivalent of Gas x 100	103%	99%	92%	100%	91%

10.4.1 Evaluation of N_{OG} and H_{OG}

The concept of the transfer unit and the equations summarised below, have been previously discussed in the theoretical section.

In general,

$$N_{OG} = \int_{y_2}^{y_1} \frac{dy}{y - y_e} \qquad \ldots\ldots 10.1$$

If the equilibrium line is linear, N_{OG} can be calculated from the terminal concentrations:-

$$N_{OG} = \frac{(y_1 - y_2)}{\dfrac{(y - y_e)_1 - (y - y_e)_2}{\ln \dfrac{(y - y_e)_1}{(y - y_e)_2}}} \qquad \ldots\ldots 10.2$$

If $y_e = 0$

$$N_{OG} = \ln \frac{y_1}{y_2} \qquad \ldots\ldots 10.3$$

For a particular absorption column of packed height Z, the number of transfer units and the height of a transfer unit are related:-

$$Z = H_{OG} \cdot N_{OG} \qquad \ldots\ldots 10.4$$

However, as previously discussed in the theoretical section, a number of linear equilibrium lines are applicable in this investigation, one for each temperature level in the column. Therefore, the resultant equilibrium conditions are not themselves linearly related and hence to be strictly correct equation 10.1 must be used to calculate N_{OG}.

The evaluation of the integral in equation 10.1 requires point values of y and y_e to be known throughout the height of the column. Hence the following information would be required for the various levels in the column:-

(a) The gas phase zinc concentration.

(b) The lead phase zinc concentration.
(c) The lead phase temperature.
(d) The equilibrium zinc partial pressure above the alloy formed by absorption.

The experimental difficulty of measuring these factors, as a function of position in the column, would be very great, particularly in the small column used in these investigations. Therefore only the terminal values were measured and the intermediate conditons evaluated using two assumptions.

An exponential decrease of the gas phase zinc concentration from the bottom to the top of the column was assumed. In cases where there is no "back pressure", i.e., no vapour pressure of the solute over the liquid ($y_e = 0$), substitution in equation 10.2 shows that the gas phase solute concentration varies exponentially with the height of the column. The assumption made was therefore only strictly valid, if there was zero equilibrium zinc partial pressure over the lead - zinc alloy formed on absorption. As the equilibrium zinc partial pressures for the alloys formed in these studies were usually small, the assumption made was unlikely to introduce any serious error.

The second assumption made was, that the lead temperature was linearly related to the position in the column. A more elegant assumption may have been that the lead temperature was exponentially related to the position, as the temperature difference causing heat transfer to the lead stream decreased as the lead flowed through the column and approached the gas temperature. However, as the exit lead temperature was in no case greater than 1.35 times the inlet temperature, the more straightforward linear relationship was used.

The zinc composition of the lead phase at any point in the column,

corresponding to a calculated gas phase zinc composition, could be determined by material balance, or more readily by plotting the "operating line", which represents the locus of all gaseous and liquid phase compositions for the particular run. It can be shown (101) that the operating line is linear provided the molar gas and liquid flow rates remain constant (very nearly the case for dilute systems) and that it passes through the points (x_1, y_1) and (x_2, y_2) representing the terminal conditions.

The gaseous zinc mole fraction (y_e) in equilibrium with a known lead phase zinc mole fraction (x) at a lead temperature (t) and under a total pressure of P_T, is given by equation 10.5.

$$y_e = \frac{P^{\circ}_{Zn} \gamma_{Zn}}{P_T} . x = m.x \qquad \ldots\ldots 10.5$$

Where m = constant in a very dilute system in which Henry's law applies for a given lead temperature (t) and total pressure P_T.

Hence once the relation between (x) and (t) was established, the equilibrium conditions could be calculated from the vapour pressure of pure zinc at the temperature (t) and the zinc activity coefficient at temperature (t) for an alloy of composition (x).

The integration was then carried out graphically by plotting $\frac{1}{y - y_e}$ versus y and integrating between limits of y_2 and y_1.

The calculation of N_{OG} and H_{OG} for Run 2D is presented as an example of the computation procedure.

SAMPLE CALCULATION - RUN 2D

Data:-

Zn mole fraction inlet gas (y_1)	=	0.00745
Zn mole fraction outlet gas (y_2)	=	0.000650
Zn mole fraction inlet lead (x_2)	=	0.000058
Zn mole fraction outlet lead (x_1)	=	0.000439
Lead inlet temperature	=	610°C
Lead outlet temperature	=	760°C
Column pressure	=	910 mm. Hg.

The expoential variation of y and the linear variation of lead temperature with respect to position in the column are shown in Fig. 10.12.

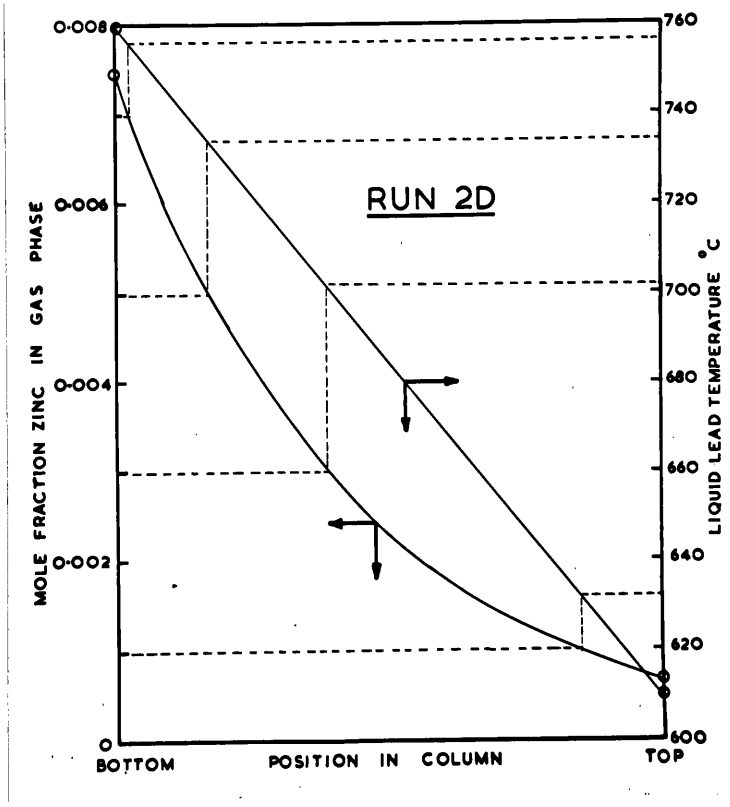

Fig. 10.12

From Fig. 10.12 the lead temperature and the gas phase zinc mole fraction can be read for various positions in the column. The figures obtained are shown in Table 10.5.

TABLE 10.5

RUN 2D

Position in Column	Gas Phase Zinc Mole Fraction (y)	Lead Temperature (°C) (t)
Top	0.000650	610
A	0.00100	632
B	0.00300	702
C	0.00500	734
D	0.00700	756
Bottom	0.00745	760

The lead phase zinc compositions, corresponding to the values of y determined, were obtained by plotting the operating line through (x_1, y_1) and (x_2, y_2) as shown in Fig. 10.13

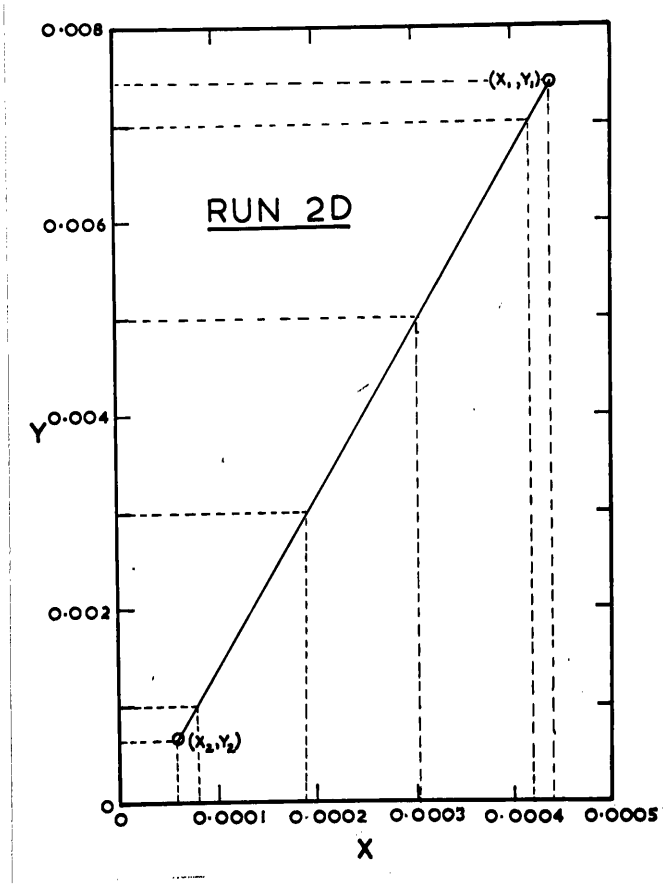

Fig. 10.13

Expected page number 247 is not in the original print copy.

TABLE 10.7

RUN 2D

Position in Column	Top	A	B	C	D	Bottom
Lead Temp. °C (t)	610	632	702	734	756	760
p^{o}_{Zn} mm. Hg.	13.8	20.6	63.3	100	138	146
γ_{Zn}	9.6	8.8	6.9	6.5	6.0	5.9
P_T mm. Hg.	910	910	910	910	910	910
$\frac{p^{o}_{Zn}\ \gamma_{Zn}}{P_T} = m$	0.145	0.200	0.480	0.716	0.912	0.945
x	0.000058	0.000080	0.000190	0.000300	0.000420	0.000439
y_e	0.000008	0.000016	0.000091	0.000215	0.000294	0.000328
y	0.000650	0.00100	0.00300	0.00500	0.00700	0.00745
$\frac{1}{y - y_e}$	1560	1020	344	209	152	144

Fig. 10.14 is a plot of $\frac{1}{y - y_e}$ versus y. Graphical integration between the limits $y_2 = 0.000650$ and $y_1 = 0.00745$ enabled $\int_{y_2}^{y_1} \frac{dy}{y - y_e}$ to be evaluated

From Fig. 10.14, $\int_{y_2}^{y_1} \frac{dy}{y - y_e} = 2.474$

i.e. $N_{OG} = 2.474$

$Z = 1.75$ ft.

$\therefore$ $H_{OG} = 0.71$ ft.

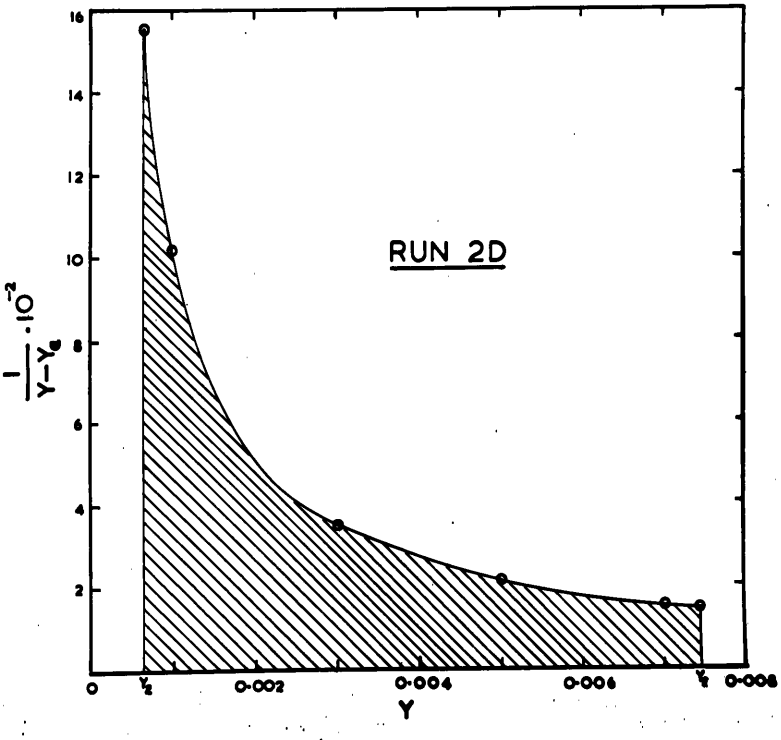

Fig. 10.14

The sample calculation of Run 2D presented is considered to be the best method of analysing zinc absorption data to evaluate the height of an overall gas phase transfer unit. This method would have general application to other data outside the range studied in this investigation. However, for these investigations the "back pressures", or the equilibrium zinc partial pressures over the alloys formed by absorption, are very small compared to the bulk gas phase partial pressures and therefore, the rigorous approach outlined was not really warranted. However, under different absorption conditions, if the "back pressure" was significant compared to the bulk partial pressure, the method outlined would have to be followed.

Under the conditions of this investigation, only a negligible error was introduced if the equilibrium conditions were assumed to be linearly related. When the equilibrium can be represented by a straight line, the more simple use of the terminal compositions to evaluate N_{OG} as given by equation 10.2 can be used. Obviously the equilibrium conditions are not linearly related. If the relation was truly linear the value of m (the slope of the equilibrium curve) would be constant. In Run 2D the value of m ranges from 0.145 at the top of the column to 0.945 at the bottom. The only reason, why the assumption of linearity introduces only a slight error in this investigation, is because the values of y_e are so much smaller than the corresponding values of y, as can be seen by inspection of Table 10.7 for Run 2D.

The extent of the error introduced by the simpler procedure can be seen in Table 10.8, in which the results of the rigorous calculation are compared with the use of equation 10.2 for several selected runs.

TABLE 10.8

COMPARISON OF METHODS OF EVALUATING N_{OG}

Run	Number of Overall Gas Phase Transfer Units	
	Rigorous Calculation Method as Presented for Run 2D	Use of Equation 10.2
2D	2.47	2.58
3D	2.58	2.57
5D	3.86	3.65
1C	1.11	1.15
2C	1.60	1.58

As the difference between the two methods of evaluating N_{OG} was small, the simpler procedure was used throughout to evaluate N_{OG} and hence H_{OG}. The values of N_{OG} and H_{OG} obtained using equation 10.2 are given in Table 10.9.

TABLE 10.9

CALCULATED VALUES OF N_{OG} AND H_{OG}

Series A						
Run	1A	2A	3A	4A	5A	6A
N_{OG}	3.95	5.71	4.62	4.33	4.72	5.03
H_{OG} (ft.)	0.45	0.31	0.39	0.41	0.38	0.35
Series B						
Run	1B	2B	3B	5B	6B	
N_{OG}	1.67	2.56	3.70	4.65	5.06	
H_{OG} (ft.)	1.07	0.70	0.48	0.38	0.35	
Series C						
Run	1C	2C	3C	5C	6C	
N_{OG}	1.15	1.58	1.78	1.64	1.86	
H_{OG} (ft.)	1.55	1.13	1.00	1.09	0.96	
Series D						
Run	2D	3D	5D	6D		
N_{OG}	2.58	2.57	3.65	3.66		
H_{OG} (ft.)	0.68	0.68	0.48	0.48		

10.5 Discussion

The heights of overall gas phase transfer units obtained for the countercurrent absorption of zinc vapour in molten lead, using a column packed with ½" mild steel raschig rings, over the range of flow rates and compositions investigated, were the end results of the packed column studies described. These values of H_{OG}, by themselves, gave no indication of the mechanism involved in the absorption process and provided no evidence, that the conventional gas absorption mechanisms and the "Two Film Theory" could be applied to the absorption at an elevated temperature of a metallic vapour in a liquid metal.

To see if the absorption of zinc vapour in molten lead had fundamentally the same mechanism as a conventional gas absorption process, the equation developed in the theoretical section, relating the height of an overall gas phase transfer unit to the individual film transfer heights, had to be applied to the results.

i.e. $$H_{OG} = H_G + \frac{G_m}{L_m} \frac{H_L}{N_{OG}} \int_{y_2}^{y_1} \frac{p^o_{Zn} \gamma_{Zn}}{P_T (y - y_e)} . dy \qquad \ldots\ldots 10.6$$

The values of the individual film transfer heights H_G and H_L required, for their evaluation, information on the diffusional resistance in both the gas and liquid phases and the flow properties and liquid holdups for molten lead irrigating the packing with the counterflow of a gas of similar properties to the nitrogen used under the elevated temperatures of the investigation. These values could not be measured directly. Therefore, two room temperature analogues of the lead - zinc absorption column were constructed.

By the use of mercury as the irrigating liquid metal and hydrogen

and nitrogen as the countercurrent flowing gas phase, an empirical correlation, enabling the static and dynamic holdup of the liquid metal to be estimated from the observed pressure drop in the gas phase, was developed. This correlation allowed an estimate to be made of the actual holdup of molten lead on the column packing under the conditions of the zinc absorption tests, based on the pressure drop across the column in the gas phase, recorded during the absorption test period.

Generalised correlations for estimating the height of a gas film transfer unit and the height of a liquid film transfer unit were obtained by absorbing ammonia and carbon dioxide in water using the same tower packing as used in the zinc absorption experiments. So that conditions in this low temperature model would simulate absorption of zinc vapour by molten lead, the tower walls and packing were made non-wetting, with respect to the irrigating liquid, by treatment with paraffin wax.

The interpretation of the zinc vapour absorption in molten lead could only be made after studying the room temperature analogues of the process. These studies are therefore presented in Chapters 11 and 12 and the final analysis of the absorption of zinc vapour in molten lead is given in Chapter 13.

10.6 Nomenclature

G_m	=	superficial molar mass velocity of the gas phase, lb.mole./(hr.)(ft.^{2})
H_G	=	height of a gas film transfer unit, ft.
H_{OG}	=	height of an overall gas phase transfer unit, ft.
H_L	=	height of a liquid film transfer unit, ft.
L_m	=	superficial molar mass velocity of the liquid phase, lb.mole./(hr.)(ft.^{2})
m	=	slope of equilibrium curve, dy_e/dx
N_{OG}	=	number of overall gas phase transfer units
P_T	=	total pressure on system, mm. Hg.
p_{Zn}	=	partial pressure of zinc in gas phase, mm. Hg.
p^o_{Zn}	=	vapour pressure of pure zinc, mm. Hg.
t	=	gas or liquid bulk temperature, °C
x	=	mole fraction of zinc in lead phase
x_1	=	mole fraction of zinc in outlet lead
x_2	=	mole fraction of zinc in inlet lead
y	=	mole fraction zinc in gas phase
y_1	=	mole fraction zinc in inlet gas
y_2	=	mole fraction zinc in outlet gas
y_e	=	mole fraction zinc in gas phase, which is in equilibrium with x in the lead phase
Z	=	height of packing in the absorption column, ft.
γ_{Zn}	=	activity coefficient of zinc in liquid lead - zinc alloy (standard state pure liquid zinc at the same temperature).

CHAPTER 11

EVALUATION OF FLOW CHARACTERISTICS OF THE PACKED COLUMN

Besides the obvious difference in operating temperature, the zinc vapour absorption in molten lead experiments differ from conventional gas absorption systems, involving aqueous or organic liquids, in two distinct ways, both of which are intimately associated with the flow of the liquid phase over the packing.

The effective interfacial area, i.e. the actual liquid surface area which is effective in the absorption process, when lead is flowing over the packing, would most certainly not be the same, as would be obtained if either an aqueous or organic phase was flowing over the packing. The flow of lead over the packing is such that non-wetting conditions prevail. However, even if the flow of water over the packing was made non-wetting by suitable treatment of the packing surface, the effective interfacial areas would be different due to the vastly different physical properties of molten lead and other liquids usually associated with absorption columns.

The second and equally important difference in the systems would be the effect of the liquid phase present in the packing under the operating conditions, called the total holdup, in altering the bed porosity and therefore the true gas velocity within the packing. Again the total holdup of liquid in the packing will be governed by the physical properties and flow of the liquid phase and to a lesser extent the properties and flow of the gas phase.

As neither of these two factors could be measured directly on the high temperature zinc absorption column, a room temperature analogue of

the column was designed. The liquid phase chosen to simulate the flow of lead over the packing was mercury. The physical properties of mercury, although not the same as lead, were considered to be of the same order with the biggest difference being in density. The relevant physical properties of the two liquids are shown in Table 11.1.

TABLE 11.1

PHYSICAL PROPERTIES OF MOLTEN LEAD AND MERCURY (65)

Property	Molten Lead		Mercury	
Density (g./cc.)	Temp. (°C) 500 600	 10.39 10.27	Temp. (°C) 20	 13.55
Viscosity (centipoise)	551 703	1.70 1.35	20	1.55
Surface Tension (dynes/cm.)	500	431	20	465

To simulate the countercurrent flow of hot nitrogen, hydrogen and nitrogen were used in the room temperature analogue.

The mercury model of the absorption system bears the same relationship to the packed column studies, as the earlier work on the gas and liquid flow characteristics of the disc column does to the use of the disc column for the zinc absorption system. In the latter case, it was realised that correlations developed on aqueous system could not be applied to the zinc absorption without first establishing the flow characteristics of the column relevant to the absorption process. However, as the effective interfacial surface area of the disc column was known, the

objective of the preliminary disc column experiments was to establish correlations, in which the properties of the liquid phase relevant to mass transfer could be adequately taken into account. This program was satisfactorily completed before the disc column was finally found unstuiable for the investigation.

The consequence of this was that a similar study had to be undertaken on the final form of absorption column used in the investigation. However, after publication of the pressure drop data on the disc column [Warner (124)] and before a similar treatment was given to the packed column finally used in the investigation, Gardner (29) published pressure drop and holdup data for a packed system, in which the liquid phase was non-wetting. The liquid phase used was water and the packings studied were various size fractions of coke treated with silicone to render them non-wetting with respect to water. The aim of the study was to give an insight into the manner of flow of slag over coke, countercurrent to a gas phase, by using a low temperature model of the process.

As Gardner's work was carried out in the Development Department of Imperial Smelting Corporation, the patentees of the new zinc blast furnace, it is also possible that besides the flow of slag over a coke column, another system of considerable interest would be the flow of molten lead down a packed column countercurrent to a gas phase containing zinc vapour.

Although the work reported dealt solely with the dynamics of flow of the two phases, Gardner (29) indicated that the results were to be used to interpret, when available, heat and mass transfer rates on the molten slag system. As yet, Gardner has not followed up the publication, but it

appears, that the pressure drop and holdup data were collected for very much the same reasons, as those which originally prompted the author to investigate the disc column from the aspect of gas and liquid flow characteristics and also to examine the flow behaviour of the packed column. The work of Gardner (29) was therefore a valuable guide to the planning of the experiments with the mercury model of this investigation.

The analysis of packed column performance in mass transfer operations is hindered because the effective interfacial area is not usually known. For this reason, the volumetric mass transfer coefficient is frequently used in the empirical correlation of packed column data. The volumetric mass transfer coefficient, or the mass transfer coefficient per unit volume, is the product of the mass transfer coefficient and the effective interfacial area per unit volume of the column.

A more fundamental approach to the analysis of packed column performance has also received the attention of several investigators. Although the volumetric mass transfer coefficients are readily obtainable experimentally and more useful to employ in practice, the second approach considers that the mass transfer coefficients per unit area and the interfacial effective areas per unit volume, should replace the volumetric mass transfer coefficient. This approach is the more elegant on theoretical grounds but the problem is to measure one or other of the quantities with sufficient accuracy to warrant the procedure.

The use of either the volumetric mass transfer coefficient or the more fundamental separation into mass transfer coefficients per unit area and transfer areas per unit volume, both require similar properties of the system to be investigated. Thus both approaches require knowledge

of the true gas velocity in the bed, any changes in gas or liquid flow behaviour occuring at definite flow rates and the amount of liquid in the bed, which is effective in the absorption process. Whereas the more fundamental approach requires exact knowledge of the effective interfacial area, the use of volumetric coefficients, together with other factors such as the effective liquid holdup, could also be used in the establishment of empirical equations for analysing the absorption data.

Therefore, before proceeding with the experimental details of the room temperature analogue, the theoretical and experimental advances in the fields relevant to the development of the analogue are briefly reviewed.

11.1.1 Fluid Flow through Fixed Beds

The existing data on single fluid phase flow through packed columns was reviewed in 1952 by Ergun (23). Reynolds (88) was the first to postulate that the fluid friction was the sum of two terms. The form of equation proposed was equation 11.1.

$$\frac{\Delta P}{L} = aV + b\rho V^2 \qquad \ldots\ldots 11.1$$

where a and b are factors which are functions of the system being studied.

The equation developed by Ergun (23) on the basis of numerous previous reported data for fluid flow in granular beds was:-

$$\frac{\Delta P}{L} g_c = 150 \frac{(1-\varepsilon)^2}{\varepsilon^3} \frac{\mu U}{D_p^2} + 1.75 \frac{1-\varepsilon}{\varepsilon^3} \frac{U^2 \rho}{D_p} \qquad \ldots\ldots 11.2$$

i.e., the pressure losses are caused by simultaneous kinetic and viscous energy losses. The firstterm on the R.H.S. of equation 11.2 respresenting

the viscous energy loss, being the most important factor at low flow rates and of little significance at high flow rates, whereas the second term in the R.H.S. of equation 11.2, representing the kinetic energy losses, is the most significant at high flow rates and of little importance at very low flow rates. The equation developed was shown to apply with reasonable accuracy to beds of spheres, cylinders, tablets and crushed materials but was not checked with beds of materials having holes through them such as raschig rings.

Carman (9) and Burke (8) had both previously indicated that packing materials such as raschig rings gave different pressure drops at high flow rates from those calculated from correlations based on solid particles. Carman (9) suggested, that in every element of solid packing the whole surface is presented equally to flow, while the interior of a raschig ring is a source of dead space and eddies at higher flow rates. However, as the same packing was used in both the zinc absorption column and the mercury model, this latter effect was of no significance when a comparison of the two columns was required.

Equation 11.2 was therefore considered as a likely form for correlating the data obtained in these experiments. As the gas flows involved in this investigation were fairly high, the viscous energy losses could be assumed negligible compared to the kinetic energy losses, and equation 11.2 was simplified:-

$$\frac{\Delta P}{L} \quad g_c = a' \rho U^2$$

Ergun (23) assigned a value of $1.75 \frac{1-\varepsilon}{\varepsilon^3} \cdot \frac{1}{D_p}$ for the term a', for the single fluid phase flow through a packed bed.

However, in this investigation the presence of a liquid phase as well

as the gas phase had to be allowed for. Under these conditions the bed porosity ε altered according to the holdup of liquid in the packing as also did the size parameter D_p. The term a' in this investigation was therefore considered to be some function of the total holdup of the liquid in the packing. Equation 11.3 was then modified to a form suitable for comparing the mercury model with the zinc absorption column, in which the same packing and height of packing were used. The true velocity (V) was used rather than the superficial velocity (U) in the modified equation 11.4.

$$\frac{\Delta P}{\chi(h_T)} = \chi' (\rho V^2) \qquad \ldots\ldots 11.4$$

The form of the function χ and χ' would have to be determined experimentally.

The form of correlation adopted by Carman (9) for plotting the results of previous investigators, who studied pressure drop in ring packings, was to plot $\frac{\Delta P g \varepsilon^3}{L \rho U^2 S}$ versus $\frac{\rho U}{\mu S}$. This type of treatment is anaolgous to the method originally proposed by Blake (6). It was Blake, who first successfully treated the problem of fluid flow in packed beds by an approach analogous to the already established method of plotting friction factor versus Reynolds number for fluid friction pipe systems. Using dimensional analysis Blake obtained the following equation:-

$$\frac{\Delta P g_c}{\rho U^2} \cdot \frac{D_p}{L} \cdot \frac{\varepsilon^3}{1-\varepsilon} = \chi \left(\frac{D_p U \rho}{\mu (1-\varepsilon)} \right) \qquad \ldots\ldots 11.5$$

By definition,

$$D_p = \frac{6}{S_v}$$

Where S_v = surface area per unit volume of packing material

The surface area per unit packed volume of bed (S) is related to S_v by equation 11.7.

$$S = (1 - \varepsilon)S_v \qquad \ldots\ldots 11.7$$

Hence by substitution of equation 11.6 and 11.7 into equation 11.5, the form originally proposed by Blake is basically the same as used by Carman.

The bed porosity ε has been one of the most controversial factors in fixed bed analysis. The form originally suggested by Blake (6) is consistent with pure fluid dynamical theory. Ergun (23) showed that this form can be transformed into functions employing the absolute values of shear stress, fluid density, viscosity and velocity, in which the fractional voids has been completely eliminated from the friction factor and the Reynolds number.

Mott (78) has suggested modification of the form, used by Blake and Carman, to allow a more direct comparison of the Reynolds number and friction factor to be made with ordinary pipe flow values and conventional Stanton plots for fluid friction in pipes. The concept of hydraulic radius (r_h) and the equivalent diameter (d_e) of the flow channels was introduced.

$$r_h = \frac{\text{Volume of Fluid in Bed}}{\text{Surface presented to Fluid}}$$

$$= \frac{\varepsilon}{S} \qquad \ldots\ldots 11.8$$

The equivalent diameter is related to the hydraulic radius as shown in equation 11.9.

$$d_e = x \cdot r_h \qquad \ldots\ldots 11.9$$

The value of x in equation 11.9 varies according to the shape of the duct. The value of four is applicable to square or circular ducts. Mott considered it desirable to use this value for packed bed analysis.

Now by definition

$$Re = \frac{d_e V \rho}{\mu} \qquad \ldots\ldots 11.10$$

$$= \frac{4\varepsilon}{S} \cdot \frac{U}{\varepsilon} \cdot \frac{\rho}{\mu}$$

$$= \frac{4U\rho}{\mu S} \qquad \ldots\ldots 11.11$$

$$= \frac{4\,V\rho\varepsilon}{\mu S} \qquad \ldots\ldots 11.12$$

i.e., the equation proposed by Mott differs only by the factor four from the equation used by Blake or Carman. Similarly the equation for friction factor suggested by Mott is of the same form as the former workers except that a factor of 2 is included in equations 11.13 and 11.14.

$$f = \frac{\Delta P\, 2g\, \varepsilon^3}{L\, S\, \rho\, U^2} \qquad \ldots\ldots 11.13$$

$$\text{or} \quad f = \frac{\Delta P\, 2g\varepsilon}{L\, S\, \rho\, V^2}$$

These types of correlation, employing the surface area per unit packed volume, are therefore suitable for examination of flow when the packing is irrigated, as they allow the total surface area exposed to the gas flow to be estimated from a measurement of the gas phase pressure drop. The unknown S can be found by cover plotting the data on a previously determined correlation in which the dry surface is known.

11.1.2 Liquid Holdup in Packed Beds

The void space in the packing, which is occupied by liquid under operating conditions, must be taken into consideration when the bed porosity is determined. The total volume of liquid in the packed bed under operating conditions is known as the total holdup. The total holdup (h_T) is considered to be the sum of the static holdup (h_S) and the dynamic

holdup (h_D). The static holdup is defined as the liquid in the packing, which does not drain from the packing, when the liquid supply to the column is discontinued. The dynamic holdup represents the liquid, which will drain from the packing, when the liquid supply is cut off. The relation between the three holdups is given by equation 11.15.

$$h_T = h_S + h_D \qquad \ldots\ldots 11.15$$

Throughout this investigation the symbols h_T, h_S, h_D are used to represent the actual volume of liquid involved and for convenience they are expressed as ml. of liquid phase. However, in the final analysis of experimental results, the dimensionless quantities H_T, H_S, H_D called the total holdup ratio, the static holdup ratio and the dynamic holdup ratio, respectively, are used. These ratios are obtained by dividing the volume of holdup by the volume of the packed bed.

Several investigators have measured or estimated liquid holdups. Two extensive studies were reported by Elgin and Weiss (21) and Jesser and Elgin (49) but there was no complete analysis of the three different types of holdup for packed columns, until the recent work of Shulman, Ullrich and Wells (111) was published. Gardner (23) reported values of the different holdup terms, for water irrigating non-wettable coke, at almost the same time as the studies of Shulman and co-workers. These latter two investigations were therefore of particular interest to this project.

Both these investigators postulated that the total holdup may be divided into two parts. One part of the holdup was considered to be due to accumulated semistagnant liquid, which resided at places, which had a natural retentive effect upon the liquid, such as points of contact between the packing elements. This liquid was considered to be

semistagnant but not entirely at rest, the flow being so slow that its volume was governed by other effects such as the surface tension of the liquid. Shulman et al. (111) considered this component of the holdup to be equal to the static holdup. Gardner (29) recognised the existence of further terms contributing to the semistagnant component. A small quantity was added to the static holdup to allow for liquid passing in and out of the sites of static holdup and a further allowance for the pressure drop across the bed creating new sites of semistagnant liquid was added.

The flowing part of the holdup was considered to be the dynamic holdup. Gardner (29) developed an empirical expression allowing the flowing part of the holdup to be analysed in a logical form, but this approach was of little significance to this investigation.

Gardner (29) and Shulman et al. (111) both reported the static holdup as being independent of the gas and liquid rate. The static holdup was found to be a function of the physical properties of the liquid phase, the shape and size of the packing and the nature of the packing surface.

In the past it had been assumed that the dynamic holdup was independent of gas rate up to the flooding point and so dynamic holdups in some of the earlier studies were determined at zero gas rate. However, both Shulman et al. (111) and Gardner (29) showed that this was not the case, as the dynamic holdup was found to increase with increase in gas rate, even before the loading point was reached. In the non-wetting case, it was suggested that the effect of gas rate on the dynamic holdup was that the liquid was retarded by frictional effects or that it was dispersed into thinner and more trickles.

Besides allowing the bed porosity to be evaluated, holdup studies are

also important in the interpretation of mass transfer data, because of the different significance, which can be attached to the components of the total liquid holdup, in so far as their being effective, in the mass transfer process. This very important aspect is discussed when the effective interfacial area, as distinct from the total interfacial area, is considered in section 11.1.4.

11.1.3 Total Surface Area of Liquid Exposed to Gas Flow

Gardner proposed, that the form of Reynolds number and friction factor employing the total surface area exposed to flow (S), as used by Mott (78) and earlier by Carman (9) and Blake (6), should be suitable for analysing an irrigated packing, in which the specific surface (S) is an unknown variable. Thus the ratio of the specific surface of the irrigated packing to that for the dry packing could be obtained, and hence if the specific surface of the dry packing was able to be calculated, the specific surface of the irrigated packing could then be evaluated. The method suggested would appear to be valuable for evaluating the specific surface of irrigated packings such as raschig rings, whose dry specific surface can be calculated from the ring dimensions, if the loss of surface area at points of contact is neglected.

The evaluation of the irrigated total specific surface would be useful for establishing the correct gas phase Reynolds number, but in itself it does not indicate the contribution to the specific surface, which is due to the liquid phase, as the specific surface obtained by such a procedure represents both solid and liquid surface presented to the gas flow.

If the liquid phase was completely non-wetting (contact angle = 90°) and if the packing was such that there could be no accumulation of liquid pockets within the bed (i.e. no static holdup), the method proposed by

Gardner (29) may then be used to evaluate the surface area of the liquid. Thus for example, if a non-wetting liquid irrigated a plane surface under conditions such that the contact angle was 90°, the method proposed would appear quite reasonable as any increase in the specific surface would be equal to the surface area of the liquid phase.

However, the application of the method for determining the liquid surface area in a packed column would appear to have a number of objections:-

(1) In a packed column, pockets of liquid are trapped in the packing, thus blanketing off portion of the packing surface area.

(2) Besides the pockets of liquid mentioned, the flow of a non-wetting liquid on a surface is characterised by the liquid phase tending to stand out from the surface and therefore, particularly in small packings, in which the size of the liquid trickle is of the same order as interstices between the packing elements, the possibility exists, that the irrigating liquid, even when flowing with a contact angle of 90°, could effectively blanket off considerable packing surface area. Thus for the small ring packing used in this investigation, it is conceivable that the liquid lead would flow through the interior of a number of rings during its descent down the column, thereby effectively reducing the specific surface of the irrigated packing below that of the dry packing. This effect, however, would be reduced as with increased packing size.

(3) Even under extreme non-wetting conditions, the liquid irrigating the packing would most probably spread out on the packing surface to a certain extent, thereby not allowing the dry surface of the irrigated packing to be known.

Because of the three reasons discussed, the liquid surface area cannot be obtained from the total specific surface. However, the evaluation of the total surface area exposed to gas flow is in itself quite significant in the analysis of a mass transfer process, as this enables the correct Reynolds number to be assigned to the gas phase.

Various other methods have been proposed for determining the liquid surface exposed to the gas stream in a packed column.

Mayo, Hunter and Nash (70) measured the extent of staining of paper raschig rings.

Grimley (36) measured the electrical conductivity of the liquid over a certain column height.

Weisman and Bonilla (125) and Shulman and DeGouff (108) attempted to separate the interfacial area (a) from the volumetric mass transfer coefficient ($k_g a$) by obtaining values of k_g for the vaporisation of naphthalene raschig rings or water from prewetted raschig rings of known transfer area and then applied their results to the various published sources of $k_g a$ to evaluate a.

However, in these latter two investigations, no liquid was used to irrigate the packing and no attempt was made to take into account the effect of liquid flowing through the packing under practical operating conditions.

A recent paper by Shulman, Proulx, Ullrich and Zimmerman (110) overcame the deficiency of the earlier work, by studying the vaporisation of naphthalene raschig rings and berl saddles, when irrigated with water at various rates and also the vaporisation rate of the dry packing. The method used was to evaluate k_g for the dry packing of known surface area and then to evaluate $k_g a$ for the irrigated packing, allowing the dry area of

naphthalene under irrigated conditions to be calculated and the wetted area to be found by difference from the total surface area. The tacit assumption in the foregoing procedure was that the total ,surface area of the dry and irrigated packing was the same. Shulman and co-workers apparently overlooked the effect, which the irrigating liquid could have on the total surface area presented to the gas. This could lead to erroneous results, particularly for small packings, because pockets of liquid having only a limited surface area could readily blanket off more extensive packing surface areas.

Although the methods proposed by Gardner (29) or Shulman et al. (110) cannot be used confidently for evaluating the liquid surface exposed to the gas stream in a packed column, a synthesis of the two procedures should enable the liquid surface area to be evaluated in cases where the surface area of the dry packing is known. By vaporisation of special elements of packing, fabricated from naphthalene or other suitably volatile material, the gas film mass transfer coefficient k_g could be evaluated, as the surface area of the dry packing would be readily calculated. The ratio of the specific surface of the dry and irrigated packing could then be obtained from pressure drop measurements using the procedure suggested by Gardner (29).

As the dry packing surface area is known, the total surface area exposed to gas flow under the irrigated conditions could be evaluated. The volumetric mass transfer coefficient k_ga for the vaporisation of the packing material under irrigated conditions could then be measured, thus allowing the area of the dry surface not irrigated to be evaluated. The surface area of the liquid could then be obtained by difference from the previously determined total surface area under irrigated conditions.

11.1.4 Effective Interfacial Area

Shulman, Ullrich and Wells (111), on the basis of holdup studies in a packed column, have proposed an explanation of an apparent mass transfer anomaly, which has existed for many years. The phenomenon referred to is the difference observed when gas phase mass transfer coefficients in a packed column are determined by vaporisation and absorption measurements, as a disagreement of as much as 300% has been observed in such cases. Shulman et al. (111) proposed that this difference was due to different effective interfacial areas in absorption and vaporisation. As this concept of effective interfacial area, as distinct from the surface area of liquid exposed to the gas, is of vital significance to the final interpretation of the zinc absorption in molten lead data obtained in this investigation, the conclusions of Shulman et al. (111) are summarised:-

(1) If a packed column is used for vaporisation, the effective interfacial area is the surface area of the moving liquid as well as of the liquid accumulated in semistagnant pockets throughout the packing. Therefore, in this case, the total wetted area or the surface area of the liquid exposed to the gas is effective in the mass transfer process.

(2) If a packed column is used for physical absorption, the semistagnant liquid pockets tend to become saturated in a short time, their surface area becomes ineffective, and so the only area effective in the mass transfer process is the area of the moving liquid. Thus for small packings, which have a large static holdup, the total surface area of the liquid is large, but the bulk of this surface area is practically useless for absorption, because it comes

to equilibrium with the gas very rapidly. In the larger packings there are fewer points of contact and resulting stagnant pockets, so that the effective area is more closely related to the wetted area.

(3) If the column is used for an absorption accompanied by an irreversible chemical reaction, such as the absorption of ammonia in acid or sulphur dioxide and chlorine in alkali solutions, the effective interfacial area becomes variable, depending on the conditions of the absorption. For example, if ammonia is absorbed in water or very dilute acid, the effective area is that of the moving liquid. As the acid concentration is increased, the semistagnant liquid, even with its slow turnover, will have an increasing capacity to absorb ammonia and at high enough acid concentrations, the semistagnant liquid or the so-called static holdup may be as effective as the moving holdup component.

(4) For the type of absorption discussed in (3), the concentration of the solute in the gas phase will influence the effectiveness of the semistagnant liquid. The greater the concentration, the more quickly the liquid becomes ineffective for further absorption.

The consequence of these proposals when applied to the absorption of zinc vapour in molten lead, a case of what would appear to be pure physical absorption, is that the dynamic holdup only would contribute to the effective interfacial area. The importance of using an absorption rather than a vaporisstion technique for evaluating the mass transfer properties of the packing in a room temperature analogue of the zinc absorption column is therefore very clear.

Although conclusion (3) and (4) were developed by Shulman et al. (111) for absorption followed by simultaneous irreversible chemical reaction,

it is felt that, even in certain cases of physical absorption, very much the same arguments could be applied. The really important factor would appear to be the rate of movement of the semistagnant liquid through the column. If this rate was only slightly less than the rate of the flowing component, then the assumption that the semistagnant liquid comes to equilibrium and is then ineffective in the absorption process, would be invalid.

Shulman et al. (111) observed the effect of injecting a dye into the water feed to a packed column. When dye was injected for about 20 seconds, some of the pockets of water in the column picked up dye, which was not completely washed out until as much as five minutes had elapsed. Shulman therefore concluded that the rate of flow of the semistagnant water through the column is very slow. He then verified this conclusion by demonstrating that ammonia absorption and water vaporisation data could be compared, if the semistagnant liquid in the column was considered ineffective.

Therefore, for the absorption of ammonia in water, there is little doubt that only the dynamic holdup is effective in the absorption process.

However, the flow of the semistagnant liquid or static holdup for the case of lead or mercury irrigating a packing under non-wetting conditions, need not necessarily be similar to that of water. Indeed, it is considered that even the static holdup in the zinc absorption studies may be almost as effective as the dynamic holdup, because the very much higher kinetic energy, associated with lead or mercury flow over the packing, could have the effect of displacing or "knocking on" the static holdup at greater rates than would be expected if water was the irrigating liquid phase.

If, however, the free flow of the static holdup was impaired by dross formation on the surface of the liquid, the result would be that the

movement of the component would be completely arrested or slowed down to such an extent, that equilibrium would be reached and the surface rendered ineffective for further absorption.

The full significance of these proposals is developed in the final assessment of the zinc absorption in molten lead results of this investigation, as described in Chapter 13.

11.2 Experimental Apparatus and Procedure

A glass column, having essentially the same dimensions as the zinc absorption column, was packed to a height of 1.75 ft. with $\frac{1}{4}$" steel raschig rings. The volume of rings in the column was obtained by weighing the rings prior to their addition to the column and using the density of steel as given by Perry (81). The volume of the packed height of the empty glass column was determined by addition of a tared quantity of water. The relevant dimensions of the column are shown in Table 11.2.

TABLE 11.2

DIMENSIONS OF MERCURY MODEL COLUMN

Column diameter	=	1.75"
Free cross sectional area	=	0.01665 ft.^{2}
Packed height	=	1.75 ft.
Volume of rings	=	231 ml.
Volume of empty bed	=	826 ml.
Dry bed porosity	=	0.72
Irrigated bed porosity	=	$(595 - h_T)/826$
Packing material	=	$\frac{1}{4}$" x $\frac{1}{4}$" x 20 gauge steel raschig rings

The mercury feed to the column was from a head tank through a pipe provided with both a plug cock and a needle valve. The needle valve was used for flow control and the plug cock served as the quick-acting valve required for measuring the mercury holdup.

The mercury flow rate was measured by weighing the discharge from the column.

Nitrogen or hydrogen were metered to the column by a venturi meter for the higher flow rates and a rotameter for the lower flows. The gas was admitted at the bottom of the column to enable counterflow conditions to exist. Manometer tappings were located in the glass column, above and below the packed bed. The pressure drop across the bed was measured using a simple manometer, with either water or mercury as the manometric fluid, depending on the magnitude.

The base of the glass column was provided with a bowl of sufficient storage capacity to collect the mercury holdup when the supply to the column was cut off and a stopcock, connecting the liquid run-off tube from the bowl to the variable lute on the mercury discharge, was closed.

The variable lute of the column was mounted vertically on a lathe cross-feed stock, which enabled the mercury level in the liquid run-off tube to be maintained accurately at a predetermined calibration mark during the run and subsequent determination of the volume of the holdup.

A line diagram of the experimental apparatus is shown in Fig. 11.1.

The experimental technique was as follows:-

(a) When steady state conditions at the desired gas and mercury flow rates were reached, the variable lute was adjusted so that the level of the liquid in the run-off tube was at the calibration mark and the pressure drop across the bed was recorded.

(b) Stopcocks A and B were then closed simultaneously, but the gas supply to the column was left unaltered.

(c) The liquid which drained from the packing, the dynamic holdup, was determined by opening stopcock B and draining off the mercury into the receiver H, until the liquid level in the run-off tube was again at the calibration mark.

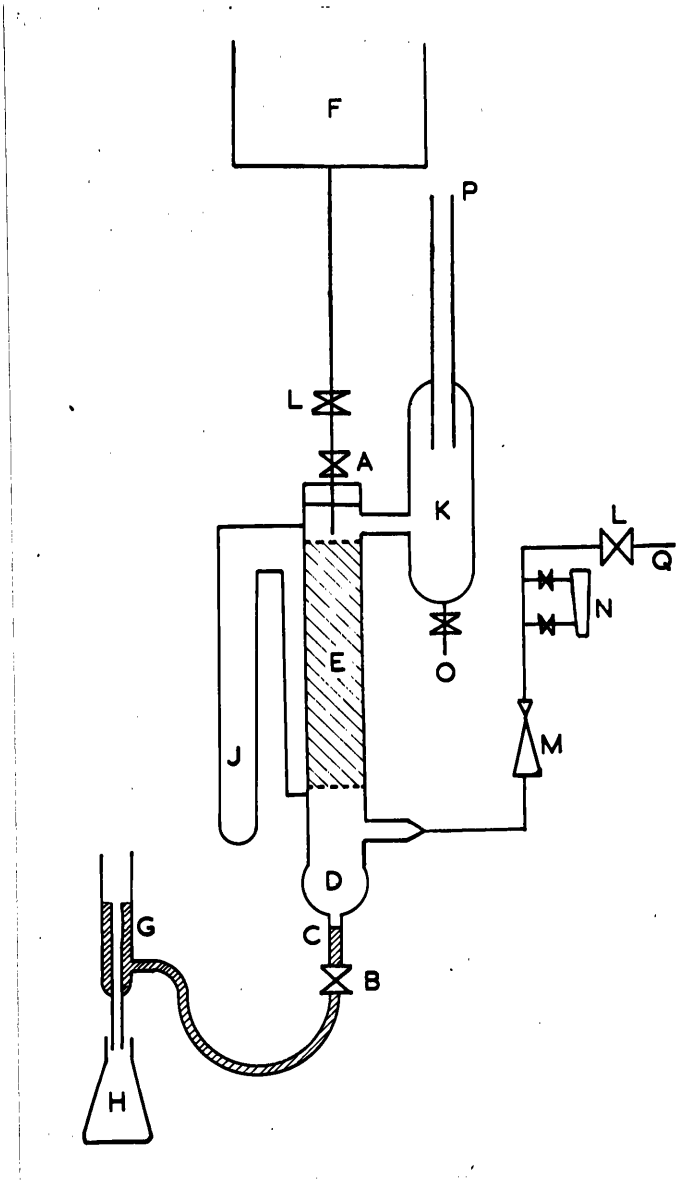

Fig. 11.1 - Line Diagram of Mercury Model

A - Stopcock on inlet liquid
B - Stopcock on outlet liquid
C - Liquid run-off tube
D - Storage bowl
E - Raschig ring packing
F - Mercury head tank
G - Variable lute
H - Receiving vessel
J - Manometer
K - Mercury entrainment trap
L - Needle control valve
M - Venturi Meter
N - Rotameter
O - Drainage cock
P - Exhaust to atmosphere
Q - Connection to Compressed gas cylinder

(d) The stopcock B was closed once this level had been reached and the gas supply to the column was then turned off. At very high gas flow rates, a further quantity of mercury drained from the column, which was measured in the same way as the dynamic holdup. This contribution to the total holdup was termed the "gas holdup".

(e) The static holdup was determined by weighing the column at the conclusion of each run and substracting the weight of the column before irrigation.

11.3 Experimental Results

The experimental results obtained using the low temperature analogue of the absorption column are given in Tables 11.3, 11.4, 11.5 and 11.6. These tables contain the relevant experimental data of pressure drop and holdup under mercury irrigation with hydrogen and nitrogen flow, the mercury holdup in absence of gas flow but with hdrogen and nitrogen atmospheres, the pressure drop across a previously mercury irrigated bed but at zero mercury rate with hydrogen and nitrogen flow and the pressure drop across the dry packing for both gas phases before mercury irrigation.

All data was obtained under approximately the same ambient conditions. A constant temperature of 20°C was used throughout in evaluating the physical properties of the gas phases. The true gas velocity takes into account the actual void space in the bed under the operation conditions and the density evaluated at the mean pressure in the bed.

TABLE 11.3

PRESSURE DROP AND HOLDUP FOR MERCURY IRRIGATION

Run	Mercury Rate lb./min.	Static Holdup h_S ml.	Dynamic Holdup h_D ml.	Gas Holdup h_G ml.	Total Holdup h_T ml.	Bed Porosity ε	Gauge Pressure at Base of Column cm. Hg.	True Gas Velocity v_g ft./sec.	Pressure Drop Across Bed ΔP cm. H_2O
			Nitrogen Gas Phase						
1	1.50	112.9	9.5	31.5	153.9	0.538	15.0	15.2	160.5
2	18.09	101.2	120	5	226.2	0.456	14.5	12.3	171.4
3	5.16	108.6	24	8	140.6	0.553	7.1	10.8	74.8
4	10.00	100.2	60	5	165.2	0.525	9.1	11.1	102.0
5	18.84	92.9	82	1	175.9	0.513	4.8	7.9	59.8
6	5.34	103.2	31	0.5	134.7	0.559	4.3	8.1	46.2
7	2.41	105.3	24	0.5	130.0	0.565	4.1	7.9	40.8
8	10.56	97.2	77.5	10	184.7	0.502	14.5	14.3	168.6
9	14.41	96.2	50.5	0	146.7	0.546	0	2.2	6.8
10	6.44	103.2	45	16.5	164.7	0.525	12.7	14.0	146.2
11	3.06	103.2	22.5	13.5	139.2	0.556	10.4	13.0	110.2
12	6.89	93.9	36	5	134.9	0.559	8.9	12.0	97.9
13	12.56	100.2	92	10	202.2	0.483	15.5	14.1	187.7
14	2.59	98.2	16	12	126.2	0.570	8.9	12.2	92.5
15	3.22	101.2	22	39	162.2	0.528	19.1	15.7	201.3
16	15.75	96.2	58	0	154.2	0.538	0	2.22	6.8
17	3.28	105.5	16	0	121.5	0.575	0	2.08	4.1
18	5.16	102.2	21	0	123.2	0.574	0	2.08	4.1
39	16.88	85.5	61	0	146.5	0.546	0	0.92	1.1
40	8.34	91.9	30	0	121.9	0.575	0	0.87	0.9
41	3.62	96.2	14	0	110.2	0.588	0	0.85	0.7
42	14.31	90.8	52.5	0	143.3	0.552	0	3.93	16.1
43	4.72	98.2	22	0	120.2	0.578	0	3.76	12.2
44	2.03	100.2	10	0	110.2	0.588	0	3.68	10.7

TABLE 11.3
(CONTINUED)

PRESSURE DROP AND HOLDUP FOR MERCURY IRRIGATION

Run	Mercury Rate lb./min.	Static Holdup h_S ml.	Dynamic Holdup h_D ml.	Gas Holdup h_G ml.	Total Holdup h_T ml.	Bed Porosity ϵ	Gauge Pressure at Base of Column cm. Hg.	True Gas Velocity v_g ft./sec.	Pressure Drop Across Bed ΔP cm. H_2O
			Hydrogen Gas Phase						
19	15.56	85.5	83	9	177.5	0.510	12.4	47.5	149.5
20	8.06	87.5	35	9	131.5	0.563	7.9	42.8	88.3
21	17.06	85.5	62	4	151.3	0.542	4.3	31.0	50.3
22	3.84	91.9	18	3	112.9	0.586	2.8	28.2	35.3
23	8.00	91.9	29	5	125.9	0.570	3.3	29.0	38.0
24	14.84	88.8	51	0	139.8	0.554	1.8	19.6	23.1
25	7.94	92.9	26	1	119.9	0.578	1.8	18.7	17.7
26	6.03	96.2	20	1	117.2	0.581	1.8	19.0	20.4
27	18.34	87.5	55.5	0	134.0	0.552	1.0	14.2	14.2
28	10.84	89.8	36	0	125.8	0.570	0.8	13.6	11.7
29	5.25	90.8	19.5	0	110.3	0.588	0.8	13.2	9.7
45	20.47	80.5	66	0	146.5	0.546	0	3.14	1.5
46	3.41	88.8	13	0	101.8	0.598	0	2.86	0.8
47	8.97	87.5	29	0	116.5	0.582	0	2.94	1.1
48	18.78	87.5	69	0	156.5	0.534	0	5.46	3.6
49	8.09	91.9	27	0	118.9	0.578	0	5.05	2.5
50	6.69	92.9	23	0	115.9	0.582	0	5.15	2.4
51	13.59	89.8	46	0	135.8	0.558	0	7.70	5.5
52	6.28	90.8	23	0	113.8	0.585	0	7.33	4.9
53	2.78	98.2	13	0	111.2	0.587	0	7.30	4.5

TABLE 11.4

MERCURY HOLDUP IN ABSENCE OF GAS FLOW

Run	Mercury Rate lb./min.	Static Holdup h_S ml.	Dynamic Holdup h_D ml.	Total Holdup h_T ml.
		Hydrogen Atmosphere		
30	20.09	89.8	59	148.8
31	11.41	92.9	30	122.9
32	5.69	96.2	16	112.2
33	3.09	98.2	10.5	108.7
		Nitrogen Atmosphere		
34	15.88	98.2	61	159.2
35	7.84	106.5	36	142.5
36	6.47	109.6	28.5	138.1
37	3.91	112.9	19	131.9

TABLE 11.5

PRESSURE DROP ACROSS PREVIOUSLY MERCURY IRRIGATED COLUMN

PREVIOUS IRRIGATION h_T = 98 ml. AND ε = 0.60

Run	Gauge Pressure at Base of Column cm. Hg.	True Gas Velocity v_g ft./sec.	Pressure Drop Across Bed ΔP cm. H_2O
	Hydrogen Gas Phase		
54	0	4.83	2.0
55	0.3	7.11	4.2
56	0.5	9.50	7.2
57	0.8	13.8	11.0
58	1.3	17.3	16.1
59	1.5	21.4	24.8
60	2.5	28.1	33.3
61	3.3	32.1	45.6
62	4.3	37.8	56.6
63	4.3	42.4	67.5
	Nitrogen Gas Phase		
64	0	0.83	0.7
65	0	1.39	1.7
66	0	1.99	3.5
67	0.3	2.70	6.0
68	0.5	3.58	9.4
69	0.8	5.40	14.1
70	1.0	6.88	24.3
71	2.5	8.73	34.0
72	5.1	12.20	66.6

TABLE 11.6

PRESSURE DROP ACROSS COLUMN BEFORE IRRIGATION

$\epsilon = 0.72$

Run	Gauge Pressure at Base of Column cm. Hg.	True Gas Velocity v_g ft./sec.	Pressure Drop Across Bed ΔP cm. H_2O
	Nitrogen Gas Phase		
73	2.3	7.4	20.4
74	5.3	10.5	42.1
75	8.9	12.6	70.7
76	1.3	5.7	13.3
77	0.8	5.0	10.3
78	0.8	4.5	8.4
79	0.3	3.0	5.6
80	0.3	2.3	3.7
81	0	1.7	2.3
82	0	1.2	1.3
	Hydrogen Gas Phase		
83	0	2.4	0.7
84	0	4.1	1.5
85	0	6.0	2.5
86	0	8.6	4.1
87	0.3	11.3	6.3
88	0.8	14.3	9.5
89	1.3	17.1	12.1
90	1.8	23.2	19.6
91	2.8	28.3	26.8
92	3.8	32.2	33.2
93	4.8	38.8	44.5

11.4 Correlation and Discussion of Results

As the aim of the mercury model experiments was to develop empirical correlations, allowing a comparison of the model with the absorption column to be made, homogeneity of units was not considered essential in dimensional correlations, provided the same units were used in analysing the absorption column and the mercury model. The units of the various terms used are not consistent amongst themselves. The reason for this apparent disregard of accepted convention was to simplify the arithmetical calculations involved by using the most convenient unit as directly measured in the actual experiments. Thus holdups are given as ml. of mercury, pressure drops as cm. of water and mercury flow rates as lb./min. The derived quantities such as true gas velocity and gas density are in f.p.s. units.

However, in the Reynolds number - friction factor correlation the various terms were later converted to consistent units to preserve the dimensionless character of this type of correlation.

11.4.1 Static Holdup

Previous investigators, who have reported static holdup data in aqueous and organic liquid systems, have observed the static holdup as being constant for a particular liquid and packing. However, the results of this investigation show that the liquid irrigation rate has a slight but definite effect on the static holdup, in that the static holdup decreases with increased liquid rate. This effect can be seen in Fig. 11.2. Although the liquid rate effects the static holdup, no consistent effect could be attributed to the gas flow rate, although the results at zero gas flow rate do appear slightly higher than the other data.

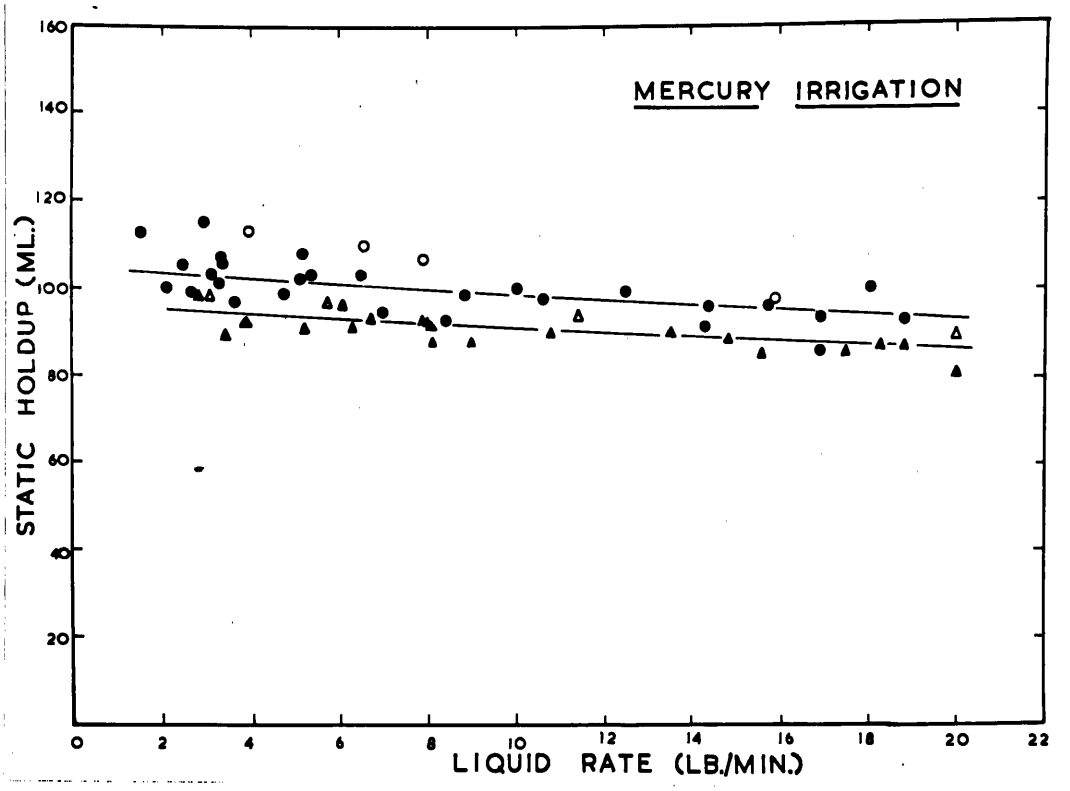

Fig. 11.2 - Mercury Irrigation Static Holdup

○ Nitrogen atmosphere, no flow
● Nitrogen flow
△ Hydrogen atmosphere, no flow
▲ Hydrogen flow

The other interesting feature of Fig. 11.2 is that the static holdup for nitrogen is displaced above the hydrogen data. This effect is thought to be due to a difference in interfacial tension between the mercury and the two gases. Perry (82) reports that the interfacial tension of mercury and nitrogen is higher than the interfacial tension of mercury and hydrogen, being 496 dynes/cm. and 470 dynes/cm. at 15°C and 19°C, respectively. The increase of static holdup with an increase in surface tension is consistent with the findings of Shulman, Ullrich, Wells and Proulx (112), who studied a surface tension range of 23 to 86 dynes/cm. by the addition of wetting agents to water.

A probable explanation of the observed effect, which the liquid rate had on the static holdup in this investigation, is that liquid metals or other high density liquids possess much greater kinetic energies than water when irrigating a packing, and therefore the possibility of dispersing or "knocking-on" semistagnant pockets of liquids is much greater and this effect increases with increased liquid rate. The significance of this would be that the semistagnant pockets of liquid, observed in packings irrigated with water, would be very much more mobile in the case of a dense liquid irrigating the packing. Under these conditions the whole concept of effective interfacial area in absorption would have to be reviewed, as the increased mobility of the dense liquids could well result in the static holdup being almost as effective as the recognised flowing component, the dynamic holdup.

11.4.2 Dynamic Holdup

The dynamic holdup for mercury irrigating the packing is not purely a function of liquid rate, and therefore supports the recent results of Gardner (29) and Shulman, Ullrich and Wells (111), who showed that the earlier practice of assuming the dynamic holdup to be solely related to the liquid rate was incorrect.

Fig. 11.3 is a plot of dynamic holdup versus the mercury irrigation rate. The dynamic holdup is clearly dependent on other factors besides the liquid rate. Increased gas rates, in general, increased the dynamic holdup. The reasons for this were outlined by Gardner (29) and have been previously discussed in the earlier section of this chapter. The high gas rates correspond to the points in Fig. 11.3 in which there was a "gas holdup". The dynamic holdup plotted is the liquid which drained from the packing before the gas flow was reduced and therefore excludes

any "gas holdup" contribution.

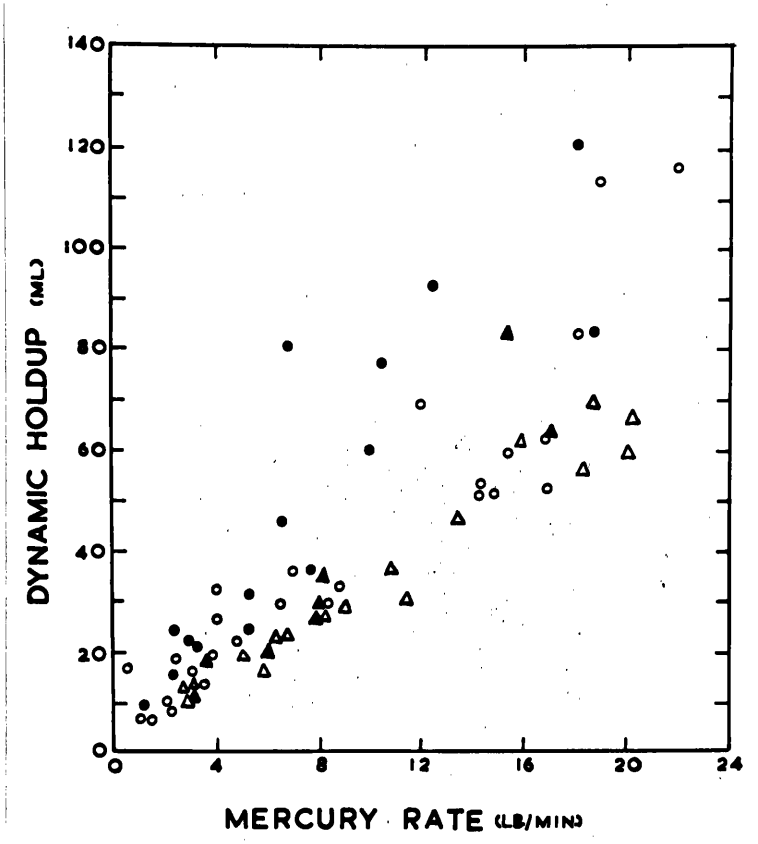

Fig. 11.3 - Mercury irrigation dynamic holdup

- ○ Nitrogen absence of gas holdup
- ● Nitrogen presence of gas holdup
- △ Hydrogen absence of gas holdup
- ▲ Hydrogen presence of gas holdup

The nature of the gas phase also has an effect on the dynamic holdup due to interfacial tension effects as can be seen in Fig. 11.3 by comparing the hydrogen and nitrogen data under similar conditions, i.e. with or without "gas holdup". Shulman, Ullrich, Wells and Proulx (112) also observed that interfacial tension affected the dynamic holdup. These authors found the effect of interfacial tension on dynamic holdup to be related to the liquid rate. At low liquid rates, decreasing surface tension

resulted in decreasing dynamic holdup, whereas at high liquid rates decreasing surface tension was found to increase the dynamic holdup. Jesser and Elgin (49) observed a similar effect. However, the results of this investigation suggest that increased interfacial tension results in an increase in the dynamic holdup irrespective of the liquid rate. The dynamic holdup effect observed in this investigation is the same as that observed for static holdup, which is what would be expected, as it is difficult to visualise interfacial tension affecting the different holdups in opposite ways.

Shulman et al. (112) commented that both their results and those of Jesser and Elgin (49) could be erroneous, because the addition of wetting agents to water to give a low surface tension liquid resulted in foaming at high liquid rates. Although antifoam agents were used, the foaming was not completely eliminated. The presence of foam could readily account for the increased dynamic holdups reported for low surface tension solutions at high flow rates.

11.4.3 Reynolds Number - Friction Factor Correlation

The method proposed by Gardner (29) for evaluating the total surface area exposed to gas flow, in which the specific surface becomes the unknown variable in the Reynolds number of equation 11.11 or 11.12 and the friction factor of equation 11.13 or 11.14, was critically examined in the earlier section of this chapter. The conclusion of this examination was that the method by itself provided no information on the surface area of liquid exposed to gas flow. As already suggested, the surface area of the liquid exposed could be obtained by a synthesis of the methods of Gardner (29) and Shulman, Proulx, Ullrich and Zimmerman (110). However, as such a suggested procedure would have been extremely time consuming,

and as the results would then have to be further analysed to evaluate, what proportion of the liquid surface was effective in absorption, the suggestion was carried no further.

The experimental data of this investigation was analysed according to the method of Gardner (29) to see if the total specific surface could be readily obtained, thus allowing the correct Reynolds number to be assigned to the gas phase.

As the specific surface appears in the denominator of both the Reynolds number and the friction factor, the most convenient method of evaluating the specific surface is to assign a value of unity to the dry packing, thus enabling the irrigated specific surface to be calculated as a ratio of the dry surface of the packing, which may be calculated, if the loss of area at the points of contact is neglected. The calculation is essentially a trial and error process of substituting values of the ratio of irrigated specific surface to the dry specific surface until the irrigated experimental point cover plots the curve representing the dry data, which is used as the datum for all calculations.

The curve representing the dry data, in which the specific surface is taken to be unity, is obtained by substituting S = 1 into equations 11.12 and 11.14 to obtain $\frac{\Delta P 2g\epsilon}{L\rho V_g^2}$ and $\frac{4V_g\rho\epsilon}{\mu}$ as the function to be plotted. As the same packed height was used throughout the mercury model experiments and the zinc absorptions, the dimension L was deleted from the expression and values of $\frac{\Delta P 2g\epsilon}{\rho V_g^2}$ and $\frac{4V_g\rho\epsilon}{\mu}$ were calculated for all the dry packing data.

The data for zero mercury flow rate, but previously irrigated packing, were also calculated in the same form, as it was expected that the two sets of data would only vary by a constant ratio and would therefore,

plot parallel to each other on a log.-log. graph.

The relevant data and calculated values pertaining to the correlation for the dry packing and the previously irrigated packing are given in Tables 11.7 and 11.8, respectively. The logarithmic plot of $\frac{\Delta P 2 g \varepsilon}{V_g^2 \rho}$ versus $\frac{4 V_g \rho \varepsilon}{\mu}$ is shown in Fig. 11.4.

TABLE 11.7

CORRELATION OF RESULTS

System	Run	Pressure Drop Across Bed ΔP cm. H_2O	Bed Porosity ε	True Gas Velocity V_g ft./sec.	Gas Density lb./ft.^{3}	$\frac{\Delta P 2 g \varepsilon}{V_g^2 \rho}$ x 10^{-2} (dimensionless)	$\frac{V_g \rho 4 \varepsilon}{\mu}$ x 10^{-5} (ft.)$^{-1}$
NITROGEN - DRY PACKING BEFORE IRRIGATION	73	20.4	0.72	7.40	0.0738	4.78	1.330
	74	42.1	0.72	10.47	0.0763	4.78	1.945
	75	70.7	0.72	12.55	0.0787	5.40	2.41
	76	13.3	0.72	5.67	0.0732	5.37	1.010
	77	10.3	0.72	4.98	0.0724	5.42	0.881
	78	8.4	0.72	4.50	0.0724	5.42	0.793
	79	5.6	0.72	3.03	0.0724	7.97	0.535
	80	3.7	0.72	2.28	0.0724	9.50	0.402
	81	2.3	0.72	1.68	0.0724	10.64	0.287
	82	1.3	0.72	1.17	0.0724	12.45	0.206
HYDROGEN - DRY PACKING BEFORE IRRIGATION	83	0.7	0.72	2.40	0.00518	22.1	0.0603
	84	1.5	0.72	4.08	0.00518	16.4	0.1026
	85	2.5	0.72	6.00	0.00518	12.62	0.1510
	86	4.1	0.72	8.60	0.00518	10.1	0.2160
	87	6.3	0.72	11.26	0.00518	9.10	0.284
	88	9.5	0.72	14.30	0.00523	8.38	0.363
	89	12.1	0.72	17.10	0.00523	7.51	0.433
	90	19.6	0.72	23.20	0.00523	6.58	0.589
	91	26.8	0.72	28.30	0.00530	5.96	0.730
	92	33.2	0.72	32.20	0.00535	5.63	0.832
	93	44.5	0.72	38.80	0.00540	5.17	1.015

TABLE 11.8

CORRELATION OF RESULTS

System	Run	Pressure Drop Across Bed ΔP cm. H_2O	Bed Porosity ε	True Gas Velocity v_g ft./sec.	Gas Density lb./ft.^{3}	$\frac{\Delta P 2g\varepsilon}{v_g^2 \rho}$ x 10^{-2} (dimensionless)	$\frac{v_g \rho 4\varepsilon}{\mu}$ x 10^{-5} $(ft.)^{-1}$
HYDROGEN - ZERO MERCURY RATE PREVIOUSLY IRRIGATED	54	2.0	0.60	4.83	0.00518	13.1	0.102
	55	4.2	0.60	7.11	0.00518	12.7	0.150
	56	7.2	0.60	9.50	0.00518	12.2	0.200
	57	11.0	0.60	13.80	0.00523	8.76	0.294
	58	16.1	0.60	17.30	0.00523	8.18	0.369
	59	24.8	0.60	21.40	0.00523	8.26	0.455
	60	33.3	0.60	28.1	0.00529	6.32	0.605
	61	45.6	0.60	32.1	0.00529	6.65	0.690
	62	56.6	0.60	37.8	0.00534	5.93	0.823
	63	67.5	0.60	42.4	0.00534	5.60	0.925
NITROGEN - ZERO MERCURY RATE PREVIOUSLY IRRIGATED	64	0.70	0.60	0.83	0.0724	11.0	0.1055
	65	11.70	0.60	1.39	0.0724	9.70	0.206
	66	3.5	0.60	1.99	0.0724	9.70	0.294
	67	6.0	0.60	2.70	0.0724	9.07	0.400
	68	9.4	0.60	3.58	0.0724	8.05	0.530
	69	14.1	0.60	5.40	0.0724	5.33	0.800
	70	24.3	0.60	6.88	0.0724	5.66	1.02
	71	34.0	0.60	8.73	0.0738	4.88	1.32
	72	66.6	0.60	12.20	0.0746	4.93	1.86

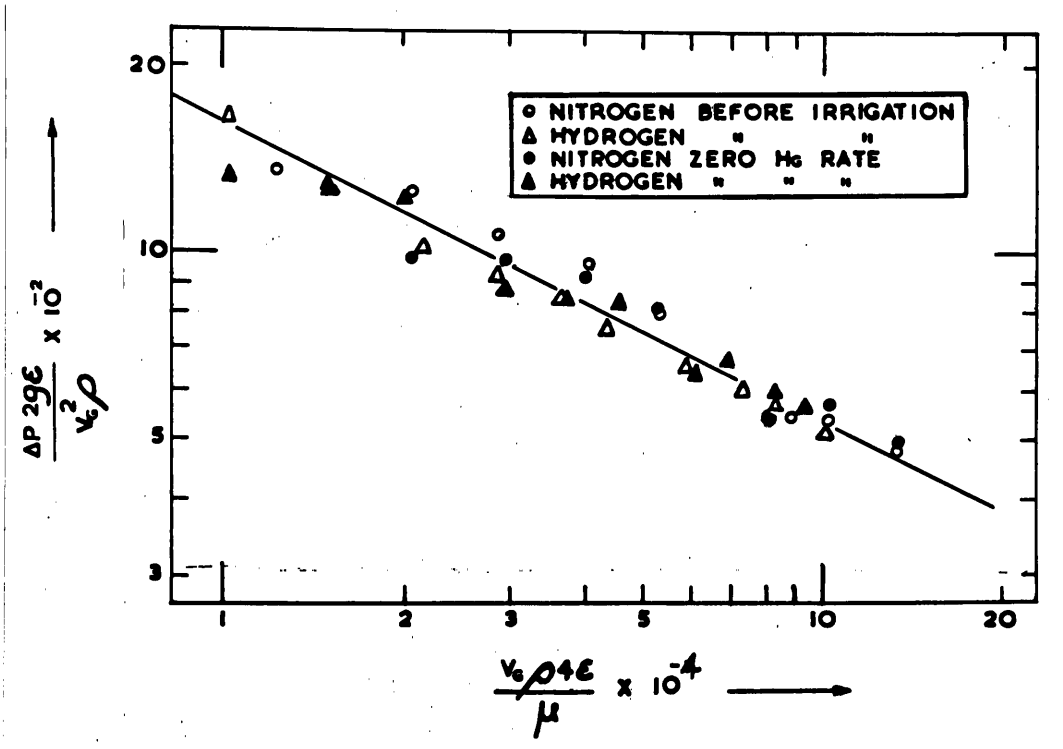

Fig. 11.4 - Dry and previously irrigated packing

The unexpected feature of Fig. 11.4 is that the specific surface of the dry and previously irrigated packing is the same. For both cases a single line represents all the data plotted. The conclusion may be reached for this particular instance, where the previous irrigation was such that a total holdup of 98 ml. remained in the packing, that the increase in surface area due to the presence of the liquid holdup is exactly compensated by the decrease in the surface area of the dry packing exposed to gas flow.

The full line in Fig. 11.4 was then used as the datum line for evaluation of the irrigated specific surfaces. Values $\frac{\Delta P 2g\varepsilon}{V_g^2\rho}$ and $\frac{4\rho V_g \varepsilon}{\mu}$

were calculated for all the irrigated data, and the results plotted on a log.-log. graph, in which the full line of Fig. 11.4 is drawn as the datum line as shown in Fig. 11.5. The relevant data and calculated values required to evaluate the irrigated specific surface are given in Table 11.9.

TABLE 11.9

CORRELATION OF RESULTS

System	Run	Pressure Drop Across Bed ΔP cm. H_2O	Bed Porosity ε	True Gas Velocity V_g ft./sec.	Gas Density lb./ft.^{3}	$\frac{\Delta P 2g\varepsilon}{V_g^2 \rho}$ x 10^{-2} (dimensionless)	$\frac{V_g \rho 4\varepsilon}{\mu}$ x 10^{-5} $(ft.)^{-1}$
NITROGEN - MERCURY IRRIGATED	1	160.6	0.54	15.2	0.0814	6.08	2.28
	2	171.4	0.46	12.3	0.0806	8.56	1.55
	3	74.8	0.55	10.8	0.0763	7.80	1.54
	4	102.0	0.53	11.1	0.0780	7.45	1.56
	5	59.8	0.51	7.9	0.0747	8.65	1.02
	6	46.2	0.56	8.13	0.0747	6.93	1.16
	7	40.8	0.57	7.9	0.0747	6.50	1.14
	8	168.6	0.50	14.3	0.0805	6.78	1.96
	9	6.8	0.55	2.20	0.0724	14.05	0.298
	10	146.2	0.53	14.0	0.0796	6.55	2.05
	11	110.2	0.56	13.0	0.0788	6.12	1.95
	12	97.9	0.56	12.0	0.0778	6.47	1.78
	13	187.7	0.48	14.1	0.0805	7.45	1.85
	14	92.5	0.57	12.2	0.0778	6.01	1.84
	15	201.3	0.53	15.7	0.0833	6.88	2.36
	16	6.8	0.54	2.22	0.0724	13.57	0.296
	17	4.1	0.58	2.08	0.0724	10.04	0.298
	18	4.1	0.57	2.08	0.0724	9.85	0.293
	39	1.1	0.55	0.92	0.0724	13.05	0.125
	40	0.9	0.58	0.87	0.0724	12.57	0.125
	41	0.7	0.59	0.85	0.0724	10.42	0.123
	42	16.1	0.55	3.93	0.0724	10.48	0.530
	43	12.2	0.58	3.76	0.0724	9.15	0.537
	44	10.7	0.59	3.68	0.0724	8.52	0.534

TABLE 11.9
(CONTINUED)

CORRELATION OF RESULTS

System	Run	Pressure Drop Across ΔP cm. H_2O	Bed Porosity ε	True Gas Velocity V_g ft./sec.	Gas Density lb./ft.^{2}	$\frac{\Delta P 2g\varepsilon}{V_g^2 \rho}$ x 10^{-2} (dimensionless)	$\frac{V_g \rho 4\varepsilon}{\mu}$ x 10^{-5} $(ft.)^{-1}$
NITROGEN - MERCURY IRRIGATED	19	149.5	0.51	47.5	0.00563	7.92	0.920
	20	88.3	0.56	42.8	0.00551	6.47	0.893
	21	50.3	0.54	31.0	0.00534	6.98	0.605
	22	35.3	0.59	28.2	0.00528	6.53	0.598
	23	38.0	0.57	29.0	0.00528	6.41	0.592
	24	23.1	0.55	19.6	0.00523	8.35	0.383
	25	17.7	0.58	18.7	0.00523	7.43	0.383
	26	20.4	0.58	19.0	0.00523	8.23	0.390
	27	14.2	0.55	14.2	0.00518	9.78	0.274
	28	11.7	0.57	13.6	0.00518	9.18	0.272
	29	9.7	0.59	13.2	0.00518	8.38	0.274
	45	1.5	0.55	3.14	0.00518	21.3	0.0610
	46	0.8	0.60	2.86	0.00518	14.9	0.0603
	47	1.1	0.58	2.94	0.00518	18.7	0.0596
	48	3.6	0.53	5.46	0.00518	16.2	0.1015
	49	2.5	0.58	5.05	0.00518	14.5	0.1030
	50	2.4	0.58	5.15	0.00518	13.3	0.1050
	51	5.5	0.56	7.70	0.00518	13.2	0.1510
	52	4.9	0.59	7.33	0.00518	13.65	0.1520
	53	4.5	0.59	7.30	0.00518	12.7	0.1510

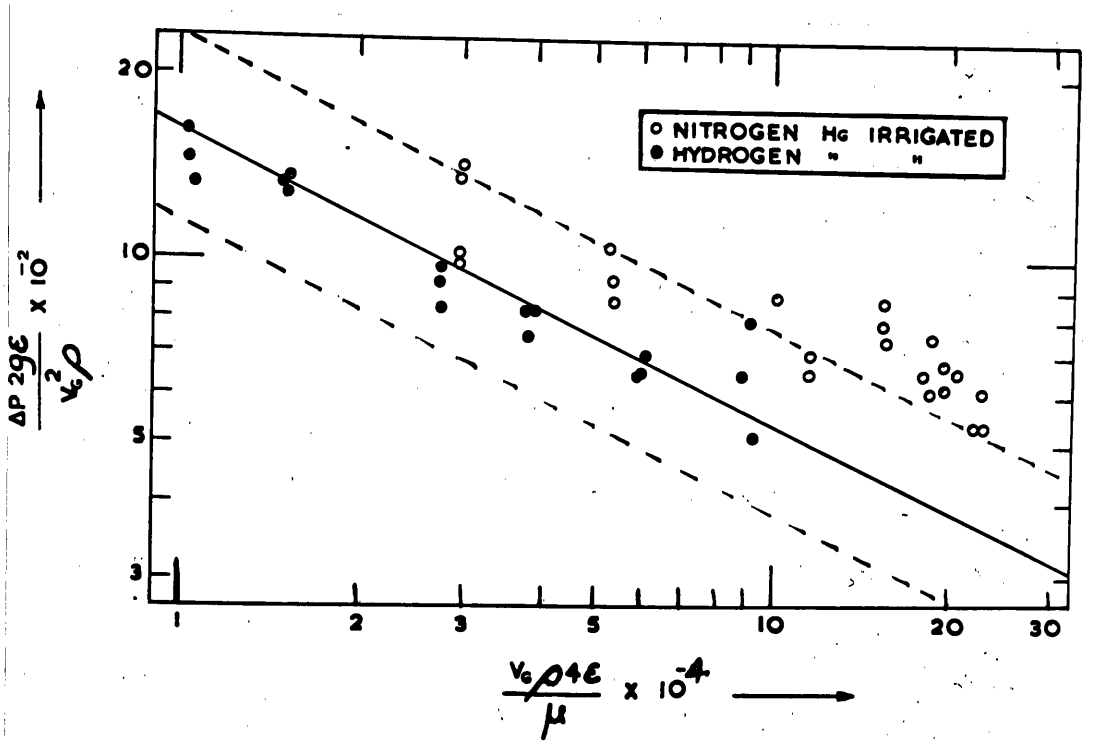

Fig. 11.5 - Mercury irrigated data

Fig. 11.5 displays an unusual characteristic in that the hydrogen data, except for the highest Reynolds number, where "gas holdup" effects were operative, exhibit specific surfaces of the same order or perhaps slightly less than the dry packing, whereas the nitrogen data suggests that the irrigated specific surfaces are quite significantly higher than the dry packing specific surface.

However, the data for the lowest nitrogen gas rate investigated, which are not plotted in Fig. 11.5, showed a reversal in trend, as the irrigated specific surfaces were less than the dry packing specific surface. As the pressure drops were measured with a simple manometer, the error involved in the measurement of the pressure drops at low gas rates was such that the low gas rate data were of doubtful accuracy.

Hence, it was decided not to plot these points but to record that they showed a reversal of trend. To be consistent all other pressure drops less than 1.5 cm. H_2O were also not plotted. It was considered that the lower pressure drop range should be investigated with a more sensitive manometer, rather than to include doubtful measurements on the plot and, in so doing, detracting from the general trend obtained from data, which were not of questionable accuracy.

A postulation, which could possibly explain the significantly higher specific surfaces of the nitrogen data, even at gas rates where there was no "gas holdup", is that differences in interfacial tension are the cause of the observed behaviour. Thus it would appear that, when nitrogen is the gas phase, the static holdup, the dynamic holdup and the specific surface for mercury irrigation are all greater than the corresponding values for hydrogen as the gas phase, because of the higher interfacial tension of nitrogen with mercury.

In cases where there is a "gas holdup", the specific surface would be expected to be somewhat greater than the other data. The group of points in Fig. 11.5 for values of $\frac{V_g \rho 4 \varepsilon}{\mu} \times 10^{-4}$ greater than 15 for nitrogen are cases, in which there were appreciable gas holdups.

The two broken lines drawn parallel to the datum line in Fig. 11.5 represent specific surfaces 30% above and below the dry packing specific surface. The only data, which show specific surface significantly outside these limits are the nitrogen data, in which the gas holdup has increased the specific surface.

The application of this type of approach, for evaluating the specific surface in the zinc absorption column, requires an estimate or a measurement of the total holdup in the packing to enable the bed porosity

and the true gas velocity to be evaluated, when lead is flowing over the packing. This information is required before the method can be used for determining the specific surface.

Shulman, Ullrich, Wells and Proulx (112) have investigated the properties of the liquid phase, which affect the holdup of aqueous and organic systems. However, the extrapolation of their results to a liquid metal of vastly different physical properties to those liquids investigated, was considered unwise. For this reason, the specific surface analysis of the zinc absorption data was not possible.

More work of a fundamental nature on the flow of liquid metals or similar dense media is required before a reliable assessment can be made of the exact effect, which the physical properties of the liquid phase have on the liquid holdup. If such information were available, it would have been possible to predict the lead holdups from the mercury holdup data, thus enabling evaluation of the bed porosity, true gas velocity and finally the total surface area exposed to gas flow using the procedure illustrated for the mercury model.

11.4.4 The Relation between Total Holdup and Pressure Drop

Because the deficiency in fundamental knowledge prevents a direct estimation of the lead holdup to be made from the observed mercury holdup on the packing, an entirely empirical approach was investigated.

The type of correlation suggested by equation 11.4, developed in the earlier section of this chapter, appeared to be satisfactory for analysing the data,

i.e. $$\frac{\Delta P}{\chi(h_T)} = \chi' (V_g^2 \rho) \qquad \ldots\ldots 11.4$$

For a particular value of $(V_g^2 \rho)$,

Let $\Delta P = \Delta P_{h_T = 0} (\chi(h_T))$ 11.16

where $\Delta P_{h_T = 0}$ is the pressure drop across the dry packing

As $h_T \rightarrow 0$

$\Delta P \rightarrow$ Finite Value

The function $\chi(h_T)$ is not known but it may be assumed to be of the form

$$\chi(h_T) = a + bh_T^c \quad \text{..... 11.17}$$

$$\therefore \Delta P = \Delta P_{h_T = 0} (a + bh_T^c) \quad \text{..... 11.18}$$

Now $a = 1$, since $\Delta P = \Delta P_{h_T = 0}$ when $h_T = o$

$$\therefore \Delta P = \Delta P_{h_T = 0} (1 + bh_T^c) \quad \text{..... 11.19}$$

$$\text{also } \chi(h_T) = \frac{\Delta P}{\Delta P_{h_T = 0}} \quad \text{..... 11.20}$$

$$\therefore \chi(h_T) = 1 + bh_T^c \quad \text{..... 11.21}$$

The constants b and c were determined by fitting an equation to the curve obtained when selected values of $\chi(h_T)$ calculated from equation 11.20 were plotted against h_T. Using this procedure the form of $\chi(h_T)$ given in equation 11.22 was obtained.

$$\chi(h_T) = (1 + 3.5 \times 10^{-5} h_T^2)$$

The calculated values of $\chi(h_T)$ for all the experimental runs and the other relevant data pertaining to the establishment of the empirical

correlation are shown in Table 11.10 appended to this chapter.

All the data of this investigation could be empirically correlated by a straight line on a log.-log. plot of $\frac{\Delta P}{(1 + 3.5 \times 10^{-5} h_T^2)}$ versus $V_g^2 \rho$ as shown in Fig. 11.6.

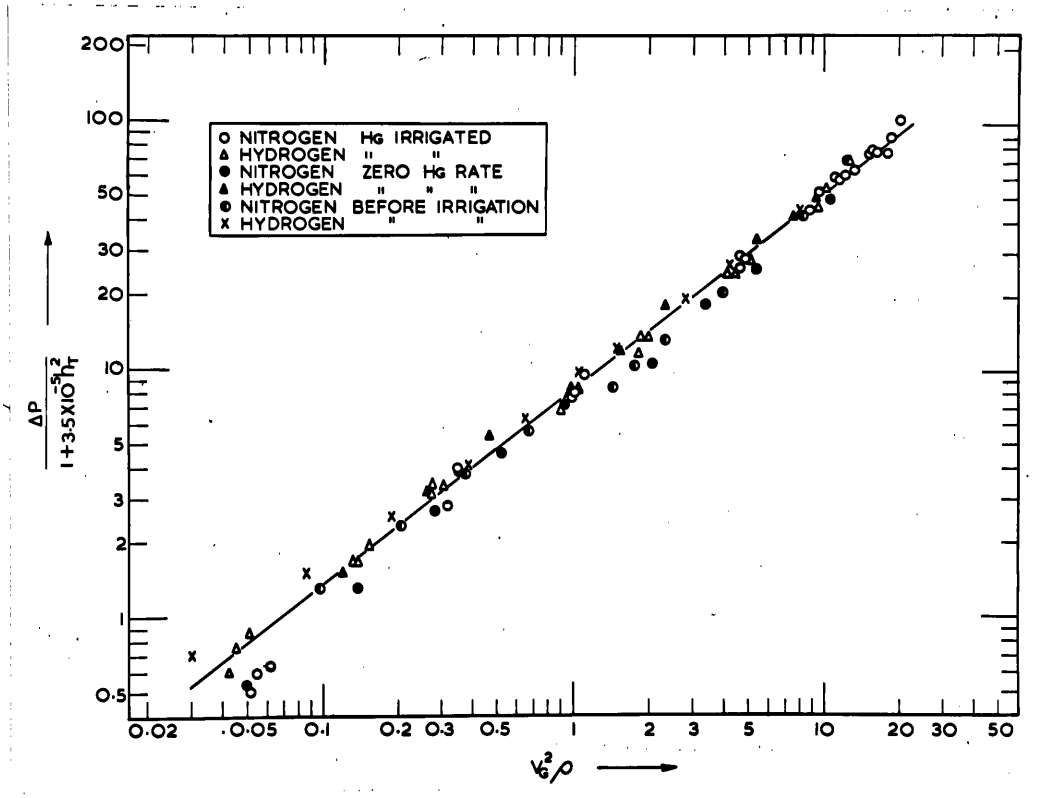

Fig. 11.6 - Empirical correlation of all data

The correlation shown in Fig. 11.6 was developed for mercury irrigation, dry packing and previously mercury irrigated packing. However, it seemed reasonable to expect the same correlation to be applicable to other liquid phases besides mercury. Tests were therefore undertaken on the same packing with water irrigation at various liquid and gas flow rates. The packing was then treated with paraffin wax to make it non-wetting to water and similar tests under non-wetting conditions were made.

The results of these tests with water as the liquid phase are shown in Table 11.11 at the end of the chapter, together with the calculated values used in the correlation. The water data are plotted in the same manner as the mercury data in Fig. 11.7. The full line in Fig. 11.7 represents the correlation obtained in the mercury model experiments.

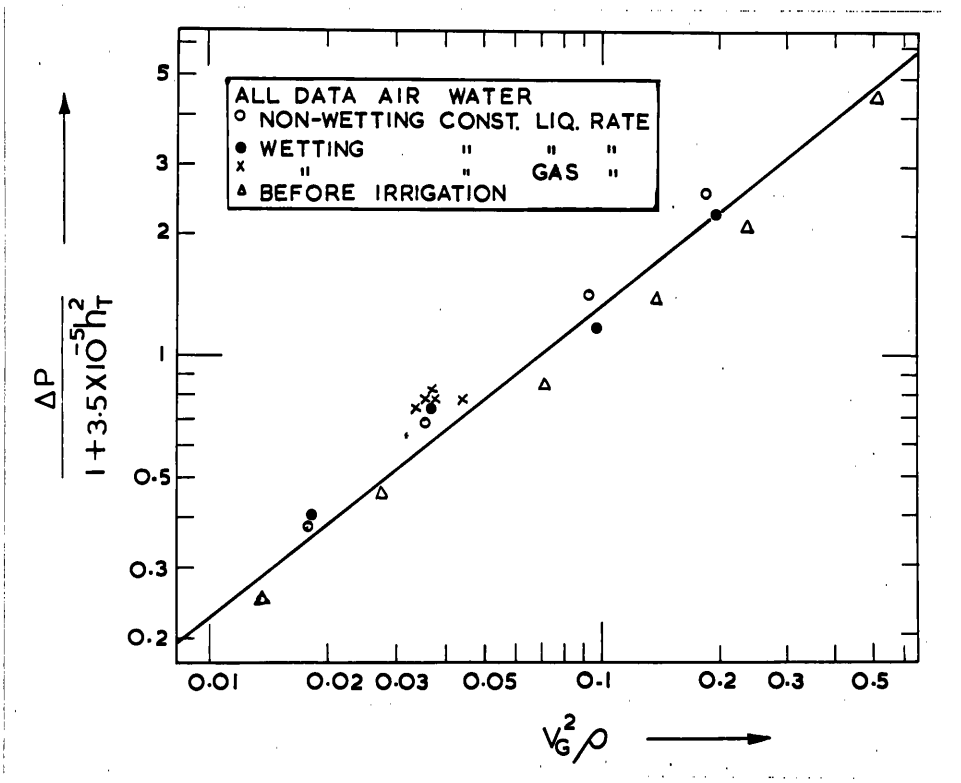

Fig. 11.7 - Comparison with water irrigation

The glass column used to obtain the data of Fig. 11.7 was the same as used in the room temperature absorption experiments described in the next chapter. This column was of slightly different construction to that of the mercury model. The pressure drop data before irrigation in Fig. 11.7 therefore refer to the modified column used in the absorption experiments.

As can be seen in Fig. 11.7 the correlation deveoped with the mercury model applies reasonably well to the water irrigated data. Although slight differences may have been observed between the two sets of data, if a more sensitive method of correlation was employed, the proposed correlation appears to be satisfactory, at least as a first approximation, for estimating the liquid holdup for any liquid system, by measuring the gas phase pressure drop, the true gas velocity and the gas density.

The other important feature of the correlation developed is that the state of the irrigating liquid, whether at rest as in the previously irrigated data or under actual irrigation, appears to make no difference to the applicability of the correlation. The correlation also holds equally well when the column is loaded, as the data, in which there were appreciable "gas holdups" in the bed, are represented by the same line as obtained for the column below the loading point. This is considered to be indicative of the close interrelationship of pressure drop and holdup, as most other forms of analysis show anomalies above the loading point.

The extension of the empirical correlation, to the case of molten lead irrigating the packing with the countercurrent flow of hot nitrogen, is considered to be justified on the basis of the experimental results discussed.

The significance of this is that either the total holdup at zero irrigation rate (i.e. the static holdup) or the total holdup with lead irrigation could be estimated from the observed pressure drops, gas temperatures and gas mass flow rates for the zinc vapour absorptions in molten lead.

As the static holdup was found to vary only slightly with the mercury irrigation rate, for the purpose of analysing the zinc absorption data,

the static holdup could be assumed constant with the introduction of only a small error. Making this assumption, the lead dynamic holdup could be evaluated by difference of the total holdup under operating conditions and the holdup of the previously lead irrigated packing.

This approach was used in the final analysis of the zinc absorption in molten lead data.

TABLE 11.10

CORRELATION OF RESULTS

System	Run	True Gas Velocity V_g ft./sec.	Gas Density lb./ft.^{3}	Pressure Drop Across Bed ΔP cm.H_2O	Total Holdup h_T ml.	$\gamma(h_T)$	$\frac{\Delta P}{\gamma(h_T)}$	$V_g^2 \rho$
NITROGEN - MERCURY IRRIGATED	1	15.2	0.0814	160.5	153.9	1.820	88.19	18.0
	2	12.3	0.0806	171.4	226.2	2.770	61.88	12.2
	3	10.8	0.0763	74.8	140.6	1.684	44.42	8.93
	4	11.1	0.0780	102.0	165.2	1.944	52.47	9.58
	5	7.9	0.0750	59.8	175.9	2.070	28.89	4.65
	6	8.1	0.0750	46.2	134.7	1.628	28.39	4.93
	7	7.9	0.0750	40.8	130.0	1.585	25.74	4.66
	8	14.3	0.0805	168.6	184.7	2.180	77.34	16.4
	9	2.20	0.0724	6.8	146.7	1.745	3.90	0.351
	10	14.0	0.0800	146.2	164.7	1.939	75.40	15.6
	11	13.0	0.0790	110.2	139.2	1.671	65.95	13.3
	12	12.0	0.0780	97.9	134.9	1.630	60.06	11.2
	13	14.1	0.0805	187.7	202.2	2.414	77.75	16.0
	14	12.2	0.0778	92.5	126.2	1.551	59.63	11.6
	15	15.7	0.0833	201.3	162.2	1.910	105.4	20.5
	16	2.22	0.0724	6.8	154.2	1.823	3.73	0.357
	17	2.08	0.0724	4.1	121.5	1.511	2.71	0.314
	18	2.08	0.0724	4.1	123.2	1.525	2.69	0.314
	39	0.92	0.0724	1.1	146.5	1.743	0.63	0.0616
	40	0.87	0.0724	0.9	121.9	1.514	0.59	0.0550
	41	0.85	0.0724	0.7	110.2	1.420	0.49	0.0521
	42	3.93	0.0724	16.1	143.3	1.710	9.42	1.115
	43	3.76	0.0724	12.2	120.2	1.500	8.13	1.020
	44	3.68	0.0724	10.7	110.2	1.420	7.54	0.977

TABLE 11.10
(CONTINUED)

CORRELATION OF RESULTS

System	Run	True Gas Velocity V_g ft./sec.	Gas Density lb./ft.^{3}	Pressure Drop Across Bed ΔP cm.H_2O	Total Holdup h_T ml.	$\gamma(h_T)$	$\frac{\Delta P}{\gamma(h_T)}$	$V_g^2 \rho$
HYDROGEN - MERCURY IRRIGATED	19	47.5	0.00563	149.5	177.5	2.090	71.53	12.7
	20	42.8	0.00551	88.3	131.5	1.598	55.26	10.1
	21	31.0	0.00534	50.3	151.3	1.792	28.07	5.13
	22	28.2	0.00528	35.3	112.9	1.441	24.50	4.20
	23	29.0	0.00528	38.0	125.9	1.548	24.55	4.45
	24	19.6	0.00523	23.1	139.8	1.676	13.78	2.01
	25	18.7	0.00523	17.7	119.9	1.497	11.82	1.83
	26	19.0	0.00523	20.4	117.2	1.475	13.83	1.89
	27	14.2	0.00518	14.2	143.0	1.708	8.31	1.05
	28	13.6	0.00518	11.7	125.8	1.548	7.56	0.960
	29	13.2	0.00518	9.7	110.3	1.421	6.83	0.903
	45	3.14	0.00518	1.5	146.5	1.743	0.86	0.0511
	46	2.86	0.00518	0.8	101.8	1.359	0.59	0.0425
	47	2.94	0.00518	1.1	116.5	1.470	0.75	0.0448
	48	5.46	0.00518	3.6	156.5	1.847	1.95	0.155
	49	5.05	0.00518	2.5	118.9	1.489	1.68	0.132
	50	5.15	0.00518	2.4	115.9	1.465	1.64	0.138
	51	7.70	0.00518	5.5	135.8	1.638	3.36	0.307
	52	7.33	0.00518	4.9	113.8	1.448	3.38	0.279
	53	7.30	0.00518	4.5	111.2	1.428	3.15	0.277

TABLE 11.10
(CONTINUED)

CORRELATION OF RESULTS

System	Run	True Gas Velocity V_g ft./sec.	Gas Density lb./ft.^{3}	Pressure Drop Across Bed ΔP cm.H_2O	Total Holdup h_T ml.	$\gamma(h_T)$	$\frac{\Delta P}{\gamma(h_T)}$	$V_g^2 \rho$
HYDROGEN - ZERO MERCURY RATE PREVIOUSLY IRRIGATED	54	4.83	0.00518	2.0	98	1.334	1.5	0.1205
	55	7.11	0.00518	4.2	98	1.334	3.15	0.262
	56	9.50	0.00518	7.2	98	1.334	5.40	0.466
	57	13.80	0.00523	11.0	98	1.334	8.25	0.995
	58	17.30	0.00523	16.1	98	1.334	12.08	1.560
	59	21.4	0.00523	24.8	98	1.334	18.60	2.383
	60	28.1	0.00529	33.3	98	1.334	24.96	4.180
	61	32.1	0.00529	45.6	98	1.334	34.20	5.43
	62	37.8	0.00534	56.6	98	1.334	42.45	7.58
	63	42.4	0.00534	67.5	98	1.334	50.63	9.56
NITROGEN - ZERO MERCURY RATE PREVIOUSLY IRRIGATED	64	0.83	0.0724	0.7	98	1.334	0.53	0.0498
	65	1.39	0.0724	1.7	98	1.334	1.28	0.139
	66	1.99	0.0724	3.5	98	1.334	2.63	0.286
	67	2.70	0.0724	6.0	98	1.334	4.50	0.524
	68	3.58	0.0724	9.4	98	1.334	7.05	0.926
	69	5.40	0.0724	14.1	98	1.334	10.58	2.100
	70	6.88	0.0724	24.3	98	1.334	18.23	3.410
	71	8.73	0.0738	34.0	98	1.334	25.50	5.50
	72	12.20	0.0746	66.6	98	1.334	49.95	10.7

TABLE 11.10
(CONTINUED)

CORRELATION OF RESULTS

System	Run	True Gas Velocity V_g ft./sec.	Gas Density lb./ft.^{3}	Pressure Drop Across Bed ΔP cm.H_2O	Total Holdup h_T	$\psi(h_T)$	$\frac{\Delta P}{\psi(h_T)}$	$V_g^2\rho$
NITROGEN - DRY PACKING BEFORE IRRIGATION	73	7.4	0.0738	20.4	0	1.0	20.4	4.03
	74	10.5	0.0763	42.1	0	1.0	42.1	8.31
	75	12.6	0.0787	70.7	0	1.0	70.7	12.35
	76	5.7	0.0732	13.3	0	1.0	13.3	2.34
	77	5.0	0.0724	10.3	0	1.0	10.3	1.79
	78	4.5	0.0724	8.4	0	1.0	8.4	1.46
	79	3.0	0.0724	5.6	0	1.0	5.6	0.663
	80	2.3	0.0724	3.7	0	1.0	3.7	0.369
	81	1.7	0.0724	2.3	0	1.0	2.3	0.204
	82	1.2	0.0724	1.3	0	1.0	1.3	0.099
HYDROGEN - DRY PACKING BEFORE IRRIGATION	83	2.4	0.00518	0.7	0	1.0	0.7	0.030
	84	4.1	0.00518	1.5	0	1.0	1.5	0.086
	85	6.0	0.00518	2.5	0	1.0	2.5	0.187
	86	8.6	0.00518	4.1	0	1.0	4.1	0.384
	87	11.3	0.00518	6.3	0	1.0	6.3	0.653
	88	14.3	0.00523	9.5	0	1.0	9.5	1.070
	89	17.1	0.00523	12.1	0	1.0	12.1	1.523
	90	23.2	0.00523	19.6	0	1.0	19.6	2.81
	91	28.3	0.00530	26.8	0	1.0	26.8	4.23
	92	32.2	0.00535	33.2	0	1.0	33.2	5.54
	93	38.8	0.00540	44.5	0	1.0	44.5	8.10

TABLE 11.11

EXPERIMENTAL AND CALCULATED DATA

WATER IRRIGATION - AIR GAS PHASE

System	Liquid Rate ml./min.	True Gas Velocity (V_g ft./sec.)	Pressure Drop Across 1.75 ft. Bed ΔP (cm.H_2O)	Total Holdup h_T ml.	$\psi(h_T)$	$\frac{\Delta P}{\psi(h_T)}$	$V_g^2\rho$
NON-WETTING CONSTANT LIQUID RATE	200	0.49	0.45	78	1.211	0.372	0.0176
	200	0.69	0.80	78	1.211	0.661	0.0353
	200	1.12	1.70	78	1.211	1.404	0.0932
	200	1.58	3.20	86	1.265	2.548	0.186
WETTING CONSTANT LIQUID RATE	200	0.49	0.503	86	1.256	0.400	0.0182
	200	0.70	0.921	89	1.272	0.724	0.0370
	200	1.14	1.50	91	1.287	1.166	0.0975
	200	1.63	3.05	103	1.367	2.231	0.197
WETTING VARIABLE LIQUID RATE	67	0.67	0.836	63	1.136	0.736	0.0334
	125	0.69	0.928	77	1.203	0.771	0.0352
	200	0.70	1.023	89	1.272	0.804	0.0368
	340	0.71	1.116	113	1.442	0.774	0.0374
	455	0.77	1.275	138	1.655	0.770	0.0443
DRY PACKING BEFORE IRRIGATION	0	0.43	0.243	0	1	0.243	0.0135
	0	0.60	0.445	0	1	0.445	0.0271
	0	0.98	0.827	0	1	0.827	0.0713
	0	1.36	1.372	0	1	1.372	0.138
	0	1.79	2.07	0	1	2.07	0.238
	0	2.73	4.48	0	1	4.48	0.518

11.5 Nomenclature

d_e = diameter of the equivalent channel, ft.

D_p = characteristic dimension of the particle, ft.

g = acceleration due to gravity, ft./(sec.^{2})

g_c = gravitational conversion factor

h_D = dynamic holdup, ml.

h_g = gas holdup, ml.

h_S = static holdup, ml.

h_T = total holdup, ml.

H_D = dynamic holdup ratio

H_g = gas holdup ratio

H_s = static holdup ratio

H_T = total holdup ratio

k_g = gas film mass transfer coefficient, lb.mole./(hr.)(ft.^{2})(atm.)

$k_g a$ = volumetric gas film mass transfer coefficient, lb.mole./(hr.)(ft.^{3})(atm.)

L = depth of packed bed

ΔP = pressure drop across packed bed, lb./ft.^{2} in equations 11.1, 11.2, 11.3, 11.5, 11.13 and 11.14, but for convenience cm. H_2O in the dimensional empirical equation 11.4 and empirical correlations of Fig. 11.6 and 11.7

$\Delta P_{h_{T=0}}$ = pressure drop for zero liquid holdup, cm. H_2O

r_h = mean hydraulic radius, ft.

S = surface area per unit packed volume of bed, ft.^{2}/ft.^{3}

S_v = surface area per unit volume of the packing material, ft.^{2}/ft.^{3}

U = superficial fluid velocity, ft./sec.

V = true fluid-velocity, ft./sec.

V_g = true gas velocity. ft./sec.

ε = fractional voids or bed porosity

ρ = fluid density, lb./ft.^{3}

μ = fluid viscosity, lb./(ft.)(sec.)

$\psi(h_T)$ = function of total liquid holdup

$\psi'(V_g^2 \rho)$ = function of gas inertia

CHAPTER 12

EVALUATION OF THE MASS TRANSFER PROPERTIES OF THE PACKED COLUMN

To interpret the zinc absorption results, generalised correlations for estimating the height of a gas film transfer unit and the height of a liquid film transfer unit were required. To develop these correlations a second room temperature analogue of the zinc absorption column was contructed.

The systems chosen were the absorption of pure carbon dioxide in water and the absorption of ammonia in water from a dilute ammonia - air mixture. So that conditions in this low temperature model would simulate the absorption of zinc vapour in molten lead, the tower walls and packing were made non-wetting with respect to the irrigating water by treatment with paraffin wax. The principal features of the low temperature absorption model are shown in Table 12.1.

TABLE 12.1

PRINCIPAL DIMENSIONS OF THE LOW TEMPERATURE ABSORPTION MODEL

Column diameter	= 1.80"
Empty cross sectional area	= 0.0177 ft.^{2}
Empty bed volume (21" height)	= 870 ml.
Empty bed volume (10.5" height)	= 435 ml.
Volume of rings in 21" bed	= 248 ml.
Dry bed porosity	= 0.72
Irrigated bed porosity for 21" packed height	= $(622 - h_T)/870$
Column packing	= $\frac{1}{4}$" x $\frac{1}{4}$" x 20 gauge steel raschig rings

The absorption of pure carbon dioxide in water is a case where there is no diffusional resistance in the gas phase and therefore the measured

height of an overall liquid phase transfer unit is equal to the height of a liquid film transfer unit. Hence, the latter, in this special case, can be measured directly by experiment.

The absorption of ammonia in water from a dilute ammonia - air mixture, because of the high solubility of ammonia in water, is controlled by diffusion in the gas phase. Hence, the measured heights of overall gas phase transfer units require a small correction for diffusional resistance in the liquid phase, to enable the height of a gas film transfer unit to be evaluated.

The experimental techniques used in this low temperature model were the same as used by Stephens and Morris (116) and Taylor and Roberts (122) for calibrating a disc column for physical absorption. As these techniques have been used frequently by other investigators and as texts such as Sherwood and Pigford (99) also outline the general approaches used for evaluating gas and liquid phase resistance in gas absorption, the experimental methods, employed in this investigation, contained no novel features and therefore, the results only will be presented together with the discussion of the significant features.

However, as a background to the discussions, the methods of correlating gas and liquid film data are first reviewed and examined critically to see if they are suitable as a basis for the interpretation of zinc absorption data.

12.1.1 Correlation of Liquid Phase Data

Sherwood and Holloway (98) proposed that liquid phase data be correlated according to equations 12.1 or 12.2

$$\frac{k_L a}{D} = \alpha \left(\frac{L}{\mu}\right)^{1-n} \left(\frac{\mu}{\rho D}\right)^{1-s} \qquad \ldots\ldots 12.1$$

or the equivalent expression

$$H_L = \frac{1}{\alpha} \left(\frac{L}{\mu}\right)^{n} \left(\frac{\mu}{\rho D}\right)^{s} \qquad \ldots\ldots 12.2$$

These equations were derived from the dimensionless form used originally by Gilliland and Sherwood (30) correlating data on vaporisation in a wetted wall column, but suitably modified for liquid phase analysis in a packed column. These equations are not dimensionless because of the omission of the length dimension from the left hand side and first group on the right in both equations. The proportionality constant α will therefore vary with the system of units employed. The length dimension was omitted because the equivalent diameter to be used in packed column analysis is not known and therefore, rather than using the nominal packing size, it was considered preferrable to delete this term.

Sherwood and Holloway (98) investigated a wide range of systems, with the result that the exponent s on the Schmidt number was found to be 0.47 in equation 12.2, i.e. the observed variation of $k_L a$ was as the 0.47 power of the liquid diffusivity. This was in remarkable agreement with the 0.5 power required for Higbie's penetration theory (39). Additional support of the 0.5 power was provided by the more recent studies of Lynn, Straatemeier and Kramers (65) and Vivian and Peaceman (123), who studied liquid phase resistance in short wetted wall columns. The value of s in equations 12.1 and 12.2 has therefore been established as 0.5, both on theoretical and experimental grounds.

The values of the exponent n and the constant α depend on the size and type of packing, the nature of the surface of the packing and the type of

flow, whether wetting or non-wetting, and therefore must be determined experimentally on the type and size of packing and flow for which the correlation is being developed.

As a preliminary examination of the zinc absorption data revealed that most of the diffusional resistance was to be located in the gas phase under the conditions of this investigation, the estimation of the height of a liquid film transfer unit was considerably less important than the evaluation of the height of a gas film transfer unit and therefore the form of correlation proposed was considered suitable for this investigation without modification.

12.1.2 Correlation of Gas Phase Data

Empirical studies of gas phase mass transfer in packed columns have been characterised by apparent disagreement and anomalies between the various reported studies, whereas liquid phase correlations since the work of Sherwood and Holloway (98) have been more successful.

However, the recent very significant contributions of Shulman and co-workers (111)(110)(112), who introduced the concept of effective interfacial area, have provided suitable explanations of the anomalies, which existed in this field, with particular reference to the difference between absorption and vaporisation in packed columns and the effects of physical properties of the liquid phase determining the wetted surface areas when organic and aqueous liquids are vaporised in packed columns. The essential features of Shulman's explanations are related to the behaviour of the liquid phase flowing through the packing and have been discussed fully in the previous chapter.

Further advances in the field were recently made by Yoshida (132), Lynch and Wilke (63) and Shulman and Margolis (109), who studied the

effect of fluid properties on the gas phase mass transfer process, by vaporisation studies with ranges of different gas phases. The first two sets of data were for water vaporisation, whilst the latter was for the vaporisation of specially prepared naphthalene raschig rings and berl saddles.

Shulman and co-workers were primarily interested in dividing the volumetric mass transfer coefficients into transfer coefficients per unit effective interfacial area and effective interfacial areas per unit packed volume. The problem of evaluating the effective interfacial area in a packed column was fully discussed in the previous chapter.

Although the effective interfacial area may be evaluated in certain cases, the use of this method for analysing the zinc absorption data was precluded, because even the total surface exposed to gas flow cannot be readily evaluated for these data without further work being first carried out to establish the effects of physical properties on the holdup of liquid metals when irrigating packings. The determination of the total surface exposed to gas flow is only the first step towards evaluating the effective interfacial area, as the surface area of the liquid has to be determined and the fraction of this liquid surface, which is effective in the mass transfer process, has to be estimated. Therefore, although division of the volumetric mass transfer coefficient may be more elegant on theoretical grounds, it is doubtful if such a procedure can be considered to have general application, because of the large amount of specialised information on the particular system, which is required, before the analysis can be undertaken.

Yoshida (132) chose to correlate his data for the vaporisation of water by a series of gases in a packed column, by a form similar to

that used by Sherwood and Holloway (98) for liquid phase resistance, i.e.

$$H_G = \beta' L^a \left(\frac{G}{\mu}\right)^b \left(\frac{\mu}{\rho D}\right)^c \qquad \ldots\ldots 12.3$$

This form of correlation, or its equivalent in terms of either the mass transfer coefficient or the volumetric mass transfer coefficient, has been used by many investigators in the analysis of gas phase mass transfer in various systems. Basically it is equivalent to the method used by Gilliland and Sherwood (30) for correlating vaporisation data in a wetted wall column, except that it has been modified for packed column usage by introducing the height of a transfer unit as originally proposed by Chilton and Colburn (12). The Chilton and Colburn j_D factor, previously discussed in the gas phase mass transfer studies of this investigation, is also basically of similar form, except that the volumetric coefficient has replaced the ordinary mass transfer coefficient and the terms of the equation have been rearranged.

Equation 12.3 can be considered as the conventional form for correlating gas phase data. However, a better form of this equation is to use the true gas velocity rather than superficial quantities as used in equation 12.3, i.e.

$$H_G = \beta'' L^a \left(\frac{G}{\mu(1-\varepsilon)}\right)^b \left(\frac{\mu}{\rho D}\right)^c \qquad \ldots\ldots 12.4$$

or

$$H_G = \beta'' L^a \left(\frac{V_g \rho}{\mu}\right)^b \left(\frac{\mu}{\rho D}\right)^c \qquad \ldots\ldots 12.5$$

The liquid rate term L in equations 12.3, 12.4 and 12.5 was introduced because the liquid rate was found to effect the gas phase transfer rate. The use of the superficial liquid phase mass velocity, to account for this observed effect, is considered to be the principal weakness of this

correlation, when examined from the aspect of application to the zinc absorption studies of this investigation. If the correlation is developed by experimentation with aqueous systems, the extension of the correlation to a system, in which the liquid phase is molten lead, would be extremely questionable.

Therefore, rather than using a liquid rate in the correlation, a term, which indicates the actual volume of liquid present in the packing, which is effective for absorption, should be used in the correlation.

It is proposed that the dimensionless quantity, "the effective holdup ratio" H_E be introduced for this purpose. The "effective holdup ratio" to be defined as the volume of liquid in the packing, which is effective in absorption, divided by the volume of the packed bed.

By the introduction of this term, it is considered that a compromise has been reached between the use of effective interfacial area as suggested by Shulman and co-workers (111)(110)(112) and the more readily achieved procedure of evaluating transfer rates per unit packed bed volume. Equation 12.5 can then be modified to the new form given in equation 12.6.

$$H_G = \beta \left(\frac{V_g \rho}{\mu}\right)^b \left(\frac{\mu}{\rho D}\right)^c H_E^{\,d} \qquad \ldots\ldots 12.6$$

A more elegant form of equation 12.6 would be to replace $\frac{V_g \rho}{\mu}$ with the correct Reynolds number form employing the total surface area exposed to gas flow, as proposed by Mott (78). However, as the specific surface could not be readily evaluated for the zinc absorption runs, equation 12.6, as such, was considered as a possible form for correlating the data.

The effective holdup ratio is a variable quantity depending on the type of mass transfer operation. Shulman, Ullrich and Wells (111) showed conclusively that the dynamic holdup was the only effective component

for the absorption of ammonia in water from a dilute ammonia - air mixture, and that the total holdup was effective in vaporisation. The full significance of the effective component of the liquid holdup was discussed in the previous chapter and also the suggestion was made that when a liquid metal irrigates a packing, the so-called static holdup could possibly be as effective as the flowing component in an absorption process such as the absorption of zinc vapour in molten lead.

Lynch and Wilke (63) proposed that the rate of mass transfer may be a function of the inertia of the gas stream ($V_g^2 \rho$) at high flow rates rather than the Reynolds number. This postulation is based on the observed pressure drop behaviour for flow past single cylinders, which shows that the drag coefficient is independent of Reynolds number at high flow rates and the pressure drop is dependent only on the inertia of the gas stream. The fact that the pressure drops in the mercury model were correlated by the gas inertia, without use of a viscosity term, may be also significant in this respect. The form of correlation suggested is given in equation 12.7.

$$H_G = \chi\left[(V_g^2 \rho), \left(\frac{\mu}{\rho D}\right)\right] \qquad \ldots\ldots 12.7$$

Equation 12.7 was proposed tentatively pending further study. Although these authors successfully correlated their data by such a method, their data can also be correlated conventionally, if the effects of interfacial velocity are taken into account, as illustrated in the discussion of gas phase mass transfer in a disc column of this investigation, where it was shown, that even a small liquid velocity of 0.1 ft./sec. could account for the apparent lack of correlation of their data by the accepted forms.

However, as no real assessment of the merits of equation 12.7 can

be made, until further experimental work is undertaken, a modified form of equation 12.7 involving the newly proposed effective holdup ratio, as shown in equation 12.8, was also considered as a possible basis for the correlation of the zinc absorption data.

$$H_G = \gamma (V_g^2 \rho)^e \left(\frac{\mu}{\rho D}\right)^c H_E^d \qquad \ldots\ldots 12.8$$

The exponent of the Schmidt number in equations 12.3 to 12.8 is considered to be $^2/_3$. Although the recent studies of Lynch and Wilke (63) and Yoshida (132) obtained different exponents on the Schmidt number, these are believed to be due to interfacial velocity effects masking the true effect of the diffusivity, as was proposed in the discussion of gas phase mass transfer in a disc column, presented earlier in this thesis. As the $^2/_3$ exponent was found to be satisfactory for correlating the disc column data of this investigation and as the most recent work, undertaken to establish the effects of fluid properties on gas phase mass transfer in a packed column, reported by Shulman and Mamgolis (109) also supported the $^2/_3$ exponent on the Schmidt number, the use of this exponent is considered to be justified. The latter work could not be affected by interfacial velocity effects, as the data were for vaporisation of solid naphthalene packing, in which there was no irrigation. The investigations supporting the $^2/_3$ exponent are very numerous. Some of these were mentioned more fully in Chapter 8 when the gas phase data for the disc column were discussed.

The gas phase mass transfer studies of Chapter 8 resulted in the introduction of a newly defined mass transfer factor, the "relative j_D

factor", in which the significant velocity term in the mass transfer process is taken to be the relative interfacial velocity, rather than the true gas velocity. As the use of this new approach is considered to have general application, a possible form of correlating the zinc absorption data of this investigation would be an equation derived from the "relative j_D factor".

If the "relative j_D factor" is introduced rather than the conventional j_D factor, the methods of correlation using the concept of the height of a transfer unit are no longer applicable, as these would also have to be modified for relative velocity effects.

The suggested form is developed in the following equations:-

By definition, from Chapter 8

$$(j_D)_R = \frac{k_g}{V_R} \frac{p_{BM}}{\rho_m} \left(\frac{\mu}{\rho D}\right)^{2/3} \qquad \ldots\ldots 12.9$$

and,

$$(j_D)_R = \chi (Re)_R \qquad \ldots\ldots 12.10$$

$$\therefore \frac{1}{(j_D)_R} = \frac{V_R}{k_g} \frac{\rho_m}{p_{BM}} \left(\frac{\mu}{\rho D}\right)^{-2/3} \qquad \ldots\ldots 12.11$$

Now

$$H_G = \frac{G_m}{k_g a} \frac{}{P} = \frac{V}{k_g a} \frac{\rho_m}{P} \qquad \ldots\ldots 12.12$$

$$\therefore \frac{1}{(j_D)_R} = a \cdot H_G \cdot \frac{V_R}{V} \cdot \frac{P}{p_{BM}} \qquad \ldots\ldots 12.13$$

$$\therefore a \cdot H_G \cdot \frac{V_R}{V} \cdot \frac{P}{p_{BM}} \cdot \left(\frac{\mu}{\rho D}\right)^{-2/3} = \chi' (Re)_R \qquad \ldots\ldots 12.14$$

For a dilute system $\frac{P}{p_{BM}}$ may be taken as unity.

As the effective interfacial area "a" is not known, the "effective holdup ratio", previously defined, can be used as a basis for correlation. Also as the "relative Reynolds number" cannot be evaluated, because the

characteristic length (or the specific surface) is not usually known, the length dimension can be omitted, as in the previous equations. The resulting form of the correlation is given by equation 12.15:-

$$H_G \cdot \frac{V_R}{V} = \alpha \left(\frac{V_R \rho}{\mu}\right)^x \left(\frac{\mu}{\rho D}\right)^{2/3} H_E^{\,d} \qquad \ldots\ldots 12.15$$

12.2 Carbon Dioxide Absorption in Water

The experimental results for the absorption of pure carbon dioxide in water under non-wetting conditions are given in Table 12.2. So as to afford a comparison of the performance of the packing, experiments were also carried out on the rings before treatment with paraffin wax. The carbon dioxide absorption data under these wetting conditions are shown in Table 12.3.

The apparent heights of liquid film transfer units in Tables 12.2 and 12.3 are the values directly measured on the apparatus, using the equilibrium data given by Perry (84). As the temperature of the liquid was different in the various runs, a comparison of the data could only be made by converting all values to a temperature of 25°C by the equation proposed by Sherwood and Holloway (98), who studied the effect of liquid temperature on carbon dioxide absorption in water. This procedure is equivalent to expressing all the data in the form of equation 12.2, but as a generalised correlation was not required at this stage, the simpler procedure of correcting all the values to the same temperature was employed.

For the non-wetting conditions, the end effects due to the absorption surface beneath the packing support, which was not taken into account in the evaluation of the apparent heights of liquid film transfer units,

were determined by using two different heights of packing. These end effects, which were found to be equal to 4.8" of additional packed height, were taken into account when the true height of a liquid film transfer unit was calculated.

The somewhat high end effects observed in these experiments are partly due to better liquid distribution at the top of the packing, where the liquid feed jet distributed the liquid into the centre of the bed. Visual observation of the column showed that, as the liquid flowed through the packing, the flow distribution was such that some of the liquid tended follow the wall of the column more after passing several inches beneath the top of the packing. The packing at the top was therefore more effective. The other factor contributing to the end effects was the "spray" section beneath the packing support.

The calculated values of apparent H_L at 25°C and true H_L at 25°C for the non-wetting runs are given in Table 12.4. As the end effects were not determined for the wetting data, only the apparent H_L at 25°C was evaluated as shown in Table 12.5. The apparent values of Table 12.5, however, can be compared directly with the apparent H_L at 25°C data for non-wetting in a 10.5" packed bed, to give an assessment of the differences between wetting and non-wetting conditions.

TABLE 12.2

EXPERIMENTAL RESULTS - CARBON DIOXIDE ABSORPTION

NON-WETTING

Run	Liquid Rate mole./hr.	Mole. Fraction CO_2 in Exit Liquor	Temperatures		$N_{OL} = N_L$	Apparent H_L ft.
			Inlet Liquid °C	Outlet Liquid °C		
		21" Packed Bed				
1A	0.49	0.000527	19.7	19.8	1.355	1.29
2A	0.49	0.000487	20.2	20.1	1.187	1.47
3A	1.15	0.000417	23.0	22.5	1.018	1.72
4A	1.15	0.000420	23.2	22.8	1.052	1.66
5A	2.20	0.000386	24.2	23.8	0.952	1.84
6A	2.30	0.000379	24.4	24.0	0.935	1.87
7A	3.35	0.000354	24.8	24.5	0.857	2.04
8A	3.35	0.000355	24.8	24.6	0.860	2.04
		10.5" Packed Bed				
9A	0.49	0.000364	24.0	22.5	0.835	1.05
10A	0.49	0.000326	24.1	22.6	0.710	1.23
11A	1.20	0.000301	24.7	23.9	0.662	1.32
12A	1.20	0.000299	24.7	24.0	0.652	1.34
13A	2.15	0.000280	25.0	24.6	0.610	1.43
14A	2.15	0.000250	25.1	24.6	0.522	1.68
15A	3.35	0.000235	25.2	24.7	0.483	1.81
16A	3.35	0.000236	25.1	24.8	0.490	1.78

TABLE 12.3

EXPERIMENTAL RESULTS - CARBON DIOXIDE ABSORPTION

WETTING

Run	Liquid Rate mole./hr.	Mole. Fraction CO_2 in Exit Liquor	Temperatures		$N_{OL} = N_L$	Apparent H_L ft.
			Inlet Liquid °C	Outlet Liquid °C		
		10.5" Packed Bed				
1	0.40	0.000595	22.1	19.9	1.920	0.456
2	0.35	0.000566	22.1	19.8	1.670	0.524
3	0.87	0.000453	23.0	21.9	1.153	0.758
4	0.87	0.000464	23.0	21.9	1.203	0.727
5	2.50	0.000330	23.6	22.9	0.725	1.205
6	2.50	0.000321	23.6	23.0	0.698	1.250
7	1.40	0.000382	23.5	22.6	0.898	0.975
8	1.55	0.000369	23.6	22.7	0.852	1.030
9	3.35	0.000289	24.5	24.0	0.627	1.395
10	3.45	0.000278	24.5	24.0	0.597	1.465
11	4.75	0.000262	26.0	25.6	0.578	1.513
12	1.47	0.000376	25.5	23.9	0.933	0.938

TABLE 12.4

EVALUATION OF APPARENT AND TRUE (H_L) AT 25°C

CARBON DIOXIDE ABSORPTION

NON-WETTING

Run	Liquid Rate mole./hr.	Apparent H_L ft.	Mean Liquid Temp. °C	Apparent H_L at 25°C ft.	True H_L at 25°C ft.	Mean True H_L at 25°C ft.
		21" Packed Bed				
1A	0.49	1.29	19.8	1.15	1.41	1.52
2A	0.49	1.47	20.2	1.32	1.62	
3A	1.15	1.72	22.8	1.63	2.00	1.98
4A	1.15	1.66	23.0	1.60	1.96	
5A	2.20	1.84	24.0	1.81	2.22	2.22
6A	2.30	1.87	24.2	1.83	2.24	2.24
7A	3.35	2.04	24.7	2.03	2.49	2.49
8A	3.35	2.04	24.7	2.03	2.49	
		10.5" Packed Bed				
9A	0.49	1.05	23.3	1.01	1.47	1.60
10A	0.49	1.23	23.4	1.18	1.72	
11A	1.20	1.32	24.4	1.30	1.89	1.91
12A	1.20	1.34	24.4	1.32	1.92	
13A	2.15	1.43	24.8	1.42	2.06	2.25
14A	2.15	1.68	24.9	1.68	2.44	
15A	3.35	1.81	25.0	1.81	2.64	2.62
16A	3.35	1.78	25.0	1.78	2.59	

TABLE 12.5

EVALUATION OF APPARENT (H_L) AT 25°C

CARBON DIOXIDE ABSORPTION

WETTING

Run	Liquid Rate mole./hr.	Apparent H_L ft.	Mean Liquid Temp. °C	Apparent H_L at 25°C ft.	True H_L at 25°C ft.	Mean True H_L at 25°C ft.
		10.5" Packed Bed				
1	0.40	0.456	21.0	0.419	-	-
2	0.35	0.524	21.0	0.480	-	-
3	0.87	0.758	22.5	0.716	-	-
4	0.87	0.727	22.5	0.690	-	-
5	2.50	1.205	23.3	1.130	-	-
6	2.50	1.250	23.3	1.190	-	-
7	1.40	0.975	23.1	0.940	-	-
8	1.55	1.030	23.2	1.000	-	-
9	3.35	1.395	24.3	1.370	-	-
10	3.45	1.465	24.3	1.430	-	-
11	4.75	1.513	25.8	1.530	-	-
12	1.47	0.938	24.7	0.930	-	-

The apparent heights of liquid film transfer units corrected to 25°C for 10.5" and 21" packed non-wetting beds and for a 10.5" packed wetting bed are plotted as a function of liquid rate in Fig. 12.1.

The apparent heights of liquid film transfer units corrected to 25°C for 10.5" and 21" packed non-wetting beds and for a 10.5" packed wetting bed are plotted as a function of liquid rate in Fig. 12.1.

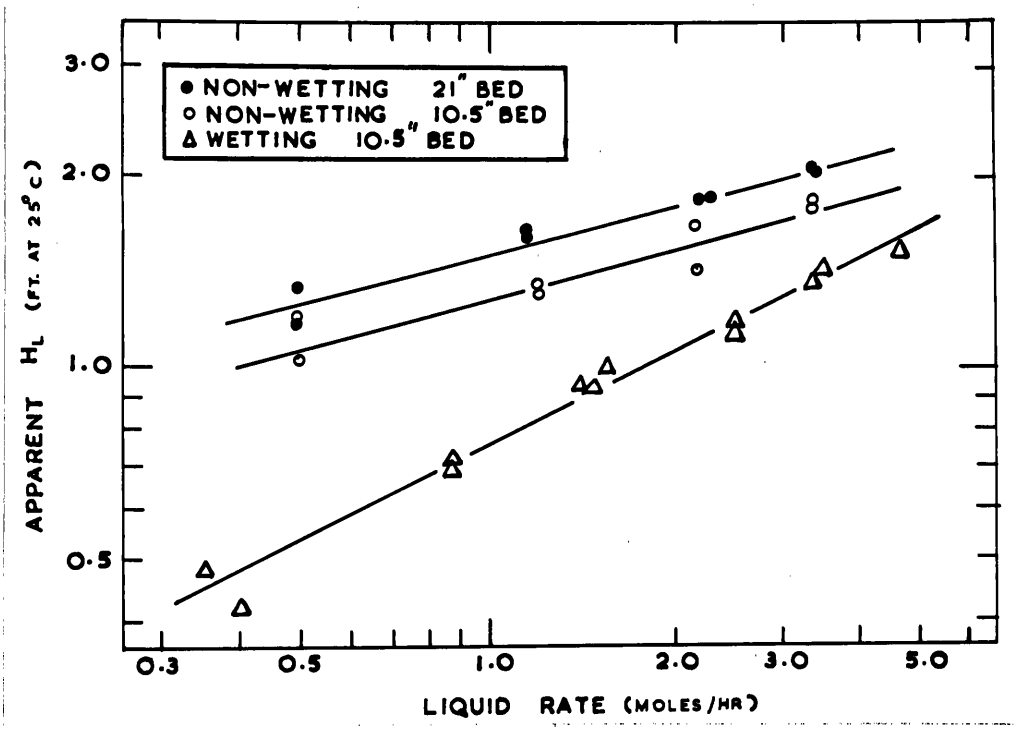

Fig. 12.1 - Apparent heights of liquid film transfer units

The wetting and non-wetting data differ in two respects, as can be seen from Fig. 12.1.

The non-wetting conditions give values of H_L significantly higher than those for wetting. This is to be expected, as the wetting interfacial area would be considerably greater than the non-wetting interfacial area.

The second effect is that the liquid rate affects the data to different extents. Thus it would appear that, if the data were extrapolated to very high liquid flows, the non-wetting conditions would give transfer rates

greater than the wetting conditions. A similar effect has been previously reported by Sherwood and Holloway (97). The explanation of this effect is considered to be a difference in turbulence in the liquid phase. Under wetting conditions, the liquid flows in thin layers over the packing but under non-wetting conditions, thick rivulets are formed rather than thin layers. These rivulets result in greater turbulence in the liquid phase, which is of utmost importance in a liquid phase controlled absorption such as carbon dioxide absorption in water. Thus this increased liquid turbulence, under non-wetting conditions, tends to offset the decreased liquid surface area resulting from the non-wetting flow. These phenomena suggest the interesting conclusion, that a non-wetting treatment of the packing, in a liquid phase controlled absorption, could possibly improve the absorption efficiency under high liquid flow conditions.

The end effects associated with the measurements can be seen in Fig. 12.1 by comparing the non-wetting 21" and 10.5" packed bed data. These end effects, which are equivalent to 4.8" of packing, are compensated when the true heights of liquid film transfer units are calculated. Fig. 12.2 shows that the single end effect correction of 4.8" of additional packing allows correlation of all the liquid film data obtained for non-wetting flow.

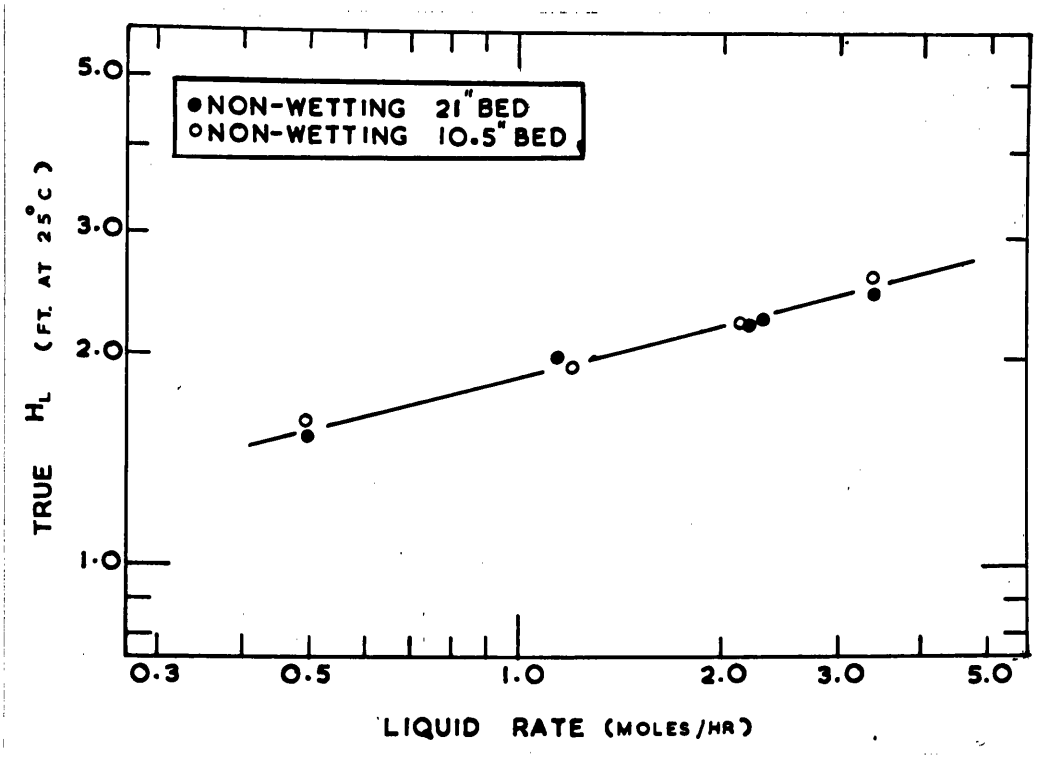

Fig. 12.2 - True heights of liquid film transfer units (corrected for end effects)

12.3 Ammonia Absorption in Water from Dilute Ammonia - Air Mixtures

As indicated in the discussion of the correlation of gas phase data, the holdup of liquid in the packed bed is very significant in the interpretation of these data. Therefore, the dynamic, static and total holdup of water irrigating the packing, under both wetting and non-wetting conditions, were measured. The results of these measurements are summarised in Table 12.6.

TABLE 12.6

WATER HOLDUP DATA

A. WETTING - 10.5" Packed Bed

Liquid Rate mole./hr.	Gas Rate mole./hr.	Static Holdup h_S ml.	Dynamic Holdup h_D ml.	Total Holdup h_T ml.	Volume of Bed ml.
1.32	0.0310	17	29.0	46.0	435
1.32	0.0500	17	27.0	43.0	435
1.32	0.0705	17	27.3	44.3	435
1.32	0.1150	17	28.5	45.5	435
1.32	0.1600	17	34.5	51.5	435
0.455	0.0705	17	14.3	31.3	435
0.860	0.0705	17	21.3	38.3	435
1.32	0.0705	17	27.3	44.3	435
2.06	0.0705	17	39.5	56.5	435
2.86	0.0705	17	51.8	68.8	435

B. NON-WETTING - 10.5" Packed Bed

Liquid Rate mole./hr.	Gas Rate mole./hr.	Static Holdup h_S ml.	Dynamic Holdup h_D ml.	Total Holdup h_T ml.	Volume of Bed ml.
1.32	0.0310	18	21	39	435
1.32	0.0500	18	21	39	435
1.32	0.0705	18	21	39	435
1.32	0.1150	18	21	39	435
1.32	0.1600	18	25	43	435
0.455	0.0705	18	14	32	435
0.860	0.0705	18	17	35	435
2.06	0.0705	18	29	47	435
2.86	0.0705	18	35	53	435
1.22	0.0705	18	21	39	435

All the experiment results for the absorption of ammonia in water from dilute ammonia - air mixtures are given in Tables 12.7 and 12.8. The data in Table 12.8, which are for wetting conditions, were obtained as a basis for comparison with the non-wetting data of Table 12.7.

As indicated in these tables, the data for the highest gas rate was generally in the loaded region. This loading could be readily detected by visual observation of the liquid in the column, as under loaded conditions, pockets of liquid, which would normally not be stagnant, ceased flowing and oscillated around fixed positions in the bed. These data were obtained at the point of incipient loading. The gas rate which caused loading under non-wetting conditions in the 10.5" packed bed, did not initiate any loading for the 21" packed bed. These visually loaded runs were not included in the final analysis of the data.

The ammonia mass balances of this investigation are inferior to those reported by previous investigators. Stephens and Morris (116) and Taylor and Roberts (122) obtained balances usually within 2 to 3% and in no case was the error greater than 6%. The balances reported by Houston and Walker (46) were also never more than 6% in error. However, in this investigation errors as great as 10% were recorded. These errors are attributed to liquid rate fluctuations, as the liquid flow during the test periods varied slightly.

As snap liquid samples were taken for analysis, any variation in liquid flow rate would be reflected in these analyses. Because composite liquid samples were not taken, the calculations of the mass transfer were based on the gas phase ammonia analyses. The outlet gas analysis was taken by sampling at constant rate throughout the run. The inlet gas analysis was determined at the commencement and conclusion of each run.

TABLE 12.7

EXPERIMENTAL RESULTS - AMMONIA ABSORPTION

NON-WETTING

Run	Gas Rate mole/hr.	Water Rate mole/hr.	Mole Fraction NH_3 in Inlet Gas	Mole Fraction NH_3 in Outlet Gas	Mole Fraction NH_3 in Exit Liquid	Temperatures °C		Mass Balance %
						Water In	Water Out	
			10.5" Packed Bed					
15	0.0310	1.32	0.0368	0.00156	0.00089	23.9	24.0	93
16	0.0310	1.32	0.0370	0.00172	0.00090	25.2	25.3	92
17	0.0500	1.32	0.0402	0.00578	0.00143	26.6	26.7	91
18	0.0500	1.32	0.0418	0.00572	0.00150	26.6	26.8	91
19	0.0705	1.32	0.0447	0.00715	0.00222	26.6	26.9	90
20	0.0705	1.32	0.0476	0.00768	0.00231	26.6	27.0	92
21	0.1150	1.32	0.0542	0.01195	0.00345	26.5	27.4	107
22	0.1150	1.32	0.0268	0.00431	0.00205	24.8	24.3	96
*23	0.1600	1.32	0.0296	0.00632	0.00268	25.1	24.5	105
*24	0.1600	1.32	0.0330	0.00715	0.00300	25.1	24.8	104
25	0.0705	0.45	0.0376	0.00872	0.00432	19.2	21.0	104
26	0.0705	0.86	0.0384	0.00617	0.00285	21.2	22.2	93
27	0.0705	2.06	0.0396	0.00376	0.00138	23.2	23.4	90
28	0.0705	2.86	0.0415	0.00327	0.00105	24.5	24.5	90
29	0.0705	1.22	0.0437	0.00625	0.00208	24.3	24.6	104
			21.0" Packed Bed					
30	0.0500	1.32	0.0490	0.00090	0.00203	22.0	22.6	90
31	0.0705	1.32	0.0499	0.00184	0.00279	22.0	23.1	92
32	0.1150	1.32	0.0519	0.00381	0.00431	22.2	23.5	97
33	0.1600	1.32	0.0547	0.00686	0.00581	21.8	23.9	100
34	0.1600	1.32	0.0558	0.00118	0.00133	22.0	22.7	96

$$\text{Mass Balance} = \frac{\text{Ammonia Lost from Gas}}{\text{Ammonia Absorbed by Liquid}} \times 100$$

* Visual Loading

TABLE 12.8

EXPERIMENTAL RESULTS - AMMONIA ABSORPTION

WETTING

Run	Gas Rate mole./hr.	Water Rate mole./hr.	Mole. Fraction NH_3 in Inlet Gas	Mole. Fraction NH_3 in Outlet Gas	Mole. Fraction NH_3 in Exit Liquid	Temperatures °C		Mass Balance %
						Water In	Water Out	
			10.5" Packed Bed					
1	0.0500	1.32	0.0553	0.00071	0.00228	22.4	22.9	91
2	0.0500	1.32	0.0598	0.00048	0.00220	23.0	23.5	102
3	0.0500	1.32	0.0643	0.00053	0.00242	23.7	24.3	100
4	0.0705	0.45	0.0337	0.00219	0.00473	19.1	21.1	103
5	0.0705	0.86	0.0343	0.00100	0.00283	21.0	21.7	97
6	0.0705	1.32	0.0367	0.00055	0.00214	21.6	22.2	90
7	0.0705	2.06	0.0378	0.00034	0.00142	22.5	22.9	90
8	0.0705	2.86	0.0418	0.00011	0.00096	24.1	24.3	107
* 9	0.160	1.32	0.0384	0.00238	0.00390	25.7	26.0	112
*10	0.160	1.32	0.0414	0.00283	0.00430	25.9	26.4	109
*11	0.160	1.32	0.0456	0.00368	0.00485	26.0	27.0	105
12	0.0310	1.32	0.0481	0.00004	0.00112	22.7	22.9	101
13	0.0310	1.32	0.0486	0.00005	0.00110	22.9	23.1	104
14	0.0310	1.32	0.0499	0.00006	0.00115	22.9	23.1	101

$$\text{Mass Balance} = \frac{\text{Ammonia lost from Gas}}{\text{Ammonia Absorbed by Liquid}} \times 100$$

* Visual Loading

The height of a gas film transfer unit was calculated from the measured height of an overall gas phase tranfer unit by correcting this value for diffusional resistance in the liquid phase. The relation between H_{OG}, for cases, in which the equilibrium curve is linear (i.e. where Henry's law holds), is given by Sherwood and Pigford (100) and other standard texts as equation 12.16.

$$H_{OG} = H_G + m \frac{G_m}{L_m} H_L \qquad \ldots\ldots 12.16$$

The values of H_L, for absorption of ammonia in water were calculated using equation 12.2, the constants and exponents being determined from the carbon dioxide absorption data. The diffusion data used were those given by Perry (83). Values of m were calculated for each run using the equilibrium data tabulated by Perry (84).

The apparent heights of gas film transfer units, using the procedure outlined, are given in Tables 12.9 and 12.10 for the non-wetting and wetting runs, respectively. The true heights of gas film transfer units were evaluated by using the same end correction as obtained in the carbon dioxide absorption experiments (i.e. 4.8" of additional packing).

The wetting data were not corrected for end effects but the wetting and non-wetting data may be compared using the apparent data, uncorrected for end effects, provided the comparison is made on the basis of the same packed height.

A summary of the ammonia absorption data for wetting and non-wetting flow is given in Table 12.11, in which the mean data for each set of experimental conditions are presented.

TABLE 12.9

EVALUATION OF H_{OG} AND APPARENT H_G - AMMONIA ABSORPTION

NON-WETTING

Run	Gas Rate mole./hr.	Liquid Rate mole./hr.	N_{OG}	H_{OG} (ft.)	Mean Liquid Temp. °C	H_L for NH_3 Absorption at Mean Liquid Temp. (ft.)	m	Apparent H_G Uncorrected for End Effects (ft.)
			10.5" Packed Bed					
15	0.0310	1.32	3.20	0.274	24.0	1.45	0.93	0.246
16	0.0310	1.32	3.11	0.281	25.3	1.40	0.99	0.252
17	0.0500	1.32	1.99	0.439	26.7	1.35	1.06	0.390
18	0.0500	1.32	2.05	0.427	26.7	1.35	1.06	0.378
19	0.0705	1.32	1.89	0.463	26.8	1.35	1.06	0.394
20	0.0705	1.32	1.89	0.463	26.8	1.35	1.06	0.394
21	0.1150	1.32	1.58	0.555	27.0	1.34	1.07	0.442
*22	0.1150	1.32	1.90	0.462	24.6	1.42	0.96	0.356
*23	0.1600	1.32	1.62	0.541	24.8	1.41	0.97	0.393
24	0.1600	1.32	1.61	0.543	25.0	1.41	0.97	0.394
25	0.0705	0.45	1.55	0.566	20.1	1.17	0.77	0.437
26	0.0705	0.86	1.90	0.461	21.7	1.32	0.84	0.376
27	0.0705	2.06	2.40	0.365	23.3	1.68	0.90	0.322
28	0.0705	2.86	2.58	0.339	24.5	1.78	0.95	0.303
29	0.0705	1.22	2.00	0.438	24.5	1.39	0.95	0.369
			21" Packed Bed					
30	0.0500	1.32	4.14	0.422	22.3	1.75	0.86	0.371
31	0.0705	1.32	3.44	0.508	22.6	1.73	0.87	0.435
32	0.1150	1.32	2.73	0.641	22.9	1.70	0.89	0.523
33	0.1600	1.32	2.19	0.800	22.9	1.70	0.89	0.636
34	0.1600	1.32	4.55	0.384	22.4	1.74	0.87	0.352

* Visual Loading

TABLE 12.10

EVALUATION OF H_{OG} AND APPARENT H_G - AMMONIA ABSORPTION

WETTING

Run	Gas Rate mole./hr.	Liquid Rate mole./hr.	N_{OG}	H_{OG} (ft.)	Mean Liquid Temp. °C	H_L for NH_3 Absorption at Mean Liquid Temp. (ft.)	m	Apparent H_G Uncorrected for End Effects (ft.)
			10.5" Packed Bed					
1	0.0500	1.32	4.48	0.195	22.7	0.96	0.88	0.166
2	0.0500	1.32	4.92	0.178	22.3	0.97	0.86	0.150
3	0.0500	1.32	5.00	0.175	24.0	0.94	0.93	0.145
4	0.0705	0.45	2.95	0.296	20.1	0.59	0.77	0.231
5	0.0705	0.86	3.70	0.236	21.4	0.78	0.82	0.187
6	0.0705	1.32	4.27	0.205	21.9	0.98	0.85	0.165
7	0.0705	2.06	4.97	0.176	22.7	1.24	0.88	0.145
8	0.0705	2.86	6.03	0.145	24.2	1.36	0.94	0.118
* 9	0.1600	1.32	3.00	0.292	25.9	0.90	1.20	0.175
*10	0.1600	1.32	2.90	0.302	26.2	0.89	1.30	0.176
*11	0.1600	1.32	2.70	0.324	26.5	0.88	1.50	0.180
12	0.0310	1.32	6.43	0.136	22.8	0.96	0.88	0.118
13	0.0310	1.32	6.33	0.138	23.0	0.96	0.89	0.120
14	0.0310	1.32	6.17	0.142	23.0	0.96	0.89	0.124

* Visual Loading

TABLE 12.11

SUMMARY OF RESULTS

MEAN DATA - ABSORPTION OF AMMONIA IN WATER

Gas Rate mole/hr.	Liquid Rate $\frac{\text{mole}}{\text{hr.}}$	Total Holdup h_T ml.	Bed Porosity ε	Velocity V_g ft./sec.	Dynamic Holdup Ratio H_D	Apparent H_G	True H_G
		Wetting - 10.5" Packed Bed					
0.0500	1.32	43.0	0.62	0.493	0.0644	0.154	-
0.0705	0.455	31.3	0.64	0.669	0.0311	0.231	-
0.0705	0.860	38.3	0.63	0.685	0.0494	0.187	-
0.0705	1.32	44.3	0.61	0.702	0.0644	0.165	-
0.0705	2.06	56.5	0.61	0.707	0.0942	0.145	-
0.0705	2.86	68.8	0.56	0.771	0.1137	0.118	-
0.1600	1.32	51.5	0.60	1.626	0.0794	0.177	-
0.0310	1.32	46.0	0.61	0.308	0.0667	0.121	-
		Non-Wetting - 10.5" Packed Bed					
0.0310	1.32	39	0.63	0.300	0.0483	0.249	0.362
0.0500	1.32	39	0.63	0.486	0.0483	0.384	0.558
0.0705	1.32	39	0.63	0.687	0.0483	0.394	0.573
0.1150	1.32	39	0.63	1.115	0.0483	0.400	0.582
0.1600	1.32	43	0.62	1.580	0.0576	0.394	0.573
0.0705	0.455	32	0.64	0.672	0.0322	0.437	0.636
0.0705	0.860	35	0.64	0.679	0.0391	0.376	0.547
0.0705	2.06	47	0.61	0.707	0.0667	0.322	0.468
0.0705	2.86	53	0.59	0.725	0.0805	0.303	0.441
0.0705	1.22	39	0.63	0.687	0.0483	0.369	0.537
		Non-Wetting - 21" Packed Bed					
0.0500	1.32	78*	0.63	0.486	0.0483*	0.371	0.456
0.0705	1.32	78*	0.63	0.687	0.0483*	0.435	0.534
0.1150	1.32	78*	0.63	1.115	0.0483*	0.523	0.644
0.1600	1.32	86*	0.63	1.580	0.0483*	0.636	0.782
0.0310	1.32	78*	0.63	0.300	0.0483*	0.352	0.432

* Not measured directly but calculated from 10.5" data.

The mean apparent heights of gas film transfer units for 10.5" and 21" packed non-wetting beds and for a 10.5" packed wetting bed are plotted as a function of gas rate in Fig. 12.3.

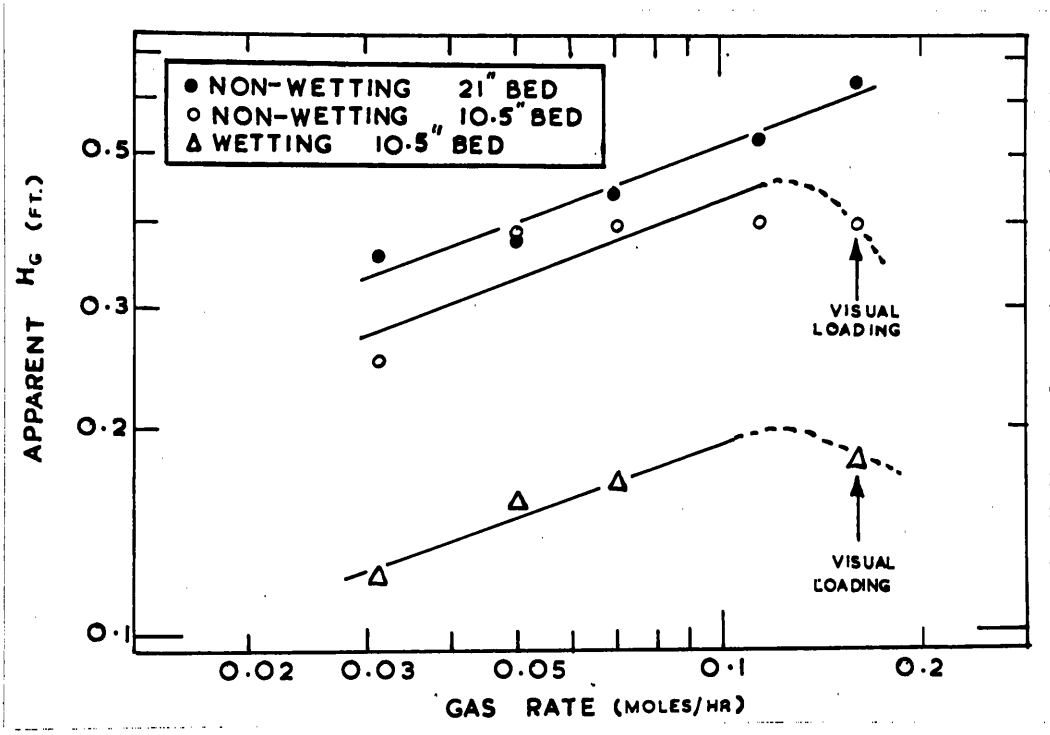

Fig. 12.3 - Apparent heights of gas film transfer units
Constant liquid rate = 1.32 moles./hr.

The non-wetting conditions give values of H_G significantly greater than those for wetting. This is to be expected, as the wetting interfacial area would be considerably greater than the non-wetting interfacial area. The effect of gas rate, however, is the same irrespective of the wetting conditions, as the data can be represented by parallel lines in Fig. 12.3. Thus the displacement of the two sets of data is apparently only due to interfacial area differences.

The results of this investigation in this respect are different to

those reported by Sherwood and Holloway (97) for gas phase mass transfer with wetting and non-wetting flow. These authors observed a different effect of gas rate on the two sets of data. No explanation of this was offered. Although both these authors' results and the results of this investigation showed that the liquid rate effects liquid phase data differently depending on the wetting conditions, as previously discussed, it is difficult to see why any effect of gas rate should be observed, which is different depending on the nature of flow, whether wetting or non-wetting.

The effect of loading on the gas film transfer unit heights observed in these experiments is the same as observed by previous investigators. Loading tends to reduce the H_G below that which would be obtained at a similar gas rate in the absence of loading.

The end effects associated with the measurements can be seen in Fig. 12.3 by comparing the non-wetting 21" and 10.5" packed bed data. These end effects can be compensated by allowing the same correction to be applied as was determined in the carbon dioxide absorption experiments. Thus if these end effects are taken as being equivalent to another 4.8" of packed height, the true values of the gas film transfer heights can be evaluated. Fig. 12.4 is a plot of the true values of H_G for both 10.5" and 21" beds for non-wetting conditions. Only the mean values of H_G for the various gas rates, at a constant liquid rate of 1.32 mole./hr., are plotted in Fig. 12.4. As can be seen in this diagram, all the non-wetting data are correlated by a single line, showing that the end effects correction is the same for either carbon dioxide absorption or ammonia absorption.

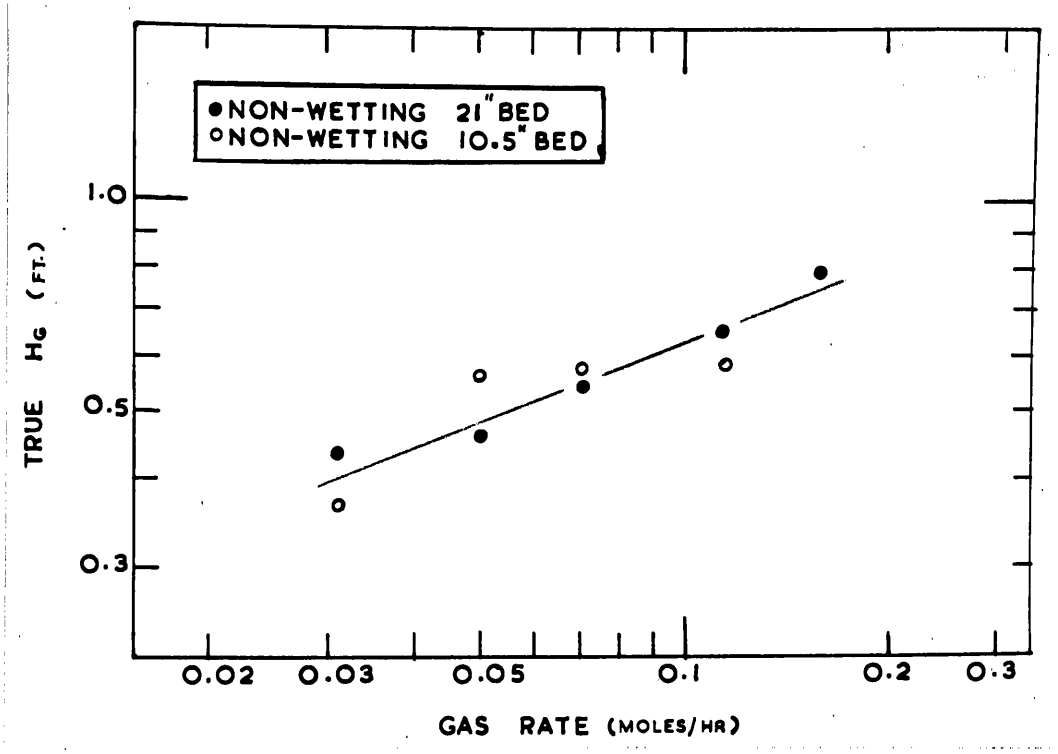

Fig. 12.4 - True heights of gas film transfer units (corrected for end effects)

Constant liquid rate = 1.32 mole./hr.

Figs. 12.3 and 12.4 were for constant liquid rate data. As discussed earlier in this chapter, the effects of liquid rate on the gas phase mass transfer process are considered to be best treated by the introduction of the new term, "the effective holdup ratio". The effective holdup ratio for ammonia absorption considered to be equal to the dynamic holdup ratio.

The exponent d on the effective holdup ratio of equations 12.6, 12.8 and 12.15 was found to be -0.42 by plotting values of H_G versus dynamic holdup ratio, for a constant gas rate, on a log.-log. graph, as shown in Fig. 12.5.

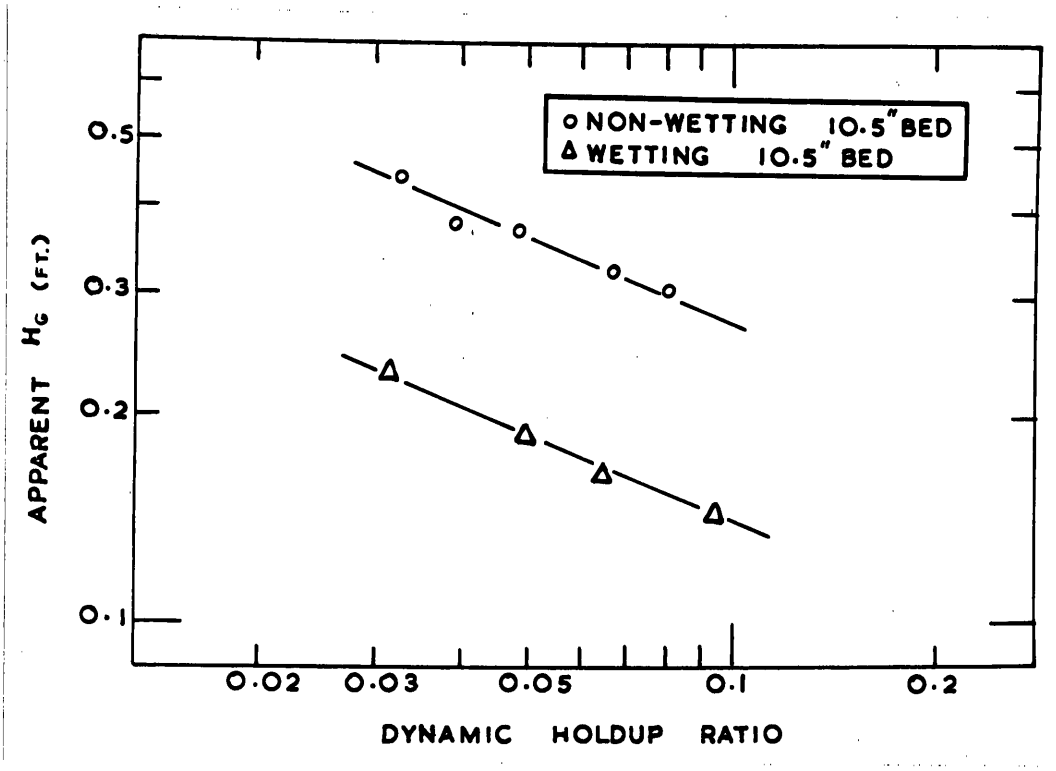

Fig. 12.5 - The effect of dynamic holdup ratio on H_G.
Constant gas rate = 0.0705 mole./hr.

The effective holdup ratio affects both the non-wetting and wetting data to the same extent, as can be seen by the parallel lines in Fig. 12.5 representing the two sets of data. An important factor about the effective holdup ratio is stressed in Fig. 12.5. This is, that the effective holdup ratio must not be considered as a substitute for the effective interfacial area in generalised correlations for all packings and types of flow. The application of the effective holdup ratio is for comparing systems, in which the type of flow, either wetting or non-wetting, and the packing are the same. Obviously, effective holdup ratio cannot be used to account

for differences in wetting and non-wetting data, as is clearly shown in Fig. 12.5 by the separate correlations obtained for each case.

12.4 Generalised Correlations

All the data required, for expressing either the carbon dioxide or ammonia absorptions in the various forms of correlation discussed at the beginning of this chapter, have been presented. However, rather than expressing the data in the various mathematical equations suggested, it was considered more desirable, for the purposes of this investigation, to extend the treatment no further at this stage, but to use the suggested correlating forms for directly comparing the results of the zinc absorption in molten lead with the data of this room temperature analogue, in the final assessment of the data, as presented in the next chapter.

12.5 Nomenclature

a = area of interphase contact, ft.^{2}/ft.^{3}

D = diffusion coefficient, ft.^{2}/hr.

G = superficial mass velocity of the gas phase, lb./(hr.)(ft.^{2})

G_m = superficial molar mass velocity of the gas phase, lb.mole./(hr.)(ft.)^2

H_D = dynamic holdup ratio

H_E = effective holdup ratio

h_S = static holdup, ml.

h_D = dynamic holdup, ml.

h_T = total holdup, ml.

H_G = height of a gas film transfer unit, ft.

H_{OG} = height of an overall gas phase transfer unit, ft.

H_L = height of a liquid film transfer unit, ft.

j_D = $\frac{k_g \; p_{BM}}{G_m} \left(\frac{\mu}{\rho D}\right)^{2/3}$

$(j_D)_R$ = $\frac{k_g \; p_{BM}}{V_R \; \rho_m} \left(\frac{\mu}{\rho D}\right)^{2/3}$

k_g = gas film mass transfer coefficient, lb.mole./(hr.)(ft.^{2})(atm.)

$k_g a$ = volumetric gas film mass transfer coefficient, lb.mole./(hr.)(ft.^{3})(atm.)

$k_L a$ = volumetric liquid film mass transfer coefficient, lb.mole./(hr)(ft.^{3})(unit ΔC)

L = superficial mass velocity of the liquid phase, lb./(hr.)(ft.^{2})

L_m = superficial molar mass velocity of the liquid phase, lb.mole./(hr.)(ft.^{2})

m = slope of equilibrium curve

N_G = number of gas film transfer units

N_{OG} = number of overall gas phase transfer units

N_L = number of liquid film transfer units

N_{OL} = number of overall liquid phase transfer units

P_{BM} = logarithmic mean of the partial pressure of the non-diffusing component at the phase boundary and in the bulk of the gas phase, atm.

P = total pressure on the system, atm.

Re = Reynolds number (dimensionless)

$(Re)_R$ = relative Reynolds number (dimensionless)

V, V_g = average true gas velocity, ft./hr.

V_R = relative velocity of the gas and liquid streams, ft./hr.

$\alpha, \beta, \beta', \beta'', \gamma$ = constants in the empirical equations.

ε = fractional voids or bed porosity

ρ = fluid density, lb./ft.^{3}

ρ_m = molar density, lb.mole./ft.^{3}

μ = fluid viscosity, lb./(ft.)(hr.)

CHAPTER 13

INTERPRETATION OF ZINC ABSORPTION DATA

Using as a basis the information derived from the two room temperature analogues, the zinc absorption data presented in Chapter 10 can be now analysed from the standpoint of the fundamental equation developed for the absorption of zinc vapour in molten lead.

i.e.

$$H_{OG} = H_G + \frac{G_m}{L_m} \frac{H_L}{N_{OG}} \int_{y_2}^{y_1} \frac{p^o_{Zn} \gamma_{Zn}}{P_T (y - y_e)} \cdot dy \qquad \ldots\ldots 13.1$$

As the value of H_{OG} is proportional to the overall resistance to mass transfer, equation 13.1 can be considered as a statement of the addition of diffusional resistances of the individual phases. The first term in the R.H.S. of equation 13.1 is a measure of the resistance to mass transfer in the gas phase and the second term accounts for resistance in the liquid lead phase.

13.1 Diffusion Resistance in Liquid Lead Phase

13.1.1 Evaluation of $\int_{y_2}^{y_1} \frac{p^o_{Zn} \gamma_{Zn}}{P_T (y - y_e)} \cdot dy$

The evaluation of the integral requires basically the same approach as used to determine the number of overall gas phase transfer units, as outlined in 10.4.1,

i.e., the following information is required for various levels within the absorption column:-

(a) The gas phase zinc concentration

(b) The lead phase zinc concentration

(c) The lead phase temperature

(d) The equilibrium zinc partial pressure above the alloys formed by absorption.

As this information could not be determined directly, the asumptions discussed fully in 10.4.1 have to be made.

i.e. (1) An exponential decrease of the zinc phase composition from the bottom to the top of the column.

(2) A linear relationship between lead temperature and position in the column.

The application of these assumptions, for obtaining the desired information for the various levels within the column, has been outlined in the sample calculations presented in 10.4.1 for Run 2D.

To illustrate the general approach used, Run 2D has been retained as typical of the calculations and therefore, the calculations presented in this chapter and those given earlier, are representative of the calculations involved for any run on the system. The relevant experimental data and the results of calculations already made on Run 2D are given in Table 13.1.

TABLE 13.1

EXPERIMENTAL AND CALCULATED DATA FOR RUN 2D

Zn mole fraction inlet gas (y_1)	= 0.00745
Zn mole fraction outlet gas (y_2)	= 0.000650
Zn mole fraction inlet lead (x_2)	= 0.000058
Zn mole fraction outlet lead (x_1)	= 0.000439
Lead inlet temperature	= 610°C
Lead outlet temperature	= 760°C
Mean lead temperature	= 685°C
Column pressure	= 910 mm. Hg.
N_{OG}	= 2.58
H_{OG}	= 0.68 ft.
Lead flow rate	= 2.62 moles./hr.
Gas flow rate	= 0.147 moles./hr.

The data previously calculated for Run 2D and presented earlier in Table 10.7 can now be used for the evaluation of $\int_{y_2}^{y_1} \frac{p^{o}_{Zn} \gamma_{Zn}}{P_T(y - y_e)} \cdot dy$

Table 13.2 includes the previously calculated data of Table 10.7 together with the new calculated data required in the evaluation of the integral.

TABLE 13.2

RUN 2D

Position in Column	Top	A	B	C	D	Bottom
Lead Temp. °C (t)	610	632	702	734	756	760
p^{o}_{Zn} mm. Hg.	13.8	20.6	63.3	100	138	146
γ_{Zn}	9.6	8.8	6.9	6.5	6.0	5.9
P_T mm. Hg.	910	910	910	910	910	910
$\frac{p^{o}_{Zn}\ \gamma_{Zn}}{P_T} = m$	0.145	0.200	0.480	0.716	0.912	0.945
x	0.000058	0.000080	0.000190	0.000300	0.000420	0.000439
y_e	0.000008	0.000016	0.000091	0.000215	0.000294	0.000328
y	0.000650	0.00100	0.00300	0.00500	0.00700	0.00745
$\frac{p^{o}_{Zn}\ \gamma_{Zn}}{P_T(y - y_e)}$	214	192	168	154	147	158

The plot of $\frac{p^{o}_{Zn}\ \gamma_{Zn}}{P_T(y - y_e)}$ versus y required for the graphical integration is shown in Fig. 13.1

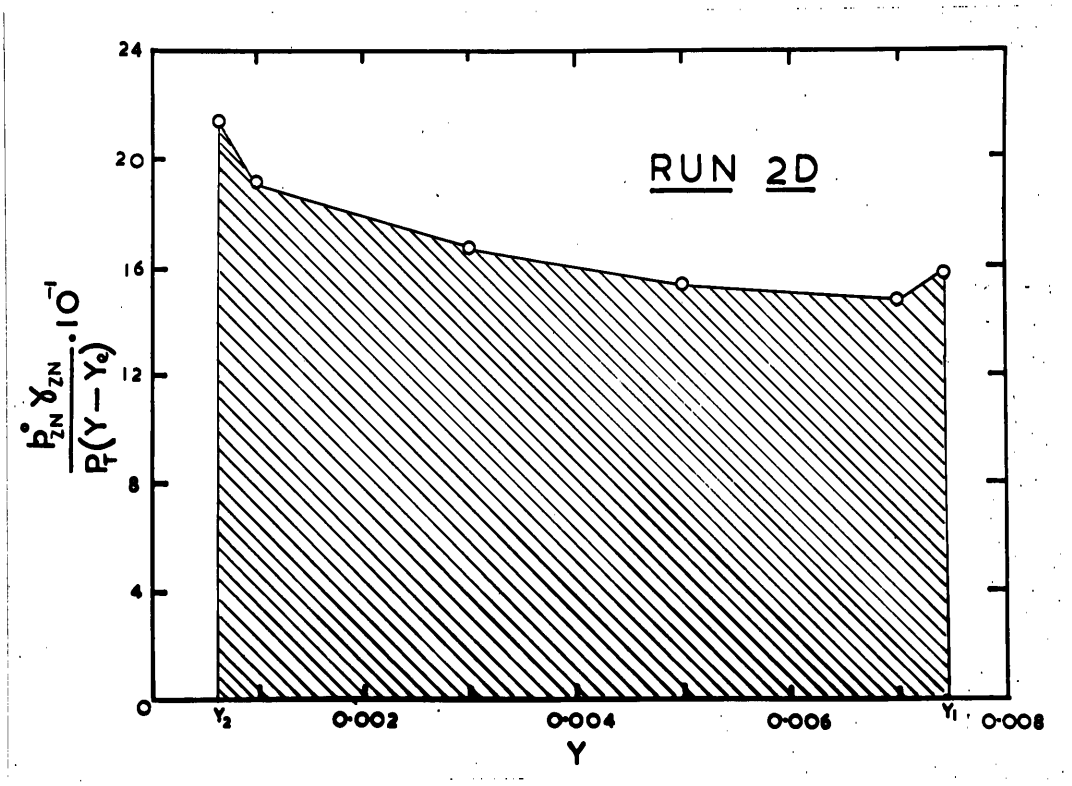

Fig. 13.1

From Fig. 13.1,

$$\int_{y_2}^{y_1} \frac{p^{o}_{Zn}\ \gamma_{Zn}}{P_T(y - y_e)} \cdot dy = 1.104$$

13.1.2 Evaluation of H_L for Zinc Absorption in Lead

H_L for zinc absorption in lead can be evaluated from the data for carbon dioxide absorption in water obtained using the room temperature analogue, by application of equation 12.2 discussed previously in 12.1.1.

i.e. $$H_L = \frac{1}{\alpha}\left(\frac{L}{\mu}\right)^n \left(\frac{\mu}{\rho D}\right)^{0.5} \quad \ldots\ldots 13.2$$

$\therefore$ At constant $\frac{L}{\mu}$,

$$\frac{(H_L)_{CO_2 - H_2O}}{(H_L)_{Zn - Pb}} = \left[\frac{\left(\frac{\mu}{\rho D}\right)_{CO_2 - H_2O}}{\left(\frac{\mu}{\rho D}\right)_{Zn - Pb}}\right]^{0.5} \quad \ldots\ldots 13.3$$

$\therefore$ For Run 2D

(a) Lead Rate = 2.62 moles./hr.
Cross Section Area of Zn Absorption Column = 0.01654 ft.^{2}

$\therefore$ $L = \frac{2.62 \times 207}{0.01654}$ lb./(hr.)(ft.^{2})

μ of Pb at 685°C = 1.37 Centipoise (interpolated from (83))

$\therefore$ $$\frac{L}{\mu} = \frac{2.62 \times 207}{0.01654 \times 1.37 \times 2.42}$$

$$= 9{,}900 \text{ ft.}^{-1}$$

(b) For $\frac{L}{\mu}$ = 9,900 ft.$^{-1}$

Water Rate in CO_2 Absorption Column = $\frac{9{,}900 \times 1 \times 2.42 \times 0.0177}{18}$

= 23.6 moles./hr.

At this water rate (H_L) apparent for CO_2 absorption in a 21" packed bed can be obtained by extrapolation of the data given in Fig. 12.1, which gives,

$(H_L)_{CO_2 - H_2O}$ = 3.3 ft.

(c) $D_{Zn - Pb}$ at 685 °C can be estimated by the procedure given in 2.1 or can be interpolated from the values of Table 2.4 by plotting log. D versus $\frac{1}{T}$.

At 685°C, $D_{Zn - Pb}$ = 6.8×10^{-5} cm.^{2}/sec.

μ of Pb at 685°C = 1.37 centipoise (interpolated from (65))

ρ of Pb at 685 C = 10.17 g./cm.^{3} (interpolated from (65))

$\therefore$ At 685°C $\left(\frac{\mu}{\rho D}\right)_{Zn - Pb} = \frac{1.37 \times 10^{-2}}{10.17 \times 6.8 \times 10^{-5}}$

$= 19.8$

At 25°C $\left(\frac{\mu}{\rho D}\right)_{CO_2 - H_2O}$ = 570 (Diffusion data from Perry (83))

(d) Hence for $\frac{L}{\mu}$ = 9,900 ft.$^{-1}$

From equation 13.3,

$$\frac{3.3}{(H_L)_{Zn - Pb}} = \left(\frac{570}{19.8}\right)^{0.5}$$

$\therefore$ $(H_L)_{Zn - Pb}$ = 0.115 ft.

13.1.3 Fraction of Total Diffusion Resistance in Liquid Lead Phase

The fraction of the overall resistance to mass transfer due to the resistance in the liquid lead phase can be calculated by rearranging equation 13.1.

$$\text{Fractional Resistance in Liquid Lead Phase} = \frac{\frac{G_m}{L_m}\frac{H_L}{N_{OG}} \int_{y_2}^{y_2} \frac{p^o_{Zn}\ \gamma_{Zn}}{P_T(y - ye)} \cdot dy}{H_{OG}} \quad \ldots\ldots 13.4$$

For Run 2D,

$$\text{Fraction Resistance in Liquid Lead Phase} = \frac{\frac{0.147}{2.62} \times \frac{0.115}{2.58} \times 1.104}{0.68}$$

$= 0.0041$

Hence, for Run 2D, only 0.4% of the total resistance to mass transfer is located in the liquid lead phase. Similar calculations on the other runs, indicated that the liquid lead phase resistances were negligible, under the conditions of the zinc absorptions carried out in this investigation.

It is important to note that the experimental conditions determine

the contribution, which the liquid lead phase makes to the overall mass transfer resistance. Thus for example, if the experiments were carried out at very high gas rates, very low liquid lead rates and much higher temperatures, inspection of the equation 13.4 indicates that the fractional resistance of the lead phase could then become appreciable.

13.2 Diffusional Resistance in the Gas Phase

For the experimental conditions of this investigation, the absorption of zinc vapour in molten lead is clearly controlled by the diffusional resistance of the gas phase, and any resistance in the liquid lead phase can be neglected.

Under these conditions equation 13.1 reduces to

$$H_{OG} = H_G \qquad \ldots\ldots 13.5$$

If the conventional gas absorption theories are applicable to the absorption of a metallic vapour in a liquid metal at an elevated temperature, the values of the heights of overall gas phase transfer units obtained for the absorption of zinc vapour in molten lead, tabulated in Table 10.9, should be directly comparable to the values of the heights of gas film transfer units for ammonia absorption in water, using one of the forms of correlation of gas phase data presented in 12.1.2.

The H_{OG} data of Table 10.9 are uncorrected for end effects as only one packed height was used in the zinc absorption experiments and hence they must be considered as apparent values of H_{OG} or H_G. It seems reasonable to assume that the end effects associated with the zinc absorptions are approximately equal to those measured in the room temperature analogue. Therefore, these values were converted to true heights of transfer units by assuming the end effects were equivalent to another 4.8" of packed height, before the comparison with the ammonia absorption data was made.

The forms of correlation suggested in 12.1.2 for comparing gas phase data, require information regarding the total and dynamic holdup of molten lead in the packing under the conditions of the experiments. Estimates of the liquid velocities in both the zinc absorption and ammonia absorption experiments are also required, if equation 12.15, in which the relative velocity is taken as the significant velocity term, is to be used for correlating the data.

13.3 Estimation of Molten Lead Holdup

The empirical correlation developed for the mercury model in which $\frac{\Delta P}{\gamma(h_T)}$ was plotted as a function of $V_g^2\rho$ as shown in Fig. 11.6 was considered to be the most suitable method of estimating the holdup of molten lead on the packing during the zinc absorption experiments. The significant features and the justification for using the correlation, based on mercury irrigation, for determining holdups for other liquid phase irrigations were fully discussed in 11.4.4.

To ensure that the zinc absorption column and the mercury model column were consistent with each other, pressure drop readings were taken across the zinc absorption column with room temperature air as the gas phase, before the column was irrigated with lead.

Further room temperature studies on the zinc absorption column were made after the column had been irrigated with molten lead. These latter studies served the dual purpose of testing the consistency of the zinc absorption column with the mercury model column, as well as providing a check on the application of the correlation, as the pressure drop was also recorded when the column was operating with hot nitrogen flow, but with the same holdup present as in the room temperature measurements. A single assumed value of the total holdup of lead on the packing allowed the data

to be compared with the mercury model correlation.

The experimental and calculated data for the two experiments just described are given in Tables 13.3 and 13.4.

TABLE 13.3

PRESSURE DROP ACROSS ZINC ABSORPTION COLUMN

AIR AT ROOM TEMPERATURE

Bed Porosity = 0.72

Gas Flow Rate x 10^4 lb./sec.	Pressure at Base of Column p.s.i.g.	Gas Density lb./ft.^{3}	True Gas Velocity ft./sec. V_g	$V_g^2\rho$	Pressure Drop Across Column ΔP cm. H_2O
6.00	0	0.075	0.67	0.0337	0.51
8.26	0	0.075	0.92	0.0637	0.91
11.05	0	0.075	1.24	0.115	1.52
14.15	0.5	0.077	1.54	0.183	2.13
17.80	0.75	0.079	1.90	0.284	3.04

TABLE 13.4

PRESSURE DROP ACROSS ZINC ABSORPTION COLUMN

PREVIOUSLY LEAD IRRIGATED

NITROGEN AT ROOM TEMPERATURE

Gas Flow Rate x 10^4 lb./sec.	Pressure at Base of Column p.s.i.g.	Gas Density lb./ft.^{3}	Pressure Drop Across Column ΔP cm. H_2O	h_T Assumed 145 ml.	
				$V_g^2\rho$	$\frac{\Delta P}{\gamma(h_T)}$
4.53	760	0.0722	0.95	0.0345	0.552
5.52	760	0.0722	1.25	0.0510	0.725
6.62	760	0.0722	1.50	0.0735	0.872
8.80	796	0.0756	2.30	0.124	1.34
11.65	827	0.0785	3.90	0.210	2.26
13.36	843	0.0800	4.90	0.270	2.85
15.66	863	0.0820	6.30	0.362	3.66
18.73	894	0.0848	8.50	0.502	4.93
23.30	942	0.0893	11.20	0.736	6.50
26.70	993	0.0943	14.10	0.913	8.18
32.80	1045	0.0992	19.80	1.310	11.50

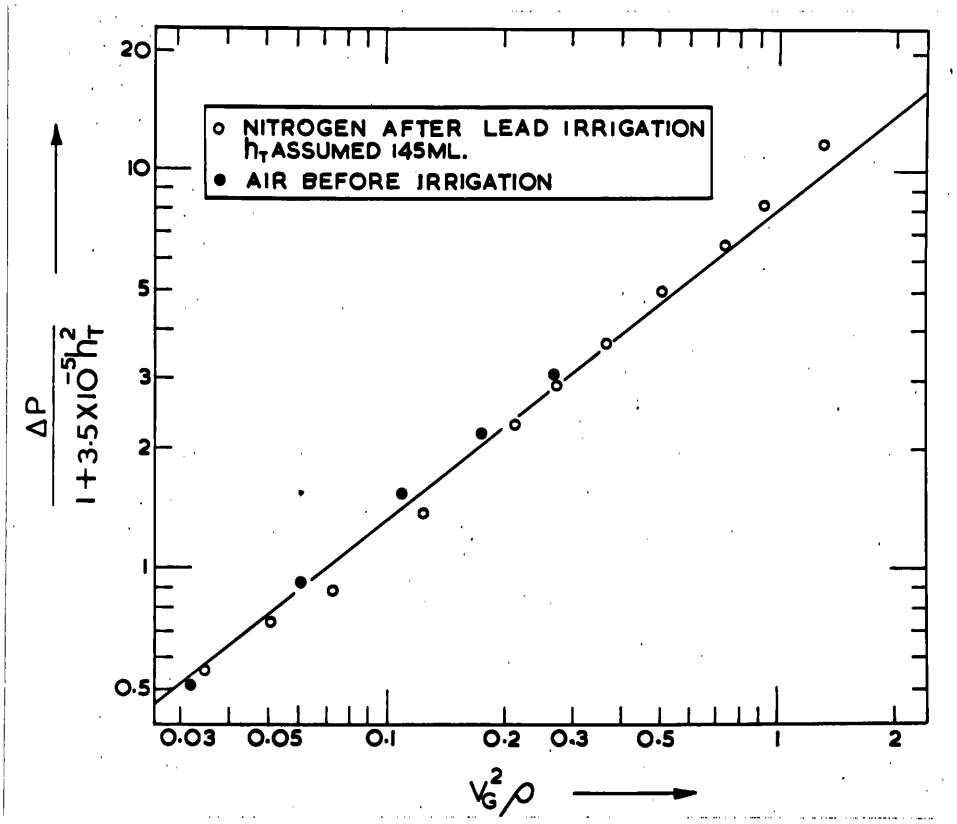

Fig. 13.2 - Empirical correlation of holdup and pressure drop

The data of Tables 13.3 and 13.4 are plotted as $\Delta P/(1 + 3.5 \times 10^{-5} h_T^2)$ versus $V_g^2\rho$ in Fig. 13.2, in which the full line represents the mercury model data of Fig. 11.6. The data are well represented by the full line and hence consistency between the two packed beds is established. The holdup of 145 ml. assumed for the previously lead irrigated data was determined by trial and error to make the observed pressure drop data fit the correlation. If for some reason, the mercury model and the zinc absorption columns were not self-consistent, a single assumed value of holdup would not have resulted in correlation of the previously lead

irrigated data with the mercury data.

The assumed static holdup of 145 ml. of cold lead is equivalent to a holdup of 160 ml. of liquid lead at 600°C, when allowance for volume change on fusion and expansion is made. Measurements of pressure drop made on the column, when hot nitrogen, at a mean temperature of 600°C, was passed through the same previously irrigated bed, required an assumed holdup of 180 ml. to enable the data to be correlated with the full line of Fig. 13.2. Thus the agreement, between the holdup of 180 ml. for the determinations made when hot and the equivalent holdup (corrected for volume changes) of 160 ml. derived from the room temperature measurements, indicates that the estimation of molten lead holdup from the observed pressure drop in the gas phase, by the empirical correlation developed, is quite reliable.

As only the total holdup of lead could be estimated using the suggested procedure, the dynamic liquid lead holdup could only be determined as the difference of the estimated total holdup under the particular operating conditions and the estimated total holdup in the absence of irrigation.

Although it was previously shown in 11.4.1 that the static holdup of mercury in the packing was dependent on the irrigation rate, the effect was so small that, for the purpose of analysing the zinc absorption data, the static holdup was considered as being unaffected by liquid rate.

The static holdup of liquid lead in the packing was obtained by observing the pressure drop across the column, the gas mass flow rate and the mean gas temperature and pressure inside the bed, immediately after the completion of an experimental run with the lead pump shut off. The estimation of the total holdup was a trial and error procedure of selecting values of h_T so that the observed experimental data cross

plotted the developed empirical correlation of Fig. 13.2. The values of h_T thus obtained and the relevant experimental and calculated data required for the estimation are shown in Table 13.5.

TABLE 13.5

ESTIMATION OF THE STATIC LIQUID LEAD HOLDUP

Description of Test	Gas Rate x 10^4 lb./sec.	Pressure Drop Across Column ΔP cm.H_2O	Mean Gas Temp. °C	Column Pressure mm. Hg	Gas Density lb./ft.^{3}	Estimated	
						$V_s^2\rho$	$h_T=h_S$
Immediately after Run 2A Previous Lead Rate = 1.73 mole./hr.	7.17	5.6	608	800	0.0254	0.277	155
Immediately after Run 4A Previous Lead Rate = 2.92 mole./hr.	9.76	8.9	575	836	0.0276	0.471	170
Immediately after Run 5A Previous Lead Rate = 5.65 mole./hr.	9.76	9.4	580	841	0.0276	0.480	175
Immediately after Run 6A Previous Lead Rate = 2.03 mole./hr.	9.76	10.9	590	836	0.0271	0.527	190
Same as above	11.0	12.2	633	837	0.0258	0.676	180
Immediately after Run 6B Previous Lead Rate = 2.31 mole./hr.	4.82	3.7	588	780	0.0254	0.134	185
Same as above	3.87	2.8	588	765	0.0249	0.0930	195

Examination of the values of $h_T = h_S$ in Table 13.5, reveals that prior to Run 5A, the holdup of liquid lead was below "saturation level" and it was only after the high liquid lead rate of Run 5A, that the static holdup sites in the packing were completely occupied by semistagnant liquid lead. After

Run 4A the estimated static holdups remain fairly constant, so that for these runs an average static holdup of 180 ml. of liquid lead was used in all subsequent calculations.

The total holdup of liquid lead under the operating conditions for each zinc absorption run of Table 10.3 were calculated in the same manner from the observed pressure drop across the column, the gas mass flow rate and the mean gas temperature and pressure in the bed. The relevant experimental and calculated data required for the estimation are shown in Table 13.6.

The dynamic holdup of liquid lead in the packing for the zinc absorption runs was obtained by difference of the total holdup data given in Tables 13.5 and 13.6.

13.4 Estimation of Average Liquid Velocities

If the form of correlation suggested by equation 12.15, in which the relative velocity of the gas and liquid phases is the significant velocity term, is to be used for comparison of the zinc and ammonia absorption data, the average liquid phase velocity must be evaluated for water and molten lead flowing over the packing.

The average linear velocity of water and mercury flowing under non-wetting conditions in the packing was experimentally determined by recording the time taken for the liquid phase to flow over a measured height of previously "saturated" packing.

The packing was "saturated" by flooding and then allowing it to drain. The liquid was introduced at the top of packing and the time between the liquid hitting the top of the packing and the appearance of flow from the bottom of the packing was measured with a stop-watch for different liquid rates in the absence of gas flow.

TABLE 13.6

ESTIMATION OF TOTAL LIQUID LEAD HOLDUP

FOR ZINC ABSORPTION RUNS

Run	Gas Rate mole./hr.	Lead Rate mole./hr.	Pressure Drop Across Column ΔP cm.H_2O	Mean Gas Temp. °C	Column Pressure mm.Hg.	Gas Density lb./ft.^{3}	Estimated	
							$V^2\rho$	h_T
1A	0.158	3.04	15.4	605	841	0.0268	0.827	185
2A	0.089	1.73	6.9	608	800	0.0254	0.304	190
3A	0.138	1.86	14.0	625	836	0.0261	0.712	190
4A	0.132	2.92	16.0	590	836	0.0272	0.716	215
5A	0.132	5.65	27.7	563	841	0.0282	0.938	270
6A	0.138	2.03	14.5	583	836	0.0274	0.715	200
1B	0.268	1.75	50.1	640	887	0.0272	2.94	215
2B	0.253	2.29	48.3	610	892	0.0282	2.67	225
3B	0.204	1.91	31.0	623	876	0.0274	1.69	215
5B	0.0219	1.46	1.9	605	826	0.0265	0.0295	280
6B	0.0438	2.31	4.2	588	841	0.0274	0.0973	255
1C	0.147	2.30	20.7	725	863	0.0243	0.995	215
2C	0.145	4.26	36.2	675	873	0.0258	1.287	275
3C	0.148	0.83	17.2	703	863	0.0248	0.890	195
5C	0.0577	2.45	7.2	690	842	0.0245	0.195	260
6C	0.0598	3.90	*-	693	842	0.0245	-	-
2D	0.147	2.62	20.8	695	910	0.0263	0.965	225
3D	0.140	4.92	50.0	650	930	0.0282	1.428	315
5D	0.0496	4.42	6.6	655	868	0.0262	0.151	280
6D	0.0450	1.77	4.4	663	878	0.0263	0.104	250

* Pressure drop not measured.

The average linear liquid velocities thus determined can be considered only approximates of the actual velocities during the absorption tests, as any traction effects because of the countercurrent gas flow were neglected. However, it is considered that the velocities measured are suitable for assessing the value of the relative velocity type of correlation as proposed by equation 12.15.

The ammonia absorption data are greatly affected by the introduction of the relative velocity, because of the low gas velocities in these studies. However, the zinc absorption data are affected only slightly, because of the high gas velocities associated with the data. Therefore, it is considered that the lead velocities can be adequately estimated, for the purpose of this investigation, by assuming the lead velocity to be equal to the mercury velocity at the same volumetric flow rate.

Interpolation or extrapolation of the velocity data, shown in Tables 13.7 and 13.8, on a log.-log. plot, allowed the average linear liquid velocities to be estimated for the ammonia absorption data of Table 12.11 and the zinc absorption data of Table 10.3.

TABLE 13.7

AVERAGE LINEAR WATER VELOCITY

Water Flow Rate ml./min.	Water Flow Rate mole./hr.	Average Linear Velocity ft./sec.
160	1.18	0.32
490	3.60	0.35
80	0.59	0.22
70	0.52	0.19
13	0.095	0.16

TABLE 13.8

AVERAGE LINEAR MERCURY VELOCITY

Mercury Flow Rate ml./min.	Equivalent Volumetric Lead Flow Rate at 550°C mole./hr.	Average Linear Velocity ft./sec.
24	0.158	0.35
106	0.658	0.37
160	1.05	0.44
14	0.092	0.26

13.5 Comparison of Zinc and Ammonia Absorption Data

To preserve the continuity of the following discussions, the calculated data required in the various correlations are presented in Tables 13.9 and 13.10 appended to this chapter.

As a preliminary analysis of the zinc absorption runs revealed anomalous behaviour in the very low inlet zinc partial pressure data, runs, in which the inlet zinc partial is less than 1 mm. Hg, are excluded from the correlations used to compare the zinc and ammonia absorption results. The reasons for their exclusion are discussed after the comparison of the two absorptions.

The exponent on the effective holdup ratio was previously determined as -0.42 as indicated in 12.3. Because there is little doubt that the dynamic holdup is the effective holdup in ammonia absorption, it was at first considered, that the dynamic holdup would be the only effective component of the total liquid lead holdup. Therefore, as a logical commencement to the comparison of the two absorption processes, the conventional form of correlation as represented by equation 12.6 was applied

with the dynamic holdup ratio being taken as the effective holdup ratio in both cases. Fig. 13.3 shows the data plotted in such form.

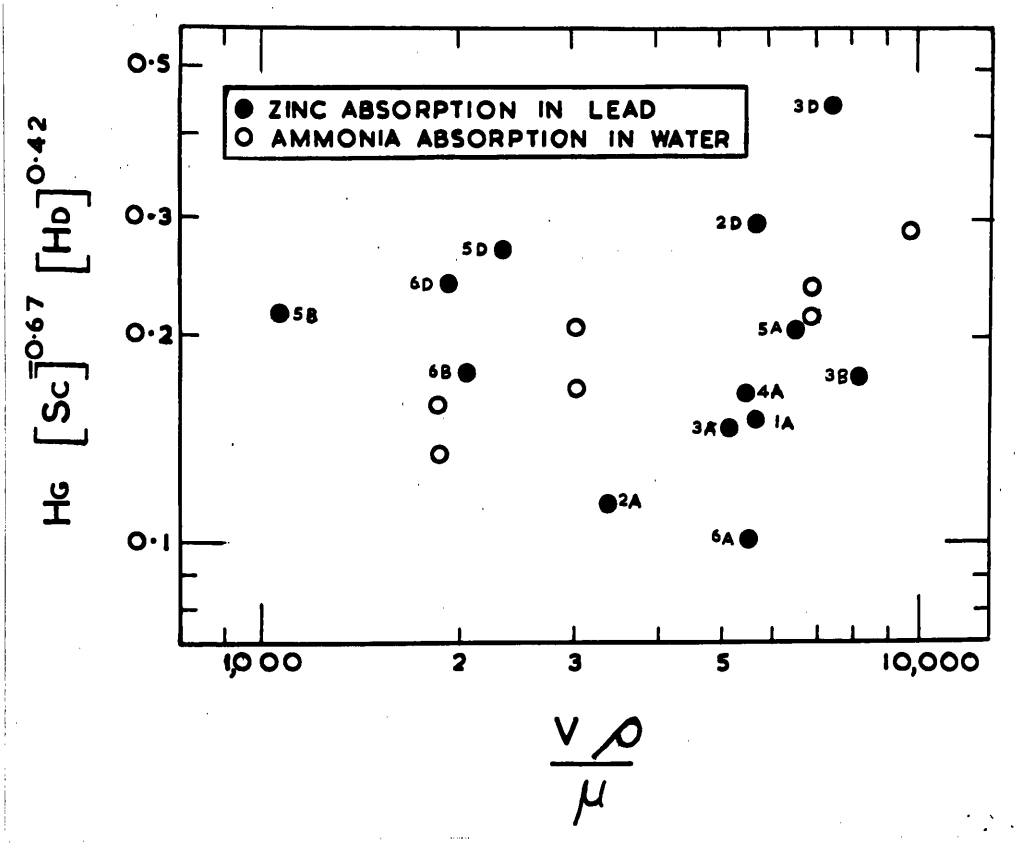

Fig. 13.3 - Correlation of zinc and ammonia absorption data

Inspection of Fig. 13.3 shows that all the zinc absorption runs up to and including Run 3B fall significantly below the ammonia data whilst the points for runs after Run 3B are displaced above.

The significance of this was not at first realised. It was only after a search of the experimental records, that the cause of the displacement of the data was believed to have been identified.

At the conclusion of Run 3B, the stainless steel inlet analysis sampling line broke due to a combination of gross overheating and zinc attack. This

mishap occurred whilst the apparatus was unattended, and therefore, for a period of about fifteen minutes, the gas circulation system was in operation with insufficient supply of nitrogen from the gasholder to compensate for the leakage through the cracked inlet analysis sampling line.

The consequence of this was that the static holdup of liquid lead in the column at the conclusion of Run 3B was exposed to oxidising conditions for about fifteen minutes and became drossed up. It is not envisaged, however, that the liquid lead was completely converted to dross but merely drossed on the surface. Had the static holdup been completely drossed, the volume of holdup would have changed considerably, but inspection of Table 13.5 shows that the static holdup volume was not significantly different after Run 3B than it was in the earlier runs once the packing had all its static holdup sites occupied (i.e. after Run 4A).

As indicated in the discussions of effective interfacial area in a packed tower (11.1.4), the significant feature, which determines the effectiveness of the semistagnant static holdup in an absorption process, is the rate of movement of this component through the packing. For water irrigation of the packing, the rate of movement is very slow and hence equilibrium in the static holdup is reached and it is then no longer effective for absorption. However, if the semistagnant static holdup moves through the packing at a rate only slightly less than the recognised flowing component (i.e. dynamic holdup), then the static holdup could be equally as effective as the dynamic holdup.

It was suggested in 11.1.4 that the rate of movement of a liquid metal or similar dense medium static holdup in a packed column would be considerably greater than that which has been observed for water. The very much higher kinetic energy of the flowing component, whether lead

mercury, or similar dense media, could have the effect of "knocking-on" or displacing the semistagnant liquid through the sites of static holdup, thereby increasing the overall rate of movement of the so-called static holdup under irrigated conditions.

Evidence of this increased mobility was given in 11.4.1, when the observed effect of liquid rate on static holdup of mercury was discussed, whereas the static holdup is unaffected by liquid rate when water is the irrigating liquid phase.

It is therefore tentatively proposed, pending further experimentation, that the concept of effective interfacial area for liquid metals irrigating a packing be modified to take into account the increased mobility of the semistagnant liquid and the so-called static holdup be considered effective in an absorption process involving the flow of a liquid metal or similar medium. It is likewise considered that the non-wetting flow of the liquid metal also facilitates an increased mobility of the semistagnant liquid holdup.

If, however, the free flow of the static holdup was impaired by dross formation or similar effects, the mobility would be seriously affected and the movement would most likely be completely arrested or slowed down to such an extent, that equilibrium would be reached and the surface rendered ineffective for further absorption.

In view of the preceding discussion, it was therefore assumed that the total holdup of liquid lead up to and including Run 3B was effective for absorption. After Run 3B, because of the dross formation on the static holdup, only the dynamic holdup was considered to be effective for absorption, as the movement of the static holdup would have been arrested by dross formation.

A qualitative test was run to check the validity of the assumption that dross formation prevented free movement of the lead retained by the rings. A quantity of steel rings were irrigated with molten lead and then partially oxidised. The rings were then quickly shaken before the lead froze. An examination of the rings, after such treatment, indicated that the drossed lead droplets were retained by the packing. A similar test carried out on clean mercury irrigated packing showed that the mercury could be readily shaken from the packing.

The correlation of the data obtained after making the appropriate amendment to the effective holdup ratio, but using the same form of correlation given earlier in Fig. 13.3 is shown in Fig. 13.4.

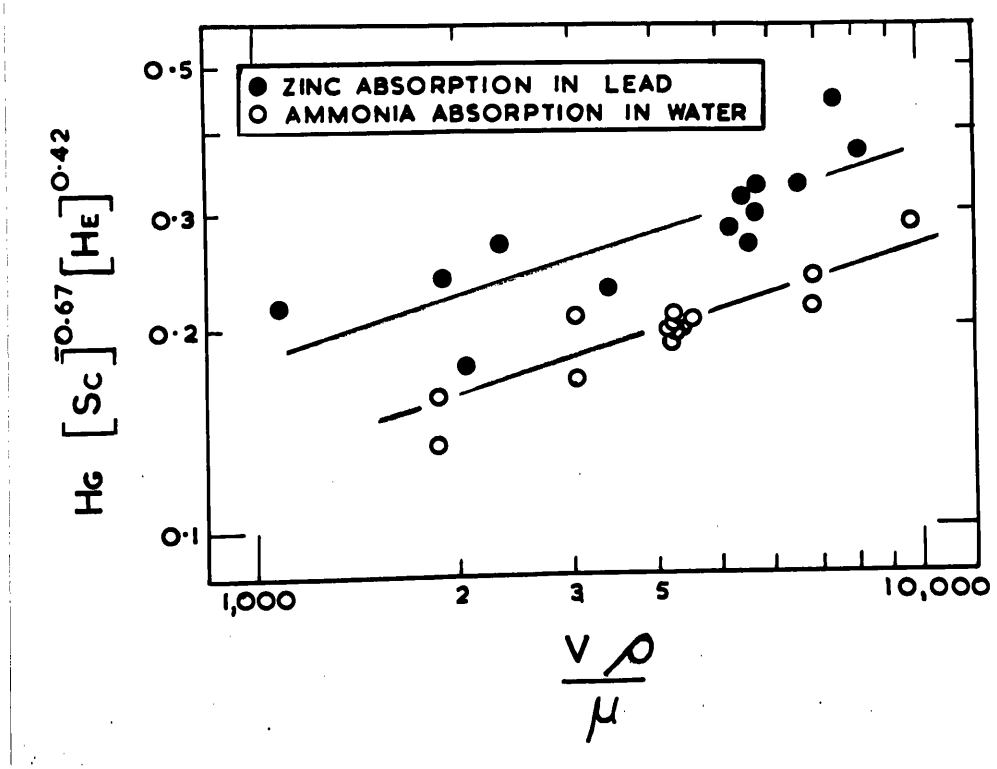

Fig. 13.4 - Correlation of zinc and ammonia absorption data

The displacement of the zinc absorption data above the ammonia data in Fig. 13.4 could possibly be due to a deficiency in the estimated values of Schmidt number or effective holdup ratio, but it also suggests that the Reynolds number, based on the gas velocity, is not a good correlating modulus, as the ammonia data of these studies are particularly sensitive to a relative velocity correction.

As a check to see if the gas inertia is the better correlating modulus, as suggested by equation 12.8, the data were replotted in Fig. 13.5 using the same ordinate as in Fig. 13.4 but with $(V_g^2\rho)^{0.5}$ as the abscissa. The square root of the gas inertia was used in this plot so as to retain the same gas velocity dependency as in the previous graph.

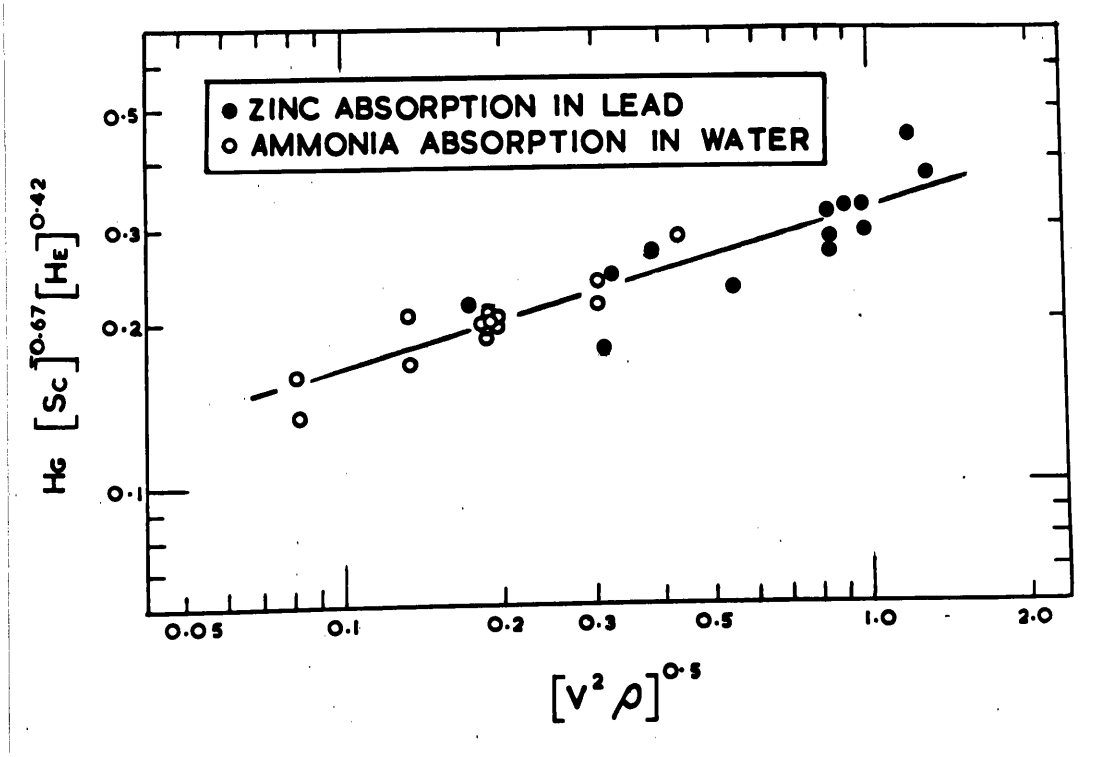

Fig. 13.5 - Correlation of zinc and ammonia absorption data

The vertical displacement of the two sets of data has been overcome using this method of correlation, as the data in Fig. 13.5 can be well represented by a single straight line.

As the newly defined "relative j_D" factor, developed from the earlier gas phase mass transfer studies with the disc column, is believed to have general application to all mass transfer studies, the new type of correlation proposed by equation 12.15, in which the relative interfacial velocity is considered the significant velocity term in the transfer process, was applied to the zinc and ammonia absorption data. The relative interfacial velocity used in the correlation of the data shown in Fig. 13.6 was taken as the sum of the gas and liquid phase average linear velocities.

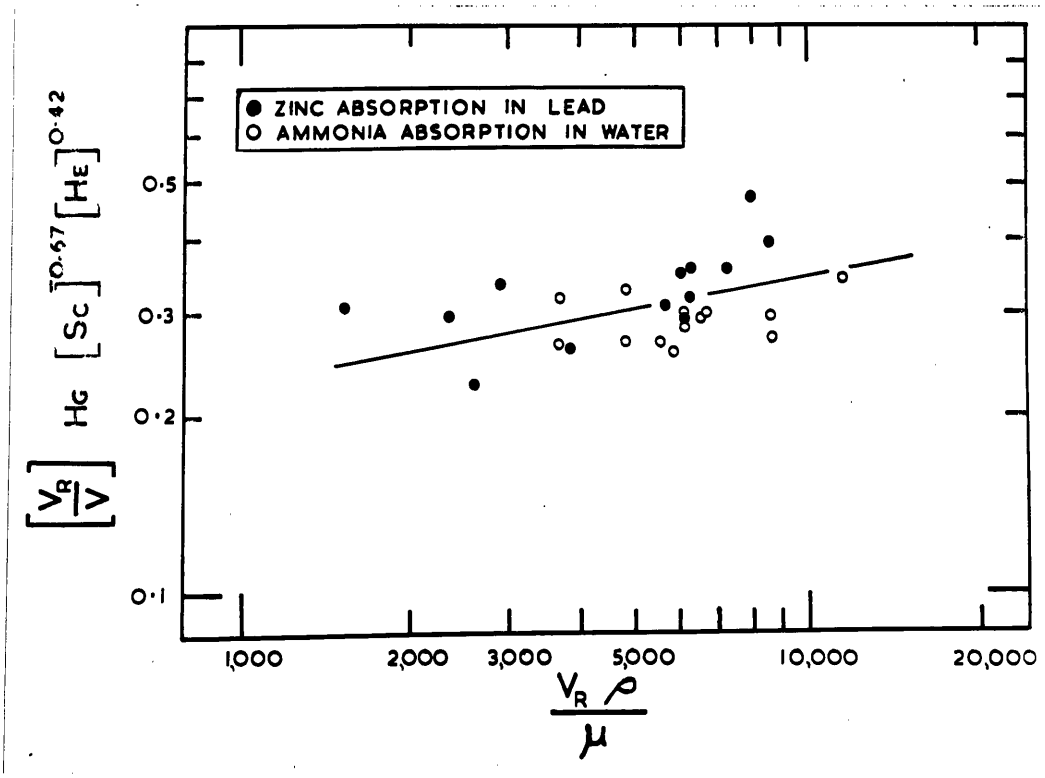

Fig. 13.6 - Correlation of zinc and ammonia absorption data

Although the experimental points in Fig. 13.6 exhibit a fair amount of scatter, the data can be represented by the single full line drawn on the graph. This is in marked contrast to the obvious displacement of the two sets of data obtained for the conventional type of correlation using the gas velocity as the significant velocity term, as can be seen by comparing Fig. 13.4 with Fig. 13.6.

The zinc absorption point showing the greatest deviation from the full line, also displayed maximum departure when the other forms of correlation were used, so that it would appear that this point is of doubtful accuracy and cannot be justly used as a criticism of a particular correlation form. Except for this one point, the observed scatter is considered to be within the range of experimental errors associated with the experimentally rather difficult conditions of this investigation.

As indicated previously, the zinc absorption runs, in which the inlet zinc partial pressure was less than 1 mm. Hg, were excluded from the preceding analysis. The anomalous behaviour of these very low zinc inlet partial pressure runs can be seen by selecting the correlation form, observed as fitting the other data with the least scatter, and replotting the data in such a form as to show the effect of inlet solute partial pressure.

Thus Fig. 13.7 is a plot of $H_G(Sc)^{-0.67}\ (H_E)^{0.42}\ (V_g^2\rho)^{-0.15}$ versus inlet solute partial pressure. Theory predicts that there would be no variation of the group plotted with the inlet partial pressure of the diffusing species.

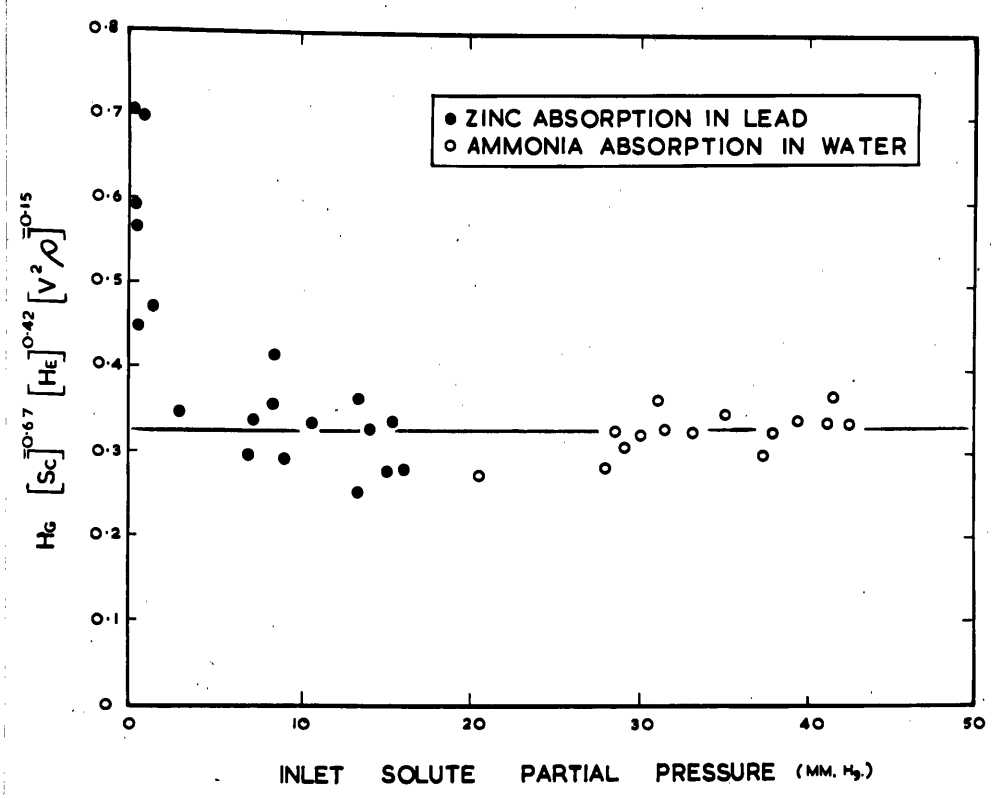

Fig. 13.7 - The effect of inlet solute partial pressure

As can be seen from Fig. 13.7, there is clearly some extraneous factor coming into the analysis, when the zinc inlet partial pressures are less than about 1 mm. Hg.

At these very low zinc concentrations, errors in the analytical procedures could be expected but these can hardly account for the very pronounced and consistent effect observed.

The only feasible explanation appears to be that the low zinc partial pressures were not effective in removing the oxygen and carbon dioxide from the gas circulation system before the runs were commenced.

As outlined in 10.1.3 commercial grade nitrogen was used in the zinc absorption experiments. Because the nitrogen was recycled, any oxygen

contamination would have been eliminated, if there were no leaks in the system, well before the runs were commenced by reaction with the zinc vaporised. Thereafter the only oxygen which could enter the system would be in the small nitrogen make-up to compensate for leaks in the system, as the entire system was maintained above atmospheric pressure. As this nitrogen passed through a bed of granulated charcoal maintained at 1000°C before coming into contact with the zinc vapour in the boiler, the effects of oxygen or carbon dioxide contamination could normally be considered as being eliminated.

However, in the low zinc partial pressure runs, it is considered that the quantitative removal of oxygen and the conversion of carbon dioxide to carbon monoxide was not completed before the runs were commenced. Under these conditions, part of the zinc entering the absorption column would be as zinc oxide, which would pass through the column in particulate form without being absorbed by the molten lead. Mechanical scrubbing would most probably be precluded because of the relatively low lead flow rates.

As the gas phase analysis methods, used in the investigation, could not detect any difference between zinc oxide and zinc vapour, the gas phase analyses under these conditions would not be truly representative of the actual zinc vapour present and hence the evaluation of the height of an overall gas phase transfer unit would be incorrect.

TABLE 13.9

VALUES USED IN CORRELATION OF AMMONIA ABSORPTION DATA

Sc = 0.67

Inlet Solute Partial Pressure mm. Hg.	Gas Rate $\frac{\text{mole.}}{\text{hr.}}$	Liquid Rate $\frac{\text{mole.}}{\text{hr.}}$	Liquid Velocity $\frac{\text{ft.}}{\text{sec.}}$	True Gas Velocity $\frac{\text{ft.}}{\text{sec.}}$	H_D	H_G Corrected for End Effects	$\frac{V\rho}{\mu}$	$\frac{V_R\rho}{\mu}$	$V^2\rho$
28.0	0.0310	1.32	0.29	0.300	0.0483	0.362	1860	3660	0.00675
31.2	0.0500	1.32	0.29	0.486	0.0483	0.558	3010	4780	0.0176
35.1	0.0705	1.32	0.29	0.687	0.0483	0.573	4270	6060	0.0353
30.8	0.1150	1.32	0.29	1.115	0.0483	0.582	6920	8720	0.0932
28.6	0.0705	0.455	0.23	0.672	0.0322	0.636	4160	5560	0.0338
29.2	0.0705	0.860	0.26	0.679	0.0391	0.547	4220	5820	0.0345
30.1	0.0705	2.06	0.33	0.707	0.0667	0.468	4380	6450	0.0372
31.5	0.0705	2.86	0.35	0.725	0.0805	0.441	4500	6660	0.0392
33.2	0.0705	1.22	0.29	0.687	0.0483	0.537	4270	6060	0.0353
37.2	0.0500	1.32	0.29	0.486	0.0483	0.456	3010	4780	0.0176
37.9	0.0705	1.32	0.29	0.687	0.0483	0.534	4270	6060	0.0353
39.5	0.1150	1.32	0.29	1.115	0.0483	0.644	6920	8720	0.0932
41.6	0.1600	1.32	0.29	1.580	0.0483	0.782	9800	11650	0.186
42.4	0.0310	1.32	0.29	0.300	0.0483	0.432	1860	3660	0.00675

TABLE 13.10

VALUES USED IN CORRELATION OF ZINC ABSORPTION DATA

Run	1A	2A	3A	4A	5A	6A	1B	2B	3B	5B
Inlet Zinc Partial Pressure (mm. Hg.)	15.3	15.1	9.0	10.6	13.9	15.9	0.98	1.30	2.86	13.3
Mean Gas Temp. (°C)	605	608	625	590	563	583	640	610	623	605
Gas Viscosity (centipoise)	0.0390	0.0390	0.0395	0.0380	0.0370	0.0378	0.0400	0.0390	0.0395	0.0390
Gas Density lb./ft.^{3}	0.0268	0.0254	0.0261	0.0272	0.0282	0.0274	0.0272	0.0282	0.0274	0.0265
Estimated Diffusion Coefficient Corrected for Column Pressure $D_{Zn - N_2}$ ft.^{2}/hr.	4.03	4.27	4.22	3.96	3.72	3.90	4.11	3.84	4.02	4.11
Sc	0.873	0.870	0.870	0.855	0.855	0.856	0.866	0.873	0.867	0.867
H_D	0.0365	0.0426	0.0487	0.0548	0.1095	0.0243	0.0426	0.0548	0.0426	0.1217
H_T	0.225	0.231	0.231	0.262	0.328	0.243	0.262	0.273	0.262	0.341

TABLE 13.10
(CONTINUED)

VALUES USED IN CORRELATION OF ZINC ABSORPTION DATA

Run	1A	2A	3A	4A	5A	6A	1B	2B	3B	5B
Av. Liquid Lead Velocity ft./sec.	0.51	0.46	0.47	0.50	0.56	0.47	0.46	0.48	0.48	0.45
True Gas Velocity ft./sec.	5.56	3.47	5.23	5.15	5.78	5.12	10.4	9.75	7.87	1.06
$V^2\rho$	0.827	0.304	0.712	0.716	0.938	0.715	2.92	2.67	1.69	0.0295
$\frac{V\rho}{\mu}$	5690	3360	5160	5480	6560	5520	10520	10500	8110	1073
$\frac{V_R\rho}{\mu}$	6200	3800	5630	6030	7220	6020	10950	11000	8580	1525
H_G. Corrected for End Effects	0.553	0.383	0.474	0.505	0.463	0.433	1.310	0.855	0.592	0.470

TABLE 13.10
(CONTINUED)

VALUES USED IN CORRELATION OF ZINC ABSORPTION DATA

Run	6B	1C	2C	3C	5C	6C	2D	3D	5D	6D
Inlet Zinc Partial Pressure (mm. Hg.)	13.3	0.48	0.48	0.58	0.39	0.50	6.78	8.37	8.30	7.16
Mean Gas Temp. (°C)	588	725	675	703	690	693	695	650	655	663
Gas Viscosity (centipoise)	0.0378	0.0427	0.0413	0.0420	0.0415	0.0417	0.0415	0.0405	0.0405	0.0408
Gas Density lb./ft.^{3}	0.0274	0.0243	0.0258	0.0248	0.0245	0.0245	0.0263	0.0282	0.0262	0.0263
Estimated Diffusion Coefficient Corrected for Column Pressure $D_{Zn - N_2}$ ft.^{2}/hr.	3.92	4.98	4.46	4.78	4.76	4.78	4.46	4.00	4.31	4.34
Sc	0.852	0.853	0.870	0.857	0.858	0.861	0.857	0.868	0.868	0.867
H_D	0.0913	0.0426	0.1156	0.0183	0.0975	-	0.0548	0.1642	0.1217	0.0852
H_T	0.310	0.262	0.335	0.238	0.317	-	0.273	0.383	0.340	0.304

TABLE 13.10

VALUES USED IN CORRELATION OF ZINC ABSORPTION DATA

Run	6B	1C	2C	3C	5C	6C	2D	3D	5D	6D
Av. Liquid Lead Velocity ft./sec.	0.48	-	-	-	-	-	0.49	0.55	0.54	0.46
True Gas Velocity ft./sec.	1.89	6.42	7.07	6.00	2.82	-	6.07	7.12	2.40	1.99
$V^2\rho$	0.0973	0.995	1.287	0.890	0.195	-	0.965	1.428	0.151	0.104
$\frac{V\rho}{\mu}$	2050	5440	6560	5280	2480	-	5730	7390	2320	1900
$\frac{V_R\rho}{\mu}$	2580	-	-	-	-	-	6200	8000	2860	2340
H_G Corrected for End Effects	0.432	1.900	1.390	1.228	1.333	1.177	0.897	0.855	0.592	0.614

13.6 Nomenclature

D = diffusion coefficient, ft.^{2}/hr.

G_m = superficial molar mass velocity of the gas phase lb.mole./(hr.)(ft.^{2})

H_G = height of a gas film transfer unit, ft.

H_{OG} = height of an overall gas phase transfer unit, ft.

H_L = height of a liquid film transfer unit, ft.

H_D = dynamic holdup ratio

H_E = effective holdup ratio

h_T = total holdup of liquid in the packing, ml.

L = superficial mass velocity of the liquid phase, lb./(hr.)(ft.^{2})

L_m = superficial molar mass velocity of the liquid phase, lb.mole./(hr.)(ft.^{2})

N_G = number of gas film transfer units

N_{OG} = number of overall gas phase transfer units

P_T = total pressure on the system, mm. Hg.

p^o_{Zn} = vapour pressure of pure zinc, mm. Hg.

ΔP = pressure drop across the packed bed, cm. H_2O

Sc = Schmidt number = $\frac{\mu}{\rho D}$, dimensionless

V_g, V = true gas velocity, ft./sec.

V_R = relative velocity of the gas and liquid streams, ft./sec.

x = mole fraction of zinc in lead phase

x_1 = mole fraction of zinc in outlet lead

x_2 = mole fraction of zinc in inlet lead

y = mole fraction of zinc in gas phase

y_1 = mole fraction of zinc in inlet gas

y_2 = mole fraction of zinc in outlet gas

y_e = mole fraction of zinc in gas phase, which is in equilibrium with x in the lead phase

Z = height of packing in the absorption column, ft.

$\varphi(h_T)$ = function of total liquid holdup

ε = fractional voids or bed porosity

ρ = fluid density, lb./ft.^{3}

μ = fluid viscosity, lb./(ft.)(sec.) or lb./(ft.)(hr.) depending on equation

γ_{Zn} = activity coefficient of zinc in liquid lead - zinc alloy (standard state pure liquid zinc at the same temperature)

CHAPTER 14

C O N C L U S I O N

The studies of this investigation clearly show the absorption of zinc vapour in molten lead to be a diffusion controlled mass transfer operation, which is fundamentally the same as a conventional gas absorption carried out at room temperature with aqueous or organic liquids as the absorbing liquid phase.

The contacting of zinc vapour with molten lead, in such processes as the recently developed zinc blast furnace, should therefore be considered as an absorption not a condensation and the units used should be termed absorbers not condensers. The use of the nomenclature existing at present in metallurgical industry, in which the zinc - vapour molten lead contacting chamber is called a condenser, can lead to erroneous conclusions being drawn with respect to the potential performance of such units.

These units may be operated with neither the lead nor gas temperatures below the dew point of the zinc vapour, as can be clearly seen by noting the temperature conditions of Run 2D and 5D, for example. For these runs the lead temperature was at no stage below the dew point of the inlet zinc vapour. Such performance obviously could not be expected of a condenser.

The most important effect of lead temperature is in determining the equilibrium zinc partial pressure above the alloy formed by absorption. As long as this figure is less than the bulk gas phase zinc concentration, diffusion of zinc from the gas phase to the liquid lead phase can be expected and, if sufficient time is allowed, the concentration in the gas

phase will be reduced until the equilibrium condition for the particular lead surface composition and temperature are reached, regardless of the fact that the gas is at no stage cooled to the dew point of its zinc vapour content.

Besides the equilibrium restriction in determining the direction of the mass transfer, the other factor, which limits the temperature of the lead phase, is that increased lead temperatures result in increased vaporisation of the liquid lead, although even operation at temperatures approaching 1000°C, the losses of lead would be very small. (Vapour pressure of lead at 987°C = 1 mm. Hg. (65))

The application of room temperature analogues, for investigating experimentally difficult high temperature operations, has been demonstrated in these studies. The zinc absorption in molten lead and the absorption of ammonia in water can be directly compared using appropriate empirical correlations suitably modified to contain the essential parameters of relative performance.

The use of room temperature analogues of other high temperature metallurgical processes, involving the transfer of mass between phases, is considered to be a potentially important method for improving existing procedures, developing new processes and techniques and for providing a better understanding of operations, which in the past have been treated largely as industrial arts rather than procedures possessing a sound scientific basis.

Considerable advances have been made by the application of physical chemistry to process metallurgy and in particular a great amount of information has been accrued for thermodynamic equilibria in many of the

high temperature metallurgical processes. However, it is considered that unless attention is also given to the rate of approach to equilibrium, which can be expected under given operating conditions, the value of such work is rather limited, as unfortunately the assumption of equilibrium attainment, as is so frequently made in theoretical treatments, can lead to misguiding conclusions.

Thermodynamics provides only the equilibrium conditions, but the extent of equilibrium reached in a process, involving the contacting of two or more phases, can only be determined experimentally. It is in this respect, that room temperature analogues of high temperature mass transfer operations should be of particular value.

Of the types of correlations discussed for gas phase mass transfer, the forms based on the gas inertia and the relative interfacial velocity gave the best correlation of the zinc absorption in molten lead and the ammonia absorption in water data.

The correlation based on the gas inertia appears slightly superior, but the relative merits of the two methods cannot be definitely established, until further experimental work is undertaken. The use of the gas inertia for correlating the data rather than a Reynolds number may be significant, as the pressure drop data for the mercury model were also correlated in terms of the gas inertia without inclusion of a gas phase viscosity term.

However, despite the slightly better correlation obtained when the gas inertia is used, it is considered that the form of correlation using the relative interfacial velocity is fundamentally the better approach. The disc column gas phase mass transfer studies have indicated that the significant velocity term in the mass transfer process is the relative

interfacial velocity and the newly defined "relative j_D" factor is therefore considered to have general application. As the equation was derived from the "relative j_D" factor, suitably modified for packed column analysis, this new type of correlation has been adequately checked in a simple system of known interfacial area. The effects of the irrigating liquid phase on the gas phase transfer process were accounted for by the use of the relative interfacial velocity and the newly proposed effective holdup ratio. It is therefore considered that the new type of equation

$$H_G \left(\frac{V_R}{V}\right) = \alpha \left(\frac{V_R \rho}{\mu}\right)^x \left(\frac{\mu}{\rho D}\right)^{2/3} H_E^{\,d}$$

is the best approach to the examination of a gas phase mass transfer in a packed column. It is suggested that this type of equation be used for predicting the rate of mass transfer for systems, in which experimental difficulty precludes direct measurement, but for which room temperature analogues may be readily established.

Although the absorptions of zinc vapour in molten lead were controlled by the diffusional resistance of the gas phase, under the conditions of this investigation, the contribution of the liquid lead phase to the overall mass transfer resistance depends entirely on the conditions, under which the absorption is carried out, as can be seen by inspection of the fundamental equation derived:

$$H_{OG} = H_G + \frac{G_m \; H_L}{L_m \; N_{OG}} \int_{y_2}^{y_1} \frac{p^{\circ}_{Zn} \; \gamma_{Zn}}{P_T (y - y_e)} \cdot dy$$

If the value of the second term on the R.H.S. of the above equation

had been significant, the interpretation of the zinc absorption data would have been very much more difficult, particularly as the values of H_L should strictly also be included within the integral, because of the variation of liquid phase Schmidt number for cases having an appreciable difference between the inlet and outlet lead temperatures.

Throughout this investigation the principal interest has been directed towards the analysis of gas phase controlled absorptions. For the absorption of a metallic vapour in a liquid metal at an elevated temperature, in which the principal diffusional resistance is located in the liquid phase, further research is definitely indicated.

The mobility of the semistagnant liquid holdup was of considerable importance in assessing the effective holdup of liquid lead, used in the interpretation of the zinc absorption data. It was suggested that the total liquid lead holdup was effective, prior to the static holdup becoming partially drossed and thereafter only the dynamic holdup was considered effective in the absorption process.

Studies with mercury flowing through a packing with the static holdup labelled by a radioactive tracer could elucidate the rate of movement of the so-called static holdup in a liquid metal irrigated packed system.

The mobility of the static holdup would also be important in either laboratory or pilot plant studies designed to predict plant performance data. As drossing is more likely to occur under plant operating conditions than in carefully controlled laboratory experiments, the design data obtained from a laboratory investigation would be misleading because of the greater effective holdup, with the result that the plant unit would be grossly under-designed. The solution to this possibility may be to

"saturate" the packing with the liquid metal and then expose the column to oxidising conditions before the laboratory tests are carried out, thereby arresting the metal in the sites of static holdup and rendering the static holdup unavailable for further absorption.

Further research in these directions would be extremely desirable.

.....

ACKNOWLEDGMENTS

Sincere thanks are due to Professor J. P. Baxter, School of Chemical Engineering, for suggesting and supervising the research topic.

The numerous helpful discussions with Dr. G. H. Roper, School of Chemical Engineering, are gratefully acknowledged and his continued support as assistant supervisor to the project was greatly appreciated.

Acknowledgment is made to Dr. R. C. Cairns, Australian Atomic Energy Commission, for helpful advice in the early stages of the program and to Dr. A. E. Jenkins, School of Metallurgy, for discussions on thermodynamic aspects.

Special thanks are due to the workshop staff of the Schools of Chemical Engineering and Metallurgy for their full co-operation in the fabrication of the research equipment, and to the following members of the School of Metallurgy: Mr. N. Salassoo and Mr. N. Kennon, laboratory assistants for general assistance when required; Mr. J. Gordon and Mr. M. Hatherly for assisting in the photographic work involved in the preparation of the thesis.

Acknowledgment is also made to the Monsanto Chemical Co. (Aust.) for the provision of the research scholarship in 1953, underwhich the research program was initiated and to the Broken Hill Associated Smelters Ltd., who kindly loaned the lead used in the investigation.

BIBLIOGRAPHY

1. Anonymous, Chem. Eng. 59, 246, August, (1952).

2. Arnold, J.H., Ind. Eng. Chem. 22, 1091, (1930).

3. Bailey, G.L.J., B.N.F.M.R.A. Report R.R.A. 898 (1951).

4. Beattie, R.E.C., B.Sc. Thesis in Chemical Engineering, N.S.W. University of Technology, (1954).

5. Bird, R.B., Hirschfelder, J.O., and Curtiss, C.F., Trans. Am. Soc. Mech. Engrs. 76, 1011, (1954).

6. Blake, F.C., Trans. Amer. Inst. Chem. Engrs. 14, 415, (1922).

7. Bonilla, C.F., Proc. International Conference on the Peaceful Uses of Atomic Energy, 9, 331, (1955).

8. Burke, S.P., and Plummer, W.B., Ind. Eng. Chem. 20, 1196, (1928)

9. Carman, P.C., Trans. Instn. Chem. Engrs. 15, 150, (1937).

10. Chapman, S., and Cowling, T.G., "Mathematical Theory of Nonuniform Gases," Cambridge University Press, Cambridge, (1939).

11. Chilton, T.H., and Colburn, A.P., Ind. Eng. Chem. 26, 1183, (1934).

12. Chilton, T.H., and Colburn, A.P., Ind. Eng. Chem. 27, 255, (1935).

13. Claasen, H., Zentralblat.f.d. Zucker-industrie, 26, 497, (1918).

14. Colburn, A.P., Ind. Eng. Chem. 22, 967, (1930).

15. Cooper, C.M., Drew, T.B., and McAdams, W.H., Trans. Am. Inst. Chem. Engrs., 30, 158, (1933-3).

16. Cooper, C.M., Christl, R. and Peery, L.C., Trans. Am. Inst. Chem. Engrs. 37, 979, (1941).

17. Cullen, E.J., and Davidson, J.E., Chem. Eng. Sci. 8, 49, (1956).

18. Danckwerts, P.V., and Kennedy, A.M., Trans. Inst. Chem. Engrs. Symposium on Gas Absorption, 32, Suppl. 1.S.58, (1954).

19. Davey, T.R.A., M. Met. Eng. Thesis, University of Melbourne, (1952).

20. Dunn, W.E., Bonilla, C.F., Ferstenberg, C., and Gross, B., A.I.Ch.E. Journal 2, 184, (1956).

21. Einstein, A., Annalen der Physik, 17, 549, (1905).

22. Elgin, J.C., and Weiss, F.B., Ind. Eng. Chem. 31, 435, (1939).

23. Emmert, R.E., and Pigford, R.L., Chem. Eng. Prog. 50, 87, (1954).

24. Ergun, S., Chem. Eng. Prog. 48, 89, (1952).

25. Ergun, S., Chem. Eng. Prog. 48, 227, (1952).

26. Fair, J.R., and Lerner, B.J., A.I.Ch.E. Journal 2, 13, (1956).

27. Fox, M.J., B.N.F.M.R.A. Report R.R.A. 771, (1948).

28. Flaschka, H., Z. Anal. Chem. 138, 332, (1953).

29. Gardner, G.C., Chem. Eng. Sci. 5, 101, (1956).

30. Gilliland, E.R., and Sherwood, T.K., Ind. Eng. Chem. 26, 516, (1934).

31. Gilliland, E.R., Ind. Eng. Chem. 26, 681, (1934).

32. Glasstone, S., Laidler, K., and Eyring, H., "The Theory of Rate Processes", 477 f.f. McGraw-Hill Book Co. Inc. New York, (1941).

33. Goodgame, T.H., and Sherwood, T.K., Chem. Eng. Sci. 3, 37, (1954).

34. Gordon, K.F., and Sherwood, T.K., Paper presented at Toronto meeting of Am. Inst. Chem. Engrs. (April, 1953).

35. Grace, R.E., and Derge, G., A.I.M.E. Trans. 203, 839, (1955); Journal of Metals, (July, 1955).

36. Grimley, S.S., Trans. Inst. Chem. Engrs. 41, 233, (1945).

37. Hamilton, W.F., Trans. Am. Inst. Chem. Engrs. 29, 292, (1933).

38. Heldvander, E.F.M., and Miesowicz, M., Physica 4, 559, (1937).

39. Higbie, R., Trans. Am. Inst. Chem. Engrs. 31, 365, (1935).

40. Hirschfelder, J.O., Bird, R.B., and Spotz, E.L., Chem. Rev. 44, 205, (1949).

41. Hirschfelder, J.O., Bird, R.B., and Spotz, E.L., J.Chem. Phys. 16, 968, (1948).

42. Hirschfelder, J.O., Bird, R.B., and Spotz, E.L., Trans. Am. Soc. Mech. Engrs. 71, 921, (1949).

43. Hobson, M., and Thodos, G., Chem. Eng. Prog. 45, 519, (1949).

44. Hoffman, R.E., J.Chem. Phys. 20, 1567, (1952).

45. Hoftyser, P.J., and van Krevelen, D.A., Trans, Inst. Chem. Engrs., 32, Suppl. 1. S.66, (1954).

46. Houston, R.W., and Walker, C.A., Ind. Eng. Chem. 42, 1105, (1950).

47. Jeans, J.H., "Dynamical Theory of Gases" 3rd ed. (1921) and "Introduction to Kinetic Theory of Gases", Cambridge University Press, Cambridge, (1940).

48. Jellinek, K., and Wannow, H.A., Z. Electrochem. 41, 346, (1935).

49. Jesser, B.W., and Elgin, J.C., Trans. Am. Inst. Chem. Engrs. 34, 277, (1943).

50. Johnstone, H.F., and Pigford, R.L., Trans. Am. Inst. Chemgrs., 38, 25, (1942).

51. Jost, W., "Diffusion in Solids, Liquids and Gases." p. 479, Academic Press, New York, (1952).

52. Kelley, K., U.S. Bureau of Mines, Bull. 383, 109, (1935).

53. Kilbanova, Pomerantsev, and Frank-Kamemetsky, J.Tech. Phys. (U.S.S.R.) 12, 14, (1942).

54. Kinnunen, J., and Merikanto, B., Chemist Analyst 41, No. 4, 76, (1952).

55. Kinnunen, J., and Wennerstrand, B., Engineering and Mining Journal 156, No. 4, 94, (1955).

56. Kleppa, O.J., J.Am. Chem. Soc. 74, 6052, (1952).

57. Landolt and Bornstein, Physikalisch-Chemische Tabellen, Springer, Berlin, (1937).

58. Le Bas, "Molecular Volumes of Liquid Chemical Compounds", Longmans, London, and Chem. News. 99, 206, (1909).

59. Lennard-Jones, J.E., Physica 4, 941, (1937).

60. Linton, W.H., and Sherwood, T.K., Chem. Eng. Prog. 46, 258, (1950).

61. Lohrisch, W., Mitt. Forsch. 322, 46, (1929).

62. Lumsden, J., Disc. Faraday Soc., No.4, 60, (1940).

63. Lynch, E.J., and Wilke, C.R., A.I.Ch.E. Journal 1, 9, (1955).

64. Lynn, S., Straatemeier, J.R., and Kramers, H., Chem. Eng. Sci. 4, 49, (1955).

65. Lyon, R.N., "Liquid Metals Handbook", pp. 40-41, U.S.A.E.C., (1952).

66. Ibid. pp. 172-173.

67. Martell, A.E., and Calvin, M., "Chemistry of the Metal Chelate Compounds", Prentice Hall Inc. New York, (1952), pp. 473-495.

68. Maxwell, J.C., Phil. Mag. 35, 185, (1868).

69. Maxwell, R.W., and Storrow, J.A., Chem. Eng. Sci. 6, 204, (1957).

70. Mayo, F., Hunter, T.O., and Nash, A.W., J.Soc.Chem. Ind. Trans. 54, 375, (1935).

71. McAdams, W.H., "Heat Transmission", McGraw-Hill Book Co. Inc. New York, (1942), p. 398.

72 Ibid. p. 414.

73. Meyer, O.E., "Kinetic Theory of Gases", (1899).

74. Mehta, J.J., and Parekh, R.H., M.S. Thesis, Mass. Inst. Technol. (1939).

75. Morgan, D.W., and Kitchener, J.A., Trans. Faraday Soc. 50, 51, (1954).

76. Morgan, S.W.K., Trans. Inst. Mining and Metallurgy, 66, 553, (1957).

77. Morris, G.A., and Jackson, J., "Absorption Towers", Butterworth, London, (1951).

78. Mott, R.A., Inst. of Physics, "Some Aspects of Fluid Flow", Edward Arnold and Co., London, (1950), pp. 242-256.

79. Mullaly, J.M., and Jacques, H., Phil. Mag. (6) 48, 1105, (1924).

80. Niwa, K., Shimoji, M., Kado, S., Watanabe, Y., and Vokokawa, T., A.I.M.E. Trans. 209, 96, (1957); Journal of Metals (Jan. 1957).

81. Perry, J.H., "Chemical Engineers Handbook", McGraw-Hill Book Co. Inc. New York, 3rd Ed., (1950), p. 118.

82. Ibid. p.363.

83. Ibid. p. 540.

84. Ibid. p. 674.

85. Ibid. p. 140.

86. Potter, O.E., Chem. Eng. Sci., 6, 170, (1957).

87. Powell, R.W., Trans. Inst. Chem. Engrs., 18, 36, (1940).

88. Reynolds, O., "Papers on Mechanical and Physical Subjects", Vol. I Cambridge University Press, Cambridge, (1900).

89. Roper, G.H., Chem. Eng. Sci. 2, 18, (1953).

90. Roper, G.H., Chem. Eng. Sci. 4, 255, (1955).

91. Rothman, S.J., and Hall, L.D., A.I.M.E. Trans. 206, 199, (1956).

92. Schlinger, W.G., Reamer, H.H., Sage, B.H., and Lacey, W.N., Report of Progress - Fundamental Research on Occurrence and Recovery of Petroleum, p.70, American Petroleum Institute, (1952-1953).

93. Schrage, R.W., "A Theoretical Study of Interphase Mass Transfer", Columbia University Press, New York, (1953).

94. Schwarts, K., "Electrolytische Wanderung in flussigen und festen Metallen", (1940).

95. Schwarzenbach, G., Schweiz Chem. Ztg. 28, 377, (1945).

96. Schwarzenbach, G., and Biedermann, W., Helv. Chim. Acta. 31, 331, 456, 459, 678, (1948).

97. Sherwood, T.K., and Holloway, F.A.L., Trans. Am. Inst. Chem. Engrs. 36, 21, (1940).

98. Sherwood, T.K., and Holloway, F.A.L., Trans. Am. Inst. Chem. Engrs. 36, 39, (1940).

99. Sherwood, T.K., and Pigford, R.L., "Absorption and Extraction", McGraw-Hill Book Co. Inc. New York, (1952).

100. Ibid. p.10.

101. Ibid. pp. 117 to 128.

102. Ibid. pp. 123 to 126.

103. Ibid. pp. 129 to 130.

104. Ibid. p. 133.

105. Ibid. pp.63 - 79.

106. Ibid. p. 61.

107. Ibid. p. 10.

108. Shulman, H.L., and DeGouff, J.J., Ind. Eng. Chem. 44, 1915, (1952).

109. Shulman, H.L., and Margolis, J.E., A.I.Ch.E. Journal 3, 157, (1957).

110. Shulman, H.L., Ullrich, C.F., Proulx, A.Z., and Zimmerman, J.O., A.I.Ch.E. Journal 1, 253, (1955).

111. Shulman, H.L., Ullrich, C.F., and Wells, N., A.I.Ch.E. Journal 1, 247, (1955).

112. Shulman, H.L., Ullrich, C.F., Wells, N., and Proulx, A.Z., A.I.Ch.E. Journal 1, 259, (1955).

113. Spier, J.L., Physica 7, 381, (1940).

114. Spiers, H.M., "Technical Data on Fuel", British National Committee, World Power Conference, (1950), pp. 352-353.

115. Stefan, J., Ann. Physik 41, 723, (1890).

116. Stephens, E.J., and Morris, G.A., Chem. Eng. Prog. 47, 232, (1951).

117. Stull, D.R., Ind. Eng. Chem., 39, 517, (1947).

118. Surosky, A.E., and Dodge, B.F., Ind. Eng. Chem., 42, 1112, (1950).

119. Sutherland, W., Phil. Mag. 38, 1, (1894).

120. Sutherland, W., Phil. Mag. 36, 507, (1893).

121. Taeker, R.G., and Hougen, O.A., Chem. Eng. Prog. 45, 188, (1949).

122. Taylor, R.F., and Roberts, F., Chem. Eng. Sci. 5, 168, (1956).

123. Vivian, J.E., and Peaceman, D.W., A.I.Ch.E. Journal 2, 437, (1956).

124. Warner, N.A., Chem. Eng. Sci. 3, 77, (1954).

125. Weisman, J., and Bonilla, C.F., Ind. Eng. Chem. 42, 1099, (1950).

126. Wells, A.F., "Structural Inorganic Chemistry", p.93, Oxford University Press, Oxford, (1945).

127. Ibid. p. 549.

128. Wilke, C.R., and Lee, C.Y., Ind. Eng. Chem. 47, 1253, (1955).

129. Whitman, W.G., Chem. Met. Eng. 29, 146, (1923).

130. Wilke, C.R., Chem, Eng. Prog. 46, 95, (1950).

131. Williams, K.C., and Davey, T.R.S., Personal Communication, Broken Hill Associated Smelters, South Australia.

132. Yoshida, F., Chem. Eng. Prog. Symposium Series, No. 16, 51, 59, (1955).

APPENDIX

PUBLISHED PAPER

Chemical Engineering Science, 1954, Vol. 3, pp. 77 to 86. Pergamon Press Ltd.

The gas flow characteristics of the disc absorption column

N. A. WARNER

School of Chemical Engineering, N.S.W. University of Technology, Broadway, N.S.W.

(*Received* 5 *February* 1954)

Summary—The gas flow characteristics of the disc column designed by STEPHENS and MORRIS [4] are studied by means of pressure drop determinations across the column. Water is run down the column with a range of gases passing countercurrent through the column. The gases studied are hydrogen, air, vinyl chloride and dichlorodifluoromethane.

Correlations for pressure drop across the column, with and without liquid flowing over the discs, and across the empty column, are presented, which enable a correlation of data for pressure drop across a single disc to be made.

The pressure drop data and gas film coefficients of mass transfer for the disc column are compared in order to show the relationship between mass transfer characteristics and gas flow characteristics. Changes in gas flow characteristics as indicated by break points in graphs relating pressure drop and gas velocity were found to be consistent with changes in the mass transfer data. Equations which enable a prediction of the location of changes in the gas flow characteristics are developed.

Data are also presented for the flooding velocities of the disc column with the system air-water.

Résumé—Au moyen de mesures de pertes de charge au travers d'une colonne à disques de STEPHENS et MORRIS, l'auteur étudie les caractéristiques de l'écoulement gazeux. On fait couler de l'eau dans la colonne où des gaz divers passent à contre-courant : hydrogène, air, chlorure de vinyle, dichlorodifluoremethane.

L'auteur présente des corrélations pour la perte de charge au travers de la colonne, avec ou sans écoulement de fluide sur les disques, avec la colonne vide, et en déduit une corrélation pour la perte de charge correspondant au disque unique.

L'auteur compare dans le cas de la colonne à disques, les résultats sur la perte de charge et ceux sur le coefficient d'échange dans le gaz de façon à établir l'interdépendance des caractéristiques du phénomène d'échange et de l'écoulement gazeux. On trouve que des changements dans le caractère de l'écoulement qui ne manifestent pas une brisure sur les courbes : perte de charge/vitesse d'écoulement, concordent avec des altérations dans le phénomène d'échange de matière. L'auteur développe des équations prédisant les altérations dans les caractéristiques de l'écoulement.

Données sur les vitesses d'inondation de la colonne à disque dans le système air-eau.

INTRODUCTION

The disc column as introduced by STEPHENS and MORRIS [4] has to date been used primarily for the investigation of gas absorption systems in which the liquid film is the major resistance. To evaluate the liquid film coefficients, the overall coefficients of mass transfer are corrected to take into account the effect of gas film resistance.

To establish the characteristics of the column with respect to the gas film, STEPHENS and MORRIS [4] applied a liquid film correction to overall coefficients obtained for the absorption of ammonia in water from dilute mixtures with air. These results were then applied to other gas mixtures by means of a general correlation applicable to wetted-wall columns [1], [2], viz.:

$$\frac{M_d k_g}{v \rho_d} = \beta \left(\frac{Dv\rho}{\mu}\right)^{-n} \left(\frac{\mu}{\rho D_v}\right)^{-m} \frac{P}{P_{BM}}$$

ROPER [3] reported data for the evaporation of water and carbon tetrachloride by air in a disc column. These data and the gas film coefficients for the absorption of ammonia in water from dilute mixtures with air were well correlated by an equation of the same form as used by STEPHENS and MORRIS.

The use of a general correlation applicable to wetted wall columns for the determination of gas film coefficients in a disc column is not entirely justified on the basis of the experimental work reported. No data have been published for gas film coefficients in a disc column for any other gas phase except air or dilute mixtures with air as the diluent.

Theoretical and experimental developments in the three fields of fluid friction, heat and mass transfer indicate that they are all closely related. It was therefore considered that an investigation of the gas flow characteristics of the disc column would provide data useful in the interpretation of gas film mass transfer coefficients. It is reasonable to expect comparable changes in the mass transfer coefficients and the conditions of gas flow. STEPHENS and MORRIS observed a change in slope of the line obtained when the gas film coefficients for a particular liquid rate were plotted against relative velocity of the air stream. The existence of such a discontinuity or " break point " in the graph is an indication that the gas flow characteristics of the disc column also undergo a change at a definite air velocity.

The gas flow characteristics of the disc column were conveniently studied by pressure drop measurements across the discs of the column. By selecting a range of gases which had extremely different physical properties it was possible to establish relationships which showed the positions of discontinuities observed in the gas flow conditions and enabled the pressure drop measurements to be correlated with the velocity and physical properties of the gas phase.

A knowledge of the limiting capacity is useful in the design of experimental work using the disc column. The air velocities at which the column ceased to function due to entrainment of the liquid were determined.

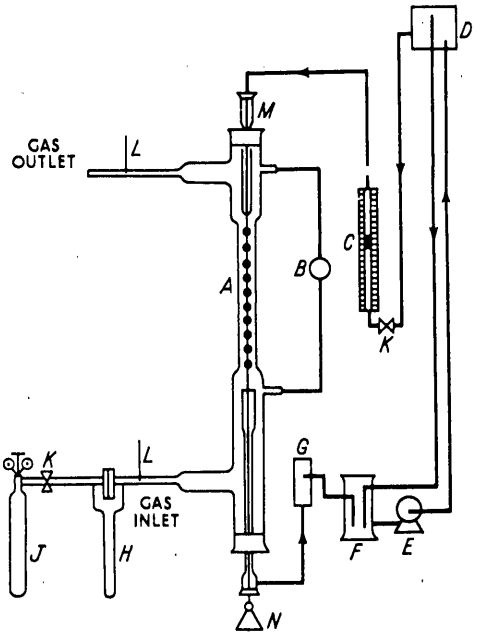

Fig. 1. Diagram of apparatus.

A—Disc column
B—Micromanometer
C—Liquid rotameter
D—Constant head tank
E—Circulating pump
F—Pump sump
G—Liquid seal arrangement
H—Calibrated orifice plate
J—Compressed gas source
K—Needle control valve
L—Thermometer
M—Liquid flow nozzle
N—Disc supporting weight

EXPERIMENTAL PROCEDURE AND RESULTS

Apparatus

The laboratory column used was developed by STEPHENS and MORRIS [4] and consisted of 27 carbon discs, 1·45 to 1·5 cm diameter, 0·44 to 0·45 cm thick, threaded edgeways on a 16 B.S.W. wire. The discs were maintained mutually at right angles by means of a plastic cement. The disc assembly forming the liquid flow path was mounted vertically inside a 2·5 cm bore glass tube through which the gas was passed. The manometer tappings for determining the pressure drop across the discs were located a short distance from each end of the disc assembly.

Table 1. *Principal dimensions of disc column*

Number of discs	= 27
Disc diameter	= 1·475 cm
Disc thickness	= 0·45 cm
Tube diameter	= 2·5 cm
Mean perimeter for liquid flow	= 0·122 ft.
Equivalent diameter for gas flow	= 0·052 ft.
Free space (dry)	= 89%
Absorption surface (dry)	= 0·1605 sq. ft.

The pressure drop readings were measured using a micromanometer graduated to read to one hundredth of a millimetre water gauge pressure differential.

The general layout of the apparatus is shown in Fig. 1 and the principal dimensions are shown in Table 1.

Procedure

The total pressure drop across the column was obtained for different liquid and gas flow rates for a wide range of gases. The gases studied were hydrogen (mol. wt. = 2), air (mol. wt. = 29), vinyl chloride (mol. wt. = 62·5) and dichlorodifluoromethane (mol. wt. = 121). As the investigation was centred on the gas phase characteristics, the liquid phase flowing over the discs was not varied and water was used in all runs.

Due to the construction of the column used it was considered necessary to determine the pressure drop over the column without the discs in position with the same range of gases. These readings enabled an estimate of the pressure drop over the discs to be made as distinct from the pressure drop over the complete column, including column walls and entrance and exit losses.

The maximum air velocities at which the column could be operated without the water being blown from the discs and the column flooding, were also investigated for different liquid rates. The liquid rate was kept constant and the gas velocity slowly increased until flooding occurred.

Results

(a) *Pressure drop across column*

The data for pressure drop across the whole column for the range of gases : hydrogen, air, vinyl chloride and dichlorodifluoromethane are shown in Table 2. The data are well correlated when ΔP_t is plotted against $v\rho^{0.41}\ \Gamma^{0.22}$ on a log-log scale as shown in Fig. 2.

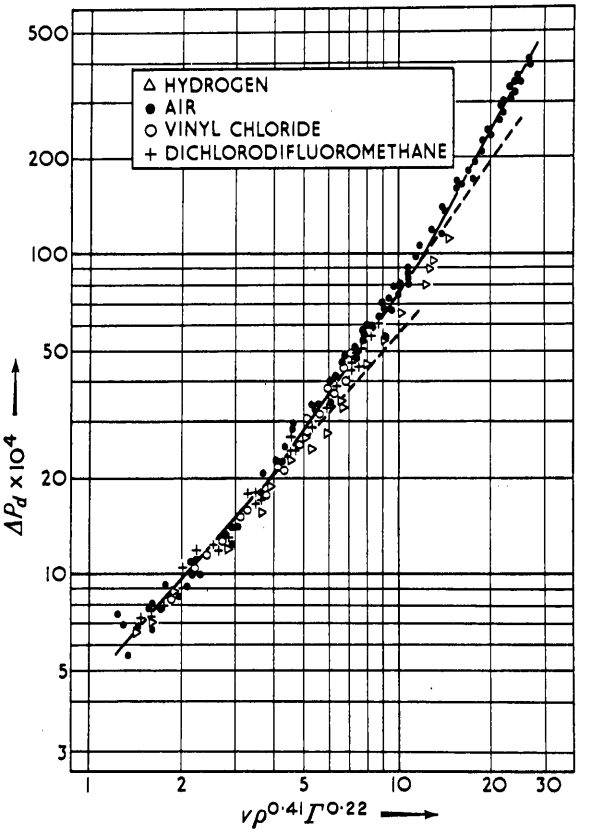

Fig. 2. Pressure drop across the column.

Table 2. Data for pressure drop across the column.

Liquid Rate lb./-hr.ft.	*Gas Velocity ft./sec.*	*Gas Re*	*ΔP_t lb./ft.²*	*Liquid Rate lb./-hr.ft.*	*Gas Velocity ft./sec.*	*Gas Re*	*ΔP_t lb./ft.²*	*Liquid Rate lb./-hr.ft.*	*Gas Velocity ft./sec.*	*Gas Re*	*ΔP_t lb./ft.²*
	Air – Water				*Air – Water*				*Air – Water*		
408	5·13	1650	0·1580	368	4·95	1590	0·1438	281	4·43	1425	0·1187
408	6·90	2210	0·2420	358	6·20	1990	0·1926	281	6·55	2100	0·2032
408	8·35	2680	0·3195	368	7·40	2380	0·2566	281	8·20	2630	0·2870
408	8·83	2835	0·3490	368	8·50	2730	0·3080	281	10·8	3470	0·4372
408	10·8	3470	0·4920	368	11·30	3630	0·4955	281	13·0	4175	0·5930
408	13·6	4370	0·6940	368	12·8	4120	0·6060	281	16·0	5130	0·8322
408	15·6	5000	0·8740	368	13·5	4330	0·6600	281	18·7	6000	1·1100
408	16·5	5290	0·9625	368	14·7	4720	0·7675	281	20·7	6650	1·3350
408	17·7	5680	1·0970	368	17·2	5530	1·0080				
408	20·6	6620	1·4430	368	19·0	6100	1·1690	255	1·05	337	0·0238
				368	19·7	6330	1·2730	255	1·35	433	0·0266
335	1·05	337	0·0226	368	21·1	6780	1·4390	255	1·80	578	0·0328
335	1·28	411	0·0266					255	1·90	611	0·0300
335	1·42	456	0·0308	166·5	0·96	296	0·0144	255	2·40	772	0·0471
335	1·75	562	0·0368	166·5	1·35	433	0·0239	255	3·16	1015	0·0737
335	2·37	761	0·0492	166·5	1·53	491	0·0246	255	4·60	1477	0·1187
335	2·85	916	0·0636	166·5	1·80	577	0·0308	255	6·40	2055	0·1826
335	3·70	1190	0·0944	166·5	2·16	693	0·0369	255	7·10	2280	0·2177
335	4·90	1578	0·1394	166·5	2·70	867	0·0470	255	8·10	2760	0·2784
335	7·35	2360	0·2440	166·5	4·05	1300	0·0881				
335	8·80	2820	0·3078	166·5	5·60	1797	0·1294	378	1·05	337	0·0188
				166·5	6·95	2230	0·01890	378	1·35	433	0·0266
188	4·23	1360	0·1043	166·5	9·04	2900	0·02650	378	1·70	546	0·0350
188	6·30	2020	0·1763					378	2·32	745	0·0492
188	7·40	2380	0·2214	188	18·2	5840	0·9415	378	3·22	1035	0·0782
188	9·40	3020	0·3074	188	20·2	6480	1·1320	378	4·30	1381	0·1169
188	10·7	3430	0·3996	188	21·2	6810	1·2475	378	5·80	1860	0·1725
188	13·0	4175	0·5280	188	22·0	7060	1·3225	378	6·90	2210	0·2210
188	14·4	4620	0·6425					378	8·50	2730	0·2996
188	16·2	5190	0·7560								
	Dichlorodifluoromethane – Water								*Hydrogen –Water*		
255	3·96	7700	0·1970	131	3·95	7680	0·1640	255	13·6	630	0·0964
255	3·41	6630	0·1620	131	3·25	6320	0·1232	255	15·2	704	0·1087
255	2·76	5370	0·1150	131	2·57	5000	0·0882	255	17·2	795	0·1312
255	2·16	4190	0·0818	131	2·02	3920	0·0613	255	20·5	950	0·1745
255	1·67	3244	0·0594	131	1·46	2840	0·0410	255	23·5	1090	0·2112
255	1·34	2608	0·0432	131	0·87	1690	0·0239	255	26·5	1230	0·2544
255	0·96	1865	0·0328					255	29·5	1365	0·3060
				355	3·93	7640	0·2113	255	16·2	750	0·1250
166·5	3·97	7720	0·1663	355	3·87	6550	0·1725	255	33·0	1530	0·3510
166·5	3·34	6500	0·1393	355	2·82	5480	0·1330	255	38·0	1760	0·4325
166·5	2·78	5400	0·1044	355	2·03	3940	0·0882	255	33·6	1560	0·3670
166·5	2·26	4390	0·0779	355	1·47	2860	0·0575	255	3·65	169	0·0226
166·5	1·82	3540	0·0574	355	1·01	1963	0·0369	255	4·1	190	0·0246
166·5	1·32	2570	0·0410	355	0·665	1293	0·0226	255	4·8	222	0·0308
166·5	0·92	1780	0·0256					255	7·3	338	0·0452
								255	9·3	430	0·0595
	Vinyl Chloride – Water							255	12·5	579	0·0881
255	4·27	5080	0·1457	355	4·22	5020	0·1636	255	10·0	463	0·0696
255	3·93	4680	0·1270	355	3·94	4690	0·1475	255	14·0	648	0·1024
255	3·52	4180	0·1087	355	3·52	4180	0·1250				
255	3·03	3600	0·0862	355	3·00	3570	0·1006				
255	2·70	3210	0·0717	355	2·43	2900	0·0718				
255	2·36	2810	0·0594	355	1·92	2280	0·0512				
255	1·94	2310	0·0493	355	1·62	1930	0·0410				
255	1·50	1785	0·0369	355	1·29	1537	0·0328				
255	1·16	1605	0·0269								

The three straight lines of Fig. 2 and the location of the " break points " are better illustrated by plotting the dimensional group $\frac{\Delta P_t}{v^2\rho}$ against gas velocity. A comparison between the two methods of plotting is shown in Fig. 3, in which ΔP_t and $\frac{\Delta P_t}{v^2\rho}$ are plotted against gas velocity for data of one of the air-water runs shown in Table 2.

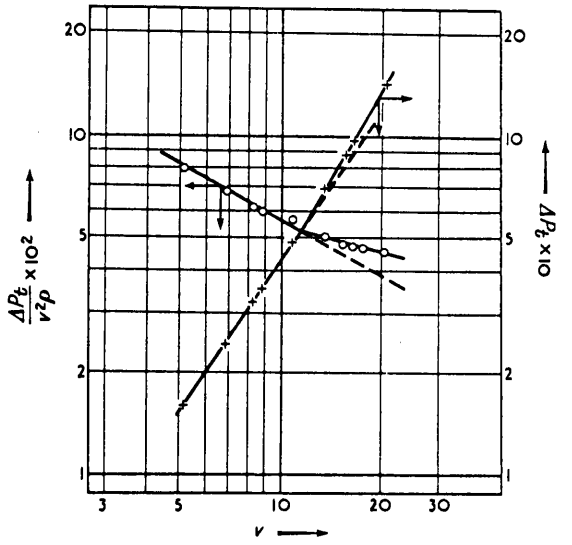

Fig. 3. Comparison of methods of plotting data

$\frac{\Delta P_t}{v^2\rho}$ versus v

ΔP_t versus v

Air-water system ($\Gamma = 408$ lb./(hr.)(ft.).

The method of plotting $\frac{\Delta P}{v^2\rho}$ was adopted for all runs to determine the " break points " but it was considered more fundamental to present final empirical correlations in terms of the pressure drop ΔP.

(b) *Pressure drop across column with zero liquid rate*

Flow through the dry column is equivalent to flow through porous media with a single fluid phase. Such data are best correlated by plotting a friction factor against Reynolds Number on log-log paper.

However, it is unnecessary to use the complete Fanning friction factor for purposes of illustrating the flow characteristics of a particular column.

The dimensional group $\frac{\Delta P_t}{v^2\rho}$ has been plotted against Re in Fig. 4 for data on the pressure drop across the dry column as shown in Table 8.

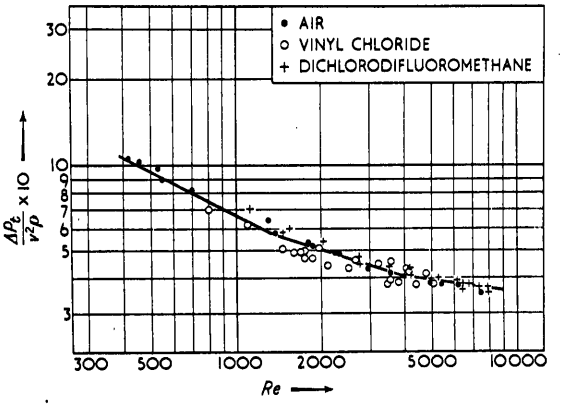

Fig. 4. Pressure drop across column at zero liquid rate.

(c) *Pressure drop across the empty column*

To evaluate the pressure drop due to the disc assembly it was considered necessary to determine the pressure drop due to the glass column itself without the discs in place.

Correlation of the data shown in Table 4 is obtained by plotting the dimensional group $\frac{\Delta P_e}{v^2\rho}$ against Re on a log-log graph as shown in Fig. 5.

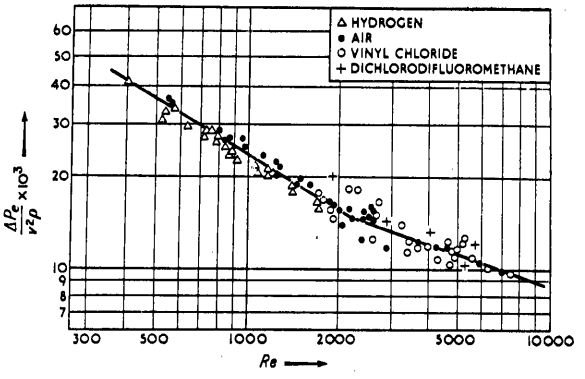

Fig. 5. Pressure drop across the empty column (discs removed).

Table 3. Pressure drop across the column at zero liquid rate.

Gas Velocity ft./sec.	*Gas Re*	ΔP_t *lb./ft.*^{2}	*Gas Velocity ft./sec.*	*Gas Re*	ΔP_t *lb./ft.*^{2}	*Gas Velocity ft./sec.*	*Gas Re*	ΔP_t *lb./ft.*^{2}
	Air			*Vinyl Chloride*			*Dichlorodifluoromethane*	
1·35	417	0·0143	4·17	4960	0·1067	4·03	7850	0·1822
1·67	537	0·0205	3·72	4420	0·0839	3·46	6730	0·1413
4·30	1380	0·0800	3·20	3800	0·0635	3·09	6000	0·1169
5·75	1845	0·1290	2·96	3520	0·0553	2·70	5250	0·0922
7·2	2310	0·1886	2·11	2510	0·0307	2·15	4175	0·0594
9·08	2920	0·2642	1·47	1750	0·0164	1·42	2760	0·0307
2·17	698	0·0286	1·23	1463	0·0123	1·04	2020	0·0185
1·42	457	0·0154	0·68	950	0·0051	0·75	1460	0·0103
1·67	537	0·0184	3·5	4160	0·0822	4·02	7820	0·1887
6·20	1990	0·1683	3·0	3570	0·0656	3·73	7250	0·1620
8·20	2630	0·2420	2·68	3190	0·0513	3·30	6420	0·1313
10·7	3430	0·3852	2·23	2660	0·0369	2·97	5770	0·1067
14·2	4560	0·5980	1·66	1973	0·0226	2·53	4920	0·0800
16·3	5230	0·7155	1·35	1605	0·0143	2·14	4160	0·0615
19·2	6160	0·9665	0·91	1082	0·0082	1·82	3540	0·0452
20·7	6650	1·0975	4·0	4760	0·1064	1·42	2760	0·0287
22·2	7130	1·2310	3·45	4110	0·0821	0·80	1566	0·0123
24·0	7700	1·3975	3·07	3650	0·0635	0·57	1108	0·0072
			2·50	2980	0·0430			
			2·10	2500	0·0307			
			1·78	2120	0·0225			
			1·47	1750	0·0174			
			1·44	1713	0·0164			
			1·56	1855	0·0185			

(d) *Corrected pressure drop due to discs*

The pressure drop across the column due to the discs was obtained by substracting the pressure drop due to the empty column (as determined from Fig. 5) from the pressure drop data due to the assembled column.

An example of the method of calculation used to approximate the pressure drop across a single disc in a disc column is shown in Table 5.

The estimated pressure drop ΔP_d due to a single disc is well correlated by plotting ΔP_d against $v\rho^{0.41}\ \Gamma^{0.22}$ on a log-log graph.

The dimensional equations for this correlation are

Let $v\rho^{0.41}\ \Gamma^{0.22} = \phi$

(a) Above $\phi = 12$

$$\Delta P_d = 9{\cdot}8 \times 10^{-5}\ \phi^{1.84}$$

(b) Between $\phi = 12$ and $\phi = 4$

$$\Delta P_d = 2{\cdot}94 \times 10^{-4}\ \phi^{1.41}$$

(c) Below $\phi = 4$

$$\Delta P_d = 4{\cdot}5 \times 10^{-4}\ \phi^{1.09}$$

(e) *Flooding characteristics*

The " flooding velocity " of the column with water flowing over the discs at various liquid rates and air passing up the column was determined visually. The first visual appearance of flooding occurred when small drops of water were blown off the periphery of the wetted discs. The column became unstable at this point and as the gas velocity was increased or the liquid rate was increased, slugs of liquid were blown off the discs and surged upward through the column.

Due to the unstable nature of the column when

Table 4. Pressure drop across the empty column (discs removed).

Gas Velocity ft./sec.	*Gas Re*	ΔP_e *lb./ft.²*	*Gas Velocity ft./sec.*	*Gas Re*	ΔP_e *lb./ft.²*	*Gas Velocity ft./sec.*	*Gas Re*	ΔP_e *lb./ft.²*
	Hydrogen			*Air*			*Air*	
8·7	402	0·0164	6·10	1958	0·0451	19·6	6280	0·2890
11·3	522	0·0205	6·85	2199	0·0553	23·5	7540	0·4020
15·8	730	0·0369	7·60	2440	0·0676	5·45	1155	0·0328
19·0	880	0·0451	8·30	2664	0·0758	6·40	2060	0·0431
23·0	1065	0·0595	1·73	555	0·0082	7·40	2380	0·0513
25·2	1165	0·0675	2·50	803	0·0133	9·10	2920	0·0717
30·3	1400	0·0863	2·74	880	0·0154	11·5	3680	0·1190
37·0	1710	0·1150	3·55	1140	0·0225	13·2	4230	0·1558
11·5	532	0·0225	3·95	1268	0·0266	14·5	4650	0·1865
12·3	570	0·0266	4·70	1509	0·0327	18·6	5960	0·2682
16·3	755	0·0389	5·85	1878	0·0429	22·3	7150	0·3668
17·2	797	0·0410	6·95	2230	0·0532			
19·7	913	0·0451	7·70	2472	0·0655		*Vinyl Chloride*	
23·0	1065	0·0573	8·20	2632	0·0820			
25·0	1157	0·0677	2·50	803	0·0164	1·62	1928	0·0061
30·3	1400	0·0862	3·02	969	0·0184	2·30	2737	0·0144
36·5	1690	0·1128	3·85	1236	0·0225	2·90	3451	0·0164
13·8	638	0·0287	4·60	1477	0·0308	3·35	3987	0·0210
15·6	722	0·0348	5·10	1637	0·0369	4·10	4879	0·0307
18·2	843	0·0431	6·35	2038	0·0472	4·00	4760	0·0266
14·7	680	0·0318	7·9	2536	0·0697	1·46	1737	0·0061
17·2	796	0·0410	8·2	2632	0·0800	1·84	2190	0·0103
19·0	880	0·0451	5·9	1895	0·0410	2·25	2678	0·0123
			8·1	2600	0·0614	2·70	3213	0·0164
	Air		10·6	3400	0·0944	3·12	3713	0·0185
			15·2	4870	0·1907	3·62	4311	0·0226
1·77	568	0·0082	17·7	5670	0·2560	3·90	4641	0·0297
2·68	860	0·0144				4·16	4950	0·0317
3·1	995	0·0184				4·45	5296	0·0389
4·04	1297	0·0267				4·40	5236	0·0389
5·10	1637	0·0369				1·95	2321	0·0113
						1·50	1785	0·0061
							Dichlorodifluoromethane	
						2·75	5350	0·0246
						0·98	1907	0·0061
						1·50	2920	0·0103
						2·1	4080	0·0184
						2·93	5700	0·0328

the flooding point is approached it was found difficult to determine accurately the flooding point.

Data based on the visual determination of the flooding velocity for different liquid rates are shown in Table 6.

Table 5. Determination of pressure drop across a disc.

Liquid rate lb./(hr.)(ft.)	*Gas velocity* ft./sec.	*Gas* R_e	ΔP_t lb./ft.^{2}	ΔP_e lb./ft.^{2} (*from Fig. 5*)	$\Delta P_t - \Delta P_e$ lb./ft.^{2}	ΔP_d lb./ft.^{2}
368	4·95	1590	0·1438	0·0328	0·1110	0·00411
368	6·20	1990	0·1926	0·0450	0·1476	0·00547
368	7·40	2380	0·2566	0·0597	0·1969	0·00729
368	8·50	2730	0·3080	0·0755	0·2325	0·00853
368	11·3	3630	0·4955	0·1200	0·3755	0·01389
368	12·8	4120	0·6060	0·1482	0·4578	0·01695
368	13·5	4330	0·6600	0·1606	0·4994	0·01851
368	14·7	4720	0·7675	0·1857	0·5818	0·02153
368	17·2	5530	1·0030	0·2400	0·7630	0·02820
368	19·0	6100	1·1690	0·2846	0·8844	0·03272
368	19·7	6330	1·2730	0·3030	0·9700	0·03590
368	21·1	6780	1·4390	0·3380	1·1010	0·04075

Table 6. Air velocities which initiate flooding.

(Flooding visually determined.)

Liquid rate lb./(hr.)(ft.)	*Air velocity* ft./sec.
101	32·0
141	27·0
188	26·5
234	23·5
281	22·5
325	21·0
368	21·5
408	20·0

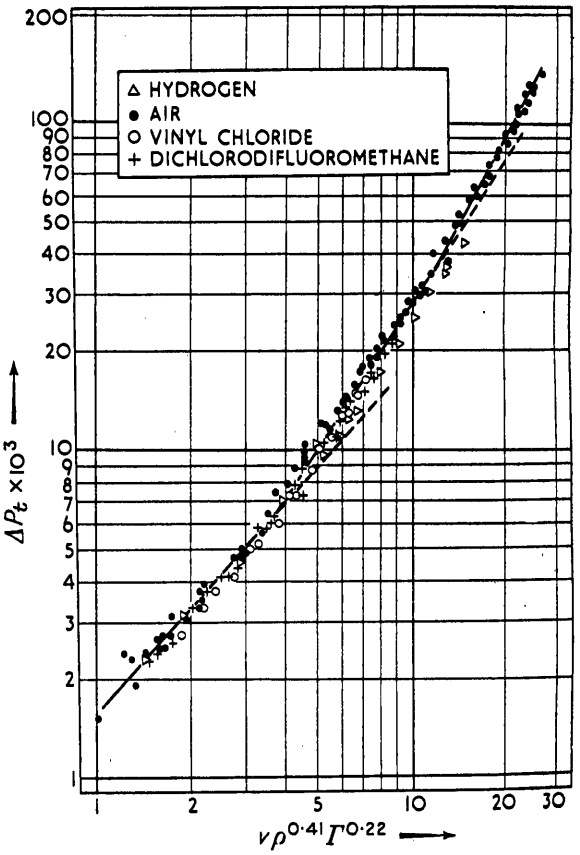

Fig. 6. Pressure drop across a disc.

DISCUSSION

The correlation for pressure drop across a disc, in which ΔP_d is plotted against $v\rho^{0.41}\ \Gamma^{0.22}$ on a log scale shows that the graph obtained is discontinuous and is characterised by two break points over the range studied. These break points are at $v\rho^{0.41}\ \Gamma^{0.22} = 4$ and $v\rho^{0.41}\ \Gamma^{0.22} = 12$. The positions of the break points for a particular system are not fixed exactly by these equations, as they tend to give high values of the critical velocities for the air runs and low values for the hydrogen and dichlorodifluoromethane runs. However, they do give an indication of the gas phase velocities, near which changes in the gas flow conditions can be expected.

The existence of these critical points is better illustrated by plotting $\frac{\Delta P_t}{v^2\rho}$ against gas Reynolds Number *Re* for individual runs with

liquid rates as parameters. Such a series of graphs is presented in Fig. 7.

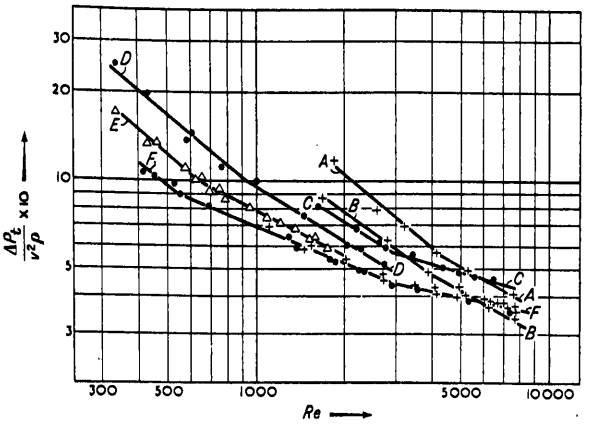

Fig. 7.

AA	dichlorodifluoromethane-water	$\Gamma = 255$ lb./(hr.)(ft.)
BB	dichlorodifluoromethane-water	$\Gamma = 131$ lb./(hr.)(ft.)
CC	air-water	$\Gamma = 408$ lb./(hr.)(ft.)
DD	air-water	$\Gamma = 255$ lb./(hr.)(ft.)
EE	hydrogen-water	$\Gamma = 255$ lb./(hr.)(ft.)
FF	air and dichlorodifluoromethane	$\Gamma = 0$ lb./(hr.)(ft.)

Referring to Fig. 7 the lines *AA* and *BB* are typical of a group of lines obtained for a particular gas phase with different liquid rates showing the existence of a break point at a Reynolds Number of approximately 4000. This break point corresponds to the lower break point of the correlation shown in Fig. 2. Lines *AA*, *DD* and *EE* are for different gas phases with the same liquid rate. The break points for these lines are approximately $Re = 4000$, $Re = 950$ and $Re = 600$ respectively. These break points all correspond to the lower break points of the correlation shown in Fig. 2. A break point corresponding to the higher break point of the correlation shown in Fig. 2 is indicated by the line *CC* at $Re = 3000$.

The inclusion in Fig. 7 of the data for the dry column shows that the flow conditions can be well correlated by graphing $\frac{\Delta P_t}{v^2\rho}$ against *Re* as shown by line *FF*. However, once the column is operating with liquid flowing over the discs the gas flow characteristics at a constant liquid rate can no longer be correlated by a Reynolds Number alone.

This can be clearly seen from the lines *EE*, *DD* and *AA*, which are for constant liquid rate with different gas phases. Hence it appears that the use of a gas Reynolds Number together with some functions of liquid rate as adopted by STEPHENS and MORRIS [4] and ROPER [3] for a correlation of gas film mass transfer coefficients, is not sufficient for a general correlation applicable to all gaseous systems.

As can be seen from Fig. 7, the line for zero liquid rate is found to intersect the line *BB* for dichlorodifluoromethane at a high Reynolds Number and then continues above the low liquid rate line. A similar effect was noticed if the low liquid rates of the air runs were plotted. The higher pressure drop of the dry column at the high Reynolds Number could be attributed to the increase in impact pressure losses on the square edges of the dry discs. The effect of liquid flowing is to round off the discs and thereby reduce the impact pressure losses. However, the liquid flowing over the discs will greatly increase skin friction and hence the general trend that pressure drop is increased with increased liquid rate.

The fact that break points are observed indicate that flow conditions in the gas phase change at definite critical points. Hence it is reasonable to expect some comparable change in the gas film coefficient under similar conditions. The data of ROPER [3] and STEPHENS and MORRIS [4] were critically examined for discontinuity in the gas film coefficient at gas velocities corresponding to the break points indicated by pressure drop measurements.

The bulk of the data reported by ROPER [3] on the evaporation of water in a disc column was for air velocities which are below the first break point on the pressure drop relations. However, data for liquid rates of 121 lb./(hr.)(ft.) and 81 lb./(hr.)(ft.) extend on both side of the first break point observed in the pressure drop relation investigated. These data have been plotted in Fig. 8 in which the pressure drop data for a low liquid rate of the air-water system are also shown.

The break point in the gas film mass transfer coefficient graph compares well with the observed break point in the pressure drop data. The data of STEPHENS and MORRIS [4] for the gas film

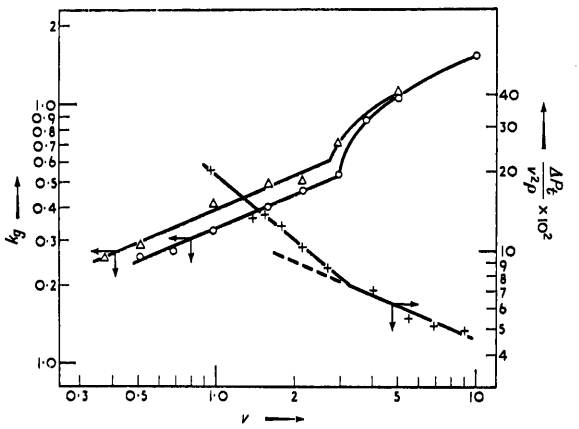

Fig. 8. Comparison of pressure and mass transfer characteristics.

- ● Γ = 121 lb./(hr.)(ft.) } Data of ROPER [3]
- ⊙ Γ = 81 lb./(hr.(ft.) } For gas film mass transfer coefficients in the evaporation of water in streams of air.
- \+ Γ = 166·5 lb./(hr.)(ft.) Pressure drop data for air-water system.

coefficient in the absorption of dilute ammonia-air mixtures by water, when plotted in the same manner, also show a break point which is consistent with that observed for pressure drop data.

ACKNOWLEDGMENTS

Acknowledgment is made to Professor J. P. BAXTER and Mr. G. H. ROPER, School of Chemical Engineering, N.S.W. University of Technology, for helpful discussion and interest in this work. Acknowledgment is also made to the *Monsanto Chemical Company* (*Aust.*) for the provision of the research scholarship which made this investigation possible.

NOTATION

- D = equivalent diameter for gas flow, ft;
- D_v = diffusivity, ft.^{2}/hr.
- k_g = gas film mass transfer coefficient, lb./(hr.)(ft.^{2})(atm.)
- M_d = molecular weight of the diffusing gas
- P_{BM} = logarithmic mean of the partial pressure of the inert gas at the phase boundary and in the bulk of the gas stream, atm.
- P = total pressure, atm.
- ΔP = pressure drop, lb./ft.^{2}
- ΔP_t = pressure drop across the whole column, lb./ft.
- ΔP_e = pressure drop across the empty column (discs removed), lb./ft.^{2}
- ΔP_d = pressure drop due to a single disc in a disc column, lb./ft.^{2}
- Re = Reynolds Number for the gas phase, $Dv\rho/\mu$
- v = velocity of the gas stream, ft./sec.
- Γ = liquor rate, lb./(hr.)(ft.)
- β = a function of liquid rate
- μ = absolute viscosity of the gas stream, lb. mass./(ft.)(hr.)
- ρ = density of the gas stream, lb./ft.^{3}
- ρ_d = density of the diffusing gas, lb./ft.^{3}
- ϕ = the dimensional function $v\rho^{0.41}\,\Gamma^{0.22}$
- n = exponent of Reynolds Number
- m = exponent of the Schmidt Number

REFERENCES

[1] GILLILAND, E. R. and SHERWOOD, T. K.; Ind. Eng. Chem. 1934 **26** 516.

[2] JOHNSTONE, H. F. and PIGFORD, R. L.; Trans. Amer. Inst. Chem. Engrs. 1942 **38** 25.

[3] ROPER, G. H.; Chem. Eng. Sci. 1953 **2** 18.

[4] STEPHENS, E. J. and MORRIS, G. A.; Chem. Eng. Progr. 1951 **47** 232.

UNIVERSITY OF KENSINGTON NEW SOUTH WALES

>006941532